



2nd International Conference DESIGN AND MANAGEMENT OF PORT, COASTAL AND OFFSHORE WORKS

Organised by:



Laboratory of
Maritime
Engineering and
Maritime Works



Laboratory of
Harbour Works



Laboratory of
Floating Structures
and Mooring
Systems



Hydraulic
Engineering
Laboratory



PROCEEDINGS VOLUME II

MAY 24-27, 2023

**Aristotle University's
Research Dissemination Center**
Thessaloniki, Greece



2nd International Conference

DESIGN AND MANAGEMENT OF PORT, COASTAL AND OFFSHORE WORKS

MAY 24-27, 2023

**Aristotle University's
Research Dissemination Center**
Thessaloniki, Greece

Proceedings of the 2nd International Conference
Design and Management of Port, Coastal and Offshore Works

ISSN: 2945-1299
ISBN: 978-960-99922-6-8

VOLUME II

ISBN: 978-960-99922-8-2

Published by: Laboratory of Maritime Engineering and Maritime Works,
Civil Engineering Department, AUTH

Edited by: T. Karambas, E. Loukogeorgaki, C. Makris

Year of Publication: 2023



Organised by:



Laboratory of
Maritime
Engineering and
Maritime Works



Laboratory of
Harbour Works



Laboratory of
Floating Structures
and Mooring
Systems



Hydraulic
Engineering
Laboratory

COMMITTEES

ORGANIZING COMMITTEE

CHAIRS

Theofanis Karambas, Professor, Director Lab. of Maritime Engineering & Maritime Works, AUTH
Eva Loukogeorgaki, Associate Professor, AUTH

MEMBERS

Spyros Christopoulos, Dr. Coastal Engineer, HYDROMARE
Christos Makris, Research Associate, AUTH
Afrodite Papageorgiou, Civil Engineer, AUTH

SCIENTIFIC COMMITTEE

Androulidakis Y., Research Assoc., AUTH, University Fellow Scholar, Un. of the Aegean
Athanasoulis G., Professor Em., NTUA
Chalmoukis I., Postdoctoral Assoc., University of Patras
Chatjigeorgiou I., Professor, NTUA
Chatzimpiros K., Professor Em., AUTH
Chlomidou K., Professor, University of Piraeus
Chondros M., Assist. Professor, NTUA
Christopoulos S., Dr. Coastal Engineer, HYDROMARE
Dimakopoulos A., Dr. Civil Engineer, Associate Director, Jacobs, UK
Dimas A., Professor, University of Patras
Fourniotis N., Assist. Professor, University of Peloponnese
Galani K., Dr. Coastal Engineer, Patras Port Authority
Grigoriadis D., Assoc. Professor, University of Cyprus, Cyprus
Grigoropoulos G., Professor, NTUA
Karambas Th., Professor, AUTH
Karmpadakis I., Assoc. Professor, Imperial College, UK
Katsardi V., Assist. Professor, UTH
Klonaris G., Dr. Civil Engineer, Research Assoc., NTUA
Kokkosis Ch., Professor, UTH
Kolokythas G., Dr. Coastal Engineer, AKTAIA
Konispoliatis D., Assist. Professor, NTUA
Koutitas Ch., Professor Em., AUTH
Koutrouveli Th., Dr. Coastal Engineer, IMDC, Belgium
Krestenitis Y., Professor Em., AUTH
Kupraios N., Dr. Civil Engineer
Leftheriotis G., Postdoctoral Assoc., University of Patras
Loizidou M., Professor, NTUA
Loizidou X., Dr. Coastal Engineer, ISOTECH, Cyprus
Loukogeorgaki E., Assoc. Professor, AUTH
Makris Ch., Dr. Civil Engineer, Research Assoc., AUTH
Mavrakos S., Professor Em., NTUA
Melissas D., Professor, NTUA
Memos K., Professor Em., NTUA
Metallinos A., Dr. Civil Engineer, Research Assoc., NTUA
Michailidis C., Assist. Professor, IHU
Mpardakis B., Dr. Civil Engineer, President of HCCE
Pallis Ath., Professor, University of the Aegean
Panagiotopoulos I., Assist. Professor, UOA
Papadopoulou M., Professor, NTUA
Papatheodorou G., Professor, University of Patras
Poulos S., Professor, UOA
Prinos P., Professor, AUTH
Samaras Ach., Assist. Professor, DUTH
Savvidis Y., Professor, IHU
Soukisian T., Dr. Naval Architecture and Marine Engineer, HCMR
Stamou A., Professor, NTUA
Sylaios G., Professor, UTH
Toumazis A., Dr. Civil Engineer, University of Cyprus
Tsanis I., Professor, University of Crete
Tsoukala V., Professor, NTUA
Vasilakis E., Assist. Professor, UOA
Zacharias I., Professor, University of Patras

EXTERNAL ADVISORY COMMITTEE

Arena F., Professor, University Mediterranea of Reggio Calabria, Italy
Benoit M., IRPHE, France
Carevic D., Professor, University of Zagreb, Croatia
Penchev V., Professor, BDCA, Bulgaria
Sánchez-Arcilla A., Professor, UPC, Spain
Taveira Pinto F., Professor, University of Porto, Portugal
Vicinanza D., Professor, University Vanvitelli, Italy



2nd International Conference
**DESIGN AND MANAGEMENT OF PORT,
COASTAL AND OFFSHORE WORKS**

CONTENTS VOLUME II

CONTENTS	7
PREFACE	11

FULL PAPERS OF DMPCO 2023 PROCEEDING VOL. II

COASTAL EROSION & MANAGEMENT

Sea Bottom Evolution considering Wave Events Sequences and Environmental Aspects: The Case Study of Kolymvari Coast, Crete <i>D. Malliouri, D. Vandarakis, S. Petrakis, V. Moraitis, F.-K. Gad, A. Skoumpaki, E. Stroglyoudi & V. Kapsimalis</i>	15
Protection of the Poti Coastal Zone from Erosion using Submerged Breakwaters <i>I. Saginadze, M. Kodua & M. Pkhakadze</i>	21
Historical Evolution and Impact of Coastal Structures on Shoreline Stability along the South Coast of Cyprus <i>S. Demetriade, D. Stagonas, S. Zervos & G. Protopapas</i>	27
Evolution and Trends of Coastal Erosion along the Nestos River Delta <i>K. Zachopoulos, N. Kokkos & G. Sylaios</i>	32
Climate Change Impacts on the Coastal Zone of Alfios River Estuary <i>M. Chondros, A. Metallinos, A. Papadimitriou & V. Tsoukala</i>	37
Perched Beach Nourishment against Coastal Erosion and Flooding: Experimental and Numerical Simulation <i>D. Spyrou, S. Christopoulos & Th. Karambas</i>	42
Wave Regime and Shoreline Evolution of the Coastal Front of Kymi (Euboea) <i>S. Lesioti, S. Poulos, A. Karditsa & C. Aggelopoulos</i>	47
A Sideways Look at 1-Line Beach Modelling <i>D. Reeve</i>	52
Effects of Flow and Sediment Parameters on Vortex Ripple Morphodynamics <i>G.A. Leftheriotis & A.A. Dimas</i>	57
Representative Waves for Estimating Annually Averaged Sedimentation and Erosion Trends in Sandy Coastal Areas using Numerical Models and Artificial Neural Networks <i>M. Diamanta & M. Chondros</i>	62
Revisiting and Enhancing the Concept of Equivalent Wave Heights <i>A. Papadimitriou, V. Tsoukala & Th. Karambas</i>	67
Wave Input Reduction Methods for Annual Bed Evolution Applications <i>A. Papadimitriou & V. Tsoukala</i>	72
Decision-Making Tool for Mitigation of the Coastal Erosion and Extreme Wave Impacts in the Coastal Zone, in the Context of Climate Change <i>S. Liaros, S.E. Poulos, N. Kampanis, J.D. Alexopoulos, G. Alexandrakis, A. Karditsa, G. Ghionis, E. Vassilakis, M. Hatzaki, P. Nastos, P. Nomikou, V. Kotinas, E.-S. Stanota, A. Nteris, V. Methenitis, G.S. Mitsika, D. Lampridou, E. Margaritou, S. Skolovas, K. Nikolaou, A. Stamatoglou, I.K. Giannopoulos, V. Gkossios, A. Konsolaki, G. Kontostavlos, M. Konstantopoulou, M. Panagou, N. Gkogkos, L. Roussos, I. Exintavelonis, H. Roukouni & K. Stamatoglou</i>	77

INTEGRATED COASTAL ZONE MANAGEMENT

Digitisation and Proactive Management of Coastal and Offshore Infrastructure and Environment	
<i>T. Onoufriou, C. Michailides & P. Christodoulides</i>	82
A Case-Study for the Water Renewal in the Rio Castle Moat in Greece	
<i>G.A. Leftheriotis, I.S. Chalmoukis & A.A. Dimas</i>	87
A Preliminary Study of Water Renewal in a Flow-Through Lake in Western Greece	
<i>N.Th. Fourniotis & G.A. Leftheriotis</i>	92
Ground Penetrating Radar for Inspecting the Core and Base of Coastal Sand Dunes	
<i>J.D. Alexopoulos, I.K. Giannopoulos, G.S. Mitsika, V. Gkosios, A. Konsolaki, E. Vasillakis & S.E. Poulos</i>	97
Coastal Marine Steel Corrosion: The Environment's Influence and In-Situ Monitoring – A Review	
<i>C. Kassinis, T. Onoufriou & C. Michailides</i>	102
Monitoring and Analysis of Coastal Eutrophication Using Remote Sensing	
<i>I. Biliani & I. Zacharias</i>	107
Carrying Capacity Indicators in Tourism – The Case of the Island of Paros Coastal Zone	
<i>D. Prokopiou & B. Tselentis</i>	110

PORTS & PORT ENGINEERING

Towards a Digital Twin for Marine and Maritime Activities: The ILIAD Project Framework	
<i>G. Sylaios, A.-J. Berre, B.L. Bye, U. Broenner & V. Kioussi</i>	117
Advancing Image Analysis Practices for Condition Assessment of Port Infrastructure with GIS Applications	
<i>C. Tsaimou, D.G. Kagkelis, P. Sartampakos & V. Tsoukala</i>	122
Expansion of Pier 6 of the Port of Thessaloniki	
<i>C. Solomonidis, K. Papadopoulos, D. Pachakis, D. Fotiadis & V. Drossos</i>	127
Creation of a Double Berth Jetty for Small Scale LNG Carriers & Barges in Revithoussa Island, Greece – A Multipurpose Terminal	
<i>C. Solomonidis, P. Biniskos & M. Aggelidis</i>	133
Numerical Modelling of Dredged Material Dispersion at Dredging and Disposal Areas	
<i>Th. Karambas & A. Papageorgiou</i>	138
Assessing the Impact of Climate Change in Wave Agitation for the Port of Piraeus	
<i>I. Kollias, A. Papadimitriou, M. Chondros, V. Chalastani, D. Spyrou, Ch. Laspidou, P. Koundouri & V. Tsoukala</i>	143
Contemporary Types and Models of Private Sector Involvement in Ports	
<i>K. Chlomoudis & M. Tozidis</i>	148
Smart and Green Ports	
<i>P. Boudouris</i>	153
Piraeus Port Authority S.A. and Thessaloniki Port Authority S.A. before and after the Privatization	
<i>M. Voudigaris & Th. Giantsi</i>	158
Revisiting Port Regulatory Governance & Substance: Towards a Holistic Supply Chain Approach	
<i>C. Chlomoudis, P. Pallis & T. Styliadis</i>	163
Expectations and Risks for Greek Ports from the Upcoming New EU Regulation for the Trans European Transport Network (TEN-T)	
<i>Th. Giantsi</i>	168
Boomer Sub-Bottom Profiler: Also Valid for Distinguishing Habitat Boundaries during Port Geological Surveys? – An example from Armenistis Coastal Zone in Ikaria Island	
<i>A. Poulos, O. Andreadis, I. Petsimeris, K.A. Chtouris, T. Hasiotis, A. Kokoromytis & D. Karamaniolas</i>	173
The Social Acceptance of Autonomous Merchant Ships in Greek Ports	
<i>C. Politopoulou, A.-F. Papathanasiou & Th. Giantsi</i>	178

COASTAL STRUCTURES

Performance of a System of Detached Breakwaters on the South Corinthian Gulf <i>E. Papafotiou & Th. Giantsi</i>	184
Kinematic Perturbations in Submerged Breakwaters under Waves <i>E. Repousis, N. Diplarakos, I. Roupas & C. Memos</i>	189
Coastal Protection Works of Liopetri's River "Potamos", Cyprus <i>S. Gouloumis & M. Karas</i>	194
Coastal Engineering Study for the Rehabilitation of the Beachfront at the Fire-Struck Area of Mati, Eastern Attica <i>C. Solomonidis & G. Fotis</i>	199
A New Time-Dependent Irregular Wave Propagation Model <i>Th. Karambas, A.G. Samaras & C. Makris</i>	204
LES of Wave Propagation on a Beach with Different Vegetation Characteristics <i>I.A. Chalmoukis, G.A. Leftheriotis & A.A. Dimas</i>	209
Coastal Engineering Applications in Greece from a Consultant's Point of View <i>A. Valsamidis</i>	215

GEOTECHNICAL & GEO-ENVIRONMENTAL ENGINEERING

Offshore Infrastructures in Greece: A New Era and a Big Challenge for Marine Geotechnical Surveying <i>T. Hasiotis & N.K. Chtouris</i>	220
Satellite Derived Bathymetry (SDB) with no Use of Field Data <i>A.K. Mavraeidopoulos</i>	225
Seabed Conditions in the Embayment of Agia Efimia (Kefalonia) Two Years after the Medicane Ianos <i>I. Petsimeris, A. Oikonomou, A. Poulos, O. Andreadis, V. Lioupa & T. Hasiotis</i>	231
The Importance of Hydrography in Local Seismic Activity Monitoring: A Case Study in Katakolo Port, Kyparissiakos Gulf, Western Peloponnese, Greece <i>D. Kioussi, E. Oikonomou, A. Sartampakou & P. Sartampakos</i>	236





PREFACE

Ports, coastal and offshore structures play a strategic role for the socio-economic development of citizens in Europe and worldwide, facilitating the sustainable and secure implementation of various human activities, such as transportation, fishing, leisure and aquaculture, the protection of coastal areas and the exploitation of energy sources in the marine environment. Contemporary societal needs, including mitigation of climate change impacts, protection against coastal flooding and extreme events, clean, affordable and secure energy, security of supplies and decarbonisation of marine facilities, have redefined, nowadays, the significance of all coastal and offshore infrastructures, and have introduced new technological challenges in the whole life-cycle of those structures. Still, a great potential for innovation and growth has been emerged taking advantage of the numerous opportunities that seas and oceans provide.

The **2nd International Conference on Design and Management of Port, Coastal and Offshore Works (DMPCO 2023)** aims to stimulate comprehensive discussions and scientific interactions among the participants about the new trends and the state-of-the-art developments in the design and management of ports, coastal and offshore structures. As a sequence of DMPCO 2019, the Conference provides a forum for presenting new ideas and enhancing scientific and applied knowledge for engineers and scientists working in the relevant fields.

DMPCO 2023 has successfully attracted the interest of 221 authors from Greece, Cyprus, United Kingdom, Belgium, Netherlands, Italy, Romania, Georgia and China. The final technical program included 89 presentations allocated into 14 sessions, as well as 5 keynotes, where worldwide recognized speakers presented cutting-edge topics. This year, the “Coastal Modelling” session was organized in the honour of Professor Emeritus Christofer Koutitas and the “Offshore Renewable Energy I” session was dedicated to the memory of Professor Emeritus Demos Angelides. The two volumes of the DMPCO 2023 proceedings include 85 papers, which are grouped in ten main thematic areas of the Conference corresponding to: Coastal Modelling, Coastal Hydrodynamics, Extreme Waves – Wave Hydrodynamics, Offshore Renewable Energy, Marine Spatial Planning & Environment, Coastal Erosion & Management, Integrated Coastal Zone Management, Ports & Ports Engineering, Coastal Structures and Geotechnical & Geo-environmental Engineering.

We would like to thank all authors and keynote speakers for their contributions, as well as all the members of the Organizing, Scientific and External Advisory Committees for their valuable help and support. All these efforts resulted to a successful Conference with active participation and stimulating discussions in the field of port, coastal and offshore structures. This success gives us the energy and the motivation to continue our strong and systematic efforts towards the organization of productive DMPCO Conferences in the future.

We are looking forward to seeing you in Patras, Greece in 2025.

Professor Theofanis Karambas
Associate Professor Eva Loukogeorgaki
Chairs of the Organizing Committee





DMP CO 2023



CONFERENCE PROCEEDINGS VOLUME II



Sea bottom evolution considering wave events sequences and environmental aspects: the case study of Kolymvari coast, Crete

D. Malliouri^{1*}, D. Vandarakis¹, S. Petrakis¹, V. Moraitis¹, F.-K. Gad², A. Skoumpaki³

E. Stroglyoudi¹, V. Kapsimalis¹

¹Hellenic Centre for Marine Research, Institute of Oceanography, 46.7 km Athens-Sounio Ave., Anavyssos, 19013, Greece

²Region of South Aegean, Tsiropina Sq., Ermoupoli, Syros, 84100, Greece

³Harbour Management Organisation of Prefecture of Chania, Peridou 24, Chania, 73100, Crete, Greece

*Corresponding author: d.malliouri@hcmr.gr

Abstract

In the present study, a numerical investigation of sea bottom evolution of the Kolymvari coastal zone is performed, which is accomplished through the use of a recently developed methodology of wave events' sequences. The adopted approach accelerates remarkably the simulation of long-term coastal morphodynamics and estimates with satisfactory accuracy the coastal evolution as a function of time. Moreover, coastal processes are simulated under the presence of coastal structures aiming to protect the coast from erosion and extreme wave conditions, without significantly degrading the suitable nesting habitat of sea turtles. Hence, the wave regime in combination with the environmental aspect of sea turtles is considered, by examining two alternative solutions. In the first solution, the coastal response to waves is examined under the presence of seven emerged breakwaters of similar characteristics, whereas a more environmentally friendly solution of four emerged and three submerged breakwaters is examined in the second case. In short, a cost-effective method is implemented, providing information on sea bottom evolution as a time function. Additionally, by considering site specific environmental aspects related to the studied coastal structures' types, a balance is attempted between a resilient coastal environment and a suitable nesting habitat for sea turtles.

Keywords Bottom evolution, Wave events' chronology, Coastal structures, Sea turtles.

1 INTRODUCTION

The short- and long-term coastal evolution are usually investigated through process-based morphodynamic models. However, the models' complexity and the inherent high computational cost, especially regarding long-term analysis, necessitate the development and implementation of wave input reduction and acceleration techniques (Benedet et al. 2016; Walstra et al. 2013). Although these acceleration techniques, e.g., the Energy Flux Method or the Sediment Transport Bins Method, are widely used in coastal engineering studies, they do not consider, in detail, wave chronology to predict the sea bottom and shoreline evolution, and, thus, are somehow inadequate for coastal zone monitoring (Malliouri et al. 2023).

In the present work, the coastal zone evolution of Kolymvari, located on the northwest coast of Crete Island, S. Greece, is estimated as a function of time, e.g., before and after extreme coastal storm events that can induce severe sea bottom changes. In the current situation, three emerged rubble mound breakwaters, were constructed in 2020, based on an experimental study performed in the Laboratory of Harbor Works (National Technical University of Athens). In the NTUA experimental study seven emerged breakwaters were proposed to be constructed to limit the wave-induced erosion phenomena that characterize the study area.

Furthermore, the beach of Kolymvari is a loggerhead sea turtle nesting area and, along with other neighboring areas of high natural value, has been included in the European Union Natura 2000 network under the code GR4340003 "CHERSONISOS RODOPOU – PARALIA MALEME -KOLPOS CHANION (<https://www.archelon.gr/contents/projects5.php?mid=3&mid2=41>). It is noteworthy that human activities and especially hard types of coastal structures, such as emerged rubble mound

breakwaters, affect sea turtles in a number of ways (e.g., Margaritoulis and Panagopoulou, 2010). Therefore, after consultation with the Sea Turtle Protection Society of Greece (ARCHELON), it is recommended that at least three of the new breakwaters should be of submerged type, since they do not hinder the turtles' ability to access the coast, the nesting conditions, and the safe access of the hatchlings to the open sea.

Hence, the present study aims to investigate the performance of the four new breakwaters, depending on their type, to ensure the coast's resistance and ecological value.

2 METHODOLOGY

The adopted methodology has two main parts, namely the wave input reduction technique that preserves wave events' chronology and the performance investigation of the two different types of breakwaters.

The performance assessment of the two different types of breakwaters regarding coastal protection necessitates the long-term (≥ 1 year) simulation of coastal morphodynamics due to wind-generated waves. In this study, the timeseries of significant wave height H_{m0} , peak wave period T_p and mean wave direction MWD , covering the annual period from 01 January 2021 to 31 December 2021, are obtained from the reanalysis dataset of ERA5 hourly data on single levels from 1959 to present, downloaded from the Copernicus database (<https://cds.climate.copernicus.eu#!/home>). The time resolution of the reanalysis data is 1 hr, while the spatial resolution is $0.25^\circ \times 0.25^\circ$ (atmosphere) and $0.5^\circ \times 0.5^\circ$ (ocean waves). The offshore wave data extraction point has the spatial coordinates of $35^\circ 33' 40.3'' N$ $23^\circ 48' 16.8'' E$.

The annual timeseries of H_{m0} , T_p , MWD have been reduced to sequences of wave events of different intensities and durations, through a wave climate schematization technique implemented to accelerate the simulations without loss of accuracy. This method is developed by Malliouri et al. 2023, according to which each wave event is determined by a segment of non-overlapped successive wave data that satisfy the statement, noted below:

$$\forall t \in [t_1, t_2]:$$

$$|H_{m0}(t) - \bar{H}_{m0}| < \Delta h \text{ and } |T_p(t) - \bar{T}_p| < \Delta t \text{ and } |MWD(t) - \overline{MWD}| < \Delta d \quad (1)$$

where t is the time variable, $[t_1, t_2]$ the time interval covered by a certain wave event, and Δh , Δt , and Δd are the maximum acceptable values of the absolute differences of $H_{m0}(t)$, $T_p(t)$, and $MWD(t)$ from their mean values \bar{H}_{m0} , \bar{T}_p , and \overline{MWD} , respectively. The values of Δh , Δt , and Δd are considered 0.5 m, 1.0 s and 15 deg., as recommended by Malliouri et al 2023, and a MORFAC (Morphological Acceleration Factor) value of 10 has also been used.

Additionally, coastal processes including wave propagation from deep waters towards inshore, coastal circulation, sediment transport, and sea bottom evolution were simulated using the MIKE 21 Coupled Model FM software package (DHI). Three sets of simulations were performed using the same wave events sequences but different bottom levels near structures of different type (see Figure 1), listed below:

1. Simulation under the presence of three emerged breakwaters (Present situation)
2. Simulation under the presence of seven emerged breakwaters (First alternative case)
3. Simulation under the presence of four emerged and three submerged breakwaters (Environmentally friendly case)

It is noted that the rock areas have been discriminated from the sand areas through the use of different Manning coefficient and initial bottom layer thickness values.

3 RESULTS

From the statistical analysis of the wind and wave data, it appears that the prevailing directions are met in a sector around 25 deg N, that is, they are northeastern. Moreover, a variety of results have been derived from the above simulations, but the most characteristic ones are chosen to be presented, for

reasons of brevity. These are the bottom evolution after an extreme wave event (see Figure 2) that started on 18 December 2021, and the results at the end of the year 2021 (see Figure 3) for the three examined cases. The extreme event corresponds to a maximum H_{m0} value of 4.51 m, a concurrent T_p value of 9.32 s, MWD of 7 deg. from North and a duration of 26 hr (Figure 2).

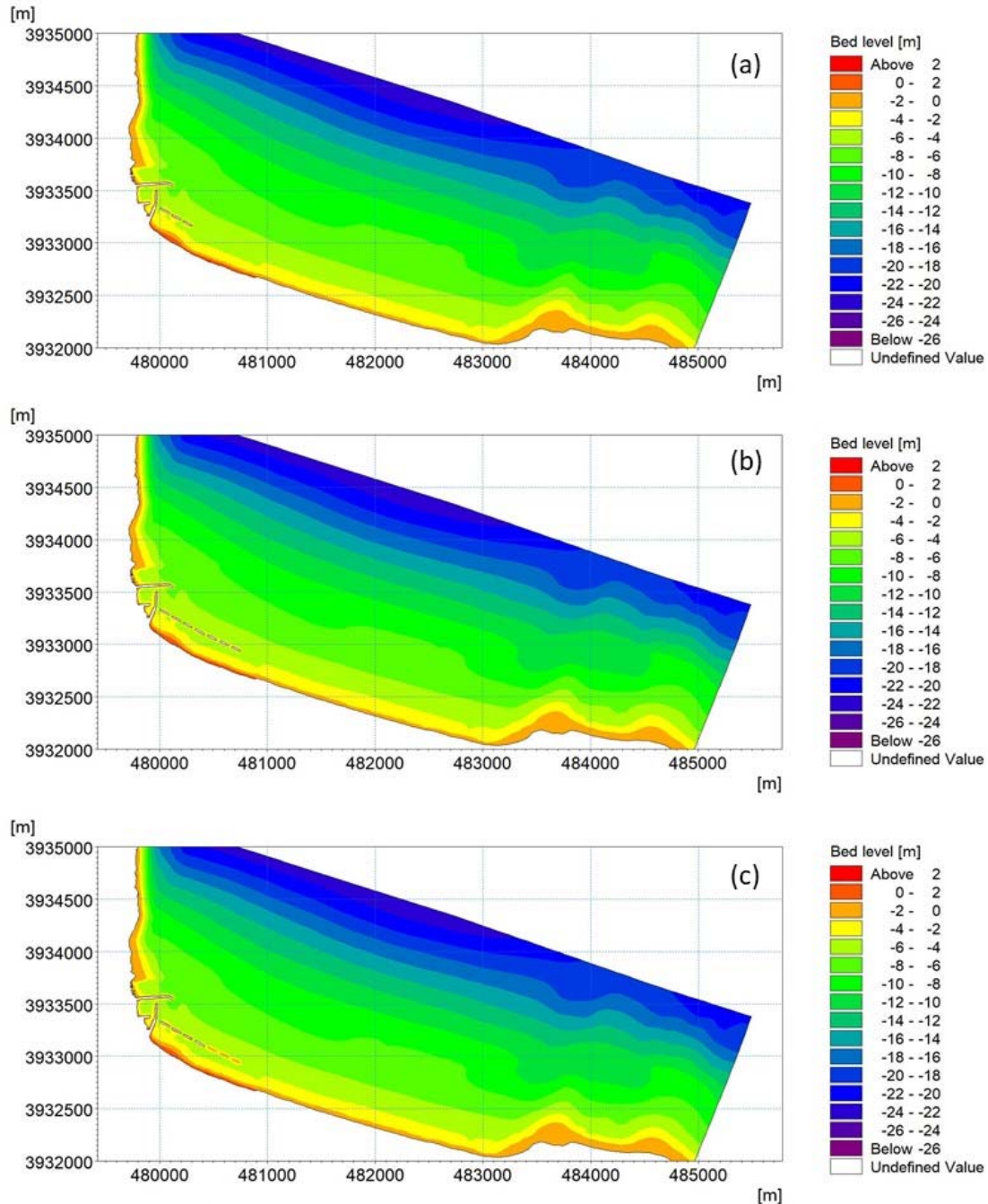


Figure 1. Bathymetry map of the study area: (a) Three emerged breakwaters (current situation), (b) Seven emerged breakwaters (first alternative solution) and (c) Four emerged and three submerged breakwaters (environmentally friendly solution).

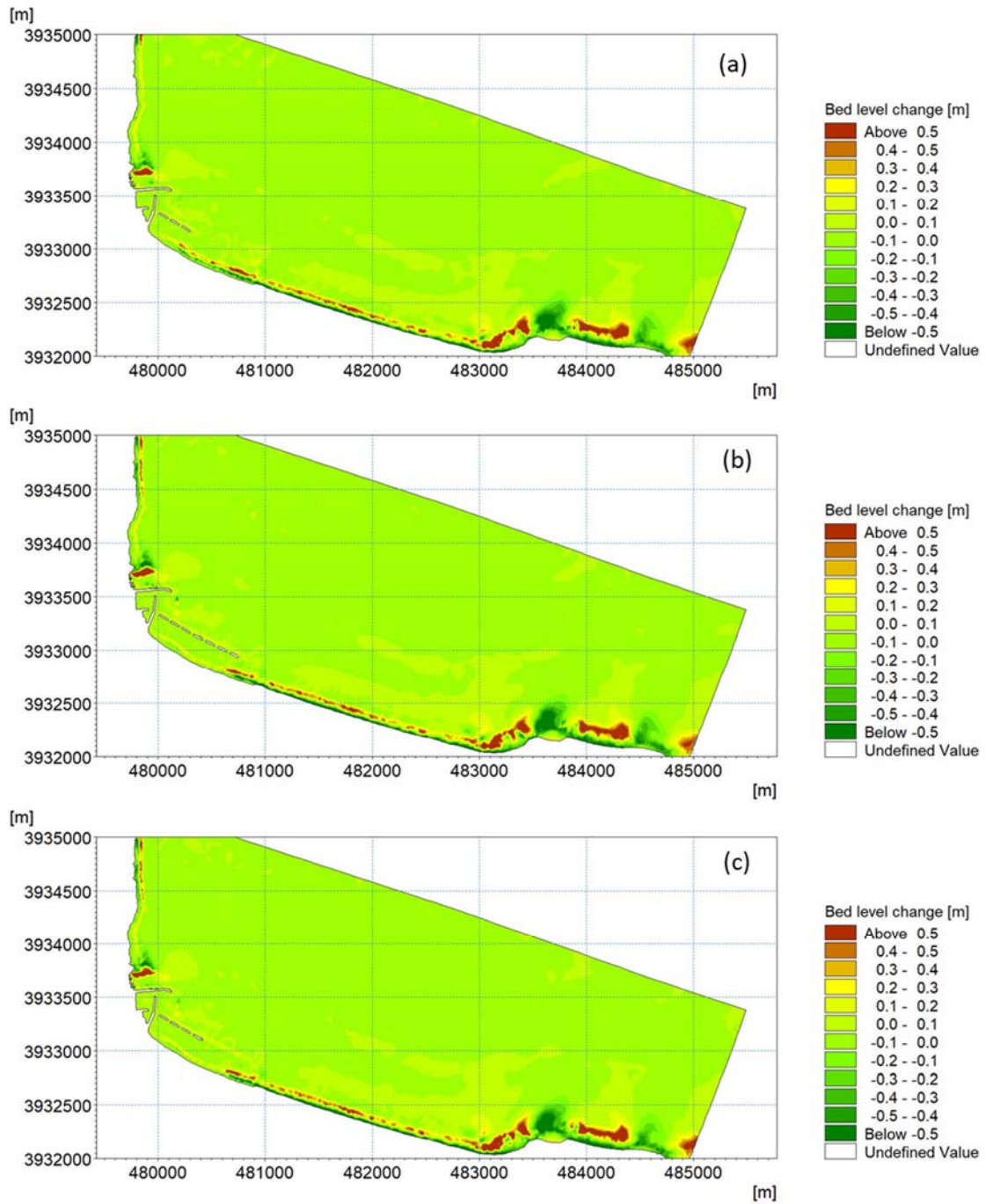


Figure 2. Bottom evolution at the end of the storm started on 18 December 2021 and lasted 26 hr: **(a)** Three emerged breakwaters (current situation), **(b)** Seven emerged breakwaters (first alternative solution) and **(c)** Four emerged and three submerged breakwaters (environmentally friendly solution).

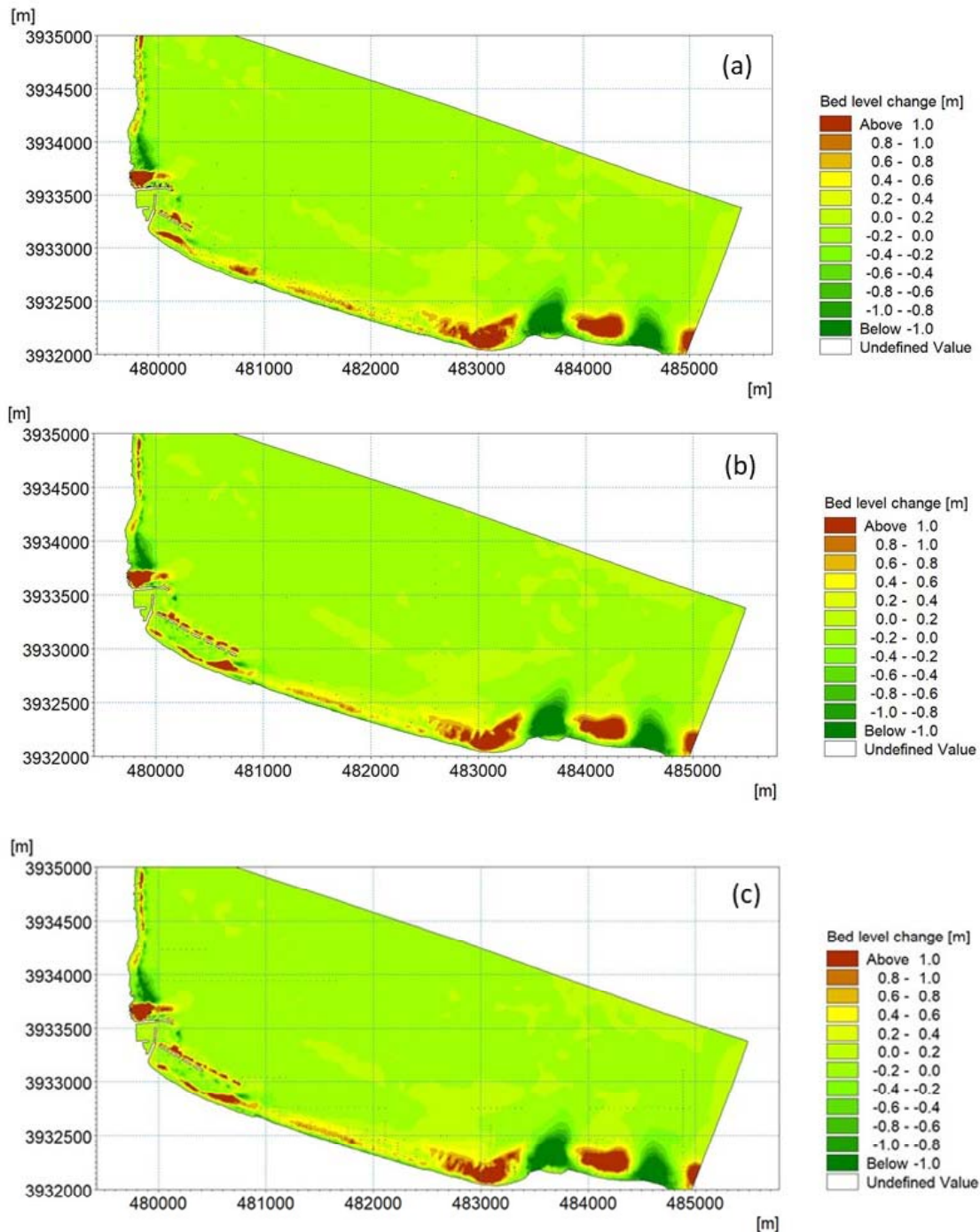


Figure 3. Bottom evolution at the end of the year 2021: **(a)** Three emerged breakwaters (current situation), **(b)** Seven emerged breakwaters (first alternative solution) and **(c)** Four emerged and three submerged breakwaters (environmentally friendly solution).

The coastal area behind the breakwaters is significantly protected from large waves and erosion phenomena, as seen in Figure 2 and Figure 3, in contrast to the coastline east of the structures. This area is exposed to extreme sea conditions, and as a result, a submerged sand bar is often formed in front of the eroded coastline (see Figures 2 and 3). The solution of the four new emerged breakwaters (Figure 2(b)) and the more environmentally friendly solution (Figure 2(c)), regrading sea turtles, seem to protect the coastline for 480 m and 450 m east of the third structure (starting from west), respectively. Furthermore, in the case of the four emerged and the three submerged breakwaters, the formation of a

tombolo in the lee of the seventh breakwater (Figure 3(c)) is less likely to occur than in the alternative case of the seven emerged breakwaters (Figure 3(b)).

4 CONCLUSIONS

A cost-effective method is implemented, providing information on sea bottom evolution as a time function. In addition, by considering site specific environmental aspects related to the studied coastal structures' types, a balance is attempted between a resilient coastal environment and a suitable nesting habitat for sea turtles. The pros and cons of the alternative solutions should be precisely weighted towards this direction. Moreover, a thorough experimental and coastal engineering study is recommended to be conducted to consider all the mentioned aspects prior to the implementation of the final solution.

ACKNOWLEDGMENTS

We acknowledge support of this work by the project "Ecological Quality Assessment of Kolymvari Coastal Zone", funded by the Harbour Management Organisation of Prefecture of Chania.

References

- Benedet, L, Dobrochinski, JPF, Walstra, DJR, Klein, AHF, Ranasinghe, R (2019) A morphological modeling study to compare different methods of wave climate schematization and evaluate strategies to reduce erosion losses from a beach nourishment project, *Coastal Engineering* 112:69–86. doi:10.1016/j.coastaleng.2016.02.005
- Malliouri DI, Petrakis S, Vandarakis D, Moraitis V, Goulas T, Hatiris G-A, Drakopoulou P, Kapsimalis V (2023) A Chronology-Based Wave Input Reduction Technique for Simulations of Long-Term Coastal Morphological Changes: An Application to the Beach of Mastichari, Kos Island, Greece, *Water* 15(3):389. doi:10.3390/w15030389
- Margaritoulis D, Panagopoulou A (2010) Greece. In: Casale P, Margaritoulis D (eds) *Sea turtles in the Mediterranean: distribution, threats and conservation priorities*. IUCN, Gland, Switzerland, p 85-111.
- Walstra, DJR; Hoekstra, R; Tonnon, PK; Ruessink, BG (2013) Input reduction for long-term morphodynamic simulations in wave-dominated coastal settings. *Coast. Eng.* 77:57–70. doi:10.1016/j.coastaleng.2013.02.001.

Protection of the Poti coastal zone from erosion using submerged breakwaters

I.S. Saghinadze¹, M. A. Kodua^{2*}, M. D. Pkhakadze¹

¹Faculty of Maritime Transportation, Akaki Tsereteli State University, Kutaisi, Georgia

²Department of Hydro-engineering, Georgian Technical University, Tbilisi, 0171, Georgia

*Corresponding author: m.kodua@gtu.ge

Abstract

The paper presents an engineering solution for the protecting and substantiality of the shoreline from the erosion of the Rioni River “City Canal”. During the investigations, the six km long coastline is divided into two parts: The 1 km long coastline adjacent, where the riparian currents arising as a result of the flow of the Rioni River into the sea are strong. The rest of the coastline, where the influence is weaker. The need to clean the bed of the canal is substantiated and an optimal cleaning plan is suggested. The need the clean the bed of the canal is substantiated and an optimal cleaning scheme is proposed. The solid material removed during cleaning should be dumped in a one km strip adjacent, which will be further processed and distributed by the waves. In order to protect the remaining shore from erosion, underwater barriers parallel to the shore are used in the sea. Sand-filled geotextile tubes are used as underwater barriers, which are both economically and environmentally sound. Graphical and analytical criteria are used to determine the parameters of underwater barriers and the nature of the morphological change of the shore (erosive, cumulative). On the basis of the analysis of the results obtained in the paper, a justified scheme for the protection of the coastline south of the “City Canal” from erosion has been developed.

Keywords Wave, Current, Shore, Geotube.

1 INTRODUCTION

The erosion processes in the city of Poti and its maritime region are mainly caused by the sedimentation of the Rioni River bed “City Canal” with solid sediment. Due to this, the cross-section of the bed has decreased by about 30-35% and instead of 500m³/s of water, it carries 200-250m³/s. As a result, the volume of solid sediment brought into the sea by the river decreased and the deficit amounted to 200,000-250,000 m³ per year (Gagoshidze et al. 2017). The sea has catastrophically washed away the coastline of Poti and pushed it back hundreds of meters. At the same time, a delta was created at the confluence of the “Nabada Channel” with the sea, which is growing over time (Figure 1). The average speed of shore washing in a multi-year cut is 6-8m/year. The volume of beach-forming sediment deposited into the river bed is approximately 1,000,000m³ (Saghinadze and Kodua. 2019).

The situation is particularly alarming in the 6 km coastal strip south of the confluence of the Rioni River “City Canal” (Figure 1). Despite many attempts, the problem remains currently unsolved, and its solution is an urgent issue.

2 MAIN PART

In order to fill the deficit of sediment in the coastal zone, it is necessary to clean the bed of the “City Canal” and dump the sediment in the coastal zone. Afterward, the Canal will cover the design flow rate and the amount of solid sediment introduced into the sea will increase. This measure will partially solve the problem. Further action is required to fully resolve the issue and will be discussed below.

The transport of sediment in the coastal zone adjacent to the “City Canal” is strongly influenced by the riparian currents generated when the Rioni River flows into the sea. Therefore, we will divide its 6-kilometer section of the coastline south of the into two parts: 1) The 1-km-long coastal strip adjacent, where the riparian currents arising from the flow of the Rioni River into the sea are strong; 2) The rest of the coastline, where the Rioni River influence is weak.

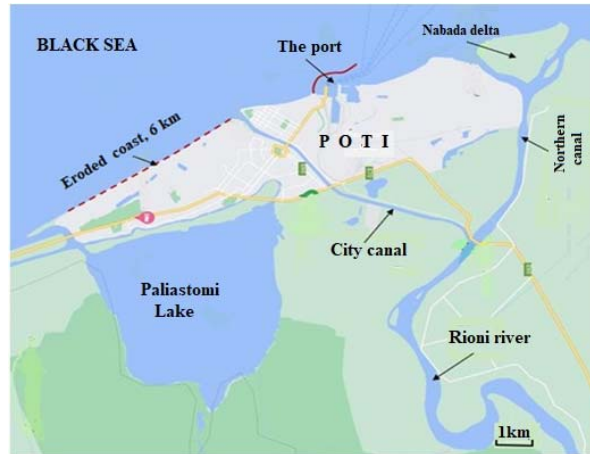


Figure 1. Scheme of the eroding coastline of Poti

2.1 The 1 km Long Coastline near the "City Canal"

In the 1 km strip adjacent to the estuary, when the Rioni flows in, a southward-directed coastal flow is generated, which carries solid sediment from this area. In addition, during southwesterly storms, the northward along-shore currents bring solid sediment into the mouth of the "City Canal", which then flows into the open sea, and this sediment is lost to the area. To prevent loss of sediment, geo-tubes filled with sand about 100 meters long should be arranged on this section of the bank (Figure 5).

In order for the bank protection scheme developed by us to work successfully, it is necessary to partially fill the sediment deficit and add additional sediment to the 1 km strip adjacent to the channel. For this, it is necessary to clean the canal bed. The extracted material will be dumped in a 1 km strip adjacent, which will be further processed and distributed by the waves.

We have developed an optimal scheme for cleaning the "City Canal", the essence of which is as follows: the cleaning should be carried out gradually over a period of five years through a suction device. 200,000 m³ of material removed annually will be dumped on the bank through a pipeline along the river bank.

2.2 The 5 km Long Coastline

In order to protect this part of the shore from erosion, we will use the method of placing multiple submerged breakwaters (SBW) parallel to the shore. Will be used geotextile pipes (geotubes) filled with sand as SBW. The use of submerged geotubes is justified both economically and ecologically (Alvarez et al. 2006).

The main geometric parameters of submerged geotube placement are: length of the geotube L_b , width - w_b , height - d , its distance from the shore x_b , distance between - L_g , and depth of geotube crest under water - a . For Poti coastline, it is convenient to place geotubes $x_b = 100; 180m$, from the shore, where the water depth is $H_b = 2; 3m$. Below are conducted the following studies for these parameters. has been taken the geotube placement parameters: $a = 0.5; 0.7 m$, $L_b = 120m, 150m$; $L_g = 60; 120; 180, 240m$.

The morphological equilibrium profile of the shore is calculated by the formula (Dean 1977):

$$h(x) = A \cdot x^{\frac{2}{3}}, A = 0.21D_{50}^{0.48} (D_{50} = 0.2mm). \quad (1)$$

In numerical calculations, we take the wave height in deep water $H_i = 1.3; 1.8m$ and the period $T_p = 9s$. The wave height in the coastline is proportional to the water depth $H = \gamma h$. in the coastline of Poti $\gamma = 0.73$ (Gagoshidze et al. 2017).

2.3 A Graphical Criterion for the Shoreline Response to Multiple SBW

The contribution of the variation of the lateral confinement ratio $m = \frac{L_g}{L_b}$ can be analyzed using the cumulative sediment displacement values in the lee of the SBW. The different degree in wave sheltering

is shown to be dependent on the relative wave height ($\frac{h_b}{H_i}$) with h_b being the depth at the location of the breakwater). Based on these relations the following equation can be derived for the location of a data point on the x - axis (Ranasinghe et al. 2010, Villani et al 2012):

$$x = \left(\frac{a}{h_b}\right)^{\frac{3}{2}} \left(\frac{L_b}{h_b}\right)^2 \left(\frac{A^3}{h_b}\right)^{\frac{1}{2}} \left[1,22 \left(\frac{L_g}{L_b}\right)^2 - 3,67 \left(\frac{L_g}{L_b}\right) + 3,22i \left(\frac{h_g}{H_i}\right)^2\right], \quad y = \frac{h_b}{H_i} \quad (2)$$

Where $i = 0.36$, H_i is the wave height at SBW, $\frac{h_b}{H_i} \geq 1.25$ and $0.25 \leq \frac{L_g}{L_b} \leq 2.5$.

The functional dependence determining the shore reaction between the system parameters is expressed by the formula (Ranasinghe et al. 2010):

$$y = 2 \log_{10} x + 0.65. \quad (3)$$

The graph of the function (1) in a semi-logarithmic scale is a line. If the points calculated for the values of the system parameters are placed on the graph to the left of the line, then the reaction of the bank is accumulative, and on the right-erosive. The results of the numerical experiments conducted are in Figure 2.

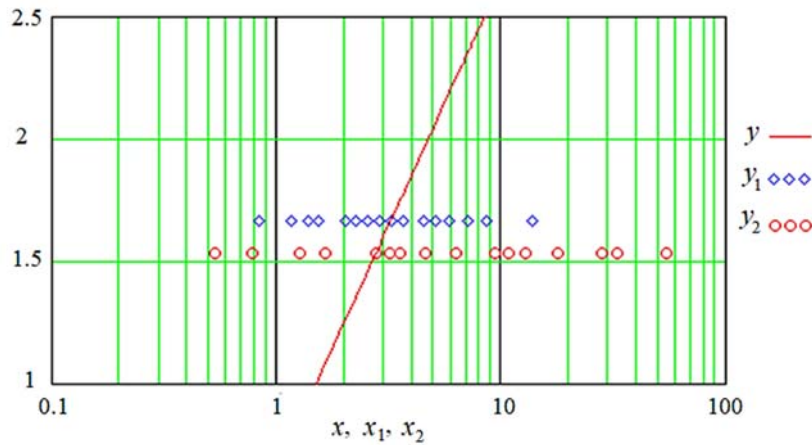


Figure 2. Determination of the morphological change of the shore graphical criteria
Shoreline response to all geotubes ratios

In Figure 2 Calculations are performed for two values of x_1 : $x_b = 180m, h_b = 3m, x_2$: $x_b = 100m, h_b = 2m$, 16 points are calculated for each parameter.

2.4 An Analytical Criterion Shoreline Response to Multiple SBW

After the placement of underwater tubes on the shore morphological change is calculated by the criteria (Bellotti. 2007; Villani et al. 2012):

$$r = \frac{\eta + \eta_b}{\eta_g} \quad (4)$$

In equation (3) η - is the rise of the water level after the transfer of water the through a geotube; η_b - the rise of the water level during the breaking of a new wave at the shore; η_g - There is a rise in the water level after the undisturbed passage of the waves between the breakwaters and breaking on the shore. The rise of the water level during the breaking of waves near the shore η_b and η_g is calculated by the following formulas (Saghinadze and Gamezardashvili. 2018)

$$\eta_{b,g} = \frac{3\gamma_{b,g}^2}{8+3\gamma_{b,g}^2} \cdot h_{b,g}, \quad (\gamma_g = 0.63; \gamma_b = 0.68) \quad (5)$$

It is known that $r > 1$ after waves pass over the geotube, 2-cell circulations of currents occur, and the shore is eroded. When $r < 1$ waves pass over the geotube, 4-cell circulations of currents occur, and the shore is accumulative (Bellotti (2007).

$$\frac{q_1^2}{g(h_2 + \eta)} - \frac{q_1^2}{h_1 \cdot g} + \mu B \frac{q_1}{g} + \eta a + \frac{\eta^2}{2} + C = 0 \quad (6)$$

$$q_1 = u_1 h_1 = C_1 \sqrt{2g\eta} \cdot h_g \cdot \frac{L_g}{L_b}, \quad (7)$$

where $\mu = f_w \frac{\gamma\sqrt{g}}{\pi}$, $\gamma = \frac{H_i}{h_b}$, $B = \int_0^{w_b} \frac{dx}{\sqrt{h(x)}}$, $f_w \approx 0.16$, $C_1 = 0.54$, $C = \beta_2 H_t^2 - \beta_1 H_0^2$, $\beta = \frac{1}{8} \left(\frac{1}{2} + \frac{2kh}{\sin 2kh} \right) + \frac{0.9kh}{2\pi}$, $k = \frac{2\pi}{L}$ wave number, L – wavelength; $H_t = K_t \cdot H_i$, where K_t is the wave transmission coefficient, which is determined by the formula (Pilarczyk and Zeidler.1996; Zanuttigh et al. 2008):

$$K_t = 0.4 \frac{a}{H_t} + 0.8 \cdot \left(\frac{w_b}{H_i} \right)^{-0.31} \cdot (1 - e^{-0.5\zeta}), \zeta = \frac{\alpha}{\sqrt{\frac{H_i}{L}}}, L = \frac{gT_p^2}{2\pi}, \alpha \approx 0.017. \quad (8)$$

The results of the obtained numerical solution of the system of equations (7)-(8) are given in Figure 4.

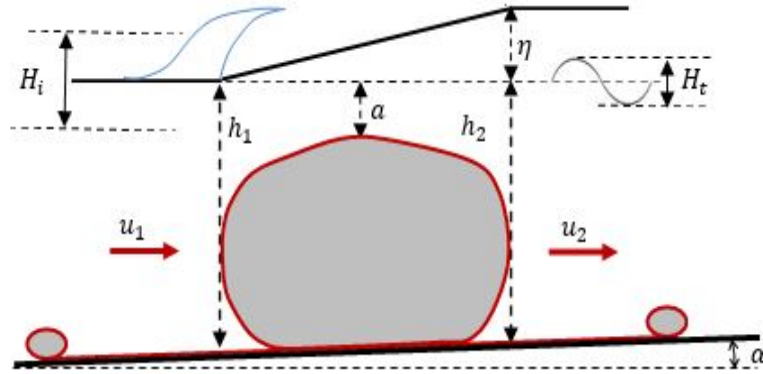


Figure 3. Cross section of submerged geotube

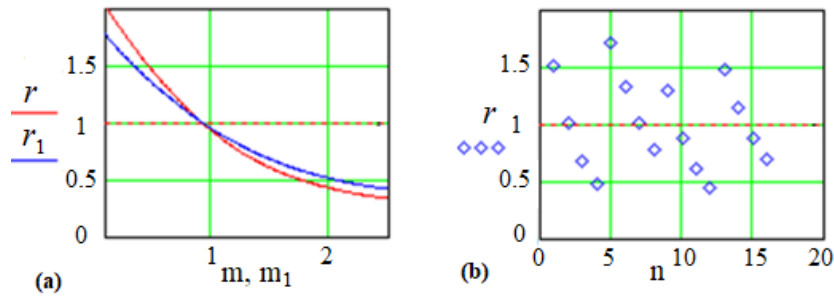


Figure 4. Dependence between the parameters of the shoreline response of the coast with the analytical criterion

Figure 4(a) is shown the relationship between the lateral confinements ratio m, m_1 and the shoreline response parameter r . The system parameters for r are: $x_b = 180\text{m}$, $h_b = 3\text{m}$, $H_i = 1,8\text{m}$. For r_1 : $x_b = 100\text{m}$, $h_b = 2\text{m}$, $H_i = 1.3\text{m}$. On Figure 4 (b) are the values of the shoreline response parameter r when ($n = 16$ is the number of points) $x_b = 180\text{m}$, $h_b = 3\text{m}$, $H_i = 1,8\text{m}$.

The results obtained for underwater geotubes are in complete agreement with the results obtained by the numerical model Delft3D for a similar coastline (Villani et al. 2012). To protect the remaining 5 km of the shore from erosion, we will use a submerged geotube (geotubes filled with sand) located parallel to the shore. Based on the calculations for the Poti coast, we choose the following values for the geotube placement parameters:

$$x_b = 180\text{m}, a = 0.5\text{m}, w_b = 5.1\text{m}, L_b = 120\text{m}, L_g = 180\text{m}.$$

For such values of the submerged geotube placement parameters, the 5 km long bank located to the south of the "city channel" will be cumulative. Based on the analysis of the obtained results, a scheme for the protection of the coastline south of the "City Canal" has been developed, which is shown in Figure 5.

3 CONCLUSIONS

Thus, during the 5 years of cleaning the “City Canal”, an additional 200,000 m³ of solid sediment will be deposited annually on the 1 km section of the adjacent bank, which will be distributed throughout the entire coastline through waves and coastal currents. As a result, erosion processes on the coast will decrease, and the shore will increase in a 1 km strip. After the cleaning of the river bed of the “City Canal”, the channel will cover the design rate and accordingly, the volume of introduced solid sediment will increase, which will have a positive effect on the morphological change of the bank. 5 years after the implementation of the proposed hydraulic measure, an 8 km long pulp pipeline with its intermediate pumps will be laid along the seashore and the Rioni “City Canal”. Then, if necessary, the pulp line can be extended by 1 km and the sediment removed in the main channel of the Rioni River in the lower basin of the watershed (Figure 1). In this part of the river, a large amount of beach-forming sediment is obtained, and if necessary, to protect the bank, this sediment can be moved to the shoreline with the existing system. In addition, if the “City Canal” becomes silted over time, the existing system can be used to clean it again. The geometric parameters of the underwater geotubes located in the 5 km long coastline are selected in such a way that after the waves pass over the geotubes, 4-cell circulations of currents occur between them and the shore. In this case, the morphological reaction of the coast is accumulative. In addition, due to the deposition of sediment, the coastline will receive additional nutrition and will be protected from erosion (Figure 5).

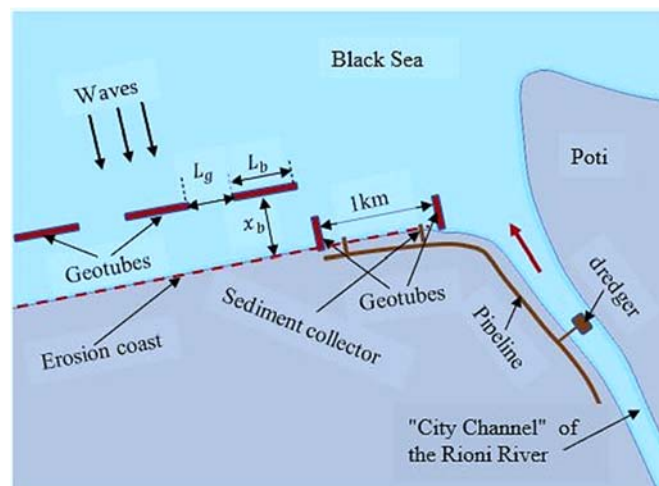


Figure 5. Erosion protection scheme of the coastline south of the “City Canal”

Acknowledgments

This research was supported by the Shota Rustaveli National Science Foundation (SRNSF) of Georgia (Grant number YS 21-108).

References

- Alvarez IE, Rubio R, Ricalde H (2007) Beach restoration with geotextile tubes as submerged breakwaters in Yucatan, Mexico. *Geotextiles and Geomembranes* 25: 233–241.
- Bellotti G (2007) An Improved Analytical Model for Estimating Water level set-up and currents induced by waves over submerged low crested coastal defense structures. *Proceedings of the 5th Coastal Structures International Conference*, p. 975-989 DOI: 10.1142/9789814282024_0086
- Gagoshidze Sh, Kodua M, Saghinadze I, Kadaria I (2017) River hydro construction and geomorphological processes of the Black Sea coast of Georgia. Technical University, Tbilisi.
- Dean RG (1977) *Equilibrium Beach Profiles: U.S. Atlantic and Gulf Coasts*. Ocean Engineering Technical Report. 12: 1-44.
- Pilarczyk W, Zeidler B (1996) *Offshore breakwaters and shore evolution control*, Balkema, Rotterdam.

- Ranasinghe R, Larson M, Savioli J. 2010. Shoreline response to a single shore-parallel submerged breakwater. *Coastal Engineering*. 57: 1006-1017.
- Saghinadze I, Gamezardashvili Z (2018) Calculation of the average change in water level during storm waves in the coastal zone of the Black Sea city of Poti. *Engineering news of Georgia*. 65(1):63-67.
- Saghinadze I, Kodua M (2019) A Mathematical Model of Sediment Transport of the Poti Coastal Zone. *J IJERT* 12: 3032-3037.
- Villani M, Bosboom J, Zijlema M, Marcel J, Stive F (2012) Circulation patterns and shoreline response induced by submerged breakwaters. *Coastal engineering*, 33:225-236.
- Zanuttigh B, Martinelli L, Lambert A (2008) Wave overtopping and piling-up at permeable low-crested structures. *Coastal Engineering*, 55: 484-498.

Historical evolution and impact of coastal structures on shoreline stability along the south coast of Cyprus

S. Demetriade^{1*}, D. Stagonas¹, S. Zervos² and G. Protopapas²

¹Department of Civil and Environmental Engineering, University of Cyprus, Nicosia, Kallipoleos, 1678, Cyprus

²Department of Coastal Unit, Public Works Department Cyprus, Nicosia, Strovolo, 165, Cyprus

*Corresponding author: sdemet04@ucy.ac.cy

Abstract

Coastal areas are dynamic environments vulnerable to anthropogenic influences and natural changes. This paper presents the historical evolution of a protected shoreline in the southern coast of Cyprus Island in the Mediterranean. Shoreline evolution was analyzed in the vicinity of coastal structures, including detached breakwaters and groins. Special attention was given to the accretion and erosional patterns prior and post construction, in identifying changes in shoreline position for two selected case studies. Shoreline positioning data and georeferenced photographs were utilized in understanding the site-specific impact of coastal structures on shoreline's stability. In the present study, coastal structures dictate, to some extent, in both cases the sedimentation process by affecting longshore sediment transport. Overall, significant accretional patterns were not observed when comparing the shorelines of 1970 and 2014 as a result of coastal defense construction. Analysis demonstrated that coastal defense structures were proven effective in attempting to battle erosional problems on one of the shorelines. However, analysis on the second area, revealed that the shoreline was advancing for a short period of time on the western side, and mainly eroding on the eastern side, with the overall performance of hard defenses proven ineffective in reducing erosion and stabilizing the coastline.

Keywords Hard engineering structures, Shoreline changes, Coastal erosion.

1 INTRODUCTION

Historically, coastal development was linked with commercial ports and defense installations, contributing to the development of major urban regions, whereas, elsewhere, coastal settlements were contributing towards fishing communities and vacation refuges (National Research Council 1990). Throughout the years, coastal areas have been the center of the communities' cultural, social and economic development, comprising some of the most productive ecosystems of the world. Due to their high ecosystem services, they are nowadays some of the most heavily degraded habitats, facing the negative effects from anthropogenic pressures and climate change. In the past 50 years, 90% of the coastal environment has suffered alterations due to anthropogenic pressures, leaving intact only 10% of the original habitats (Pasquali and Marucci 2021). The increase of urbanization in coastal areas along with the combination of natural phenomena, such as storm surges, have been the main factors for modifications in coastal dynamics. Problems amplify due to the continues human intervention, leading to changes in sediment supply, limiting their ability to reach and nourish coastal areas (Bird 1996).

Due to the dynamic coastal environment, and the erosional problem that most of the coastlines are facing, attempts in battling erosion and stabilizing the shoreline involved, in most cases, the construction of hard engineering structures. Shore-parallel structures such as detached breakwaters and shore-normal structures such as groins, can be used in stabilizing coastlines that are facing severe erosional problems, by blocking further long-shore sediment transport (Vaidya et al. 2015). It's important to note, however, that the presence of coastal structures induces morphological changes not only to the shoreline that they are present, but on adjacent shorelines as well. Blockage of sediments on the updrift site of the coastal structures reduces sediment availability for adjacent shorelines, causing erosional problems on the downdrift sides.

The present paper would aim to describe shoreline evolution and local morphodynamics for two case study areas in Limassol, southern Cyprus, as a result of the historical development of coastal defenses.

The following sections of this paper give the general and environmental setting of the study area, the methodology followed including data processing and conclude with the result findings and the discussion.

1.1 South Coast of Cyprus and Environmental Setting

Cyprus island is located in the northeastern section of the Levantine Basin, approximately 65km off Turkey's southern coast and 100 km west of Syria. The coastline and coastal areas of Cyprus, cover around 772.49 km, and they are entirely depended on local sediment supply from the mainland. Mountain rivers were responsible for alluvial sediment transport through river deltas. Minor sediment depositions from eroding sea cliffs and accumulation from decomposed organic material such as corals and shells contribute locally to shaping the coastlines (Nir 1993). The sediment contribution from rivers has decreased over time, mainly due to the major dam construction projects in Cyprus that started in 1980s (Omorphos and Ioannou 2000).

Regarding wave energy, the Mediterranean Sea is less energetic due its sheltered geographical setting (Mattiazzo 2019). The most frequent wave heights for southern Cyprus are in the range of 0.25 m to 1.25 m, prevailing from west and northwestern directions. The probability that wave heights exceed 1.75 m is 4% prevailing from southwestern and northwestern directions (255° – 285°). Generally, the predominant wave directions for Cyprus are from the west and northwestern, with some occurrences from southwest. The most frequent wave periods are in the range of 0 s to 5.5 s, reaching 7.5 s during winter season. The probability that wave periods are longer than 13.5 s is 0.2%. On the Southern Cypriot coast, longshore sediment transport is usually in an eastern-moving direction, as the incoming waves are approaching the coast from the western and northwestern directions (Loizidou and Dekker 1994).

2 MATERIALS AND METHODS

In characterizing erosional and accretional patterns prior and post constructional events, satellite derived shoreline (SDS) positions for the following years; 2003, 2008 and 2014 were extracted from satellite images by the Public Works Department (PWD) of Cyprus. Shorelines of 1963 and 1993 were extracted from aerial photographs, whereas shoreline position for 2003, 2008 and 2014 was estimated at mean sea level from satellite images. PWD data are covering a coastal stretch of 8.5km, starting from 34°40'44.26" N, 33°3'8.04" E to 34°42'32.9" N, 33°8'13.02" E. An additional satellite dataset with a position accuracy of <15 m between the SDS position and the in-situ shoreline, indicating shoreline position for 33 years (1984-2016) was extracted from Luijendijk et al. (2018) which overlaps the area covered by the PWD of Cyprus.

Shoreline data obtained from the PWD of Cyprus were imported and plotted in AutoCAD 2023 software, allowing for the visual comparison between different time periods and locations. From Luijendijk et al. (2018) data, shoreline change rates in m/yr at transects with an alongshore spacing of 500 m were derived for the shorelines of interest. The indicated change rates (m/yr) were obtained by fitting a line-of-best fit to the shoreline position data.

3 RESULTS AND DISCUSSION

Coastal defense structures have an important role in shaping shorelines and beaches as they actively influence wave dynamics by affecting their refraction and diffraction patterns, and sedimentary processes by impacting longshore and cross-shore sediment transport (Rosa-Santos et al. 2009). Most of the Cypriot coastline is heavily protected by various coastal defense structures including sea walls, groins and offshore parallel breakwaters. In southern Cyprus, specifically in Limassol, coastal defenses have important dimensions regarding their total coverage length, with a total of 51 breakwaters and 28 groins. In this analysis, particular focus was drawn in two case studies in Limassol, Southern Cyprus. Vathia beach area (Fig.2) presents the first case study in which shoreline evolution and beach shape was analyzed with respect to major construction phases. Construction in the greater area of Limassol

approximately began in 1986 aiming to battle erosional problems and extend the beachfront. Prior to that, from the analysis of aerial image datasets (Fig.1) in 1963 coastal development in the area was limited. SDS data collected for 1970 and 2014 are indicating a clear pattern of accretion for the sectional area located western of Π3 groin (Fig.2).



Figure 1. Aerial photograph of Vathia area (Study Area 1) and Germasogia area (Study Area 2) in 1963 and the catchment area of Vathias and Germasogia rivers, respectively (PWD, 2023)

been observed, in the shadow of the structure. In the coastline of 1970, three smaller groins were found, adjacent to Π4 groin, thus, it can be assumed that sedimentary material distributed in the area was previously trapped by the smaller groins, which gave rise to the accretion observed in the shadow of Π4 groin in the 2014 shoreline. The presence of six breakwaters in the 1989 directly in front of Vathia beach area, support this hypothesis when comparing the shoreline of 1970 and 1993 (Fig.2). Due to breakwaters' proximity to the shoreline, and to the three smaller groins that were present from 1970, it is believed that sedimentary material transported through longshore currents was indeed trapped in the area. Additionally, it is believed that the fast downdrift accumulation of sediments in this stage occurred not only due to natural reasons, but also due to construction factors. However, due to the limited hydrographic and bathymetric data for that period of time, this assumption is inconclusive and cannot be fully proven.

Further erosional problems in Vathia beach area, led to two nourishment events in the 1996 and 1997, easternly of Π4 groin. Port deepening activities in the 1993, performed by the PWD of Cyprus, led to the extraction of fine sands, and to the total placement of 3646 m³ of artificial material over the two consecutive years. Observations from the PWD of Cyprus concluded that the two nourishment interventions were not as successful as it was hoped. SDS data of Transect C, located approximately 500 m easternly from the nourished side, are indicating minor erosion for the years of 1998-2000, thus reassuring observations made by the PWD. The choice of nourishing the beachfront of Vathia area with fine sands could potentially be the reason why its stabilization was unsuccessful when taking into consideration that Limassol's coastline is composed of coarse gravel and sands (Nir 1993). In 2003, three additional breakwaters were constructed (Fig.2; 11-14), with the eastern breakwater constructed first. After breakwater construction the sand started to accumulate on both sides of Π3 and Π4 groins, with the updrift and downdrift sides extending 28 cm and 12 cm, respectively, seaward when comparing the shoreline data of 2003 and 2008. SDS data of Transects A and B located westerly of Π3 groin and Transect C located easternly of Π4 groin are found in agreement with the PWD data, as all transects are indicating a clear pattern of accretion from 2003, breakwaters' construction year, until 2016.

This finding was expected when taking into consideration that the accreted area, covering approximately an area of 500 m, is in the upstream side of the structure. Previous calculations on the sediment transport rates in Limassol (Delft Hydraulics, 1996) resulted in the estimation of approximately 21,000 m³/year of sandy material being transported by longshore currents in an eastern moving direction. Accretional patterns observed western of Π3 groin were found in agreement with indicated change rates of Transects A and B, which demonstrated an overall accretional behaviour in the magnitude of 0.6 ± 0.1 m/yr and 0.5 ± 0.2 m/yr, respectively, for 1984-2016.

The area located easternly of Π4 groin, representing the downdrift side, minor erosional patterns have been observed when the shoreline position of 2008 was compared with the one of 2014. Contradicting this, directly adjacent to Π4 groin, significant accretion has



Figure 2. Satellite derived shoreline for Vathia area in Limassol, southern Cyprus with shoreline positions over time indicated with different colors. Transect locations, A, B and C are indicated with white dashed lines (left to right) demonstrating a behaviour of 0.6 ± 0.1 , 0.5 ± 0.2 and 0.2 ± 0.01 m/yr, respectively

upstream direction, from Germasogia beach. Construction of the reservoir in the 1968 was one of the major water projects for Cyprus with its water capacity reaching 13.5 million m^3 (Socratous et al. 2001). Construction of such a major project undoubtedly led to the depletion of fluvial sediment reaching the downstream coast, resulting in beach erosion, and giving rise to the construction of a series of coastal defenses in the 1975.

Construction of the majority of groins was completed by the early 1980s, aiming to minimize erosion and protect the seafront. Supplementary SDS data for the area is demonstrating a fast erosional trend from 1984 to 1993. This can also be observed from shoreline positions, when comparing SDS of 1993 with 2003, extracted from the PWD of Cyprus, proving that groin construction was found unsuccessful in stabilizing the shoreline. By 2004, the majority of groins were dismantled completely, whereas Π9, Π13 and Π15 – Π17 were reconstructed to a different length. Additionally, in 2004, six breakwaters (Fig.3; 20-24α) were constructed by the PWD of Cyprus. Breakwater construction seemed to have a positive impact in aiming to stabilize the yearly erosional rates for the western side of the area from 2004 until 2008. However, when analyzing the eastern coast of Germasogia, the opposite trend was observed, where yearly erosional rates post construction, have been intensified. This trend is also visible when observing SDS of 2003, 2008 and 2014 (Fig.3) with the eastern side demonstrating a small overall accreting trend whereas the western side is showing an overall eroding trend.



Figure 3 Satellite derived shoreline for Germasogia area in Limassol, southern Cyprus with shoreline positions over time indicated with different colors. Transect locations, E, F and G are indicated with white dashed lines (left to right) demonstrating a behaviour of -0.3 ± 0.1 , -2.1 ± 0.2 and -2.0 ± 0.3 m/yr, respectively

4 CONCLUSIONS

In this paper, the historical effects of different types of coastal defenses on the shoreline were studied for two locations along the south coast of Cyprus island. For the southern coast of Cyprus, specifically for Limassol, hard defenses have important dimensions regarding their overall coverage length, with a total of 51 breakwaters and 28 groins established in a coastline of 8 km length. For the two case studies multiple groins, normal to the shore and breakwaters, parallel to the shore are established. The demonstrated effects of groins' construction were found more severe in comparison with breakwaters' construction as they appear to heavily interfere with alongshore sediment transport carried by drift currents. This interference was very clear when observing Vathia and Germasogia study sites, where groins in the upstream section, Vathia area, are believed to have blocked alongshore sediment transport by currents, thus, further impacting the downstream coastal section. The effects of groin construction were worsened when taking into consideration that sediment flow regimes were disrupted as a result of the major dam construction projects in Cyprus that started in 1980s. Due to the nature of the Cypriot coastline, heavily depended on local sediment supply from the mainland, hard defenses were only able to minimize erosion on small shoreline stretches in their updrift site, however, not stabilize them. Accumulation of sediments on the downdrift site of current defenses is believed to be due to the presence of previous structures, trapping sediments in the area that were then redistributed as a result of defense demolition and reconstruction. Overall, the presence of coastal structures in Vathia beach area were proven effective in attempting to battle erosional problems, with the shoreline from 1970 to 2014 showing a general accreting behavior with minor erosional patterns. However, analysis presented for Germasogia beach area, located in the downstream direction of Vathia beach area, revealed that the shoreline was advancing for a short period of time on the western side, and mainly eroding on the eastern side. Observations and conclusions drawn from this study provide an insightful base for the implementation of numerical modeling in understanding and foreseeing future morphodynamic responses under different climate change scenarios. Forecasting shoreline responses under different climatic scenarios would advance knowledge on the effectiveness of the currently established coastal defenses in protecting and stabilizing the shorelines against undesired future erosional events.

References

- Bird EC (1996) Beach Management. John Wiley and Sons Limited. Hoboken, NJ, USA, Volume 5
- Delft Hydraulics (1996) Coastal Zone Management for Cyprus – Unified Report. PWD, Cyprus
- Loizidou X, Dekker J (1994) Coastal Zone Management for Cyprus – Nearshore Wave Climate Analysis. Public Works Department Cyprus
- Luijendijk A, Hagenaars G, Ranasinghe R, et al (2018) The State of the World's Beaches. Scientific Reports, 8(1)
- Mattiazzo G (2019) State of the Art and Perspectives of Wave Energy in the Mediterranean Sea: Backstage of ISWEC. *Frontiers in energy Research*, 7
- National Research Council (1990) Managing Coastal Erosion. Washington, DC: The National Academies Press
- Nir Y (1993) The Coast of Cyprus. Geological Survey Department Ministry of Agriculture, Natural Resources and Environment Department, Cyprus
- Omorphos Ch, Ioannou E (2000) Southern Conveyor Project. Ministry of Agriculture, Natural Resources and Environment. Water Development Department, Cyprus
- Pasquali D, Marucci A (2012) The effects of urban and economic development on coastal zone management. *Sustainability*
- Public Works Department (2023) Aerial photograph of Limassol's Coastline in 1963. Public Works Department, Cyprus
- Rosa-Santos P, Veloso-Gomes F, Taveira-Pinto F, et al (2009) Evolution of Coastal Works in Portugal and their Interference with Local Morphodynamics. *Journal of Coastal Research*, 56, 757-761
- Socratous G, Omorphos C, Ioannou E (2001) Dams of Cyprus. Ministry of Agriculture, Natural Resources and Environment. Water Development Department, Cyprus
- Vaidya AM, Santosh KK, Kudale MD (2015) Shoreline response to coastal structures. *Aquatic Procedia*, 4, 333-340

Evolution and trends of coastal erosion along the Nestos River delta

K. Zachopoulos¹, N. Kokkos¹, G. Sylaios^{1*}

¹ Democritus University of Thrace, Department of Environmental Engineering, Vas. Sofias 12, 67100 Xanthi, Greece

*Corresponding author: gsylaios@env.duth.gr

Abstract

Coastal zones are facing intensified natural and anthropogenic disturbances resulting in coastal erosion. The shoreline changes are directly related to waves, tides, winds, storms, extreme events, sea level change, and human activities affecting the geomorphologic processes of the coast. Climate change, expressed as the more intense and frequent storm occurrences may exacerbate coastal erosion. Coastal zone monitoring involves satellite-borne shoreline extraction and detection of change rates over time. The shoreline evolution along the study site of the Nestos River Delta, in the North Aegean Sea, was assessed by analysing historic satellite images, covering the area during the latest three decades (1985 - 2020). The standard methodology was applied in four steps: a) the creation of a data list with all satellites and satellite images available, referring to the coastal area of interest, b) the historic shoreline extraction from the relevant satellite images, c) the evaluation of the shoreline movement throughout the study period, and d) the offshore and nearshore wave analysis (extreme wave events, incident wave energy, longshore sediment transport, etc.), using data from the Copernicus Marine Environmental Monitoring Service (CMEMS) reanalysis products.

Keywords Coastal processes; Shoreline evolution; Satellite image classification; incident wave energy.

1 INTRODUCTION

The coastal zone is a dynamic geomorphologic system in which multiple changes occur at diverse temporal and spatial scales (Mills et al., 2005), mostly affecting the shoreline position response through erosion/deposition actions. Factors of natural (such as incident waves, tides, storms, tectonic processes, and sediment loads through the hydrologic network) and anthropogenic origin (such as mismanagement of coastal structures, dredging activities, dam construction upstream a river) are responsible for the coastal erosion. In parallel, climate change is expected to exert further pressure on coastlines due to the Sea Level Rise (SLR) effect and the increase in storminess (Zhang et al., 2004). Coastal authorities are faced with the increasingly complex task of balancing development and managing coastal vulnerabilities and risks. In that sense, the Integrated Coastal Zone Management (ICZM) provides a framework to resolve conflicts, mitigate the impacts of short-/long-term uses, and support strategies for sustainable coastal management (Anfuso et al., 2011).

The methodology used to assess coastal erosion is based on the processing and analysis of historical satellite images, as well as on the analysis of historic wave data time-series. This methodology entails the procedure of shoreline delineation using a semi-automatic image classification technique. All historic shorelines were extracted by processing satellite images from the Sentinel 2 satellite sensor. Image selection was based on the correct geo-reference and image clarity, i.e., minimal cloud cover. Then, the pixels of each satellite image were classified in two classes: land and water, and the historic shorelines were extracted. The evaluation of the shoreline evolution was performed using the Digital Shoreline Analysis System (DSAS), provided by the United States Geological Survey (USGS), capable to produce auto-generated transects. The methodology was validated using a GeoEye-1 satellite imagery having very high spatial resolution (0.46 m in panchromatic). In parallel, using a series of algorithms, data from existing oceanographic databases describing coastal currents and waves were retrieved from external platforms and systems (e.g., from CMEMS). These data were further analyzed to assess extreme waves (e.g., POT) and to apply a simple Ray Wave Model from the open sea to the nearshore zone computing all wave characteristics at the wave breaker and estimating the wave-induced nearshore current and the theoretical wave-induced sediment transport.

2 METHODOLOGY

2.1 Study area

The study area includes both shorelines of the Nestos River Delta. The Nestos River is a transboundary river that springs in the Rila Mountains in central Bulgaria, flows through Bulgarian territory, enters Greece, and discharges into the Thracian Sea in Northern Greece (24°48'14.54"E, 40°50'48.80"N). Long sandy beaches and a complex lagoon system define the area. More specifically, the study area's coastline is interrupted by several irrigation channels and numerous streams that outflow to the open sea. Furthermore, the runoff from the Nestos River transport fresh water and suspended sediments to the coastal zone. The coastal area is vulnerable to extreme storms, which have become more frequent and intense in recent decades, as a consequence of climate change. The entire coastal zone is characterized by intense erosion due to the operation of three hydroelectric and irrigation dams along the course of the Nestos River. Their construction began in the early 1960s, and they were completed by the end of 1996, resulting in a gradual disturbance in the erosion–deposition balance, especially in the vicinity of the deltaic zone (Sylaios et al., 2012). Andredaki et al. (2008) estimated a sediment supply reduction of 84 %, in relation to historic sediment yields at the deltaic zone, due to the Nestos River damming. Nestos River presently supplies the coastal zone with fresh water, having a total annual runoff ranging between 600×10^6 and 800×10^6 m³, with limited seasonal variability (Sylaios et al., 2012). Plume water shows a limited hydrographic signature in the form of local, shallow, freshwater lenses covering the first surface meter of the water column throughout the year (Kamidis et al., 2011).

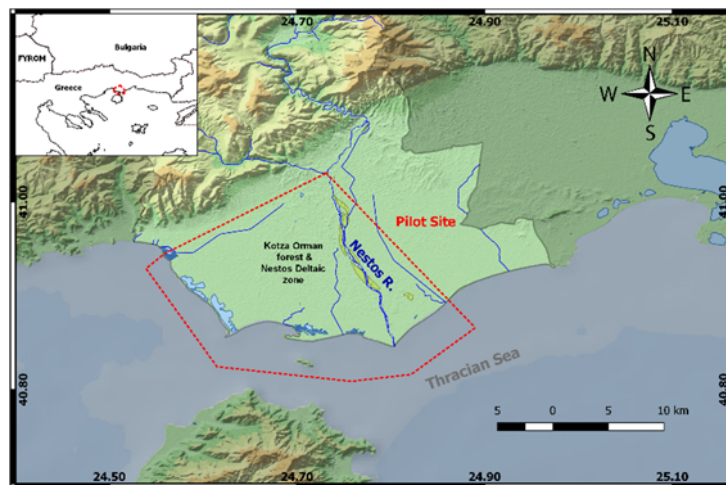


Figure 4 Map of Study area

2.2 Wave data analysis

Offshore wave time-series data retrieved from the CMEMS reanalysis product at sixteen points along the coastline (at hourly time-step), covering the period 2015-2019. For the period 2019-2020 the forecast product of CMEMS was used. The retrieved parameters were the following: the spectral significant wave height (H_{m0}), the zero up-crossing wave period (T_{M10}), and the wave propagation direction, relative to the North (ϕ_0). These data were imported into a simple ray model, as open sea significant wave height (H_o), wave period (T), and open sea direction (ϕ_o), to transform the offshore wave characteristics into the wave characteristics at the nearshore and at the breaker zone. All parameters were produced following the equations described by the Coastal Engineering Manual (2008). Additionally, the Peaks Over Threshold analysis (POT) analysis was applied on the storm events recorded from 2014-2019. POT is a systematic way to analyze the distribution of the exceedances over a specified threshold and to estimate the probability of occurrence of extreme events. The method is based on the observation that the extreme tail of distribution often has a relatively standardized and straightforward form, regardless of the shape at the central parts of the distribution.

2.3 Satellite image selection extraction and validation

Satellite images were retrieved from various satellite imagery repositories, covering the period from the early 1980s to late 2020. All images were retrieved during the summer months (May to September) and in the same tidal phase (ebb tide phase) to minimize the error of the tidal effect. The shoreline movement analysis was carried out in two different periods, based on the spatial resolution of the examined satellite images: a) Five satellite images from Landsat 4-5 TM and one Landsat 8 OLI, covering almost 25-year time period (from 1985 to 2015), were retrieved from the Earth Explorer database, provided by the United States Geological Survey Global Visualizer (USGS - <https://earthexplorer.usgs.gov/>), and b) six satellite images from Sentinel 2 sensor, covering 5 years (from 2015 to 2020), were retrieved from the Copernicus Open Access Hub, provided by Copernicus and European Space Agency (<https://scihub.copernicus.eu/>).

Images were processed following the semi-automatic classification technique, allowing the identification of land and sea pixels in an image. The technique trains a Machine Learning model based on pixel's spectral signature. The Normalized Difference Water Index (NDWI), introduced by McFeeters (1996), was utilized for the classification process. As water bodies strongly absorb light in the visible to the infrared electromagnetic spectrum, NDWI uses green and near-infrared bands to highlight water bodies. NDWI was calculated, according to the McFeeters (1996) formula. The produced NDWI image was imported to the Semi-Automatic Classification Plugin (SCP) for QGIS (Congedo, 2016), and around 30 Regions of Interest (ROIs) were manually determined and used for training the algorithm. This process was repeated for each satellite image, and consequently, all historic shorelines were finally extracted. The validation of the semi-automatic classification method and the error assessment was estimated by comparing the shoreline polyline, extracted by the semi-automatic technique, with a very high-resolution satellite image Geo-Eye-1 (<0.5 m spatial resolution).

3 RESULTS

3.1 West Coast of Nestos River delta

The 2.5 km long western shoreline is changing dynamically over time. Approximately 0.054 km² has changed throughout the study period. Approximately 53% of the total land has been retreated (-0.049 km²) and 47% has been accumulated (0.005 km²), thus the area seems balanced in terms of sediment budget. Four main hotspots of erosion and accretion along the coastal zone are observed. The average shoreline change (SCE) is around 28.2 m, with an average Net Shoreline Movement (NSM) of around -29 m and an average erosion rate of around -2.0 m/year. Significant land loss is observed at the central-western coast of the study site (around -0.29 km² and erosion rate up to -13.0 m/year) and at the coastline near the western Nestos River mouth (approximately -0.29 km²). On the other hand, the area with the higher sediment accumulation lies to the western end of the study site (about 0.048 km² and accretion rate up to 5 m/year), while another accretion zone is located at the central-eastern part of the study site (around -0.014 km²).

Table 1 Erosion rates per study period, annual incident wave energy, annual longshore sediment transport and wave-induced longshore current at the western coastline of Nestos River Delta.

Period	Erosion (m/yr)	Annual incident wave energy (J m ⁻¹ s ⁻¹)	Annual Theoretical Sediment Longshore flux (m ³ /yr)	Wave Induced Longshore Current (m/s)
2020- 2019	0.6	153.82	758.56	0.395
2019-2018	-3.8	181.23	903.99	0.388
2018-2017	0.1	158.51	785.24	0.329
2017-2016	7.2	150.02	747.79	0.348
2016-2015	-4.8	158.48	782.09	0.347

The sediment influx is directly linked to the Nestos River discharge and the SPM concentration exported from the river mouth. At the western Nestos River delta, sediment moves from east to west, transporting

on average 795 m³/year, peaking at 904 m³/year in 2018-2019. The most energetic periods were 2018-2019 (incident wave energy equal to 181.23 J m⁻¹s⁻¹), leading to significant shoreline retreat (about -3.8 m/year). The sedimentation rates in that area are strongly affected by the river sediment flux. The ray wave model applied can only explain the longshore sediment transport (from east to west) and redistribution.

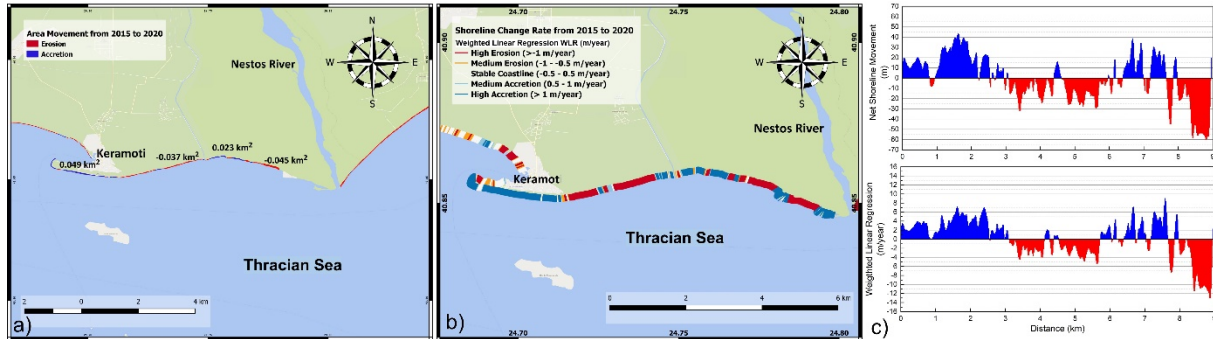


Figure 2 Shoreline evolution from 2015 to 2020. a) Map of coastal areal change, b) Map of the estimated annual shoreline change (WLR), and c) The estimated statistical parameters (NSM, and WLR) per transect along the Western Coast of Nestos River delta

3.2 East Coast of Nestos River delta

The eastern coastal zone consists of two erosion “hotspots”, and the sediment is transferred from the eroded regions to the regions with accretion. The average shoreline change (SCE) is around 19 m, the mean NSM is approximately 6.1 m and the average accretion rate reached 0.6 m/year. High erosion is observed in an extended area of about 7 km in length, extending from Nestos River mouth to Erasmio beach. In this area, high erosion rates (up to -18.8 m/year) are observed, and the shoreline retreated by up to -113.5 m. On the other hand, the central-east shoreline (around 9 km) shows significant sediment accumulation, with accretion rates of up to 6.2 m/year and maximum net shoreline movement of up to 31.5 m. The areas with the higher accretion rate are located at the eastern end of Erasmio beach (WLR: 1-2.6 m/year), at Maggana Beach (WLR: 1.5-6.2 m/year), and the western part of Myrtofyto beach (WLR: 1-5.0 m/year). Over these 5 years, approximately 0.159 km² of the coastal zone has been altered. Of this area, about 53% has retreated, representing -0.085 km² while 47% has accumulated (or 0.074 km²). Significant land loss is observed at the coastline between Nestos River mouth and Erasmio beach (around -0.12 km²). On the other hand, the area with the higher sediment accumulation is Maggana beach (about 0.048 km²) and the western part of Myrtofyto beach (around 0.022 km²).

Overall, the sediment transport in the study area appears strongly linked to the Nestos River discharge and SPM fluxes, as well as to the wave-induced longshore sediment transport. To the east of the Nestos River delta, sediment moves eastwards with mean sediment transport of approximately 240 m³/year. The maximum sediment transport has been estimated in the 2018-2019 period at about 383 m³/year. The most energetic periods are 2018-2019 (74.88 J m⁻¹s⁻¹) and 2016-2017 (65.24 J m⁻¹s⁻¹), resulting in increased shoreline movement. On the other hand, the low incident wave energy (3.8 J m⁻¹s⁻¹) in 2017-2018 resulted into negligible shoreline movement (almost zero erosion rate).

Table 2 Erosion rates and Ray-Wave model results for the West Coastline of Nestos River delta.

Period	Erosion (m/yr)	Annual incident wave energy (J m ⁻¹ s ⁻¹)	Annual	
			Theoretical Sediment Longshore flux (m ³ /yr)	Wave-Induced Longshore Current (m/s)
2020- 2019	-1.3	59.78	301.33	0.241
2019-2018	-4.4	74.88	382.75	0.228
2018-2017	0.0	3.08	18.77	0.166
2017-2016	7.5	65.24	332.56	0.205
2016-2015	-7.8	31.33	159.8	0.172

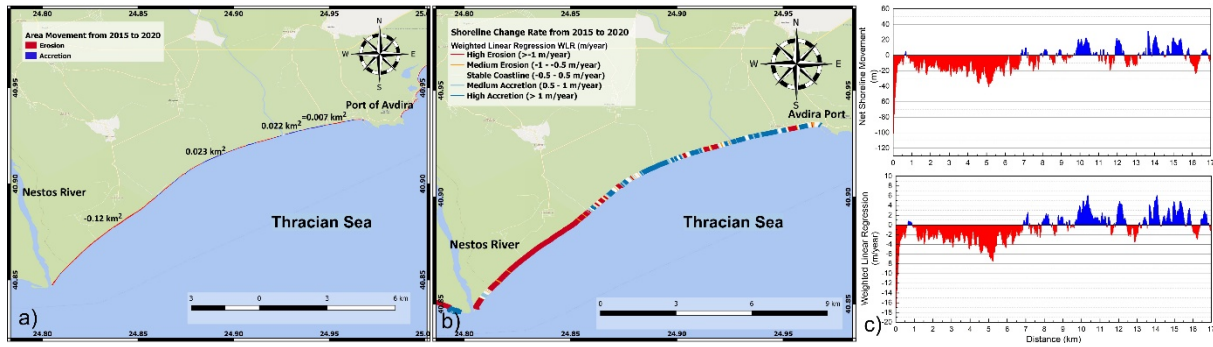


Figure 3 Shoreline evolution from 2015 to 2020. a) Map of coastal areal change, b) Map of the estimated annual shoreline change (WLR), and c) The estimated statistical parameters (NSM, and WLR) per transect along the Eastern Coast of the Nestos River delta

4 CONCLUSIONS

The assessment of shoreline change using satellite images reveals that the study area experienced high rates of erosion and accretion along the coastline during 2015 - 2020. The erosion in the study area is affected by the incident wave energy, the direction of wave propagation, and the sediment grain size. The higher erosion rates correspond to periods of increased incident wave energy from directions favoring the longshore sediment transport. The present study constitutes a successful effort to correlate the offshore wave data given from the Copernicus Marine Environmental system to coastal erosion rates produced by historic satellite images. An additional parameter that influences the coastal erosion in the entire study site is evident from 2015 and onwards. The constant low discharge rates in the Nestos River influence the sediment transport in the river estuaries, leading to coastal erosion events. Focusing on the areas of economic interest: a) the eastern side of Keramoti beach, and especially from the Keramoti Military Summer Camp until the drainage canal high erosion rates are reported ranging from -0.40 up to - 5 m/year. The shoreline retreats by up to -30 m. b) The Erasmio beach is divided into four sections according to its erosion activity. The higher shoreline retreat (up to -18 m) is presented at the central western part of the beach, showing a rate of up to -2.6 m/year.

References

- Andredaki M, Hrissanthou V, Kotsovinos N (2008) Calculation of sediment reduction at the outlet of Nestos River basin, due to the dams. IV Intern Symp Transb Water Manag, Thessaloniki, 15–18/10/2008, CD-ROM
- Anfuso G, Pranzini E, Vitale G. (2011) An integrated approach to coastal erosion problems in northern Tuscany (Italy): Littoral morphological evolution and cell distribution. *Geomorphology*, 129, 204-214. doi: <https://doi.org/10.1016/j.geomorph.2011.01.023>
- Congedo L (2016) Semi-Automatic Classification Plugin, available from: doi: 10.13140/RG.2.2.29474.02242/1
- Kamidis N, Sylaios GK, Tsihrintzis VA (2011) Modeling the Nestos River plume dynamics using ELCOM, *Desalination and Water Treatment*, 33:1-3, 22-35, doi: 10.5004/dwt.2011.2627
- McFeeters SK (1996) The use of the Normalized Difference Water Index (NDWI) in the delineation of open water features. *International Journal of Remote Sensing*, 17(7), 1425-1432. doi:10.1080/01431169608948714
- Mills MJ, Toon OB, Thomas GE (2005) Mesospheric sulfate aerosol layer. *Journal of Geophysical Research: Atmospheres*, 110(D24). doi: 10.1080/01431169608948714.
- Sylaios GK, Anastasiou S, Tsihrintzis VA (2012) Restoration of a seashore eroded due to dam operation through beach nourishment. *Ecology and Hydrobiology*, 12(2), 123–135. doi: <https://doi.org/10.2478/V10104-012-0010-6>
- Zhang K, Douglas BC, Leatherman SP (2004) Global warming and coastal erosion. *Climatic Change* 64, 41-58, doi: <https://doi.org/10.1023/B:CLIM.0000024690.32682.48>

Climate change impacts on the coastal zone of Alfios River estuary

M.K. Chondros^{1*}, A.S. Metallinos¹, A.G. Papadimitriou¹, V.K. Tsoukala¹

¹ Laboratory of Harbour Works, School of Civil Engineering, National Technical University of Athens, 15780, Zografou, Greece

*Corresponding author: michondros@mail.ntua.gr

Abstract

The present study investigates the impact of climate change on the nearshore wave and hydrodynamic fields, as well as on the erosion and accretion trends in the coastal area of Alfios River estuary in Pyrgos, Greece, which is a flood prone area due to its low-lying topography. Sea state data (offshore wave climate and sea water levels) are obtained from open databases both for the previous and for the coming decades. Numerical modelling is implemented to investigate the coastal processes for various climate change scenarios in comparison to the historical dataset. Based on the findings of the present study, the coastal zone of Pyrgos will become more vulnerable to erosion and coastal flooding events. The mean sea level rise in conjunction with the wave action will lead to alteration of coastal processes, regarding the observed erosion/accretion trends.

Keywords Climate change, sea level rise, coastal erosion, coastal flooding

1 INTRODUCTION

Several coastal areas are experiencing the adverse impacts of climate change, with sea level rise (IPCC, 2019), increased storm surges, and changes in wave patterns (Hemer et al., 2013), leading to coastal erosion and flooding. Retreat of the shoreline due to sea level rise, makes previously stable areas vulnerable to wave action. As waves continue to ride on the retreated shoreline, they can travel farther landwards, inundating low-lying areas and leading to coastal flooding. Furthermore, the increase in storm surges exacerbate the risk, leading to even higher water levels and causing significant damage to coastal areas. Therefore, numerous researchers have significantly contributed to the investigation of climate change impacts on coastal areas (Tsoukala et al., 2016, Garner et al., 2017). Nevertheless, most of the research is conducted on a regional or global scale, while this study focuses on a local scale, investigating the impacts on the coastal area of Alfios River estuary in Pyrgos, Greece, and in that sense is pioneering. The findings provide valuable insights into how climate change will affect the coastal study area and pave the way for developing advanced tools for mitigating the adverse impacts and ultimately protect the coastal community.

2 METHODOLOGY, DATA AND MODELS

2.1 Methodology

The methodology followed herein is based on the following steps. First, offshore wave characteristics and sea water level data are obtained from reliable open databases. These data are statistically analyzed to draw the first conclusions on the change of offshore wave patterns, due to climate change, up to year 2100. As a next step, the bathymetric grid is constructed based on data retrieved by nautical charts and field surveys and accounting for different mean sea water levels. Subsequently, the Initial Sedimentation and Erosion modelling concept (Chondros et al. 2022) is adopted to determine the sedimentation and erosion trends in the coastal study area. Particularly, sediment transport equivalent waves are determined in order to estimate the annually averaged sedimentation and erosion trends both for the current situation (based on past historical wave data) and for the coming decades (based on various climate change scenarios). Having defined the wave and sea level rise scenarios to be investigated, numerical simulations are performed. The selected wave scenarios are given as input to a numerical wave model for simulating wave propagation from offshore to nearshore and providing the nearshore wave field and the radiation stresses. The latter serve as input to a hydrodynamic model to simulate the wave generated

flow field and provide the current speed and direction. Next, simulation of sediment transport field is performed by implementing a sediment transport model for simulating the erosion and accretion areas by calculating the rate of bed level change in the entire coastal zone. Finally, an annual integration of the rate of bed level change results for all the considered scenarios is carried out to calculate the annually averaged rate of bed level changes, providing the erosion/accretion areas, for each considered period.

2.2 Past and future sea state data

2.2.1 Offshore wave climate

Historical and projected data incorporating the climate change impact, were extracted from the Copernicus Climate Data Store (cds.climate.copernicus.eu) and in particular from the product titled “Ocean surface wave time series for the European coast from 1976 to 2100 derived from climate projections”. Data were obtained for three different climate scenarios: the current climate, also termed historical, for the time period 1976-2015 and two Representative Concentration Pathway (RCP) scenarios that correspond to an optimistic emission scenario where emissions start declining beyond 2040 (RCP4.5) and a pessimistic scenario, where emissions continue to rise throughout the century (RCP8.5), both for the time period 2041-2100. This period is further broken down to 30-year periods, i.e., 2041-2070 and 2071-2100. Given the orientation of the shoreline and the wider geomorphology, the study area is exposed to waves coming from SSE, S, SSW, WSW, W and WNW sectors, and hence these sectors are investigated herein. The datasets were statistically analyzed to derive a mean annual offshore wave climate. The wave characteristics were grouped in 30-degree directional bins (i.e., 12 sectors) and in equally spaced wave height groups with a step of 0.5m. The wave rose diagram for the historical dataset is given in Figure 1, while the respective roses for RCP4.5 and RCP8.5 are given in Figure 2. In addition, the mean annual frequencies of occurrence per each wave height group are given in Table 1, for the considered datasets and for the most dominant sectors, i.e., the SSW, WSW and W.

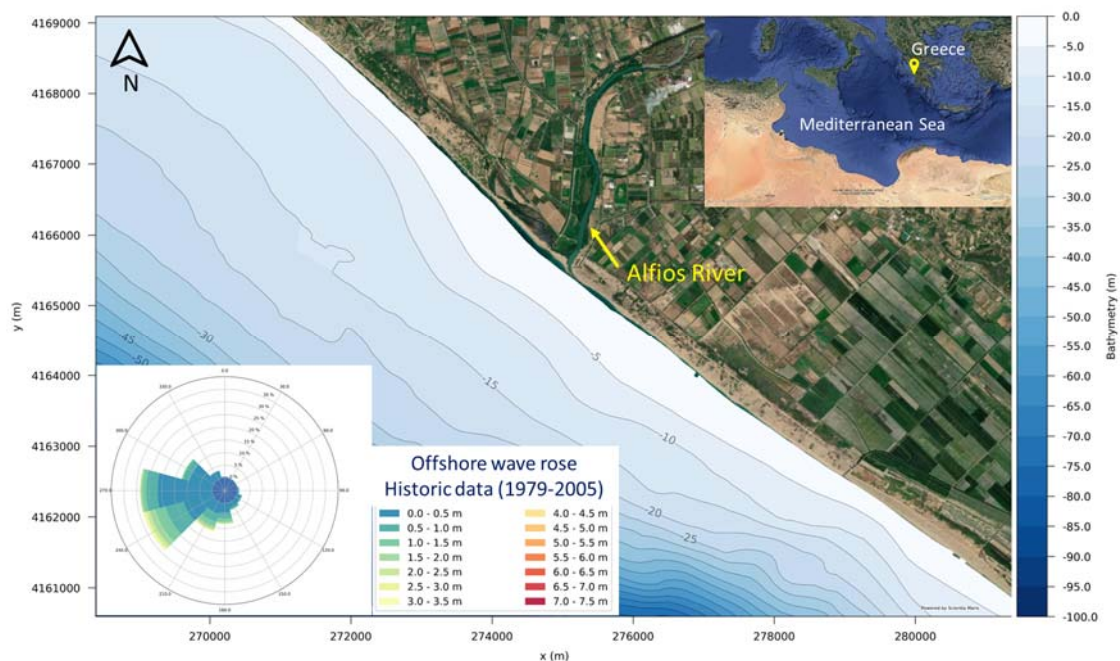


Figure 1. Bathymetry of the coastal area of Alfios River Estuary, Pyrgos, Greece. Upper right corner: Location of the study area in the Mediterranean Sea; Lower left corner: offshore wave rose diagram for 1976-2005

2.2.2 Sea water levels

Sea Level Rise (SLR) projection data were obtained from the National Aeronautics and Space Administration Sea Level Projection Tool (sealevel.nasa.gov) based on the Intergovernmental Panel on Climate Change 6th Assessment Report (IPCC, 2019). An average SLR of 0.25 m and 0.29 m is anticipated for the period of 2041-2070 for the SSP2-4.5 and SSP5-8.5 scenarios respectively, while an

average SLR of 0.46 m and 0.58 m is anticipated for the period of 2071-2100, and hence these values are considered herein.

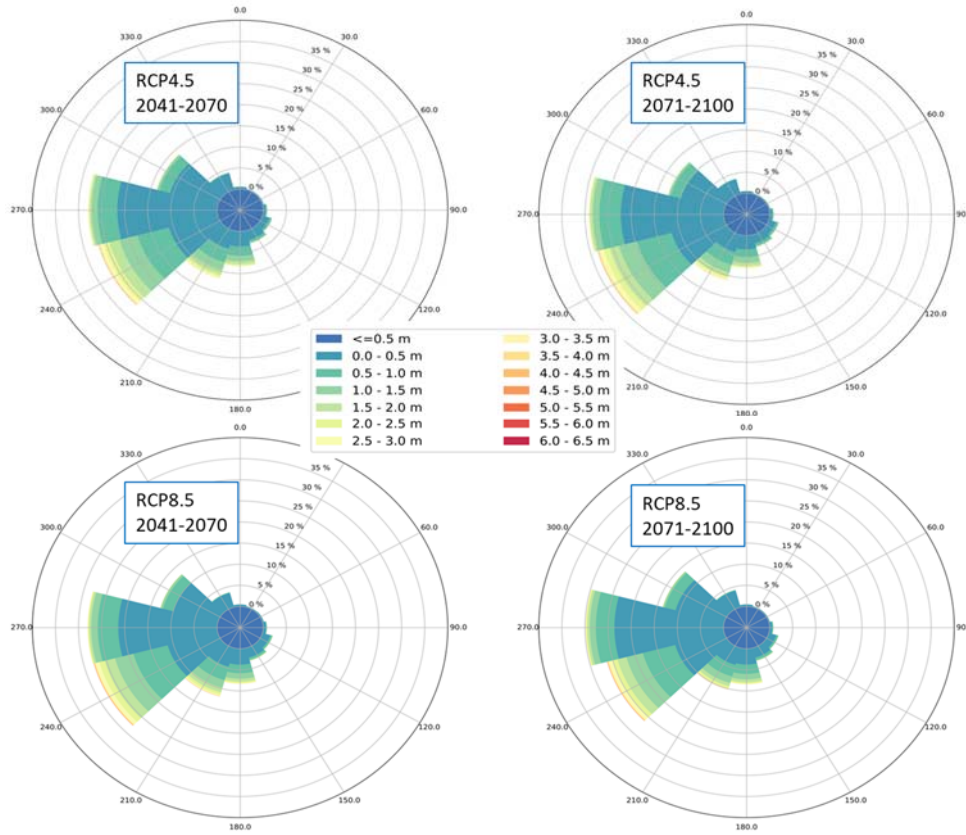


Figure 2. Offshore wave climate rose for RCP4.5 and RCP8.5, for periods 2041-2070 and 2071-2100

Table 1. Mean annual wave frequencies of occurrence per each wave height group and dominant sector

Wave Height (m)	Historic (1976-2005)			RCP4.5 (2041-2070)			RCP8.5 (2071-2100)		
	SSW	WSW	W	SSW	WSW	W	SSW	WSW	W
[0-0.5]	4.366%	11.764%	21.673%	4.444%	10.945%	21.630%	4.142%	10.988%	23.627%
(0.5-1]	3.333%	7.514%	4.518%	3.331%	7.078%	4.262%	2.826%	7.276%	4.019%
(1-1.5]	1.950%	4.185%	1.503%	1.947%	4.069%	1.268%	1.618%	3.689%	1.319%
(1.5-2]	1.057%	2.394%	0.580%	1.108%	2.254%	0.444%	0.796%	2.009%	0.541%
(2-2.5]	0.518%	1.292%	0.205%	0.552%	1.250%	0.183%	0.446%	1.035%	0.232%
(2.5-3]	0.255%	0.734%	0.089%	0.227%	0.612%	0.067%	0.202%	0.628%	0.084%
(3-3.5]	0.138%	0.333%	0.039%	0.084%	0.299%	0.029%	0.081%	0.364%	0.026%
(3.5-4]	0.074%	0.142%	0.006%	0.029%	0.115%	0.006%	0.038%	0.165%	0.014%
(4-4.5]	0.023%	0.063%	0.003%	0.008%	0.054%	0.002%	0.018%	0.063%	0.001%
(4.5-5]	0.010%	0.024%	0.003%	0.005%	0.034%	0.002%	0.012%	0.028%	0.001%
(5-5.5]	0.003%	0.013%	0.001%	0.002%	0.020%	-	0.003%	0.015%	0.000%
(5.5-6]	0.002%	0.004%	0.001%	0.002%	0.005%	-	0.000%	0.006%	0.000%
(6-6.5]	0.003%	0.001%	-	-	0.004%	-	-	0.006%	-
(6.5-7]	0.002%	-	-	-	-	-	-	0.002%	-
(7-7.5]	0.001%	-	-	-	-	-	-	-	-
(7.5-8]	0.002%	-	-	-	-	-	-	-	-
SUM	11.736%	28.462%	28.622%	11.738%	26.738%	27.893%	10.182%	26.274%	29.866%

2.3 Implemented numerical models

The suite of advanced numerical models (Scientia Maris, 2022) applied herein, includes the wave model Maris PMS, the hydrodynamic model Maris HYD, and the morphological model Maris SDT. The wave model is a nonlinear mild-slope irregular model of parabolic approximation (Chondros et al., 2021) capable of simulating accurately all the dominant phenomena in the coastal study area (i.e., shoaling, refraction, diffraction and energy loss due to depth-induced breaking and bottom friction). The hydrodynamic model is based on the well-known incompressible depth-averaged Reynolds Averaged Navier Stokes equations, simulating the wave-driven coastal currents and providing the surface elevation and the current velocity components (Chondros et al., 2022, Papadimitriou et al., 2022). Finally, the morphological model can simulate the non-cohesive sediment transport field and the subsequent bed evolution, based on the sediment mass balance or “Exner” equation, in coastal areas due to the combined effect of waves and currents (Papadimitriou et al., 2022).

3 NUMERICAL MODELLING RESULTS

The steps presented in the methodology were applied in the coastal zone of Alfios River estuary. The bathymetry was resolved with a constant spatial step of 5.0 m in both directions, totaling 2600 cells in the x direction and 1700 cells in the y direction, covering an area of approximately 13 km x 8.5 km. The bathymetry of the study area is showcased in Figure 1. The bed is comprised mostly of coarse sand material. A comparison between the annually averaged rates of bed level change, for the historical dataset, the RCP4.5 2041-2070, the RCP4.5 2071-2100 and the RCP8.5 2071-2100, obtained by assessing the impact of the 6 representatives (from each sector of interest) is showcased in Figure 4.

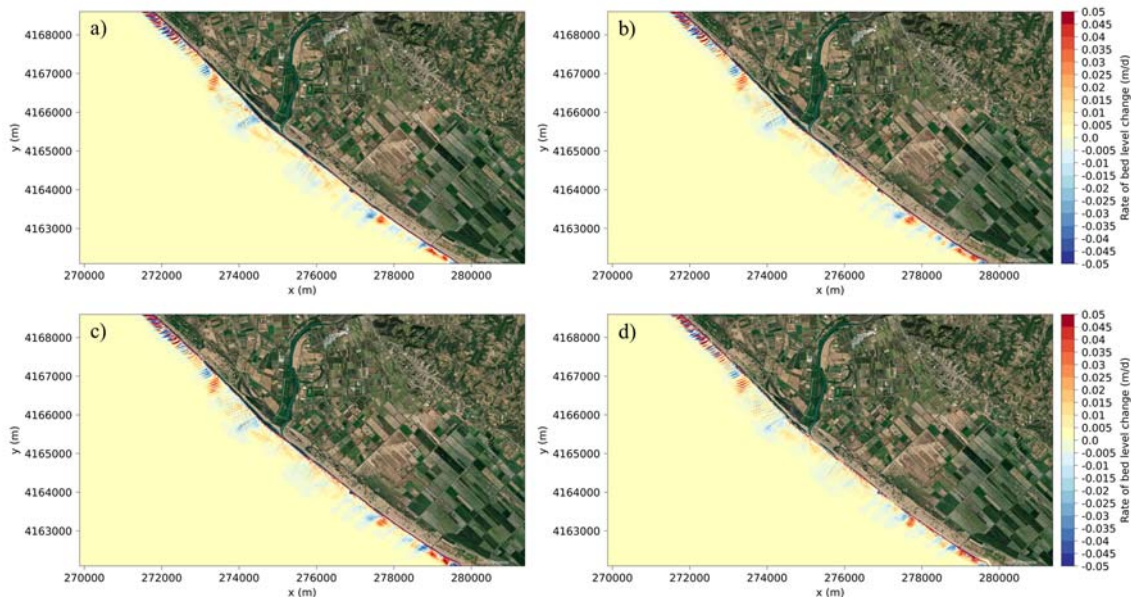


Figure 4. Annually averaged rates of bed level change for: a) Historical dataset; b) RCP4.5 2041-2070; c) RCP4.5 2071-2100; d) RCP8.5 2071-2100

4 DISCUSSION AND CONCLUSIONS

Based on the projected offshore wave climate it is observed that the cumulative frequencies of occurrence per each sector are comparable and of the same magnitude between the Historical, RCP4.5 and RCP8.5 datasets. Nevertheless, it is worth mentioning that in both RCP datasets a decrease in the maximum expected wave heights is observed. According to the historical dataset, wave heights occurred in the groups of (7-7.5] and (7.5-8], while for both RCP datasets the maximum wave heights remain lower than 7 m, up to 2100. Moreover, an alteration to the direction of the maximum wave heights is observed. Namely, the maximum wave heights, according to the historical dataset, are coming from the SSW sector, while for both RCP datasets the maximum wave heights are coming from the WSW sector. This is particularly interesting because waves coming from the SSW sector generate longshore currents

with direction from NW to SE (the shore normal points to 220° clockwise from the North, see Figure 1) while waves coming from WSW generate currents with the opposite direction, i.e., from SE to NW.

Based on the morphological results it can be deduced that, in general, alternating patterns of erosion and accretion are observed throughout the domain. It can be observed that the rates of bed level change are comparable and of the same magnitude between the Historical, RCP4.5 and RCP8.5 datasets. Nevertheless, it is worth mentioning that in all considered RCPs a wider zone of erosion/accretion trends is observed due to the retreated shoreline because of the SLR. Comparing rates of bed level change for RCP4.5 2041-2070 with the ones for RCP4.5 2071-2100 it can be deduced that no significant changes are observed. The comparison of rates for RCP8.5 for the similar period shows a slight increase in the intensity of erosion and accretion trends for 2071-2100 in comparison to 2041-2070.

In the light of the above-mentioned, it is understood that the major risk for the coastal area of Alfios River in the coming years is the rise of sea level. A mean water level shift of 0.60 m can lead to a horizontal shoreline retreat of approximately 20 m. Furthermore, storm surges will exacerbate the risk, leading to even higher water levels. This retreat will inevitably ease the way for the waves to runup and reach further inland, eroding the coast and inundating the coastal area.

Acknowledgements

This research is carried out in the context of the project “Adaptation to Climate Change Through the Development of an Early Warning System for Compound Coastal Flooding: Implementation in the Alfios River Estuary in the Coastal Zone of Municipality of Pyrgos, Greece - EWS_CoCoFlood” under the call for proposals “Physical Environment & Innovative Actions 2022 - Priority Axis 3 “Research and Application””. The project is financed by the Green Fund (3523 - 699/2022).

Furthermore, the authors wish to thank the National Cadastre of Greece for providing the valuable Digital Elevation Models of the study area and acknowledge the fruitful collaboration with the Municipality of Pyrgos.

References

- Chondros MK, Metallinos AS, Memos CD, Karambas TV, Papadimitriou AG (2021) Concerted Nonlinear Mild-Slope Wave Models for Enhanced Simulation of Coastal Processes. *Appl. Math. Model* 91, 508–529. doi.org/10.1016/j.apm.2020.08.027
- Chondros MK, Metallinos AS, Papadimitriou AG, Tsoukala VK (2022) Sediment Transport Equivalent Waves for Estimating Annually Averaged Sedimentation and Erosion Trends in Sandy Coastal Areas. *J. Mar. Sci. Eng.*, 10(11), 1726. doi.org/10.3390/jmse10111726
- Garner AJ, Mann ME, Emanuel KA, Kopp RE, Lin N, Alley RB, Horton B, DeContok RM, Donnellyl JP, Pollard D (2017) Impact of climate change on New York City's coastal flood hazard: Increasing flood heights from the preindustrial to 2300 CE. *Proc. Natl. Acad. Sci. U.S.A.* 114, 11861–11866. Doi 10.1073/pnas.1703568114
- Hemer MA, Fan Y, Mori N, Semedo A, Wang XL (2013) Projected changes in wave climate from a multi-model ensemble. *Nat. Clim. Change* 3, 471–476. doi 10.1038/nclimate1791
- IPCC (2019) Summary for Policymakers. In: IPCC Special Report on the Ocean and Cryosphere in a Changing Climate [H.-O. Pörtner, D.C. Roberts, V. Masson-Delmotte, P. Zhai, M. Tignor, E. Poloczanska, K. Mintenbeck, A. Alegría, M. Nicolai, A. Okem, J. Petzold, B. Rama, N.M. Weyer (eds.)]. Cambridge University Press, Cambridge, UK and New York, NY, USA, pp. 3–35. <https://doi.org/10.1017/9781009157964.001>
- Papadimitriou AG, Chondros MK, Metallinos AS, Tsoukala VK (2022) Accelerating Predictions of Morphological Bed Evolution by Combining Numerical Modelling and Artificial Neural Networks. *J. Mar. Sci. Eng.* 2022, 10(11), 1621. doi.org/10.3390/jmse10111621
- Scientia Maris (2022) Maris PMS, HYD, SDT User Guides, v02-2022
- Tsoukala VK, Chondros MK, Kapelonis ZG, Martzikos N, Lykou A, Belibassakis K, Makropoulos C (2016) An integrated wave modelling framework for extreme and rare events for climate change in coastal areas—The case of Rethymno, Crete. *Oceanologia* 58, 71–89. doi.org/10.1016/j.oceano.2016.01.00

Perched beach nourishment against coastal erosion and flooding: Experimental and numerical simulation

D. Spyrou¹, S. Christopoulos², Th. Karambas^{1*}

¹Department of Civil Engineering, Aristotle University of Thessaloniki, University Campus, 54124 Thessaloniki, Greece

²HYDROMARE, Consulting engineering company, 20 L.Sofou, 57001 Thermi, Thessaloniki, Greece

*Corresponding author: karambas@civil.auth.gr

Abstract

The paper illustrates the results of an experimental and numerical research, carried out to reproduce the cross-shore evolution of a perched beach nourished with sand. An extensive two-dimensional laboratory investigation was performed, in order to study the cross-shore profile evolution of a perched beach, after the application of beach nourishment method. The morphology evolution is also simulated by an improved version of the Boussinesq type nonlinear wave and sediment transport model.

Keywords Perched beach, Beach nourishment, Morphodynamic model.

1 INTRODUCTION

Beach nourishment combined with a submerged structure is a very common method against beach erosion and flooding. The response of the cross-shore hydro-morphodynamics depends on the interaction between the waves, the submerged reef, and the characteristics of the artificial beach. The reef dissipates and reflects the wave energy and obstruct the sand from drifting seawards (Gonzalez et al. 1999).

2 EXPERIMENTAL METHODOLOGY

The experiment has been conducted (in a 1:20 scale) in the Laboratory of the Department of Hydraulics and Environmental Engineering, Aristotle University of Thessaloniki, Greece. A sandy beach was formed in a 14.05 m long wave flume (Fig. 1). The flume was 0.40 m. wide. The slope of the surf-zone was set equal to 1:10. The water level was 0.28 m. A submerged structure, made of geotextile material, was placed one meter (towards the shore) from the point where bed slope (1:10) begins. The freeboard was 9 cm. A well sorted fine natural sand of $d_{50}=0.2$ mm is used in the experiments.



Figure 1. The experimental perched beach

Four wave periods were selected, $T = 1.00$ sec, $T = 1.25$ sec, $T = 1.54$ sec, $T = 2.00$ sec. The wave height was constant and equal to 0.1 m ($H = 0.1$ m) and 0.04 m ($H=0.04$ m). The beach fill slope was 1:2 and 1:4 respectively. The berm height of the beach fill was $B=0.05$ m.

3 NUMERICAL MODEL

Cross-shore morphology evolution of a nourishment project is simulated by an improved version of the Boussinesq nonlinear wave model described in Spyrou and Karambas (2021). The hydrodynamic model (wave and undertow model) provides to the sediment transport model all the required information (wave height, bottom velocity, wave energy dissipation, mean sea level).

The bed load transport (q_b) (including sheet flow sediment transport rate and suspended load over ripples) is estimated with a quasi-steady, semi-empirical formulation, developed by Camenen, and Larson (2007) for an oscillatory flow combined with a superimposed current:

$$\frac{q_b}{\sqrt{(s-1)gd_{50}^3}} = a_n \sqrt{\theta_{w,net}} \theta_{w,m} \exp\left(-b \frac{\theta_{cr}}{\theta_w}\right) \quad (1)$$

where $s (= \rho_s/\rho)$ is the relative density between sediment (ρ_s) and water (ρ), g the acceleration due to gravity, d_{50} the median grain size, a_w , a_n and b are empirical coefficients (Camenen and Larson 2007), $\theta_{w,m}$ and θ_w the mean and maximum Shields parameters due to wave, and θ_{cr} the critical Shields parameter for the inception of transport. The net Shields parameter $\theta_{w,net}$ is given by:

$$\theta_{w,net} = (1 - a_{pl,b}) \theta_{w,on} - (1 + a_{pl,b}) \theta_{w,off} \quad (2)$$

where $\theta_{w,on}$ and $\theta_{w,off}$ are the mean values of the instantaneous Shields parameter over the two half periods T_{wc} and T_{wt} ($T_w = T_{wc} + T_{wt}$, in which T_w is the wave period and $a_{pl,b}$ a coefficient for the phase-lag effects (Camenen and Larson, 2007).

Phase-lag effects in the sheet flow layer were included through a coefficient proposed by Camenen and Larson (2007)

In order to incorporate the suspended sediment transport rate, the depth-integrated transport equation for suspended sediment is solved. Here we adopt the transport equation proposed by Kobayashi and Tega (2002):

$$\frac{\partial(hC)}{\partial t} + \frac{\partial(hCU_s)}{\partial x} = S - w_s C / \beta_d \quad (3)$$

where C is the depth-averaged volumetric sediment concentration, U_s is the horizontal sediment velocity, S is the upward sediment suspension rate from the bottom and w_s is the sediment fall velocity. The horizontal sediment velocity U_s is assumed to be given by $U_s = (U - w_s)$.

The suspension rate S per unit horizontal area is related to the wave energy dissipation (Camenen and Larson 2007) $S = c_R w_s$, where c_R is the reference concentration at the bottom.

The bed reference concentration is written as follows based on the analysis of a large data set on sediment concentration profiles (Camenen and Larson 2007):

$$c_R = 3.51^{-3} \exp(-0.3d_*) \theta_{cw,m} \exp\left(-4.5 \frac{\theta_{cr}}{\theta_{cw}}\right) \quad (4)$$

where $d_* = \sqrt[3]{(s-1)g/v^2 d_{50}}$ is the dimensionless grain size.

The coefficient β_d is given by: $\beta_d = \frac{\varepsilon}{d_{50} h} \left[1 - \exp\left(-\frac{w_s h}{\varepsilon}\right)\right]$

where ε is the sediment diffusivity (Spyrou and Karambas, 2021).

4 EXPERIMENTAL AND NUMERICAL RESULTS

Figures 2 and 3 show the profile evolution and the final profile at the end of the experimental process respectively. Under erosive wave conditions (0-120 min), together with beach face erosion a bar begins to form near the shore and then it moves seawards as the experiment evolves. It ends up in a position in contact with the submerged breakwater.

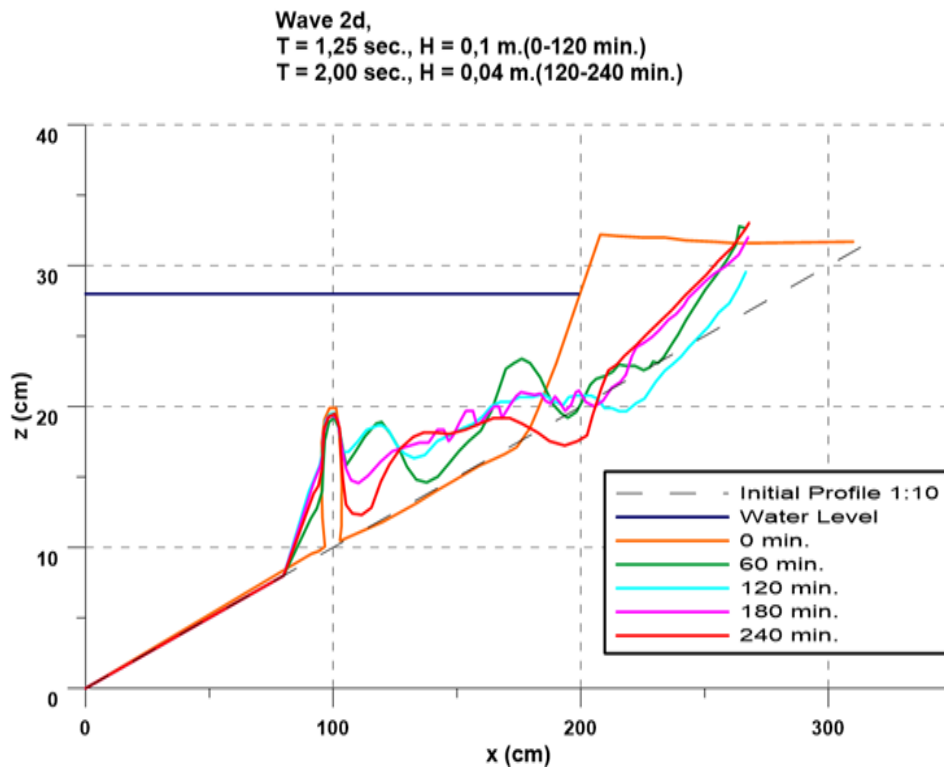


Figure 2. Profile evolution under erosive (0-120 min) and accretive (120-240 min) wave conditions; slope 1:2, B=0.05 m

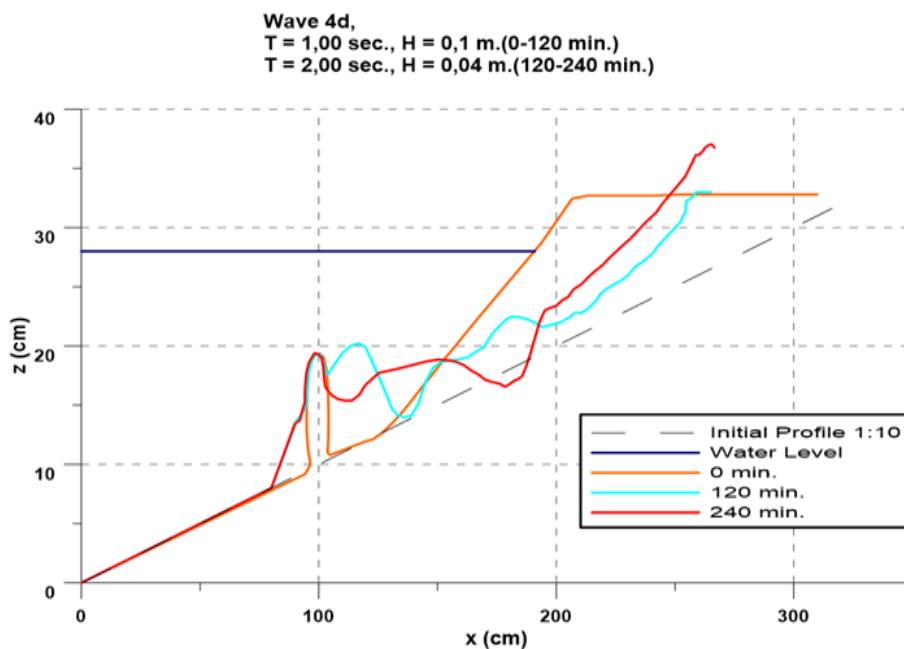


Figure 3. Final profiles under erosive (0-120 min) and accretive (120-240 min) wave conditions; slope 1:2, B=0.05 m

The submerged structure is an obstacle to further movement of the sand. The sand is not carried seawards but remains trapped between the constructed layout and the shoreline. Also, in comparison with the previous experiments, under the same conditions but without submerged structure (Spyrou and Karambas 2021), the coastline recession and coastal flooding is decreased. Consequently, the method can be considered as an improvement of the beach nourishment method and can be used against beach erosion and flooding. Under accretive wave conditions (120-240 min) beach is partially recovered. Similar results are obtained for the case of 1:4 slope.

Figures 4 and 5 show the instantaneous surface elevation, the initial profile, the sediment transport rate, the final profile at the end of the experimental process, together with the results from the mathematical model. The presence of the geotextile artificial reef leads to wave reflection and additional dissipation of the wave energy, mitigating the erosive wave conditions. The cross-shore profile resulting from the numerical application is very well related to the experimental one.

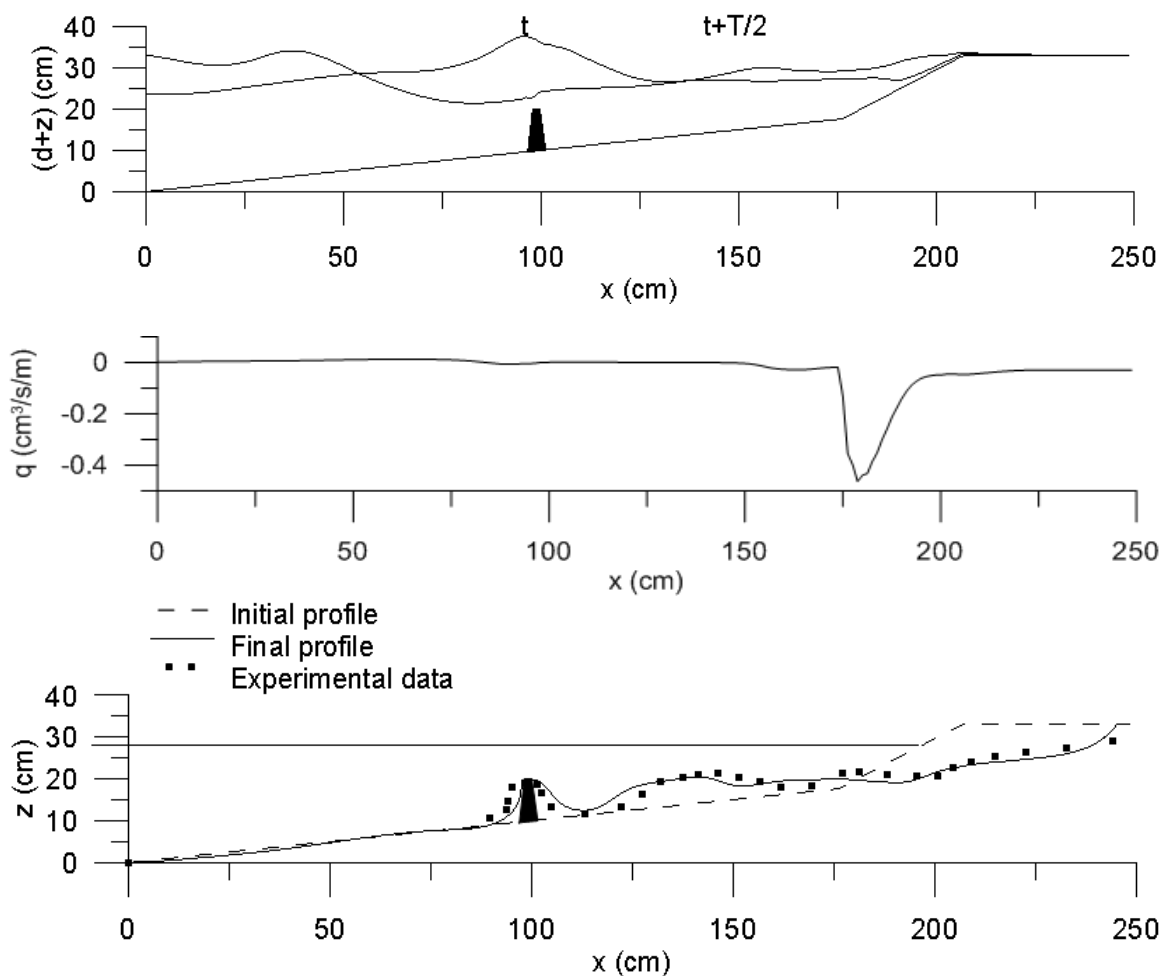


Figure 4. Instantaneous surface elevation (top), sediment transport rate (middle) and cross-section morphology evolution (bottom); $H=0.10$ m, $T=1.54$ sec, slope=1/2

5 CONCLUSIONS

- The submerged structure is an obstacle to further movement of the sand. The sand is not carried seawards but remains trapped between the constructed layout and the shoreline.

- In comparison with the previous experiments, under the same conditions but without submerged structure (Spyrou and Karambas 2021), the coastline recession and coastal flooding is decreased.
- Consequently, the method can be considered as an improvement of the beach nourishment method and can be used against beach erosion and flooding. Finally, the cross-shore profile resulting from the numerical application is very well related to the experimental one.

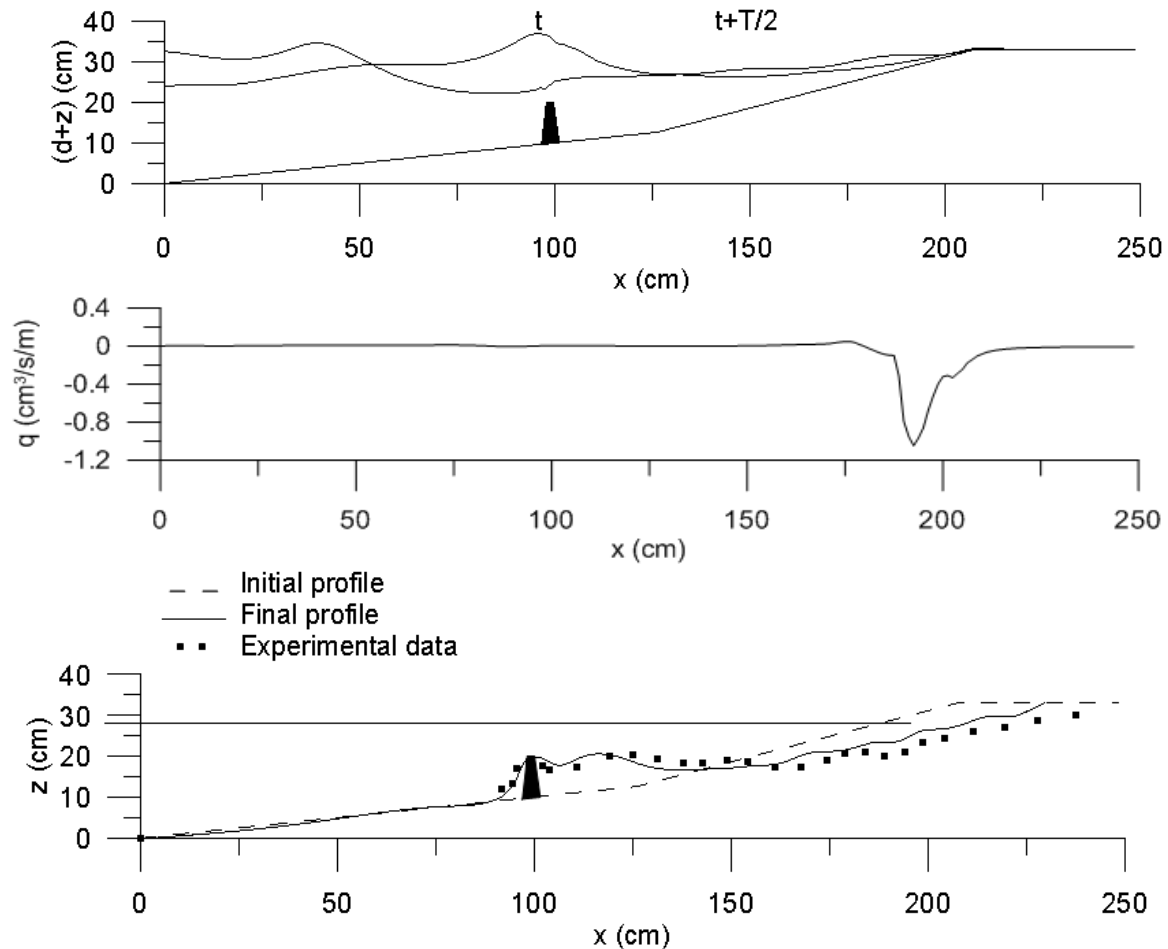


Figure 5. Instantaneous surface elevation (top), sediment transport rate (middle) and cross-section morphology evolution (bottom); $H=0.10$ m, $T=1.54$ sec, slope=1/2

References

- Camenen, B., Larson, M. (2007) A unified sediment transport formulation for coastal inlet application, Technical report ERDC/CHL CR-07-1, US Army Engineer Research and Development Center, Vicksburg, MS
- Gonzalez M., R. Medina, M. A. Losada (1999) Equilibrium beach profile model for perched beaches, *Coastal Engineering* 36(4): 343-357.
- Kobayashi N. and Y. Tega (2002), Sand Suspension and Transport on Equilibrium Beach, *Journal of Waterway, Port, Coastal, and Ocean Engineering* 128 (6): 238– 248. doi:10.1061/(ASCE)0733-950X(2002)128:6(238)
- Spyrou D., Th. Karambas (2021) Experimental and Numerical Simulation of Cross-Shore Morphological Processes in a Nourished Beach. *Journal of Coastal Research* 37 (5): 1012–1024. doi:10.2112/JCOASTRES-D-20-00098.1

Wave regime and shoreline evolution of the coastal front of Kymi (Evia)

S. Lesioti¹, S. Poulos¹, A. Karditsa², C. Aggelopoulos¹

¹ Department of Geology & GeoEnvironment, National And Kapodistrian University Of Athens,
Panepistimioupolis-Zografou, 15784, Attiki

² Department of Ports Management and Shipping, Evripus Campus, National & Kapodistrian University of
Athens, Psachna Evias, 34400, Evia

*Corresponding author: e-mail: poulos@geol.uoa.gr

Abstract

In this paper the wave regime of the broader coastal area of Kymi (Evia) is investigated, utilizing wind data from various sources and different mathematical approaches (i.e., CEM 1984, 2006), as well as the ERA5- ECMWF wave data. Moreover, the spatial evolution of coastal front over time is investigated through the comparison of the shoreline position a series of aerial photographs and satellite images. According to the results shoreline evolution is controlled by both natural processes and anthropogenic interventions. Stability and small progradation is provided in sectors of minimal human intervention, while shoreline retreat is mainly associated with coastal artificial constructions. Remarkably, there are no implications that the port of Kymi has affected the nearby shoreline evolution.

Keywords: Coastal zone management, sea level rise, environmental indicators, coastal works

1 INTRODUCTION

Since the last century, 26% of the Greek coastline has been under erosion (EUROSION, 2004) due to natural (e.g., inner-shelf/coastal slides, coastal subsidence) and anthropogenic (e.g. construction of river dams, ports and other coastal works) causes. Sea level rise is expected to further enhance coastal erosion with considerable impacts on the low-lying coasts (i.e., beaches, deltas), coastal cliffs and dunes. Apart from SLR impacts, climate change will further affect coastal zones through other phenomena such as changes in winds intensity and direction, storm surges or wave activity.

In this paper the wave regime of the broader coastal area of Kymi (Evia) is investigated, using wind data from various sources and different mathematical approaches (i.e., CERC 1984, CEM, 1995), as well as the ERA5- ECMWF wave data. Moreover, the spatial evolution of coastal front over time is investigated by comparing the shoreline position via a series of aerial photographs and satellite images.

2 THE STUDY AREA

The study area is located in the east coast of Evia facing the Aegean Sea, extending from Kalogeros beach (at the north) to Kefala beach (at the south). This coastal sector consists mainly of coastal cliffs fronted by a beach zone, which hosts the mouths of three torrential streams i.e., Melas (158,4 km²), Manikiatis (47,9 km²) and Stomio (12,6 km²). The main anthropogenic intervention is the port of Kymi (constructed in the early 19th century) and the construction of the coastal road along its northern part (Fig. 1). Geologically, the area belongs to the Pelagonian Zone and, in particular to the Kymi Basin, which is the largest Neogene basin in Evia. The upper sequence of the Kymi basin is circa 800 m thick and consists entirely of alluvial fan deposits and conglomerates of Late Miocene age (Kokkalas 2001). The Neogene deposits that dominate the coastal sector of the area under investigation are dominated by the presence of terracotta marls that appear strongly stressed by tectonic action and are characterized as semi-permeable materials. Moreover, the hydrogeological behavior of the formations favors the penetration of rainwater at depth, causing creep and landslides phenomena (Koumantakis et al., 2008). The Kymi Basin has undergone two phases of extensional deformation; the former is associated with a ENE–WSW extension, while the latter with a NNE–SSW extension. The ENE–WSW extension is associated with a large-angle normal fault (deepening to the west) extending along the coastline with a NW-SE orientation.

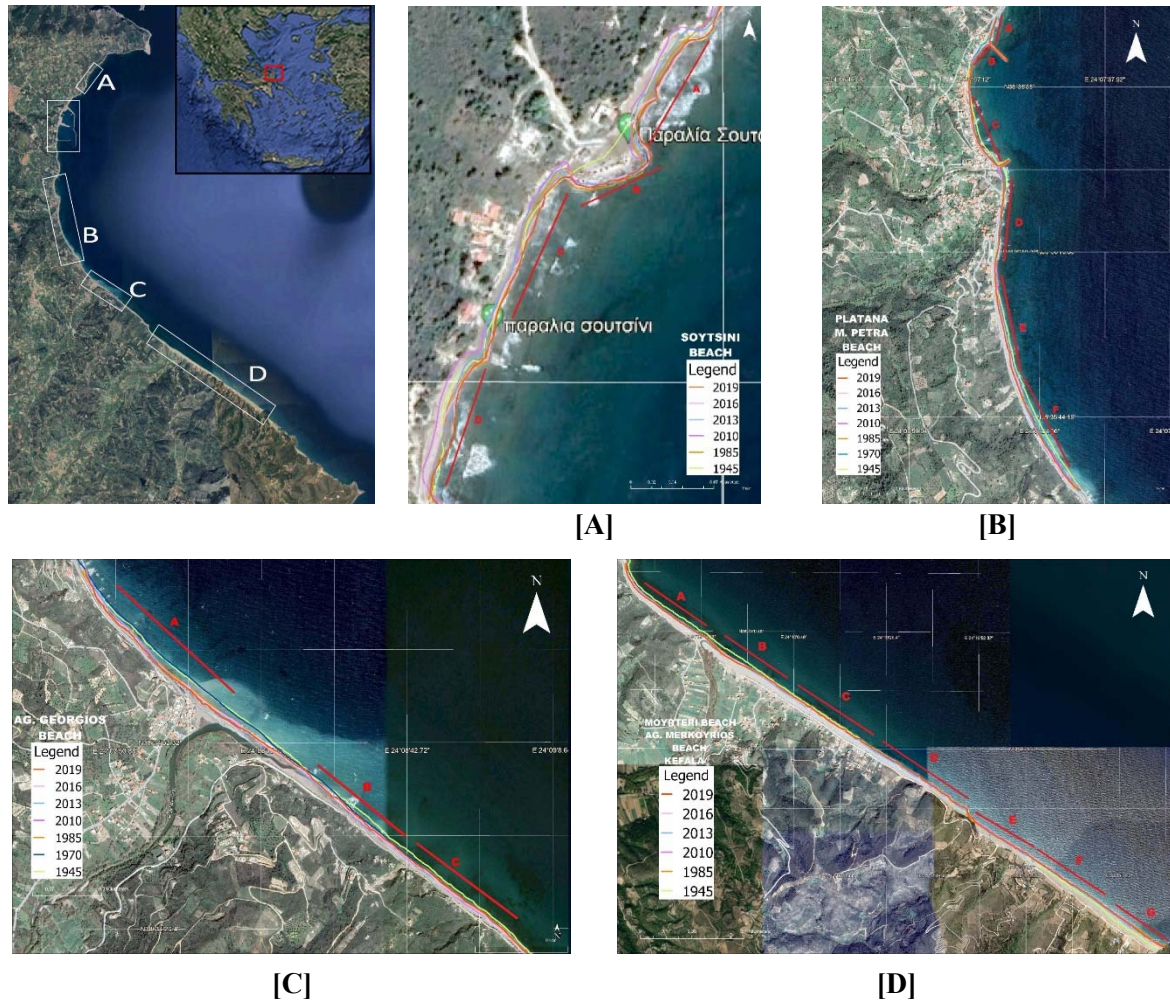


Figure 1. Study area and shoreline evolution in different sectors of the study area

3 METHODOLOGICAL APPROACH

The determination of the wave regime was carried out using (i) wind data timeseries from the HNMS weather station in Skyros (1955-2021) and the hourly values of ERA5- ECMWF (wave height, period and direction) (Mediterranean Sea Waves Reanalysis | Copernicus Marine MyOcean Viewer (https://data.marine.copernicus.eu/product/MEDSEA_MULTYEAR_WAV_006_012/description)). Sverdrup-Munk (CERC 1984) and Bretschneider and Joswap (CEM, 1995) equations were used to calculate the wave parameters from wind data, while the fetch distance calculations were based on the methodology proposed by Smith (1991) and CEM (1995), respectively. The ERA5- ECMWF wave data refer to 38°33' 55,16" N and 24°9' 41,00" E coordination point and includes the hourly values for the period 2011-202: (i) VHM0_WW [m]: Sea surface wind wave significant height; (ii) VMDR_WW [°]: Sea surface wind wave from direction; and (3) VTM01_WW [s]: Sea surface wind wave mean period. Regarding gravity waves those having $H_{m0} < 0,064$ m (i.e., $H_s < 0,04$ m) and $T_{m01} < 1$ s are accepted. In addition, the following relationships (CEM, 1984; Gouda, 2000) were used:

$$H_s = 0,95 H_{m0}; T_s \approx 1,2 T_{m01}; H_{1/10} \approx 1,27 \times H_s; \text{ and } T_s \approx T_{1/10}$$

The calculation of potential longshore sediment transport was based on Kamphuis' equation, for the immersed load, which transformed to dry weight using equation:

$$Qt (im) = 2.23 \cdot T^{1.5} \cdot \tan\beta^{0.75} \cdot d_{50}^{-0.25} H_b^2 \cdot (\sin 2\alpha_b)^{0.6}$$

$$Qt (dry) = Qt(im) \cdot \frac{\rho_s}{(\rho_s - \rho_w)}$$

The determination of H_b was calculated based on Rattanapitikon and Shibayama (2006) relationship:

$$H_b = (-0.57 \cdot m^2 + 0.31 \cdot m + 0.58) \cdot L_o \cdot \left(\frac{H_o}{L_o}\right)^{0.83}$$

The breaking parameter (γ_b) was calculated using the equation given by Larson and Kraus (1988):

$$\gamma_b = 1.14 \cdot \xi_o^{0.21}$$

where (ξ_o) is the surf similarity parameter provided by (Iribarren & Nogales, 1949):

$$\xi_o = m / \left(\frac{H_o}{L_o}\right)^{0.5}$$

where (m) is the subaqueous slope of the surf zone ($=\tan\beta$).

The particle size analysis of the surface sediment samples was carried out at the Laboratory of Physical Geography (Department of Geology and Geoenvironment) following Folk's (1974) dry sieving procedure.

The study of the evolution of the coastal front was based on the comparison of shoreline position via aerial photographs (1945, 1960, 1978), cadastral orthophoto maps (1998) and recent Google Earth satellite images (2010, 2020).

4 RESULTS – DISCUSSION

The calculation of wave characteristics ($H_{m,0}$ and T_p) presents particular difference when predicted by the Sverdrup-Munk method (CEM 1984) and when predicted by the Bretschneider and Joswap method; this difference is related to the altered approach in fetch calculation (cf. Table 1) with Sverdrup-Munk uses a 24 directional arc with the CEM (1984) method (as suggested by Smith, 1991) while Bretschneider and Joswap use a 82 arc according to CEM (1995) (see Table 2).

Table 1. Wave characteristics of the significant wave height and period for the 1/3, 1/10 and 1/100 highest occurrent waves.

		(1/3)			(1/10)			(1/100)		
		CEM	Jon.	ERA40	CEM	Jon.	ERA40	CEM	Jon.	ERA40
N	Hs	1,86	1,28	0,74	2,81	1,87	2,35	4,42	2,87	4,99
	Ts	5,72	3,96	3,55	6,55	4,49	5,85	7,61	5,17	7,59
	f(%)	7,97	7,97	17,04	2,39	2,39	6,89	0,24	0,24	0,91
	Dir	0	0	8	0	0	16	0	0	18
NE	Hs	1,71	1,96	0,99	2,38	2,66	3,12	3,13	3,46	5,95
	Ts	4,91	4,80	3,95	5,48	5,31	6,61	6	5,79	8,1
	Dir	45	45	30	45	45	30	45	45	27
	f(%)	5,59	5,59	4,85	1,68	1,68	29,57	0,17	0,17	0,24
E	Hs	1,22	0,92	0,24	2,32	1,48	0,34	4,2	2,54	1,32
	Ts	5,38	4,79	2,18	6,93	4,54	2,41	8,43	5,43	4
	Dir	90	90	90	90	90	97	90	90	77
	f(%)	1,45	1,45	0,83	0,44	0,44	97,27	0,04	0,04	0,05
SE	Hs	-	-	0,44	-	-	1,47	-	-	3,81
	Ts	-	-	2,86	-	-	4,7	-	-	6,16
	Dir	135	135	143	135	135	148	135	135	139
	f(%)	-	-	4,08	-	-	0,74	-	-	0,10

Furthermore, a difference in wave characteristics calculations is found when comparing the wave characteristics predicted by the wind data with those provided by the ERA5- ECMWF hourly values covering a 20-year period (2011-2020). Besides, the processing of the wave direction data shows that the offshore wave directions deviate from the proposed directions. Moreover, there is a difference in the annual frequency of occurrence between the wind/wave directions and the wave directions given by the ERA5- ECMWF database.

Table 2. Fetch distances calculated for the four main directions for the location A,C and D

	Location [A]				Location [C]			Location [D]		
	N	NE	E	SE	N	NE	E	N	NE	E
arc 82		45,4	162,3	171,7	79,7	119,6	162,8	80,0	107,2	108,6
arc 24		0,8	188,6	295,0	88,5	42,2	183,7	153,0	40,7	153,8

In terms of incoming wave power, the northern part of the coastal area under investigation receives the highest power from the 10% of the highest waves, estimated to be some 1500 W/m, while the remaining part receives approximately 700 W/m. This difference is due to the long SE wave fetches. The potential longshore sediment transport, based on the wave characteristics of the largest 10% of the incoming waves, calculated for segmented sectors of the study area is given in Table 3. The calculation shows that, except for the northern part (Soutsini beach) where the transport is eastward, the transport along the coastal sectors is southwards with rates in the order of 150-170 Mt at its central part (e.g., beaches Platana, Mourteri) and more than 300 Mt at its southern end (Megali Petra beach). With respect to the terrestrial sediment fluxes, the tree torrents with a total drainage area of 219 km² are estimated to contribute annually some 50-100 10³ tonnes (assuming that sediment yield is in the order of 250-500 t/km², according to Woodward et al., 1995). In addition, a significant sediment budget may be provided by the coastal cliffs consisting of erodible lithology and extending the shore in most of the study area.

The shoreline evolution for the different sectors of the study area is given in Table 4. Hereby, it has to be mentioned that the aggregated error in the calculation of shoreline displacement, introduced by digitization accuracy, coastline definition, georeferenced processes etc is estimated in the order of a few meters. In general, the northern part of the study area [A] presents variable changes either positive (up to 25 m) or negative (up to -12,5 m). The coastal area nearby the port of Kimi (Figure 2B) presents minimal changes. Along the sector [B] shoreline presents a clear progradation, reaching locally 25 m; this progradation is mostly related to the riverine sediment influx. Sector [C] (Platana beach) undergoes a profound erosion that locally is 20-45 m. The latter process is attributed to the presence of groins at both ends of the beach, which prevents the lateral influx of sediments, the artificial construction of the coastal road and the offshore sediment transport due to its orientation. Most of the northern part of section [D] retreats, while its southern part prograde by 20-40 m; this is attributed to the southward longshore sediment transport.

Table 3. The estimated potential longshore sediment transport (dry mass) along the different coastal sectors

Beach	Soutsini	Mourteri		Platana			Megali Petra		
Slope (%)	0,03	0,03		0,025			0,025		
d50 (mm) depth(m)	0,24 (-2 m)	4,33 (-2)	0,61 (-4)	0,185 (-4)			0,185 (-4)		
Shoreline orientation	22E	73W	77W	7E	6W	16W	11W	25W	33W
Q (kamfuis) (x10 ⁶ ton)	679	-171	-162	-171	-153	-132	-469	-425	-73

Table 4. Rates of progradation (+) or retreat(-) of the shoreline between 1945 and 2010

Sector	A	B	C	D	E	F	G
[A]	-12,5	+25	+3,5	-4	+8,5		
[B]	+(4-12,5)	+(6-25)	+(1-16)				
[C]	-(1-44)	-(1-29)	-(1-24)				
[D]	-(1-28)	-(1-24)	-(0-12)	-(0-12)	-(0-7)	+(2-19)	+(2-36)

5 CONCLUSIONS

The calculation of wave characteristics from different sources of wind data presents variations that are attributed mostly to the procedure of fetch calculation. The use of ERA5- ECMWF metadata seems to be a good choice for the determination of offshore wave characteristics. Shoreline evolution is controlled by natural processes and anthropogenic interventions. Stability and small progradation is provided for those sectors of minimal human intervention, while shoreline retreat is associated with coastal artificial constructions that reduce beach sediment budget.

References

- EUROSION, 2001, "Coastal erosion – Evaluation of the need for action" Directorate General Environment, European Commission [research programme for the erosion in Europe]
- CEM 1995. Coastal Engineering Manual. Engineering and Design COASTAL GEOLOGY, DEPARTMENT OF THE ARMY, U.S. ARMY CORPS OF ENGINEERS, CECW-EG Washington, DC 20314-1000 Manual N. 1110-2-1810
- CERC 1984 (COASTAL ENGINEERING RESEARCH CENTER. *Shore Protection Manual* (4th edition U.S. Army Corp of Engineers: U.S. Government Printing Office: Washington, DC.
- Goda, Y., 2000. Random seas and design of maritime structures, Advanced Series on Ocean Eng, Vol 15, World Scientific Publishing, Singapore
- Iribarren, R. and Nogales, C., 1949. Protection des ports. XVII International Navigation Congress, Lisbon, Section II-4.
- Kamphuis, J. W. (1991). Alongshore sediment transport rate. *Journal of Waterway, Port, Coastal, and Ocean Engineering*, 117(6), 624-640.
- Kokkalas, S., 2001. Tectonic evolution and stress field of the Kymi-Aliveri basin, Evia island, Greece. *Bull. Soc. Geol. Greece* 34, 243–249.
- Koumantakis, I., Rozos, D., Markantonis, K., Iliia, I., Tsagaratos, P., 2008. Landslide Phenomena of Kimi Municipality. Research Program founded by the Prefecture of Euboea Island.
- Kraus, N. C., & Larson, M. (1988). *Beach profile change measured in the tank for large waves 1956-1957 and 1962*. Coastal Engineering Research Center Vicksburg MS.
- Pe-Piper, G., Piper, D.J.W., 1994. Miocene magnesian andesites and dacites, Evia, Greece: Adakites associated with subducting slab detachment and extension. *Lithos* 31, 125–140.
- Rattanapitikon, W., & Shibayama, T. (2006). Breaking wave formulas for breaking depth and orbital to phase velocity ratio. *Coastal Engineering Journal*, 48(04), 395-416.
- Ring, U., Glodny, J., Will, T., & Thomson, S. (2007). An Oligocene extrusion wedge of blueschist-facies nappes on Evia, Aegean Sea, Greece: implications for the early exhumation of high-pressure rocks. *Journal of the Geological Society*, 164(3), 637-652.
- Smith J.M., 1991 Wind-Wave Generation on Restricted Fetches. Coastal Engineering Research Center, Department Of The Army, Vicksburg, Mississippi Miscellaneous Paper CERC-91-2
- Woodward, J. C., Foster, I. D. L. (Ed.), Gurnell, A. M. (Ed.), & Webb, B. W. (Ed.) (1995). Patterns of erosion and suspended sediment yield in Mediterranean river basins. In *Sediment and Water Quality in River Catchments* (pp. 365-389). John Wiley & Sons Ltd.

A sideways look at 1-line beach modelling

D.E. Reeve^{1*}

¹Department of Civil Engineering, Swansea University, Swansea, Wales, SA1 8EN, United Kingdom

*Corresponding author: d.e.reeve@swansea.ac.uk

Abstract

Predicting changes to beach orientation in response to variations in prevailing wave conditions or man-made interventions such as groynes is an important element of beach management. The ‘1-line’ beach shape model is a well-established means of providing such predictions. For certain conditions the model reduces to a simple linear equation that can be solved analytically. For more general cases, computational packages have been developed and are commercially available. Here, we return to analytical solutions; in addition to their pedagogical uses we investigate their potential for informing probabilistic design and management. Considering the wave conditions to be random, and by extension the beach movements also, solutions for the mean and variance of beach position can be derived. This information may also be used in combination with reliability theory to estimate the probability that a groyne fills or a beach nourishment erodes over a particular period. Such ideas can be extended to derive equations for the evolution of the statistical moments of beach position and in some cases, expressions for these moments directly. These can yield the mean and variance of beach position, information useful in beach and coastal management.

Keywords Beach, 1-line model, stochastic, reliability.

1 INTRODUCTION

This introduction provides a very brief history of the origins of the 1-line beach model concept and some of the subsequent developments.

1.1 The 1-line beach model

The 1-line model is based on the concept of conservation of sediment and a longshore sediment transport equation with highly simplified physics. It has found widespread application in predicting medium to long-term changes in shoreline morphology. The primary assumptions are that the beach profile is in equilibrium (so that bathymetric contours are parallel to each other) and that the longshore sediment transport occurs only out to a fixed depth, (the depth of closure D_c). Additionally, for analytical work, it is assumed that: wave conditions are uniform and constant; waves approach the shore close to normal and the local beach orientation does not vary greatly from its trendline. Under these conditions the 1-line equations may be condensed into a single equation for the position of a single beach contour (Pelnard-Considère, 1956):

$$\frac{\partial y}{\partial t} = \varepsilon \frac{\partial^2 y}{\partial x^2} \quad (1)$$

where y is the distance of the chosen beach contour in the offshore direction from a longshore datum line, (taken as the x -axis), t is time, the parameter ε takes the role of a diffusion coefficient and is equal to twice the maximum longshore sediment transport divided by D_c . Pelnard-Considère (1956) gave a solution to this equation for the case of a single groyne on an initially straight beach:

$$y(x, t) = \tan(\alpha_b) \left(\frac{2\sqrt{\varepsilon t}}{\sqrt{\pi}} \exp\left(-\left(\frac{x}{2\sqrt{\varepsilon t}}\right)^2\right) - x \operatorname{erfc}\left(\frac{x}{2\sqrt{\varepsilon t}}\right) \right) \quad (2)$$

where α_b is the angle between the beach and the incoming breaking wavefront. Solutions for other cases including detached breakwaters, nourishments and river deposits have been derived, (see e.g. Larson et al., 1997; Wind, 1990; Walton, 1994). More recently, analytical solutions that allow arbitrarily varying

wave conditions have been derived for the cases of a single groyne, a groyne compartment and river deposits, (see e.g., Reeve, 2006; Zacharioudaki and Reeve, 2008; Walton and Dean 2011; Valsamidis and Reeve 2017).

Computational solution of the more general 1-line model requires the simultaneous solution of the longshore transport equation, the conservation of sediment equation and a geometrical constraint linking the local angle of wave attack, the local beach orientation and the offshore wave angle, (Hanson 1989). The flexibility of computational solutions allows the inclusion of additional processes such as nearshore wave transformation, wave diffraction and reflection, spatially and time varying wave conditions, as well as more sophisticated wave breaking treatments (see e.g., Larson et al 2003).

2 RELIABILITY APPLICATIONS

Here, we consider how some simple analytical solutions can be used to assess the uncertainty in various cases of interest. Uncertainty in the sediment transport rate, wave angle and depth of closure are represented by assigning a probability distribution to each.

2.1 Reliability of a groyne

From Equation (1) we know that the accumulation of sand immediately updrift of a groyne, L , is given approximately by:

$$L = \alpha_b \sqrt{\frac{4\epsilon t}{\pi}} = 2\alpha_b \sqrt{\frac{2Q_0 t}{\pi D_c}} \quad (3)$$

where Q_0 is the maximum sediment transport rate. The situation is shown in Figure 1 below, where waves are driving a longshore sediment transport rate Q from left to right.

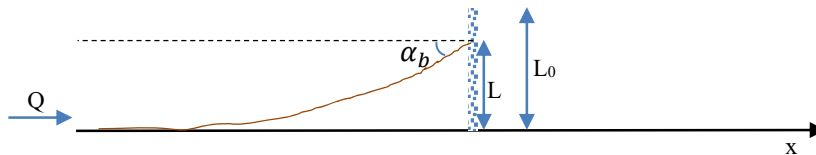


Figure 1. Diagram of accretion updrift of a groyne

Let the length of the groyne, L_0 , be 60m. In standard first order reliability methods, (FORM), (see e.g. Melchers, 1999; Thoft-Christensen and Baker, 1982; Reeve, 2010), uncertain or stochastic variables are assumed to follow a Normal distribution and are assigned a mean and standard deviation. After various calculations a probability of the loading exceeding the strength can be evaluated. In the current context the ‘loading’ is the extent of the accretion, L , and the strength is the length of the groyne, L_0 . Table 1 below summarises an illustrative example set of values.

Table 1. Variable settings for groyne reliability calculation

	Mean	Std. Dev.	Units
Q_0	11800	3400	m ³ /year
α_b	0.2	0.05	Radians
D_c	10	2	m

Setting Q_0 , α_b and D_c equal to their mean values, we can perform a deterministic calculation with Equation (3) to confirm that $L > L_0$ when $t = 30$. That is, the groyne will be full and by-passing will

occur after 30 years. If we use a FORM calculation with the values in Table 1 we find that the probability of $L > L_0$ is 0.38 after 25 years and 0.6 after 35 years. Such calculations provide not only a deterministic estimate of the active lifetime of the groyne but also a guide as to the variation about that value that might be experienced in any particular case. The value of the guide will reflect the accuracy with which the statistical properties of the key variables can be estimated!

2.2 Reliability of a simple nourishment

A similar approach can be applied to the solution for a rectangular nourishment of depth L running from $x = -a$ to $x = a$. The solution in this case is, (Wind 1990):

$$y(x, t) = \frac{L}{2} \left(\operatorname{erf} \left(\frac{a-x}{2\sqrt{\varepsilon t}} \right) + \operatorname{erf} \left(\frac{a+x}{2\sqrt{\varepsilon t}} \right) \right) \quad (4)$$

As before, knowing that $\varepsilon = 2Q_0/D_c$, assigning mean and standard deviations to Q_0 and D_c we can calculate the probability that the depth of the nourishment has halved, (say), after a particular time.

One issue with this approach is that not all variables follow a Normal distribution. FORM has been adapted to account for non-Normal distributions as well as correlated variables, but it remains an approximate method. An alternative to this is to try to predict the statistics of beach position directly.

3 MOMENTS OF BEACH POSITION

One method of estimating the statistics of beach position is to solve the 1-line equation as part of a Monte Carlo simulation such as proposed by Vrijling and Meijer (1999). This requires two extra elements beyond a good sequence of wave conditions: an accurate means of simulating trivariate sequences of wave height, period and direction with the correct statistics and temporal correlation functions; an increased computational load as simulations must be performed over many realisations (or independent sets of wave time sequences). The first element is not straightforward. Borgman and Sheffner (1991) pioneered a method for coastal applications. While reasonable, it suffered from the variables showing intermittent and unrealistic jumps over time. Many other methods have been developed but tend to suffer either from deficiencies in reproducing the statistical properties of the original wave sequence or becoming very computationally demanding. The second element has receded somewhat in importance as computing power has increased significantly over the last few decades, although it remains a consideration for long term or very large ensemble simulations.

An alternative to Monte Carlo simulation is to derive equations for particular statistical moments of the shoreline. In the context of Equation (1) this would entail considering the diffusion coefficient to be of the form $\varepsilon(t) = \langle \varepsilon \rangle + \delta(t)$ where angle brackets denote an ensemble average and $\delta(t)$ is a mean zero stochastic variable with known probability density and temporal correlation function. With suitable provisos, it is possible to combine this expression for $\varepsilon(t)$ with Equation (1) to obtain closed-form expressions for the mean and variance of $y(x, t)$. Approximate solutions for the evolution of beach nourishment were derived by Reeve and Spivack, (2004), who used a truncated Normal distribution for $\delta(t)$ and Gaussian and exponential correlation functions to model the temporal correlation. Important conclusions from this work were that:

- 1) the mean shoreline position is not obtained by inserting mean forcing conditions into the governing equation. The temporal fluctuations in the wave conditions have a cumulative effect on how the shoreline evolves which is dependent upon the distribution function and the autocorrelation properties of the fluctuations;
- 2) The solutions also show that the fluctuations in wave conditions, when taken cumulatively, act to accelerate the diffusive effect in the ensemble mean. This provides an explanation of why beach nourishment is often observed to spread at a faster rate than predicted using representative values of wave variables in a deterministic one-line model.

Such solutions are extremely valuable in providing a validation test for computational Monte Carlo simulations. Nevertheless, they apply to quite restrictive situations and remain approximate.

4 ENSEMBLE AVERAGING SOLUTIONS

Returning to Equation (1), if we treat the shoreline position and wave conditions as random variables, with $y = \langle y \rangle + y'$ and $\varepsilon = \langle \varepsilon \rangle + \delta$, by substituting these expressions into Equation (1) and taking ensemble averages we can form an equation for the evolution of the ensemble average of y :

$$\frac{\partial \langle y \rangle}{\partial t} = \langle \varepsilon \rangle \frac{\partial^2 \langle y \rangle}{\partial x^2} + \langle \delta \frac{\partial^2 y'}{\partial x^2} \rangle \quad (5)$$

where it is understood that $\langle y' \rangle = \langle \delta \rangle = 0$, $\langle \langle y \rangle \rangle = \langle y \rangle$ and $\langle \langle \delta \rangle \rangle = \langle \delta \rangle$. It is clear from Equation (5) that the time evolution of the ensemble average shoreline depends not only on the ensemble averaged wave conditions, $\langle \varepsilon \rangle$, but also on the correlations between the variations in wave conditions and beach plan shape. This latter term can be viewed as a form of ‘morphodynamic turbulence’, whose quantification is analogous to the ‘turbulence closure problem’ in fluid mechanics. An obvious approximation is to neglect the correlation term, setting it equal to zero. However, we know from the work on shoreline moments, (Section 3), that this does not give satisfactory results. Another alternative is to parameterise the correlation in terms of the ensemble average terms, using a mixing length-type idea. Yet another possibility is to use existing deterministic analytical solutions for $y(x, t)$ and to perform the ensemble averaging directly. To elucidate, suppose we have an analytical solution $y(x, t) = f(\varepsilon, \alpha_b, x, t)$, where f is a solution of the diffusion equation (Equation 1). Now, in practice, ε is typically a function of wave height, period and direction, (and possibly other variables relating to beach geometry and material which will be neglected for the moment). The ensemble average of $y(x, t)$ may be obtained by integrating the function f over all possible values of the stochastic variables:

$$\langle y(x, t) \rangle = \int_0^{2\pi} \int_0^{\infty} \int_0^{\infty} f(H, T, \alpha_b, x, t) \cdot p(H, T, \alpha_b) dH dT d\alpha_b \quad (6)$$

where $p(H, T, \alpha_b)$ is the trivariate probability density function of the waves. The righthand of equation (6) is the formal definition of the ensemble average of f , and similar expressions exist for the higher moments of y . Equation (6) may be evaluated by performing the triple integral once both f and p have been established. Alternatively, it may be estimated from the average of many evaluations of f for different realisations of the wave conditions. Reeve et al. (2014) investigated the statistics of beach movement near a groyne using Equation (6). Six hundred realisations of a 4-year record of offshore waves were produced using the method of Borgman and Sheffner (1991). The 600 realisations of wave sequences were then used to calculate 600 separate solutions of f (as a function of x and t). The average and variance of f for any chosen x and t could be estimated directly from these solutions. One important finding was that although the wave heights, periods and directions were correlated in time, the correlations with wave direction were much more short-lived. This effectively decoupled beach changes that were dependent on wave direction from those that were more strongly related to wave height and period. In the case of a groyne this meant that details of the beach shape near the groyne, which are strongly dependent on wave angle, fluctuated over shorter time scales than the larger scale pattern of accretion updrift of the groyne.

5 CONCLUSIONS

To conclude, the analytical solutions of the 1-line model, while often considered of primarily pedagogical value, can still be useful and lead to new insights when probabilistic design is concerned. They are important in being able to provide independent solutions against which computational models run for Monte Carlo simulation can be checked to ensure they are producing the correct statistics for beach position. While not as flexible as computational models they can still provide valuable insights,

often at very modest computational cost. Future work is aimed at evaluating Equation (5) for a wider range of cases and also investigating appropriate means of parameterizing the turbulence term in Equation (5).

References

- Borgman, LE, Sheffner, NW (1991) Simulation of time sequences of wave height, period and direction. Technical Report. US Army Corps of Engineers.
- Hanson, H (1989) Genesis: a generalized shoreline change numerical model. *J. Coast Res.* v. 5, 1–27.
- Larson M, Hanson H, Kraus NC (1997) Analytical solutions of one-line model for shoreline change near coastal structures. *J. Wtrwy, Port Coastal and Ocean Engineering*, 123, p180-191.
- Larson M, Kraus NC, Hanson H (2003) Simulation of regional longshore sediment transport and coastal evolution — The “Cascade” model. *Coastal Engineering 2002*, 2612–2624.
- Melchers, RE (1999) *Structural Reliability Analysis and Prediction*. 2nd Edition, J Wiley & Sons, Chichester, p437.
- Pelnard-Considère R (1956) Essai de théorie de l'évolution des formes de rivage en plages de sables et de gâlets. Societe Hydrotechnique de France, IV^{ème} Journees de L'Hydraulique Question III, rapport 1, p. 74-1-10.
- Reeve DE (2006) Explicit expression for beach response to non-stationary forcing near a groyne. *ASCE J. Waterway, Port, Coastal & Ocean Engineering*, 132, p125-132.
- Reeve DE (2010) *Risk and Reliability: Coastal and Hydraulic Engineering*, Spon Press, London, 304p.
- Reeve DE, Pedrozo-Acuña A, Spivack M (2014) Beach Memory and ensemble average of the shoreline evolution near a groyne. *Coastal Engineering*, 86, p77-87.
- Thoft-Christensen P, Baker MJ (1982) *Structural Reliability Theory and Its Applications*. Springer, Berlin.
- Valsamidis A, Reeve DE (2017) Modelling shoreline evolution in the vicinity of a groyne and a river. *Continental Shelf Research Continental Shelf Research*, 132, p49-57.
- Vrijling JK, Meijer GJ (1992) Probabilistic coastline position computations. *Coastal Engineering*, 17, p1-23.
- Walton TL (1994) Shoreline solution for tapered beach fill. *J Wtrwy, Port, Coast., & Oc. Engrg, ASCE* 120 (6), 651–655.
- Walton TL, Dean RG (2011) Shoreline change at an infinite jetty for wave time series. *Cont. Shelf Res.* 31, 1474–1480.
- Wind HG (1990) Influence functions. In: *Proceedings of the 21th International Conference on Coastal Engineering*. pp. 3281–3294.
- Zacharioudaki A, Reeve DE (2008) Semi-analytical solutions of shoreline response to time varying wave conditions. *ASCE J. Waterway, Port, Coastal & Ocean Engineering*, Vol 134(5), p265-274.

Effects of flow and sediment parameters on vortex ripple morphodynamics

G.A. Leftheriotis^{1*}, A.A. Dimas¹

Department of Civil Engineering, University of Patras, Patras, 26504, Greece

*Corresponding author: gletheriot@upatras.gr

Abstract

In the present work, numerical simulations were performed to study the effect of sediment characteristics and flow intensity on the creation and morphological evolution of orbital vortex ripples under oscillatory flow conditions. The numerical methodology is based on large-eddy simulations of turbulent oscillatory flow, fully coupled with the induced bed and suspended sediment transport, as well as the corresponding morphodynamic evolution of the bottom surface. The Immersed Boundary method is implemented for the imposition of both fluid and sediment boundary conditions on the mobile bottom surface. Results are presented for ripple creation and propagation under different flow and sediment parameters.

Keywords Vortex ripples, Large-eddy simulation, Navier-Stokes equations, Immersed boundary method.

1 INTRODUCTION

The complex interactions between sand and wave-generated flows lead to the generation of sand ripples. These structures are created due to the flow vortices developed on the leeside of their crests during each half cycle of the oscillatory flow, and they are described in the literature as vortex ripples (Bagnold, 1946). Clifton and Dingler (1984), proposed a classification of ripples into two main categories: (a) orbital ripples, whose length depends the wave orbital amplitude a_o , and (b) anorbital ripples whose length depends on the sediment grain diameter, D_g . The presence of ripples is quite important in terms of engineering, since they play a major role in phenomena like wave attenuation and coastal sediment transport. The size of ripples is crucial for the sediment transport processes in coastal environments, since it affects the bottom friction and the wave boundary layer. Thus, a number of researchers have developed predictive formulae for ripple equilibrium dimensions, for given sediment and flow characteristics. Nielsen (1981) described the ripple dimensions as a function of the mobility parameter, ψ . Based on laboratory/regular wave conditions, he proposed the following equations for the prediction of the ripple length, L_r , and the ripple height, h_r ,

$$\frac{L_r}{a_o} = 2.2 - 0.345 \cdot \psi^{0.34} \quad \text{and} \quad \frac{h_r}{a_o} = 0.275 - 0.022 \cdot \psi^{0.5} \quad (1)$$

The objective of the present study is to investigate numerically the effect of different values of the mobility parameter, ψ , and the normalized sediment size parameter, a_o/D_g , on the morphodynamical development of vortex ripples. An LES model is utilized for the numerical simulation of the three-dimensional (3D) turbulent oscillatory flow, coupled with the corresponding sediment transport mechanisms. The evolution of the mobile bed is achieved by the numerical solution of the conservation of sediment mass (Exner) equation.

2 METHODOLOGY

2.1 Numerical Methods

The governing 3D fluid motion equations are the continuity equation and the Navier-Stokes (NS) equations, which are made dimensionless using the velocity amplitude, U_o , and a_o , in the following form:

$$\frac{\partial u_i}{\partial x_i} = 0 \quad (2)$$

$$\frac{\partial u_i}{\partial t} + \frac{\partial}{\partial x_j} (u_i u_j) = -\frac{\partial p}{\partial x_i} - \frac{\partial \tau_{ij}}{\partial x_j} + \frac{1}{\text{Re}} \frac{\partial^2 u_i}{\partial x_j \partial x_j} + f_i \quad (3)$$

where u_i are the velocity components, t is the time, x_i are the spatial coordinates, p is the dynamic pressure, τ_{ij} are the subgrid-scale (SGS) stresses, and f_i is the Immersed Boundary (IB) method term (Dimas and Chalmoukis, 2020) for the imposition of the non-slip velocity boundary condition on the bed surface. The SGS stresses are modelled using the standard eddy-viscosity model in Smagorinsky (1963), and their influence was gradually damped close to the bed surface by reducing the SGS eddy-viscosity smoothly, using the formula in Van Driest (1956). Both bed and suspended sediment transport are taken into account in the sediment transport model, using the semi-empirical formula in Engelund and Fredsøe (1976) for the computation of the bed load transport rate, and an advection-diffusion equation for the computation of the concentration of the suspended sediment.

$$\frac{\partial c}{\partial t} + u_j \frac{\partial c}{\partial x_j} - \frac{W_s}{U_o} \frac{\partial c}{\partial x_3} = -\frac{\partial \chi_j}{\partial x_j} + \frac{1}{\text{Re} \cdot \sigma} \frac{\partial^2 c}{\partial x_j \partial x_j} + f_c \quad (4)$$

where W_s is the dimensional settling velocity of the sediment, χ_j is the SGS turbulent flux of sediment, σ is the Schmidt number, and f_c is the IB method term for the appropriate sediment concentration boundary condition on the bed surface. The coupling between the evolution of bed morphology and the sediment transport fluxes was obtained by the numerical solution of the Exner equation:

$$\frac{\partial h}{\partial t} = -\frac{1}{1-n_p} \left(\frac{\partial q_1}{\partial x_1} + \frac{\partial q_2}{\partial x_2} \right) \quad (1)$$

where h is the bed level, n_p is the bed sediment porosity (assumed to be constant), and $q_i = q_{bi} + q_{si}$ is the total sediment flux in the horizontal directions.

A fractional time-step scheme is utilized for the time discretization of the NS equations, with an intermediate velocity field computed in the first stage of the time-step, using a 2nd order Adams-Bashforth scheme. In the second stage of the time-step, the final velocity field is computed. 2nd order central finite differences are used for the spatial discretization of the NS equations on a staggered Cartesian grid. Detailed information regarding the coupled hydrodynamic and sediment transport model and the numerical methods are provided in Dimas and Leftheriotis (2019). The coupling between the morphological evolution of the bed and the sediment transport fluxes is obtained by solving numerically the conservation of sediment mass equation (also called the Exner equation). The sediment flux comprises both bed load, q_b , and suspended load, q_s , transport rates. An avalanche algorithm is included in the morphodynamical model to mimic as possibly the natural process in the vicinity of ripple crests, when the bed slope exceeds a certain limit. The Exner equation was discretized in time using a 3rd order Adams-Bashforth scheme applied in both horizontal directions, while 2nd order central differences were used for the spatial gradients. Detailed information about the morphodynamical model is available in Leftheriotis and Dimas (2022).

2.2 Simulation Setup

Ripple formation and propagation was examined initiating from a flat bed with a small perturbation in the middle of the computational domain (Figure 1). The streamwise length of the computational domain, L_x , was selected to be sufficient for a number of three consecutive ripple wavelengths to be formed, based on the simulation parameters. The width of the computational domain, L_y , was set equal to L_x so that ripples development is not affected by the periodic boundary conditions. The height of the domain, L_z , was selected at least equal to $5 \cdot a_0$ to ensure that the upper boundary does not affect the development of the boundary layer.

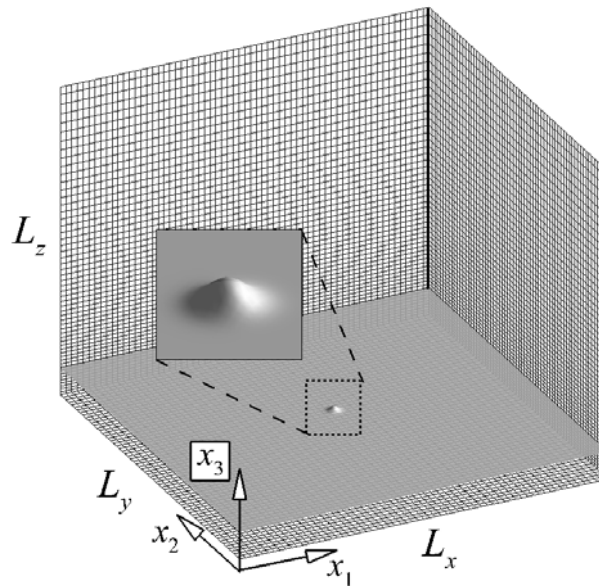


Figure 1. The computational domain with the initial bed geometry immersed in the Cartesian grid.

The resolution of the computational grid is uniform in the horizontal directions, while it is non-uniform in the vertical direction, where a finer resolution is applied near the bed level. The resolution of the computational grid is sufficient ($\Delta x_3^+ \sim 3$) for the resolution of the wave boundary layer for all cases examined. The flow time-step was selected so that both convective (CFL) and diffusive (VSL) criteria are satisfied. The morphological time-step is 20-50 times larger than the flow time-step, and it is numerically restricted by the Courant Friedrichs Lewy condition for the morphological equation ($CFL_m < 1$). Periodic boundary conditions were applied in the horizontal directions (x_1, x_2), for all variables (velocity, pressure, sediment concentration and bed level), so ripple development is not spatially limited. A zero Dirichlet boundary condition is applied at the bottom boundary, $x_3 = 0$, while appropriate rigid-lid boundary conditions are applied at the upper boundary, $x_3 = L_z$ for all variables.

3 RESULTS

The numerical model has been validated in terms of fluid flow, sediment transport and bed morphodynamics. The validation results for flow velocity and suspended sediment concentration can be found in Dimas and Leftheriotis (2019), while validation results for the morphological evolution of the bed have been presented in Leftheriotis and Dimas (2022).

The objective of the present study was to examine the effect of non-dimensional flow and sediment parameters on the morphodynamics evolution of ripples. Ripple creation and propagation was examined initiating from a flat bed with a small perturbation in the middle of the computational domain (Figure 1 **Error! Reference source not found.**). Two values of ψ ($= 20, 50$) were selected, for $a_o/D_g = 500$. The bed sediment corresponds to quartz sand with specific gravity equal to $S = 2.65$, and the porosity of the bed sediment was equal to $n_p = 0.4$, typical value for coastal sediments. The dynamic friction coefficient, μ_d , was chosen equal to 0.35. The simulations started with the fluid and the sediment at rest, 200-700 wave periods (depending on the case examined) were required for the bed geometry to reach an equilibrium shape and another 20 wave periods were used for sampling and averaging.

3.1 Ripple Creation and Propagation

In the first case ($\psi = 20, a_o/D_g = 500$), due to the small value of the mobility parameter, the net sediment transport rate is quite small, especially in the beginning of the simulation. It takes almost 50 wave periods for the initial hump to grow and cause the creation of ripples (Figure 2). After that time the computational domain is almost fully covered with small ripples that grow slowly and begin to present spanwise two-dimensionality (see Figure 2 at 100T). After about 200 wave cycles, the bed geometry

consists of five consecutive ripples. During the next 200 waves, phenomena of ripple merging occur, with ripple number 4 slowly dividing and merging with ripples number 2 and 4. After 400 wave cycles, the bed geometry consists of four consecutive ripples, which is close to the predicted final form. During the next 300 waves, phenomena of ripple annihilation occur, with ripple number 5 slowly vanishing, due to the larger vortices generated by ripples 1 and 4. The phenomenon of ripple annihilation occurs when a ripple is located between two ripples that generate larger vortices and remove sediment away from the crest of ripple 5, until the ripple completely vanishes. After 700 wave cycles the bed finally converges to its equilibrium geometry, composed of three consecutive ripples, with lengths equal to $1.25 \cdot a_o$ and heights equal to $0.171 \cdot a_o$. The calculated ripple dimensions are well within the range of the experimental data used to fit the empirical formulas in Nielsen (1981), which give $L_r = 1.25 \cdot a_o$ and $h_r = 0.177 \cdot a_o$ for $\psi = 20$. Afterwards, for the next 500 wave periods the ripples retain these equilibrium dimensions and present onshore migration with a velocity of $5 \cdot 10^{-4} \cdot U_o$.

In the second case ($\psi = 20$, $a_o/D_g = 500$), due to the larger value of the mobility parameter, the net sediment transport rate is larger than in case 1, especially in the beginning of the simulation. In Figure 3 **Error! Reference source not found.**, typical snapshots are presented during ripple development from a flat bed with a small perturbation in the middle of the computational domain. The initial hump grows rapidly in height and it expands in the spanwise direction during the first wave periods. At the same time, a number of small perturbations are emerging on each side of the initial hump. After 20 wave periods, the bed is almost fully covered in small rolling grain ripples, which is the first stage of ripple development according to Miller and Komar (1980). During the next wave periods merging phenomena take place, with the bed geometry being fully covered with ripples that present spanwise three-dimensionality and close to the predicted final form after about 100 waves. During the next periods, phenomena of ripple merging and annihilation occur, the spanwise three-dimensionality vanishes, which eventually leads to ripples that present spanwise two-dimensionality. The equilibrium geometry of the bed is reached after about 150 wave periods, and comprises three consequent ripples with dimensions of $L_r = 0.9a_o$ and $h_r = 0.139a_o$. The calculated ripple dimensions are well within the range of the experimental data used to fit the empirical formulas in Nielsen (1981), which give $L_r = 0.9 \cdot a_o$ and $h_r = 0.2 \cdot a_o$ for $\psi = 50$. For the next 200 wave periods the ripples do not present significant morphological changes, they retain the equilibrium dimensions and migrate with a small offshore velocity of $5 \cdot 10^{-5} \cdot U_o$.

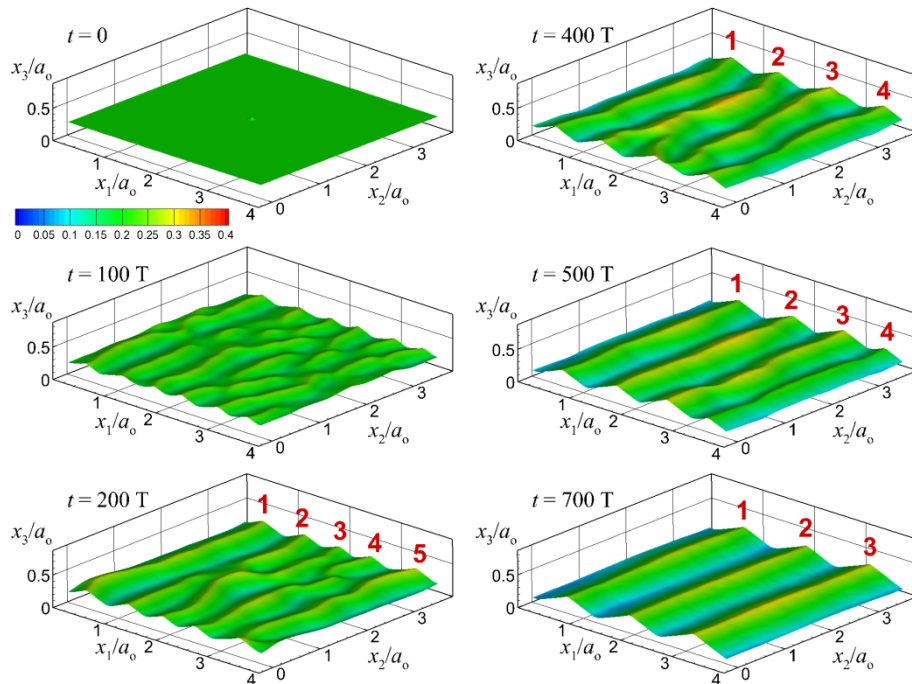


Figure 2. Numerical result of ripple creation from a flat bed for $\psi = 20$ and $a_o/D_g = 500$. The equilibrium state is reached after about 700 wave cycles.

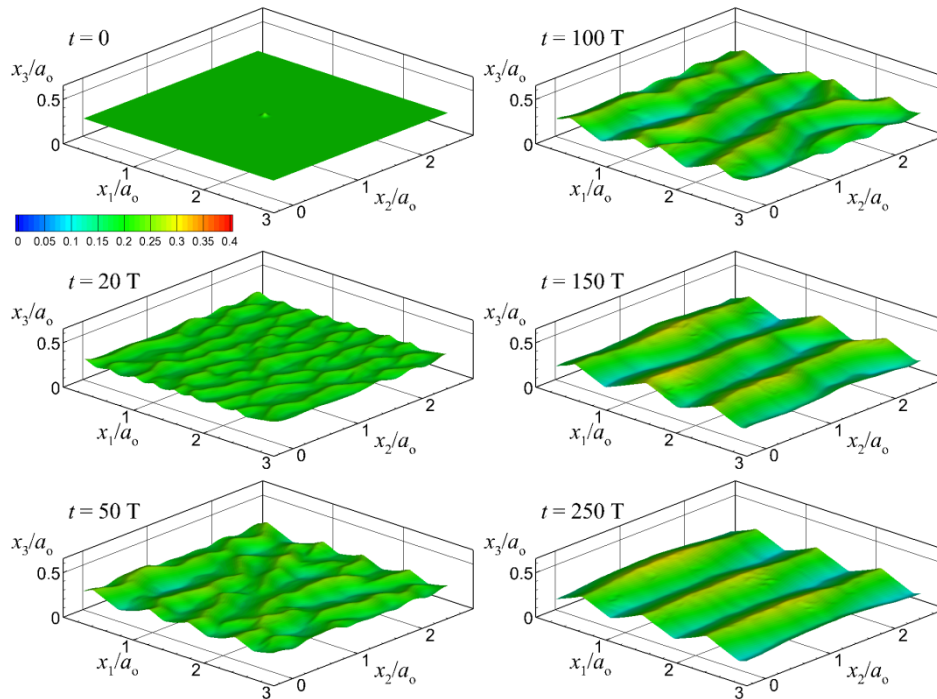


Figure 3. Numerical result of ripple creation from a flat bed for $\psi = 50$ and $a_o/D_g = 500$. The equilibrium state is reached after about 150 wave cycles.

4 CONCLUSIONS

Large-eddy simulation of turbulent oscillatory flow coupled with sediment transport and bedform evolution were performed. The objective of the present study is to study the effect of sediment characteristics and flow intensity on the creation and morphological evolution of orbital vortex ripples under oscillatory flow conditions. Ripple creation and propagation from an initially flat bed with a small perturbation in the middle of the computational domain until the bed reached an equilibrium state, adapting to oscillatory flow conditions based on ψ . The numerical model demonstrated the ability to simulate phenomena of ripple formation, growth, annihilation, widening, shortening, merging, and migration, resulting in equilibrium ripples with wavelengths in agreement with those predicted by empirical equations.

References

- Bagnold RA (1946) Motion of waves in shallow water, interaction between waves and sand bottoms. Proceedings of the Royal Society A, 187(1008), 1-15. doi:10.1098/rspa.1946.0062
- Clifton HE, Dinger JR (1984) Wave-formed structures and paleoenvironmental reconstruction. Mar Geol 60(1-4) 165-198. doi:10.1016/0025-3227(84)90149-X
- Dimas AA, Chalmoukis IA (2020) An adaptation of the immersed boundary method for turbulent flows over three-dimensional coastal/fluvial beds. Appl Math Model 88, 905–915. doi:10.1016/j.apm.2020.07.007
- Dimas AA, Leftheriotis GA (2019) Mobility parameter and sand grain size effect on sediment transport over vortex ripples in the orbital regime. J Geophys Res Earth Surf 124 (1), 2-20, doi:10.1029/2018JF004741
- Engelund F, Fredsøe J (1976) A sediment transport model for straight alluvial channels. Hydrol Res 7(5), 293-306. doi:10.2166/nh.1976.0019
- Leftheriotis GA, Dimas AA (2022) Morphodynamics of vortex ripple creation under constant and changing oscillatory flow conditions. Coast Eng 177, 104198. doi:10.1016/j.coastaleng.2022.104198
- Miller MC, Komar PD (1980) Oscillation sand ripples generated by laboratory apparatus. J Sediment Res 50(1), 173–182. doi:10.1306/212F799B-2B24-11D7-C
- Nielsen P (1981) Dynamics and geometry of wave-generated ripples. J Geophys Res 86(C7), 6467– 6472. doi:10.1029/JC086iC07p06467
- Smagorinsky J (1963) General circulation experiments with the primitive equations I. The basic experiment. Mon Weather Rev 91, 99–165. doi:10.1175/1520-0493(1963)091<0099:GCEWTP>
- Van Driest ER (1956) On turbulent flow near a wall. J Aeronaut Sci 23(11), 1007–1011. doi:10.2514/8.3713

Representative waves for estimating annually averaged sedimentation and erosion trends in sandy coastal areas using numerical models and artificial neural networks

M. Diamanta^{1*}, M. Chondros¹

¹Laboratory of Harbour Works, School of Civil Engineering, National Technical University of Athens, 5, Heron Polytechniou Str., 15780, Zografou, Greece

*Corresponding author: mardiamanta@gmail.com

Abstract

Process based numerical models are widely recognized as a valuable tool for simulating and predicting changes in coastal bed morphology. However, despite their prevalent use in coastal research studies, they are highly intensive in computational resources and processing capacity, therefore requiring the employment of wave schematization methods in order to reduce the required wave input data and accelerate the simulation processes. This paper introduces a new methodology of wave schematization, combining the use of numerical modelling and Artificial Neural Networks (ANN), in order to derive a set of representative wave conditions that is morphologically equivalent to the full wave climate. The proposed approach utilizes time series of offshore wave characteristics (height, period and direction) that can be obtained from open databases and bathymetric data for the coastal area while the representative sea states are calculated by a trained ANN and are then used as inputs in the simulations carried out by the numerical models in order to obtain predictions on the evolution of coastal bed morphology. The proposed methodology is applied and evaluated against two other well-established methods of wave schematization in the coastal zone of the archaeological site of Archontiki in Psara Island, in Greece, proving its better performance.

Keywords Representative waves, Sediment transport; Coastal Erosion, Artificial Neural Networks.

1 INTRODUCTION

Coastal erosion is a major risk for communities in coastal zones, especially with climate change and increasing human interventions. To that end, coastal engineering scientists have developed powerful numerical models in order to predict changes in seabed morphology overtime, which allows to test and optimize protection schemes for the affected coastal areas. However, the vast majority of these models is computationally intensive, especially for longer time horizons. The Initial Sedimentation and Erosion (ISE) modeling concept (de Vriend, 1993; Roelvink and Reniers, 2012) was developed as a solution to this problem, since it involves using numerical models to simulate wave, hydrodynamic, sediment transport, and morphological processes only once, without updating the bed level after each morphological time-step. This approach allows for the calculation of rates of bed level change for each incident wave scenario, based on the same initial bathymetry, by multiplying the resulting rate of bed level change fields by the annual frequency of occurrence of each wave scenario, and using the sum of these fields to provide an estimate of sedimentation and erosion trends in a coastal study area over one year.

Nevertheless, the implementation of coastal engineering studies typically requires multiple simulations to fully investigate the complex processes that take place in coastal areas, even when employing the ISE modelling approach. Moreover, additional simulations are often necessary to optimize the design of coastal protection works and to test their stability and effectiveness of the structures under various climate change scenarios. To reduce the computational burden of such simulations, offshore wave climate schematization, also known as wave input reduction, is commonly used to reduce the input wave data required for process-based models (Walstra et al., 2013; Benedet et al., 2016; Papadimitriou et al., 2020). The proposed herein approach offers a potential solution to the challenges posed by the increased time and computational demands of numerical simulation models allowing for more efficient and effective simulation of wave processes in coastal environments. This involves the use of wave climate data time series, drawn from open wave databases, which are used to train an Artificial Neural Network

to compute the representative wave conditions which are then used as inputs to the numerical models to predict morphological seabed evolution.

2 PROPOSED METHODOLOGICAL APPROACH

The proposed herein methodology, building upon the concept of Initial Sedimentation and Erosion (ISE) modelling and existing methods of wave schematization, aims to reduce the number of simulation scenarios required to predict the evolution of coastal bed morphology, by training an Artificial Neural Network, to select the equivalent sea states based on the sediment transport potential. Similar to the method proposed by Chondros et al. (2022) a single representative wave is determined for each directional sector of interest. However, with the utilization of the ANN, the proposed methodology aims to achieve a higher level of accuracy in the results while attaining an equally reduced amount of computational effort.

The method, comprises of two main parts, the first of which involves training the ANN, while the second involves the computation of the representative wave scenarios and the implementation of the numerical models in order to obtain the full morphodynamic profile of sedimentation/erosion in the coastal area. The distinct steps of each part are presented as follows.

2.1 Artificial Neural Network (ANN) programming and training

1. The different incident wave scenarios used to train the ANN are determined in this step. The parameters defining each training scenario are the significant wave height (H_s), the peak period (T_p) and the mean wave direction (MWD), while the different combinations of these parameters are selected in order to cover a wide range of possible values that can be encountered in a multivariate wave climate.
2. The bathymetric grid of an idealized shore of uniform bottom slope, equal to that of the study area, is constructed.
3. Simulations are carried out for each of the selected training scenarios, using the characteristic parameters (H_s , T_p , MWD) as inputs. The numerical models (developed by Scientia Maris) utilized, include a parabolic mild slope wave model (Maris PMS) a hydrodynamic model (Maris HYD), and an initial sedimentation/erosion and morphological model (Maris SDT). The outputs of the morphological model, i.e., the rates of bottom level change, will be used as target outputs for the training of the ANN.
4. The ANN is programmed and trained using the collected input and target datasets as described above. Different network architectures are considered in order to select the optimal structure for the ANN, i.e., the number of hidden layers and neurons in each layer. The Mean Square Error and the correlation value, R , between the generated outputs and the target outputs are used to evaluate the network performance.

2.2 Determining the Sediment Transport Equivalent Waves

1. The multivariate wave climate is divided into equally spaced directional bins of 22.5° which subsequently grouped by significant wave height with an interval of 0.5 m. The mean values of the characteristic parameters (H_s , T_p , MWD) are then calculated for each of the abovementioned directional and wave-height bins.
2. For each directional sector, the input data is subjected to a pre-processing procedure which includes the normalization of the mean values that were calculated in step 1 in order to be fed to the trained ANN.
3. The output of the ANN's processing is the longshore sediment transport rate Q (m^3/s), which is used to derive the characteristic parameters of the representative wave of each directional bin, based on the empirical equations developed by Chondros et al. (2022). The determined quantities include the equivalent wave height H_e (m), the equivalent period T_e (s), the equivalent mean wave direction $MWDe$ ($^\circ$) and the equivalent frequency f_e (%).
4. Simulations are performed for each of the equivalent sea-states calculated. The results produced (i.e., the rates of bed level changes calculated by the SDT) are then integrated by assigning the equivalent frequencies of occurrence as weights to the different incident wave scenarios in order to obtain the full sedimentation/erosion profile of the coastal area.

3 APPLICATION AND RESULTS

The proposed methodology is applied in a real-life case study, in the coastal zone of the archaeological site of Archontiki in Psara Island, in Greece, and is evaluated against the Classical Approach and the methodology proposed by Chondros et al. (2022), in order to assess its performance.

3.1 Study Area

The coastal area of Archontiki, extends over an area of about 1.5 km of the NW coastline of Psara Island and houses an ancient archaeological site which was discovered in 1962 consisting of a Mycenaean settlement, a cemetery and a vaulted tomb, parts of which are covered by the sea. Opposite the coast of Archontiki is the isle of Daskalio, which in ancient times was connected to the mainland forming a small peninsula with a natural harbor. To provide a detailed representation of the wave climate in the study area, wave data were obtained from Copernicus Marine Service database utilizing the data package MEDSEA_MULTIYEAR_WAV_006_012, which is the product of a multi-year reanalysis of hourly recorded wave parameters at $1/24^\circ$ horizontal resolution in the area covering the Mediterranean Sea. Given the orientation of the coastline and the wave climate in the area, it is observed that the coast is mainly exposed to waves generating from the NNW, NW, WNW, W, SSW and S directions while being protected by the island of Antipsara from the SW and WSW directions, as shown in Figure 1.

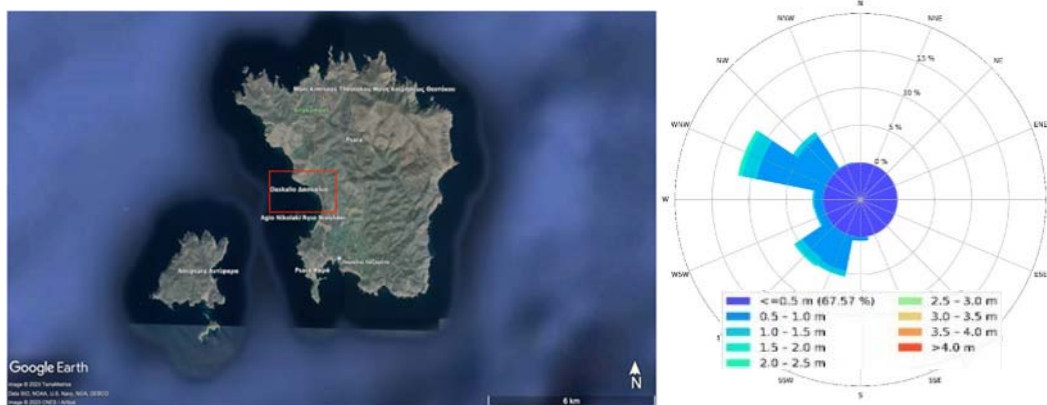


Figure 1. Overview of the study area: (a) The island of Psara and the study area (indicated with red), Google Earth (2022) (b) Wave rose plot of the mean annual wave climate for the study area

In order to illustrate the bathymetry of the seabed in the area, a bathymetric grid was constructed using the Maris BTG numerical tool (Scientia Maris, 2022) and hydrographic charts. The grid, containing a total of 1200 cells in the horizontal x direction and 1080 cells in the vertical y direction was constructed with a fixed spatial step of $dx=dy=2.5$ m. The sediment in the area consists mainly of coarse grain sand, therefore a constant value of $d_{50}=1.8$ mm was assumed throughout the numerical domain.

3.2 ANN Training and Architecture

In order to implement and train the ANN, in the context of the proposed methodology, it is required to select a representative dataset of the characteristic parameters' values, which will adequately cover a range of possible wave conditions. These incident wave scenarios include combinations of wave height H_s (m), peak period T_p (s) that follow the distribution of the actual sea-state dataset that was obtained for the study area and include the maximum and minimum values for which the characteristic parameter pairs occur. The network is then trained using the Levenberg-Marquadt optimization algorithm, which adjusts the weights and biases of the network to minimize the error between predicted and actual outputs. At the end of the process, the ANN should be able to identify the complex relationships between the characteristic parameters (H_s , T_p , MWD) of the input incident wave scenarios and the potential shift in coastal bed morphology that they result in. Various alternative structures of Multilayer Feedforward Neural Networks are considered in order to select the optimal architecture (number of hidden layers and hidden neurons) based on the network's performance. The metrics used for the performance evaluation are the mean square error, MSE, and the correlation coefficient R, and the results of the comparative evaluation of the examined network architectures is illustrated in Figure 3. It is observed that the optimal

network structure has two hidden layers, each containing 12 hidden neurons since it produces the minimum MSE, equal to 1.000236, with the highest correlation factor, R, equal to 0.999. The selected network architecture is shown in Figure 4.

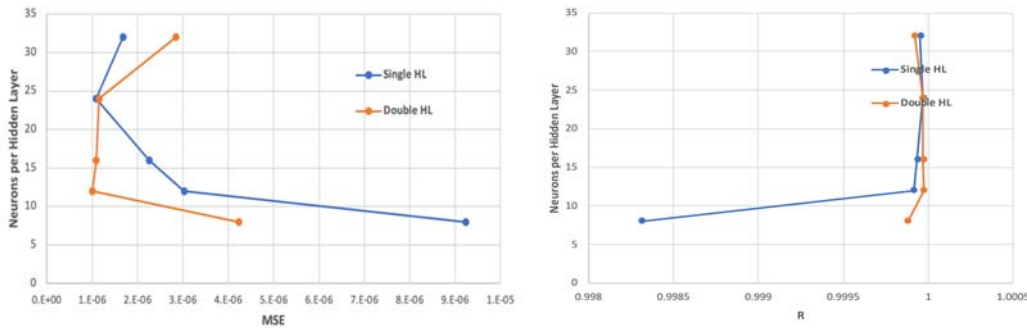


Figure 3 (a) Mean squared errors, MSE, and (b) correlation factors, R, for the considered ANN architectures of single (blue) HL1, and double (orange), HL2, hidden layer networks and various numbers of neurons

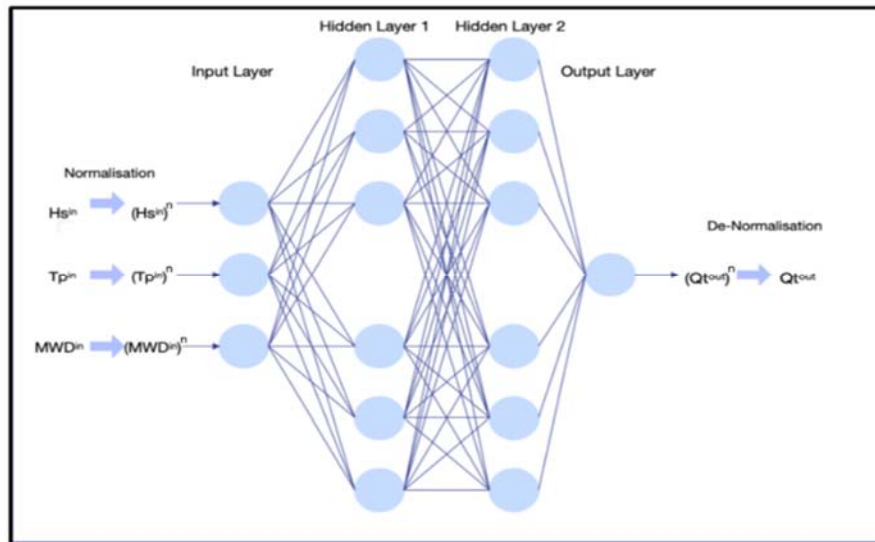


Figure 4. Optimal ANN architecture selected to predict the representative sea-states

3.3 Morphological Modelling Results

After deriving the equivalent waves using the trained ANN, following the process described in section 2.2, and executing in sequence the PMS, HYD, and SDT models for each representative sea-state of the six directional sectors of interest, an integrated rate of bed level change was obtained for the coastal area. The results of the proposed methodology as well as the ones obtained by the implementation Classical Approach and the method proposed by Chondros et al. (2022) are shown in Figure 5. The results of the CA are then used as a benchmark in the evaluation of the accuracy of the proposed method compared to the Chondros et al. (2022) method. The main performance metric considered is the Brier Skill Score, an index widely used in evaluating the performance of morphological evolution models, as shown in Table 1.

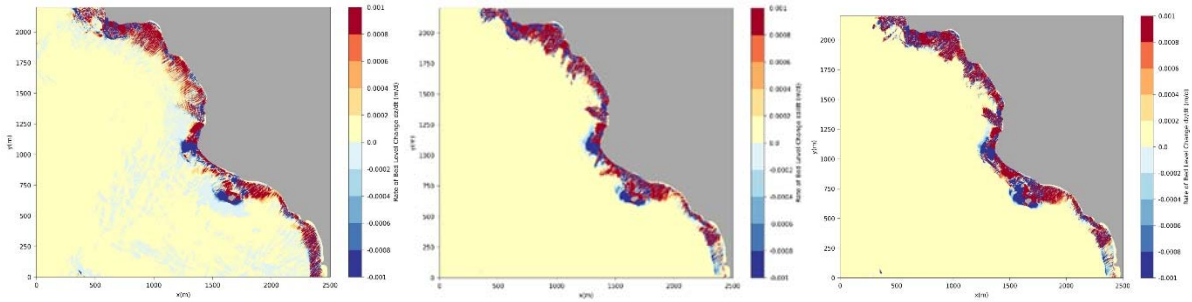


Figure 5. Calculated rates of bed level change obtained by implementing: (a) the CA (b) the Chondros et al. (2022) method and (c) the PA

Table 1. Brier Skill Score of the morphological model adopting the PA and the Chondros et al. (2022) method

	PA	Chondros et al. (2022)
BSS	0.595	0.562

4 DISCUSSION AND CONCLUSIONS

In the light of the abovementioned findings, it can be deduced that the innovative methodology proposed by this research can determine representative waves that can drastically reduce the required simulation effort while simultaneously preserving the accuracy and reliability of the results. The innovative methodology proposed by this research can determine representative waves that can significantly reduce the required simulation effort while maintaining the accuracy and reliability of the results. The proposed methodology is based on the recent approach established by Chondros et al. (2022) and extended by incorporating the development of an Artificial Neural Network (ANN). Compared to the former approach, the proposed methodology does not further reduce the computational burden but offers higher accuracy while maintaining the same required number of simulations. Thus, the proposed methodology provides a valuable tool for engineers and scientists to accelerate the simulations of sedimentation and erosion trends in coastal areas.

To further improve the methodology, the training of the developed ANN could be enhanced by incorporating additional parameters such as bottom slope, sediment grain size, and wave characteristics to generalize the network so that it can be applied to calculate wave representatives in any coastal area. Future research could therefore focus on investigating the appropriate parameters and training methods for the ANN in order to provide a more comprehensive tool for engineers and scientists in the field of coastal engineering.

References

- Benedet, L., Dobrochinski, J. P. F., Walstra, D. J. R., Klein, A. H. F., & Ranasinghe, R. W. M. R. J. B. (2016). A morphological modeling study to compare different methods of wave climate schematization and evaluate strategies to reduce erosion losses from a beach nourishment project. *Coastal engineering*, 112, 69-86.
- Chondros, M., Metallinos, A., Papadimitriou, A., & Tsoukala, V. (2022). Sediment Transport Equivalent Waves for Estimating Annually Averaged Sedimentation and Erosion Trends in Sandy Coastal Areas. *Journal of Marine Science and Engineering*, 10(11), 1726.
- de Vriend, H. J., Zyserman, J., Nicholson, J., Roelvink, J. A., Pechon, P., & Southgate, H. N. (1993). Medium-term 2DH coastal area modelling. *Coastal engineering*, 21(1-3), 193-224.
- Papadimitriou, A.; Panagopoulos, L.; Chondros, M.; Tsoukala, V. A Wave Input-Reduction Method Incorporating Initiation of Sediment Motion. *J. Mar. Sci. Eng.* 2020, 8, 597.
- Roelvink, D. & Reniers, A. (2012). *Guide to Modeling Coastal Morphology*, 1st ed.; Word Scientific: Singapore; p. 292.
- Walstra, D.J.R.; Hoekstra, R.; Tonnon, P.K.; Ruessink, B.G. Input Reduction for Long-Term Morphodynamic Simulations in Wave-Dominated Coastal Settings. *Coast. Eng.* 2013, 77, 57-7.

Revisiting and enhancing the concept of equivalent wave heights

A. Papadimitriou^{1*}, Th. Karambas², V.K. Tsoukala¹

Laboratory of Harbour Works, NTUA, 15780, Zografou, Greece

²Laboratory of Maritime Engineering and Maritime Works, AUTH, 54124, Thessaloniki, Greece

*Corresponding author: andrewtnt@mail.ntua.gr

Abstract

The prediction of coastal bed evolution in timescales of months to years has been at the forefront of coastal engineering research for several decades, due to the implications to the economy, environment, and community safety. Traditionally, process-based models are employed to simulate the morphological bed level changes, however these models are excessively demanding in computational resources. To alleviate somewhat the computational effort levels, the method of reducing the forcing input by computing “equivalent wave heights” has been extensively used in engineering practice. The scope of this research is to examine possible enhancements to the traditional method, by introducing principles driving the long-term bed evolution and incorporating Machine Learning Techniques. In total, 3 alternative configurations to the default “equivalent wave heights” method have been examined, each with different features and assumptions, but all achieving to improve model performance. The findings of this research have strong implications on the reliable prediction of coastal bed evolution with a simultaneous reduction of the required computational effort.

Keywords Equivalent waves, Input reduction, Wave modelling, Process-based models.

1 INTRODUCTION

Process-based models have been traditionally employed to simulate the morphological coastal bed evolution at an inter-annual scale. Despite their widespread usage these models are associated with staggering computational burden. To alleviate this burden, methods to reduce the forcing wave input needed to perform the morphological simulations. To this end, the method of calculating equivalent wave heights (EWH), capable of replicating the morphological bed level evolution induced by the full timeseries of offshore wave characteristics, has been utilized in coastal engineering practice for several decades (Chonwattana et al. 2005, Karambas et al. 2013). This method, based on separating the tri-variate wave climate in fixed directional bins and calculating equivalent wave characteristics based on the energy flux potential of each bin, aims to reduce the required model run-time for the demanding morphological simulations. Despite the widespread usage of this method, a research effort concentrating on examining enhancements of this method and systematically evaluating model results has not been undertaken yet. The objective of this research is to further expand on the concept of EHW, provide and evaluate possible enhancements to increase the reliability of model results, while keeping computational effort at a minimum.

2 MATERIALS AND METHODS

2.1 Methodology and examined configurations

In the present research, the method of Chonwattana et al. (2005) was utilized to compute the equivalent wave characteristics. This method is based on the conservation of the wave energy flux along a way ray and on each directional bin the longshore sediment transport rate is used to calculate a set of constants through the following system of equations:

$$\begin{cases} H_s^2 T_p \sin a_o = C_1 \\ H_s^2 T_p \cos a_o = C_2 \\ H_s^{2.5} \cos(a_o^{0.25}) \sin(2a_o) = C_3 \end{cases} \quad (1)$$

where H_s is the significant wave height, T_p is the peak wave period, a_o the wave incidence angle with respect to the shore normal and C_1, C_2, C_3 as set of constants.

The equivalent values of the constants C_1, C_2, C_3 are calculated as the mean values on each pre-defined directional bin:

$$\begin{cases} C_{1,eq} = \frac{\sum f_i C_{1,i}}{\sum f_i} \\ C_{2,eq} = \frac{\sum f_i C_{2,i}}{\sum f_i} \\ C_{3,eq} = \frac{\sum f_i C_{3,i}}{\sum f_i} \end{cases} \quad (2)$$

where f_i is the frequency of occurrence of each sea-state.

Finally, the offshore equivalent wave characteristics are computed by solving the following set of equations.

$$\begin{cases} a_{o,eq} = \tan^{-1} \frac{C_{1,eq}}{C_{2,eq}} \\ H_{s,eq} = \left[\frac{C_{3,eq}}{(\cos a_o)^{0.25} \sin(2a_{o,eq})} \right]^{2/5} \\ T_{p,eq} = \frac{C_{2,eq}}{H_{s,eq}^2 \cos a_{o,eq}} \end{cases} \quad (3)$$

The default configuration of the EWH method will be thereafter denoted as test EHW-01. In conjunction to this test three additional configurations were considered, aiming to enhance the results of this method, and are briefly described below:

- Test EWH-02: Each directional bin is further subdivided depending on if the energy flux capacity of each individual sea-state exceeds the average energy flux of said directional bin. Effectively, this configuration aims to: a) more adequately describe the diversity of the wave climate more adequately and b) better describe the effect of more energetic sea-states in altering the coastal morphology.
- Test EWH-03: This test does not consider directional bins of fixed size, but it is based on the premise of defining “Transition Zones” where the longshore and cross-shore sediment transport affect the morphological bed evolution interchangeably. Given an arbitrary number of wave incidence angles, three distinct zones can be defined based with the following characteristics: (a) for oblique wave incidence angles relatively parallel to the coastline, the longshore component drives the sediment transport through the wave energy flux, (b) for almost perpendicular wave incidence angles the cross-shore transport is the main driver and its influence can be quantified with the Dean parameter and (c) for the remaining cases of the oblique wave incidence angles, the dominance of longshore and cross-shore transport is interchangeable and can be quantified through the CERC transport formula. When the zones are defined, the equivalent wave characteristics are readily calculated following the principles of EWH-02, but utilizing the appropriate proxy quantity depending on if longshore or cross-shore sediment transport drives the morphological evolution.
- Test EWH-04: This test incorporates the training, validation and implementation of an Artificial Neural Network (ANN), to eliminate sea-states unable to initiate sediment motion based on the Shields criterion of incipient sediment motion, considering only the influence of waves. Then the calculation of the equivalent waves is based on the principles of EWH-02 test. For more details on the training and validation of the ANN, the reader is referred to the publication of Papadimitriou et al. 2022.

2.2 Study area and numerical model

The performance evaluation of the alternative configurations was carried out in the coastal area near the port of Rethymno in Crete, Greece. The simulated area of interest includes the aforementioned port, located in the northern end of Crete within the homonymous bay and the adjacent coastline to the east, which extends approximately 8 km. The numerical simulations were carried out utilizing the MIKE21 CM FM (DHI 2023), an integrated suite containing a spectral wave model, a hydrodynamic and a sand transport/morphology model. A full year of wave records, selected arbitrarily to be the year 2012, are extracted for the execution of the numerical simulations. As a benchmark, a “brute force” simulation containing a detailed representation of the annual wave climate (68 sea-states, obtained by dividing the wave height in 0.5m and the wave incidence angle in 15° intervals) is also executed. The evaluation of model performance will be carried out based on the calculation of the Brier Skill Score (BSS) metric (Sutherland et al. 2004), for an area of interest extending about 4 km from the port’s easternmost breakwater. The wave rose of the offshore wave climate, as well as the numerical mesh and model evaluation area, are showcased in Figure 1.

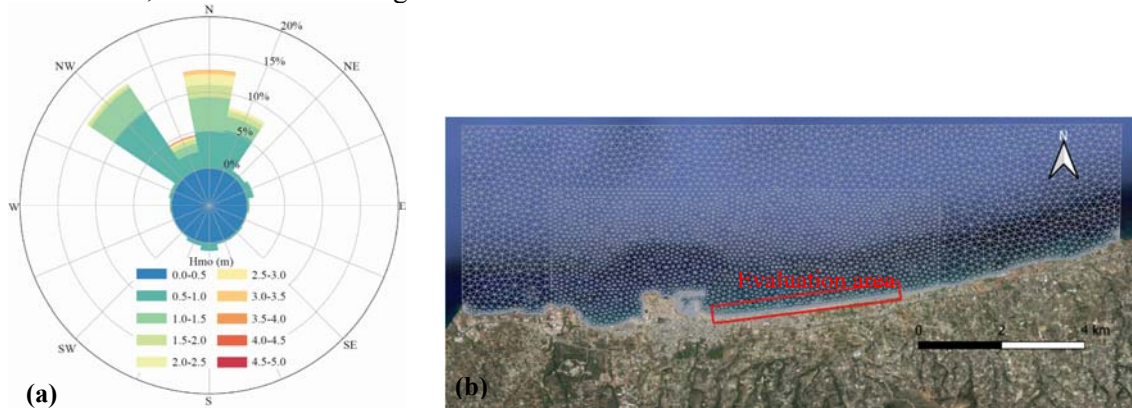


Figure 1. Offshore wave climate and study area: (a) Wave rose (b) Numerical mesh and evaluation area

2.3 Obtained representative wave conditions

For a fair intercomparison, a fixed number of twelve (12) representative wave conditions was considered for all the EHW configurations. The representative wave conditions for EWH-02 and EWH-04 are shown in Table 1, and as a scatter plot for all four methods is depicted in Figure 2.

Table 1. Comparison of representative wave conditions for the EWH-02 and EWH-04 methods

	EWH-02				EWH-04			
	H_s (m)	T_p (s)	a_0 (°)	f_i (%)	H_s (m)	T_p (s)	a_0 (°)	f_i (%)
1	0.43	5.71	-76.33	0.69	0.73	5.02	-71.75	0.32
2	0.43	4.45	-42.54	17.55	0.85	5.21	-46.48	8.97
3	0.79	4.63	-8.39	21.39	1.15	5.23	-7.74	11.12
4	0.54	5.16	12.82	21.81	0.96	5.76	9.74	14.13
5	0.27	5.74	42.71	4.92	0.68	5.5	41.45	0.45
6	0.31	5.96	70.29	1.93	0.71	6.02	67.84	0.82
7	0.94	4.33	-67.08	0.34	1.32	6.76	-69.8	0.11
8	1.06	5.05	-46.8	12.13	1.42	5.88	-46.07	4.33
9	2.42	5.22	-7.49	5.17	2.57	5.74	-6.97	4.31
10	1.71	5.68	7.04	11.72	2.01	6.33	6.61	5.44
11	0.69	5.91	41.05	1.17	0.87	6.62	39.33	0.37
12	0.87	5.98	72.06	1.17	1.29	5.8	76.79	0.24
total				100.00				50.61

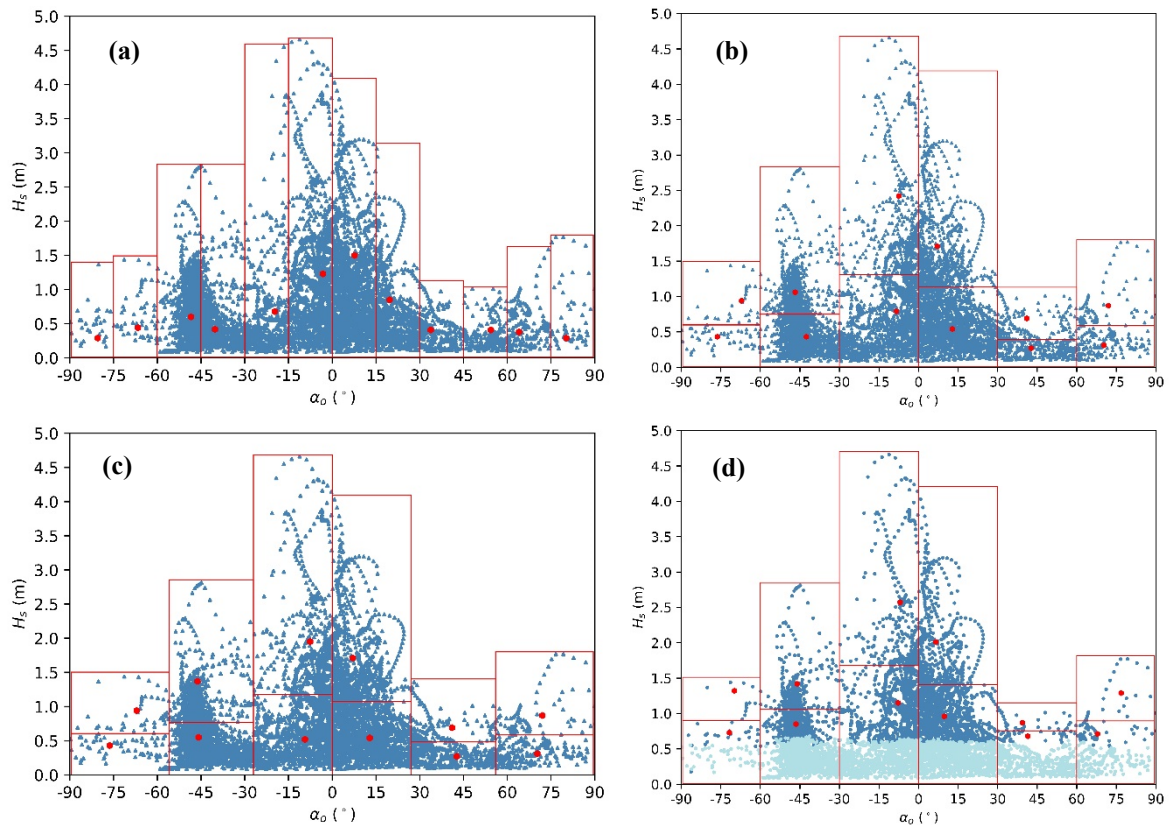


Figure 2. Obtained 12 representative wave conditions: **(a)** EWH-01, **(b)** EWH-02, **(c)** EWH-03, **(d)** EWH-04

As shown in Figure 2, the default method (EWH-01) does not describe in a concise manner the more energetic sea-states that are present especially in the range of $\alpha_o = [-30^\circ, 15^\circ]$. On the other hand, the subsequent subdivision in each directional bin (EWH-02 & EWH-03) seems to lead to a better prescription of the diversity of the wave climate. It should be noted that the representatives obtained from EWH-03 are quite similar to those obtained in EWH-02, however EWH-03 is far more complex in conceptualization & implementation. Finally, the elimination of lowly energetic sea-states (denoted with light-blue markers in Figure 2d) by implementing a trained ANN (EWH-04) shifts the representatives to a set of more energetic wave characteristics compared to the other tests.

3 RESULTS

To intercompare and evaluate the four examined methods, both a visual inspection of model results and calculation of the BSS will be undertaken. It is noteworthy that for all tests, a significant model run time reduction was observed when reducing the forcing input from 68 to 12 sea-states (reduction of about 450%).

In Figure 3, the bed level change results calculated by implementing the MIKE21 CM FM model forced with the wave characteristics of the brute force simulation (top) and EWH-04 (bottom) are shown.

Inspecting the results visually, it can be deduced from Figure 3 that EWH-04 simulation can capture in a very satisfying manner the morphological bed level change patterns induced by the “brute force” simulation. In particular, in both simulations the accretion at the port’s entrance and the adjacent shore to the easternmost breakwater is reproduced adequately.

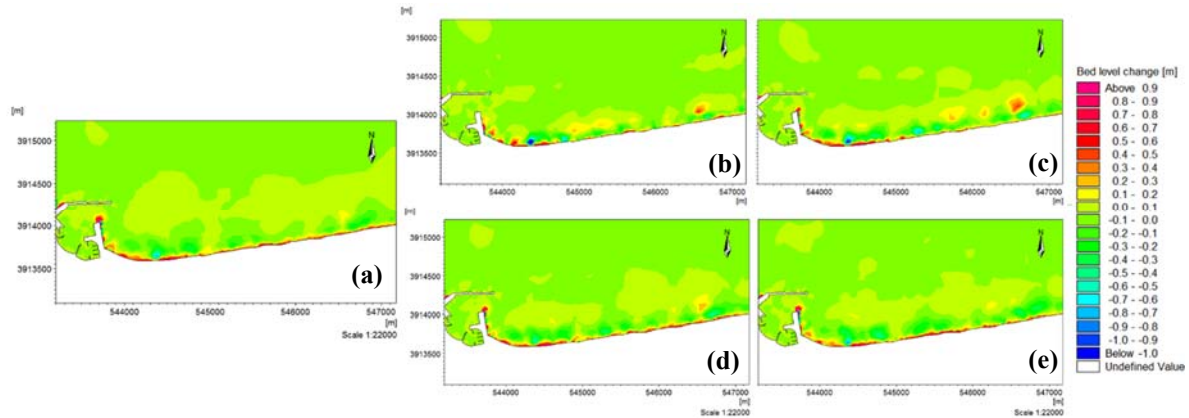


Figure 3. Computed bed level change by implementing the: (a) “brute force” simulation, (b) EWH-01, (c) EWH-02, (d) EWH-03, (e) EWH-04.

The calculated BSS values of each test are shown in Table 2.

Table 2. Calculated BSS values for each EWH test simulation

	EWH-01	EWH-02	EWH-03	EWH-04
BSS	0.24	0.56	0.58	0.65

It is observed that a significant model performance increase is achieved in all tests (EWH-02, EWH-03 and EWH-04) compared to the default test (EWH-01). With respect to the BSS classification (Sutherland et al. 2004), the default test gave a “Good” model performance, while all the newly conceptualized tests are classified as “Excellent”. Ultimately, the best performing test is considered EWH-04, which incorporates an ANN to eliminate sea-states that are deemed insignificant in shaping the morphological bed evolution. The inclusion of the trained ANN in EWH-04 requires minimal computational effort and user interference but also provides reliable results with respect to the “brute force” simulation.

4 CONCLUSIONS

From the thorough evaluation of the equivalent wave heights method examined in the framework of this research it is observed that all examined configurations provided a significant enhancement of the results compared to the default implementation. The best performing method is EWH-04, which incorporates an Artificial Neural Network to eliminate lowly energetic sea-states. The methodologies presented in this research can aid in obtaining more accurate model results while simultaneously reducing the computational burden, based on the principles of a method implemented widely in practical applications.

References

- Chonwattana S, Weesakul S, Vongvisessomjai S (2005) 3D Modeling of Morphological Changes using Representative Waves. *Coast Eng J* 47:205-229. doi:10.1142/S0578563405001240
- Karambas T, Koutandos E, Kampanis N (2013) Numerical simulation of wave-induced morphology evolution. Paper presented at the ICE - Maritime Engineering Conference, London, United Kingdom.
- DHI (2023) MIKE21 Flow Model FM User Guide. Copenhagen, Denmark
- Papadimitriou A, Chondros M, Metallinos A, Tsoukala V (2022) Accelerating predictions of morphological bed evolution by combining numerical modelling and Artificial Neural Networks. *J of Mar Sci and Eng* 10:1621. doi:10.3390/jmse10111621
- Sutherland J, Peet AH, Soulsby RL (2004) Evaluating the performance of morphological models. *Coast Eng* 51: 917-939. doi:10.1016/j.coastaleng.2004.07.01

Wave input reduction methods for annual bed evolution applications

A. Papadimitriou¹*, V.K. Tsoukala¹

¹ Laboratory of Harbour Works, NTUA, 15780, Zografou, Greece

*Corresponding author: andrewtnt@mail.ntua.gr

Abstract

The numerical prediction of the annual coastal bed evolution is mandatory to identify possible erosion areas and establish the corresponding remediation measures. However, the models tasked with this prediction are associated with significant computational burden, especially considering the vast amount of wave input data that are used to force them. To alleviate somewhat the computational effort, input reduction methods concentrating on reducing the required forcing input have been employed in many applications. The scope of this research is twofold, to develop new input reduction methods that can improve the reliability of model predictions and provide a comprehensive evaluation on which is the optimal method depending on the model configuration. Based on the evaluation carried out during this research the best performing method incorporates an Artificial Neural Network that is tasked with eliminating sea-states considered unable to initiate sediment motion. The findings of this research provide initial guidelines and recommendations on the advantages and limitations of each examined input reduction method to be implemented in practical coastal engineering applications.

Keywords Input reduction, Wave modelling, Coastal area models, Morphological evolution.

1 INTRODUCTION

The prediction of coastal bed level change at an annual scale is of particular interest to engineers, scientists and the public due to the strong implications to the environment, economy and community safety. In the scales of interest to engineers (e.g., for areas extending up to a few kilometers and for a time span of 1-10 years) and when distinction between cross-shore and longshore processes is not evident, coastal area models are applied to predict the coastal bed evolution. However, these models are associated with staggering computational burden, rendering the prediction of coastal bed evolution a tedious task. Hence, various wave input reduction (IR) methods have been developed (Papadimitriou et al. 2020) all aiming to reduce the forcing input of the numerical models and reproduce the morphological bed evolution induced by the full timeseries of wave characteristics. The input reduction methods can be divided in three branches:

- Representative Morphological or Equivalent Wave Height (EWH) selection methods (Chonwattana et al. 2005)
- Binning input reduction methods (Papadimitriou et al. 2020)
- Clustering algorithms (Papadimitriou et al. 2022)

Depending on the exchange of feedback between waves and hydro-morphodynamics, two distinct approaches can be distinguished depending on the operation of the coastal area models: (a) the “Morphostatic Approach” where the wave, hydrodynamic and wave simulations are executed in sequency considering the same initial bathymetry and (b) the “Morphodynamic” approach where the constant feedback between waves, hydrodynamics and morphodynamics is considered and bed updating in undertaken at each model time step.

Considering the implications of each of the two approaches on the accuracy of the results, as well as the increased availability of offshore sea-state characteristics from metocean databases, the scope of this research is to further expand on the concept of wave IR methods and provide a thorough evaluation and practical guidelines on the selection of the optimal IR method for each case.

2 MATERIALS AND METHODS

2.1 Methodological approach and implemented Input Reduction methods

Hereafter, a brief overview of widely used IR methods, as well as new ones developed in the framework of this research will be provided for each IR branch.

2.1.1 Binning Input Reduction Methods

Binning methods constitute the most widely used category of IR methods (Papadimitriou et al. 2020). They are based on the notion of dividing the wave climate into wave height and wave direction bins, with each containing an equal fraction of a proxy quantity considered vital in shaping the morphological bed evolution at annual timescales (e.g., wave energy flux, longshore sediment transport rate). In the framework of this research, a novel IR method based on the elimination of sea-states considered unable to initiate sediment motion, and thus further reducing the computational effort, is conceptualized and tested alongside the widely used method of Binning IR based on the wave energy flux capacity.

- EF Method: Definition of bins utilizing as a proxy quantity the wave energy flux.
- PR Method: Elimination of sea-states considered unable to initiate sediment motion in the nearshore and utilizing the sediment pick-up rate function as the proxy quantity to define the bins. For more details the reader is referred to Papadimitriou et al. 2020.

2.1.2 Clustering algorithms

Clustering algorithms have been employed in big data analysis in various disciplines and belong to the unsupervised machine learning techniques. In general, clustering algorithms divide a multivariate dataspace (timeseries of offshore sea-state wave characteristics in this case) by initially selecting an arbitrary number of centroids and grouping the dataset into clusters and then recomputing the centroids by an iterative procedure. In total, two methods were used and evaluated in this research, namely:

- KM-01: Default implementation of the widely used K-Means clustering algorithm.
- KM-02. Centroid initialization based on ones initially obtained by implementation of the PR Binning method, in an attempt to introduce a quantity influencing the nearshore morphological evolution and somewhat alleviate the unsupervised nature of the K-Means algorithm.

2.1.3 “Equivalent Wave Height” selection methods

The principles of the branch of Equivalent Wave Height (EWH) reduction methods are quite similar to the Binning ones. In EWH methods however, the bins are defined in the wave incidence angle directional space only and have a fixed size. In each bin, a wave representative condition is calculated based on the conservation of the wave energy flux (Chonwattana et al. 2005). In total, two methods were implemented:

- EWH-01 Method: Default method presented in Chonwattana et al. 2005.
- EWH-02 Method: This test incorporates the training, validation and implementation of an Artificial Neural Network (ANN), to eliminate sea-states unable to initiate sediment motion due to the effect of waves. Then the calculation of the equivalent waves follows by further subdividing each directional bin and creating two new classes based on the exceedance of the average energy flux potential. For more details on the training and validation of the ANN, the reader is referred to the publication of Papadimitriou et al. 2022.

2.2 Study area and numerical model setup

Performance evaluation of all the IR methods was undertaken in the coastal area near the port of Rethymno in Crete, Greece. The area of interest includes the aforementioned port and the adjacent coastline, which is approximately 8 km in length. The numerical simulations were carried out utilizing the MIKE21 CM FM (DHI 2023), an integrated coastal area model containing a spectral wave model, a hydrodynamic and a sand transport/morphology model. A full year of wave records, chosen to be the year 2012, was extracted for the execution of the numerical simulations. Two “brute force” simulations representing the full timeseries of offshore sea-state characteristics were considered as a benchmark for the model evaluation. It is noted that for the “Morphodynamic” approach the “brute force” simulation

contained the full timeseries, while in the “Morphostatic” approach it was a detailed representation of the full timeseries, containing 68 sea-states, obtained by dividing the wave climate in 0.5 wave height intervals and 15° incidence wave angle bins. The evaluation of model performance was based on the calculation of the Brier Skill Score (BSS) metric (Sutherland et al. 2004), for an area of interest extending about 4 km from the port’s easternmost breakwater. To obtain a fair intercomparison between each method a fixed number of 12 representative conditions were considered throughout the simulations. The wave rose of the offshore wave climate, as well as the representatives obtained by implementing the PR method of input reduction, are showcased in Figure 1.

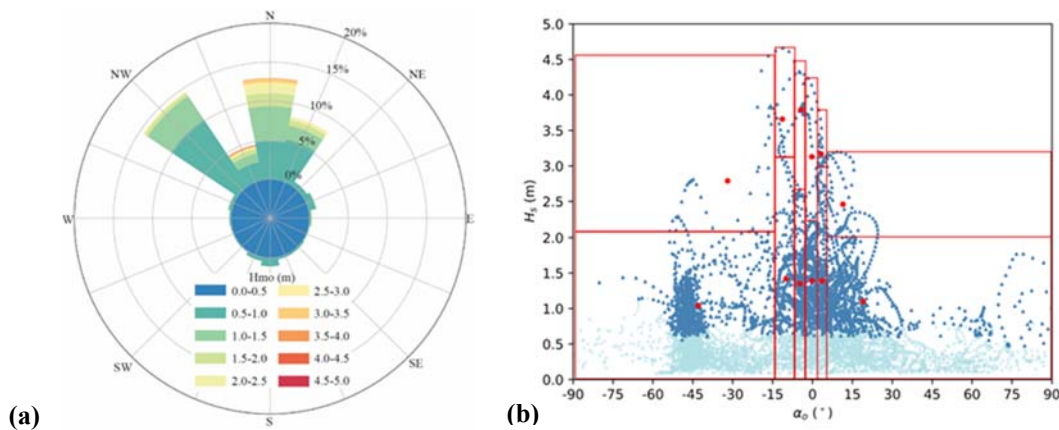


Figure 1. Offshore wave climate and study area: **(a)** Wave rose for the year 2012, **(b)** obtained 12 representative waves conditions of the PR method of input reduction (light blue markers denote eliminated sea-states)

To provide a comparative overview of the differences between the IR methods, the representative wave conditions with the respective obtained by implementing the EF and PR methods are shown in Table 1. Observing the respective classes and due to the elimination of sea-states considered unable to initiate sediment motion, it can be deduced that the PR method contains more extreme sea-states (e.g. bin 6) while also reducing the frequency of occurrence of lowly energetic sea-states compared to the EF method.

Table 1. Comparison of representative wave conditions for the EF and PR Input Reduction methods

	EF method				PR method			
	H_s (m)	T_p (s)	α_0 (°)	f_i (%)	H_s (m)	T_p (s)	α_0 (°)	f_i (%)
1	0.51	5.05	-43.60	30.68	1.04	6.26	-42.93	29.29
2	1.44	6.87	-45.15	3.78	2.79	8.35	-31.88	1.22
3	0.83	5.20	-12.99	8.52	1.42	6.62	-9.98	8.64
4	3.53	8.77	-12.95	0.52	3.66	8.88	-11.35	0.60
5	0.94	5.59	-4.86	7.93	1.35	6.50	-4.72	10.68
6	2.91	8.17	-5.02	0.78	3.79	8.99	-4.42	0.60
7	0.90	5.43	-0.14	8.52	1.39	6.49	-0.19	10.94
8	2.61	7.98	0.54	1.00	3.13	8.41	-0.31	0.99
9	0.91	5.39	5.00	8.22	1.39	6.37	3.57	9.03
10	2.97	8.20	4.20	0.80	3.17	8.44	3.25	1.05
11	0.54	4.61	28.72	26.95	1.10	5.98	19.03	24.83
12	1.85	7.01	16.33	2.29	2.46	7.65	11.45	2.13

3 RESULTS AND DISCUSSION

The evaluation of the wave IR methods concerned not only the model performance based on the obtained BSS values but also the achieved levels of model run-time reduction. In Figure 2, the bed level change

results calculated by implementing the MIKE21 CM FM model forced with the wave characteristics of the brute force simulation and each examined IR methods are shown. It is noted that these results concern simulations conducted through the “Morphodynamic” simulation approach.

Inspecting the results visually, it was observed that all the simulations forced with the representative inputs can capture in a very satisfying manner the morphological bed level change patterns induced by the “brute force” simulation. In particular, the accretion at the port’s entrance and the adjacent shore to the easternmost breakwater were reproduced adequately, however differences mostly in the magnitude of the observed accretion were spotted. Out of the methods shown in Figure 2, the best reproduction of the accretion/erosion patterns of the “brute force” simulation was achieved through method EWH-02, while the most notable differences were identified in the KM-01 method.

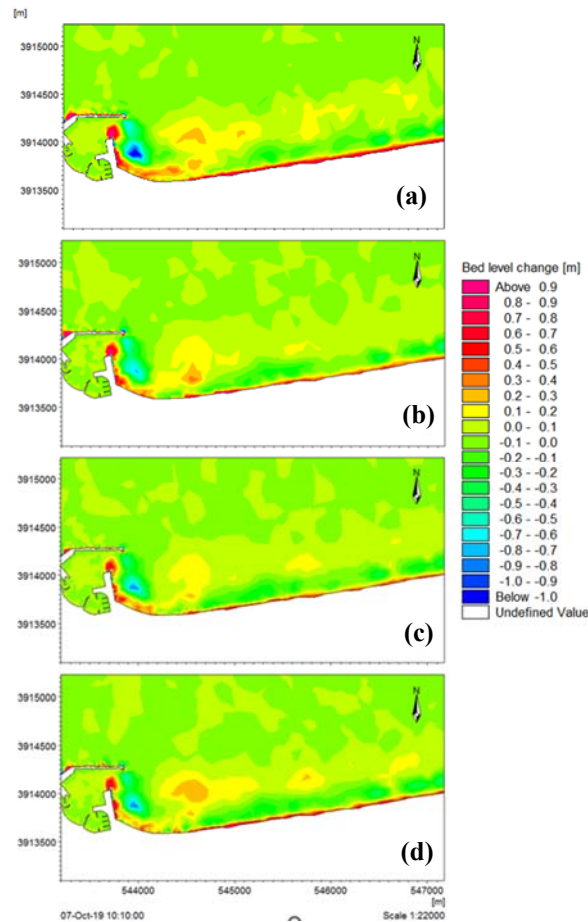


Figure 2. Computed bed level change by implementing the: (a) “brute force” simulation (b) EF method (c) KM-01 method (d) EWH-02 method

The calculated BSS values of each test are shown in Table 2, along with the model run-time reduction (compared to the benchmark “brute force” simulation) and the respective simulation approach that was followed.

Concerning the “Morphodynamic” simulation approach, it was observed that the highest BSS values were obtained by the EF method of wave schematization. However, it is noted that in this approach, the time reduction is relatively small compared to the brute force simulation, since the total model-run time is the same for the “brute force” as well as for the simulations with reduced set of input. In contrast, only for a small penalty in model performance, the effective reduction of the dataset for the PR and EWH-02 methods, due to the elimination of lowly energetic sea-states, led to a significant percentage reduction of 60-63% with regards to model run-time. For the “Morphostatic” approach the model run-time reduction is far more noticeable, due to the shear reduction of the number of simulations to be performed. It is noted that the default implementation of the EW-01 method showed the worse

performance out of all the tested IR methods. On the other hand, the method EWH-02 was associated with the highest BSS values, closely followed by the EF method. The exemplary performance of the EWH-02 method can be attributed to the added value of incorporating a properly trained ANN, with minimal computational effort requirements and user interference, that also produced reliable results with respect to the benchmark “brute force” simulation.

Table 2. Calculated BSS values for each examined test simulation.

IR method	BSS (Classification)	Model run-time reduction (%)	Simulation approach
EF	0.84 (E)	13	Morphodynamic
PR	0.72 (E)	63	Morphodynamic
KM-01	0.63 (E)	17	Morphodynamic
KM-02	0.71 (E)	16	Morphodynamic
EWH-02	0.73 (E)	60	Morphodynamic
EF	0.52 (G)	462	Morphostatic
EWH-01	0.24 (G)	485	Morphostatic
EWH-02	0.58 (E)	468	Morphostatic

4 CONCLUSIONS

The evaluation of the IR methods, conducted in the framework of this research, focused on not only the obtained BSS values (the higher the BSS the better the performance), but also the computational efficiency. After the comparative analysis, it was determined that elimination of lowly energetic sea-states either outright led to higher BSS values (in the Morphostatic approach) or greatly reduced the computational burden, albeit with a small penalty in performance (in the Morphodynamic approach). The method EWH-02 was found to be the best one based on these two factors, achieving reliable results and significant model run-time reduction. Consequently, based on the assessment conducted in the framework of this research, it is advised to use this method for practical applications. Building upon additional investigations of this research, it is also advised to select a number of 12 representative wave conditions to replicate the morphological evolutions induced by an annual wave climate.

The findings of this research have strong implications and provide the engineering community with guidelines and recommendations on which IR method is optimal based on the model configuration, as well as the adequate number of wave representative conditions that should be selected.

References

- Chonwattana S, Weesakul S, Vongvisessomjai S (2005) 3D Modeling of Morphological Changes using Representative Waves. *Coast Eng J* 47:205-229. doi:10.1142/S0578563405001240
- DHI (2023) MIKE21 Flow Model FM User Guide. Copenhagen, Denmark
- Papadimitriou A, Panagopoulos L, Chondros M, Tsoukala V (2020) A wave input reduction method incorporating initiation of sediment motion. *J Mar Sci Eng* 8:597. doi:10.3390/jmse8080597
- Papadimitriou A, Chondros M, Metallinos A, Tsoukala V (2022) Accelerating predictions of morphological bed evolution by combining numerical modelling and Artificial Neural Networks. *J of Mar Sci and Eng* 10:1621. doi:10.3390/jmse10111621
- Papadimitriou A, Tsoukala V (2022) Performance evaluation of the K-Means clustering algorithm for the prediction of annual bed morphological evolution. Paper presented in the 7th IAHR Europe Congress, Athens, Greece
- Sutherland J, Peet AH, Soulsby RL (2004) Evaluating the performance of morphological models. *Coast Eng* 51:917-939. doi:10.1016/j.coastaleng.2004.07.015

Decision-making tool for mitigation of the coastal erosion and extreme wave impacts in the coastal zone, in the context of climate change

S. Liaros¹, S.E. Poulos^{2,3*}, N. Kampanis², J.D. Alexopoulos³, G. Alexandrakis², A. Karditsa^{2,4}, G. Ghionis³, Emm. Vassilakis³, M. Hatzaki³, P. Nastos³, P. Nomikou³, V. Kotinas³, E-S. Stanota¹, A. Nteris¹, V. Methenitis², G.S. Mitsika³, D. Lampridou³, E. Margaritou², S. Skovolias¹, K. Nikolaou¹, A. Stamatoglou¹, I.K. Giannopoulos³, V. Gkossios³, A. Konsolaki³, G. Kontostavlos³, M. Konstantopoulou³, M. Panagou¹, N. Gkogkos¹, L. Roussos¹, I. Exintavelonis¹, H. Roukouni¹, K. Stamatoglou¹

¹ Ilida Consulting Engineers S.A., 63 Arch. Elis, 27059, Havari, Ilia (info@ilida-eng.gr)

² Institute of Computational Mathematics, Foundation for Research and Technology, 100 Nikolaos Plastira, Vasilika Vouton, 70013 Heraklion, Crete (kampanis@iacm.forth.gr)

³ Faculty of Geology & Geoenvironment, National and Kapodistrian University of Athens, Panepistimiopoli – Zografou, 15784, Attiki (jalexopoulos@geol.uoa.gr)

⁴ Department of Ports Management and Shipping, National and Kapodistrian University of Athens, Psachna Evias, 34400, Evia (kkarditsa@pms.uoa.gr)

*Corresponding author: e-mail: poulos@geol.uoa.gr

Abstract

The tool assesses natural factors and the impact of human activities as well as the available mitigation measures in a cost-benefit perspective and with a view to mitigating the impacts of climate change. Therefore, the tool is designed to respond to both erosion (as a natural disaster) and erosion due to human (inappropriate) intervention, as well as CM&D (e.g., sea level rise, extreme wave events). The innovation of the project is based on the creation of a multi-parameter decision making tool (ILIDA_KIT) related to climate change mitigation and resilience to coastal erosion and extreme wave events in the context of integrated coastal zone management. ILIDA_KIT relies on a multi-disciplinary interactive platform in a GIS environment that through the development of a set of appropriate indicators (environmental, anthropogeographic, economic) can be parameterised. The ultimate purpose of the tool is to select the most appropriate intervention (intensity, size, time horizon) measure, based on the cost-benefit analysis, considering both the protection and the sustainable development of the coastal zone.

Keywords: Coastal zone management, sea level rise, environmental indicators, coastal works

1 INTRODUCTION

The coastal zone, which represents an interface space, between ocean and land areas, is highly dynamic but also sensitive to natural changes and human interventions (Martins et al., 2002). Coastal areas are essential also to many local and national economies as it hosts about 10% of the world's population that live or work in it. On the other hand, coastal populations are highly vulnerable to climate change, being particularly affected by rises in sea level and wave height, coastal erosion, cyclones, and flooding (Carmo, 2018).

In particular sea-level rise may cause coastal flooding, seawater intrusion, inundation of land habitat changes in shorelines and a series of environmental impacts (e.g., lead to the degradation of coastal ecosystems such as salt marshes, mangrove forests, seagrass beds, soft sediments, kelp forests and coral and oyster reefs. Moreover, as marine economy corresponds to a considerable proportion of national GDP and employment in many coastal countries, extreme weather fluctuations, sea-level rise and other climatic changes will affect sectors such as tourism, fisheries and aquaculture (Allan, et al., 2021). It is also clear that human action (strong urban and industrial pressures), has been the primary cause of the current imbalances, both, directly (through local actions) and indirectly (through contributions, to global warming and climate change) (Bullimore, 2014). It is, therefore, crucial to discuss schemes of intervention that are acceptable to stakeholders and local communities. Meanwhile, coastal managers and policymakers should make effective and, timely decisions on the use of appropriate adaptation measures, for the immediate and longer time-periods.

The objective of the project is the development of a multi-parameter decision making tool (ILIDA_KIT) for the successful management of coastal erosion and the impacts of extreme wave events, with emphasis on coastal zones of tourist interest, in the context of integrated coastal zone adaptation management and, in particular, on mitigation and resilience to the already manifested climate change.

2 METHODOLOGICAL APPROACH

The methodological approach of the ILIDA_KIT implementation includes the following stages:

Stage-1: In the first stage, the causes of erosion (as a natural disaster, human intervention, or climate change) are identified, as well as the frequency and magnitude of extreme wave events and their evolution over time. An optimal methodological approach is sought to assess the contribution of natural factors to the evolution of coasts, and in particular beaches facing erosion, and the impact of extreme wave events. Next, the contribution of anthropogenic factors to coastal evolution, whether direct (e.g., coastal structures) or indirect (e.g., river dams). The existing institutional framework is recorded and evaluated and good practices in addressing the impacts of climate change from Greece and elsewhere are analyzed. Considering the above physical and social information, the critical coastal area for the implementation of the tool is spatially defined.

Stage-2. In the 2nd stage, all the information needed to manage coastal erosion (current and future) and extreme storms in general are gathered, in order to be applied to the pilot area. The information to be collected concerns the geo-environment, socio-economic characteristics, as well as the institutional framework in national and European context (ILIDA CONSULTING ENGINEERS S.A.). The physical and human geographic characteristics will be extracted from satellite data, historical aerial photographs, existing maps and environmental studies, and additional field work will be carried out. The western coastal zone of the Peloponnese and the northern coast of the Messinian Gulf were selected for the development of the tool (Fig.1); this choice is based on the fact that ILIDA CONSULTING ENGINEERS S.A. and the Department of Geology and Geoenvironment (NKUA) have long experience in research of these areas.

Stage-3: In Stage 3, the vulnerability of the coastal zone to erosion and extreme wave events is parameterized (development / use of indicators) based on the intensity, frequency of occurrence of the phenomena and their spatial impact (current and future) on the coastal ecosystem (geo-environment). Subsequently, their impact on human presence and activity (society-economy) is assessed through the development and use of appropriate indicators. In addition, the available technical interventions (indirect or direct), the institutional framework and the physical parameters governing their selection and, finally, an estimate of their implementation (construction) costs, are described and analyzed.

Stage-4: In stage 4, the ILIDA_KIT will be developed, which through a multi-criteria analysis will be used to select the action (no intervention, mild technical intervention, hard technical intervention), which methodologically results from a computational process on an interactive information platform from information layers structured in GIS and quantified in the form of indicators. The tool will be applied to the selected area and then tested with other coastal areas (e.g., Katerini Beach, Kokkini Hani in Crete) that have already suffered erosion and host coastal projects to address it.

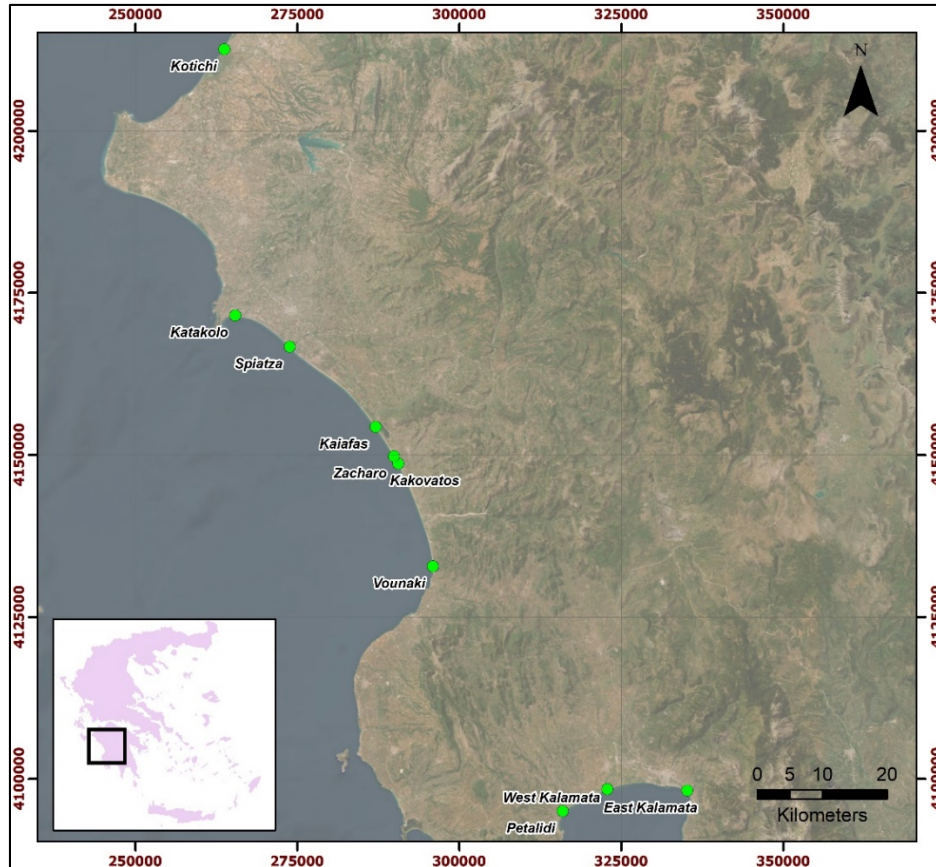


Figure 1. Coastal sites under investigation

Table 1. Work packages (WP) and the scope

<p>WP-1. Assessment of natural processes related to coastal zone formation/evolution and to disasters due to climate change and extreme wave events.</p>	<p>The scope of WP-1 is to identify the factors that control the morphological evolution of the coasts and in particular of the beaches and the factors that cause coastal erosion (CE) and extreme wave events (EWE).</p>
<p>WP-2. Registration of the current state of the coastal zone</p>	<p>The purpose of WP-2 is to obtain all the necessary data and information to develop the assessment indicators (WP-3) for the evaluation of the impacts of coastal erosion (CE) and extreme wave events (EWE), which will then be integrated into the ILDA_KIT (WP-4).</p>
<p>WP-3. Development of an Evaluation Indicator System</p>	<p>The objective of the WP-3 is to develop the scientific methodology to exploit the data selected in WP-1 and WP-2 by developing a system of indicators that provide a basis for assessing both the vulnerability of the coastal zone to erosion (current and future) and the spatio-temporal occurrence of extreme wave events together with the socio-economic evaluation of their impacts.</p>
<p>WP-4. Design - build - implement a decision making system tool – ILIDA_KIT</p>	<p>WP-4 aims at the design, operational implementation and subsequent actions for the commercialization of the ILIDA_KIT decision making tool.</p>

3 COLLABORATIVE ORGANISATIONS

The project is materialized by three partners: (1) Ilida Consulting Engineers S.A.; (2) Institute of Computational Mathematics (Foundation for Research and Technology); and (3) Department of Geology & Geoenvironment (National and Kapodistrian University of Athens).

ILIDA CONSULTING ENGINEERS S.A. undertakes the preparation of implementation and supervision studies regarding Environment and sustainable development, Topography – GIS, Spatial planning – Urban planning, Project Management-Technical Consulting, National Cadastre, Hydraulic and Architectural works, Reenactments and Transportation Projects. It also participates in research projects related (directly and indirectly) to the above objects and the utilization of research products. The company also develops computer software and services related to the design or supervision of technical projects and the provision of services in the fields of business organisation, time and cost management of projects and planning.

Institute of Computational Mathematics (ICM) conducts research in applied mathematics and simulation science belonging to the Foundation for Research and Technology-Hellas (FORTH). Within ICM, the Laboratory of Coastal and Marine Research is active in research and applications related to the coastal environment, with applications in coastal hydrodynamics, hydrology, development of high resolution monitoring systems, and integrated environmental planning systems. It focuses on innovative scientific and research activities, in areas such as risk assessment and prevention measures regarding the socio-economic impacts of climate change and in the planning and management of activities in the coastal zone.

Department of Geology and Geoenvironment of the NKUA, participates with three (3) laboratories: (1) *Geophysics Laboratory* specialized in applied studies of geological and lithological conditions, geo-environmental investigations, determination of aquifer quality, investigation of landslides and subsidence, through the application of sophisticated techniques of high resolution (electrical resistivity tomography, ground penetrating radar, seismic refraction tomography, etc.); (2) *Laboratory of Climatology and Atmospheric Environment*, focusing on the study of climate variability, both on a regional and global scale, the impact of weather and climate on public health, the investigation of causes and processes related to extreme weather events (heat waves, droughts, floods, tornadoes, etc.); and (3) *Laboratory of Physical Geography* which is involved in the investigation of processes related to the evolution of the landscape (including human activities) with the synergy of GIS and remote sensing technologies.

4 PROJECT'S OUTPUTS

ILIDA_KIT, in the context of integrated coastal zone management, relies on a multi-disciplinary interactive platform in a GIS environment that through the development of a set of appropriate indicators (environmental, anthropogeographic, economic) can be parameterised. The results of the tool are as follow:

- Assessment of the main causes (natural and human) of erosion, including assessments of beach retreat due to climate change.
- Provide a response to the relationship between extreme wave events and climate variability and change, including future approaches (2050 and 2100).
- Comprehensive assessment of the impacts and costs of climate change on different components of the natural (ecosystem) and socio-economic coastal environment.
- Selection of the most appropriate interventions (answer to the question: No intervention - No intervention but with change in human presence and action - Mild technical intervention – Hard technical intervention) to address erosion and the effects of extreme wave events based on realistic construction cost/benefit (socio-economic) estimates.
- The creation of an integrated (WEB-GIS) geo-spatial data base with emphasis on the geo-environmental and socio-economic conditions, which can be integrated/utilized in general management (spatial) plans of the coastal zone, in an ecosystemic direction, while

contributing to the fulfillment of contractual legal obligations of Greece (e.g., Directive 2014/52/EU).

- Significant contribution to the economy at local, regional and national level by protecting the domestic product produced in the coastal zone through appropriate interventions and saving money by avoiding unnecessary interventions (e.g., failures of costly technical projects).
- Finally, the decision-making tool produced can be used both in other coastal areas of Greece and in other countries in the SE Mediterranean region, where coastal zone management needs to be adapted to or mitigate the effects of climate change.

Acknowledgements

Project ILIDA_KIT is funded by the project “Decision-making tool for the confrontation of coastal erosion and extreme wave events in the coastal zone, in the context of climate change” (GSRT_T2EDK-02795 with MIS 5129417), financed by the Sectoral Operational Programme «Competitiveness, Entrepreneurship and Innovation» (NSRF 2014–2020) and co-financed by Greece and the European Regional Development Fund (ERDF).

References

- Allan, R. P., Hawkins, E., Bellouin, N., & Collins, B. (2021). IPCC, 2021: summary for Policymakers.
- Bullimore, B., 2014. Problems and pressures, management and measures in a site of marine conservation importance: Carmarthen Bay and Estuaries. *Estuarine, Coastal and Shelf Science*, 150(B), 288–298. doi:10.1016/j.ecss.2014.05.005
- Carmo, J. S. A. D. (2018). Climate change, adaptation measures, and integrated coastal zone management: The new protection paradigm for the Portuguese coastal zone. *Journal of Coastal Research*, 34(3), 687-703.
- Martins, F.; Alves, F.; Pinho, L.; Gomes, A., and Lopes, A.M., 2002. A novel way for the management of maritime public domain (MPD) in the coastal zone of central Portugal. In: Veloso-Gomes, F.; Taveira-Pinto, F., and Neves, L. (eds.), *Proceedings of the Littoral 2002—The Changing Coast* (Porto, Portugal), Volume 1, pp. 433–441.

Digitisation and proactive management of coastal and offshore infrastructure and environment

T. Onoufriou^{1*}, C. Michailides², P. Christodoulides¹

¹Department of Civil Engineering and Geomatics, Cyprus University of Technology, Limassol, Cyprus

²Department of Civil Engineering, International Hellenic University, Serres University Campus, Greece

³Department of Electrical Engineering, Computer Engineering and Informatics, Cyprus University of Technology, Limassol, Cyprus

*Corresponding author: tonoufriou@cut.ac.cy

Abstract

A huge development of coastal and offshore structures is anticipated in near future; in order to meet efficiently this development safety and environmental protection should be assured. Effective management schemes for those assets during conception, installation, operation, maintenance and dismantling should be used. East Med Energy Research for Growth and Education Centre of Excellence (EMERGE CoE) has been established within Cyprus University of Technology for improving the understanding of the physical behavior, ageing and degradation of marine engineered assets with the use of smart technologies. The EMERGE research group developed and installed in-field monitoring laboratories as real-time test beds in cooperation with industry stakeholders in two different coastal areas off the coasts of Cyprus which provide valuable data for research and development.

Keywords Proactive Management, Digitisation, Coastal and Offshore Infrastructure, Monitoring Techniques.

1 INTRODUCTION

Recent findings of natural gas discoveries in the offshore Eastern Mediterranean Region, i.e., Leviathan in Israel, Aphrodite and Calypso in Cyprus and Zohr in Egypt, as well as future planned exploration by major international offshore operators could contribute significantly to energy security and economic prosperity for the countries in the region. At the same time, renewables are the largest source of energy growth and are set to penetrate the global energy system more quickly than any fuel in human history. In addition to the offshore oil and gas structures and systems that already have been developed and installed, but are still being developed with a growing rate, ocean renewable energy systems (e.g. offshore wind turbines, wave energy converters, combined/hybrid concepts) are currently in the consideration, assessment and design phase.

While the potential benefits of offshore oil and gas as well as the rest of renewable energy technologies exploration are substantial, there are also significant possible negative impacts on the Mediterranean ecosystem which may affect all Blue Growth sectors since infrastructure assets development in coastal and offshore areas is required. Negative impacts may result from accidental or operational hazards, extreme environmental events or other security related risks resulting in loss of life, waste discharge and significant oil spills into the Mediterranean Sea. Such events would have dramatic consequences with main impacts on coastal tourism and fisheries and huge associated financial losses and other catastrophic effects.

The safe and efficient development of offshore and coastal infrastructures and operational processes as well as the development of the relevant skills to support these industries is of paramount importance. Challenges in connection with condition monitoring, systems integration, materials performance, data, and development of safety codes and standards are already met. Those challenges are related with the use of smart technologies for improving the understanding of the physical behavior, ageing and degradation of marine engineered assets and smart proactive management of the whole life cycle from design through to operation, maintenance, life extension and decommissioning.

Towards those needs a National Centre of Excellence has been established for promoting Cyprus as a regional hub for energy, research, innovation, education, and training. East Med Energy Research for

Growth and Education Centre of Excellence (EMERGE CoE) has been established within Cyprus University of Technology by faculty members of the Civil Engineering and Geomatics Department.

The creation and installation of in-field monitoring laboratories in cooperation with industry stakeholders has been a key strategic element of the EMERGE CoE's actions, which in turn provides a strong foundation which facilitates many of the above activities. All the aforementioned activities are interconnected and are essential pieces of the puzzle for a successful center. The two initial operational monitoring systems (Figure 1) for measuring the response of marine infrastructures (e.g. accelerations at various coastal jetty and fixed bottom breakwater positions) and environmental factors (wind direction, wind velocity, wave height, temperature, humidity, atmospheric pressure) at two distinct marine locations in Cyprus (the Vasiliko Energy Centre and Ayia Napa Marina) have been augmented by a new monitoring system for water quality parameters installed at the Ayia Napa Marina.

The EMERGE research group is using those significant in-field laboratories as real-time test beds, which will enable many other crucial related activities in line with the center's goals. Over the past few years, the EMERGE research team has worked with two key industry stakeholders, VTTV Vasiliko and Ayia Napa Marina, who provided access to their infrastructure and valuable in-kind support to build up, validate, and operate these systems. In order to facilitate the scopes of the EMERGE CoE's planned study topics, real-time monitored data from the two systems already have been used. It is worth mentioning that three years' worth of data from one of the two systems is currently saved in EMERGE database and is steadily growing. Data analysis already resulted in research publications (Demetriou et al., 2021, 2022) and daily forecasting reports.



Figure 1 Monitoring system in Vasiliko VTTV (left) and Ayia Napa Marina (right), Cyprus

2 RATIONALITY AND FUNCTION OF EMERGE COE

EMERGE offers significant added value by moving away from an unfocused and fragmented level of knowledge which is created through various ad hoc actions in this area to an integrated, systematic and high-quality framework which will result in:

- Establishing a National Centre of Excellence and promoting Cyprus as a regional hub for energy, research, innovation, education & training
- Retaining and investing capital expenditure in Cyprus, attracting further international funding and creating jobs
- Providing a structured programme with national and international outreach for research, innovation, education and training
- Perform strategic studies of national, regional and international importance and provide support for effective and coherent development of the energy sector.

While all the above activities are interrelated and are all necessary pieces of the puzzle for a successful centre a key strategic element of the EMERGE has been the development and installation of in-field monitoring laboratories. Two already functioning monitoring systems for measuring the response of

marine infrastructures and environmental processes exist in two different marine locations in Cyprus. These key in-field laboratories will serve as real time test beds for the purposes of the EMERGE research group which will facilitate many other important related essential activities in line with the centre's objectives. These systems have been set up, validated and run by the EMERGE research group in collaboration with industry stakeholders VTTV Vasiliko and Ayia Napa Marina during the past four years. Real time monitored data from the two systems are utilized and will form an essential in field research laboratory and database for facilitating the scopes of the EMERGE proposed research topics. They will also ensure that the research and education activities of EMERGE will stay in tune with the industry needs and promote industry uptake of the centre's output and support future development of further activities including training programs and entrepreneurship. Furthermore, the utilization of the two networks as test-beds and the accompanied data in EMERGE activities signifies the commitment and interest of major Energy players in the outcomes of EMERGE activities as well as potential uptake from other stakeholders in the area, and progresses the EMERGE activities from the fundamental/theoretical to the applied research realm.

This increase in research capacity, both in terms of infrastructure and staff, has already produced significant scientific results. Several research studies have been conducted and distributed to the scientific community in this regard, while others have matured and are being readied for publication. These studies are based on the Center's elaborated flagship project, which was envisioned at the Center's inception and extensively evolved throughout the years in response to stakeholder needs and modern technology advances. The research projects included in this paper are at the heart of the Centre's research efforts, and they provide the groundwork for a long-term scientific effect that will benefit both industry and academia.

3 INFIELD LABORATORIES

3.1 VTTV infield laboratory

The infield laboratory at VEC is located within the premises of VTTV and it consists of a high-quality monitoring system that is installed on the fixed-bottom coastal jetty responsible for the berthing of vessels and for loading and unloading of petroleum products. The monitoring system is designed to monitor key structural and environmental parameters and comprises of two triaxial accelerometers, an anemometer and a wave radar. The readings of the sensors are recorded on an industrial computer and communicated to the server located at the premises of EMERGE via the cloud. More recently, a weather station has been incorporated to the monitoring system to enhance the R&D activities and the installation of an accelerometer with ATEX certificate in the offloading platform of the jetty.

With regards to the recording, storing and transmission of measured data, all the sensors are wired connected to an independent industrial computer that is placed on the structure. All the data are stored temporarily to the memory of the industrial computer and in a relatively short time interval the data are transmitted automatically to the data storage internet space to EMERGE's servers. From the data storage space and through a File Transfer Protocol (FTP) authorized users can upload all the monitoring data in file format ready for further analysis and post-processing.

3.2 Ayia Napa Marina infield laboratory

This infield laboratory is located at the premises of Ayia Napa Marina near the entry point of the newly developed port. The monitoring system consists of an underwater pressure reader, an accelerometer, a weather station and an industrial computer. The sensors are supported by a high-performance industrial computer which is set to communicate the recording to EMERGE's servers. In a similar manner and with regards to the recording, storing and transmission of measured data, all the sensors are wired connected to an industrial computer that is placed on the breakwater of Ayia Napa Marina. All the data are stored temporarily to the memory of the industrial computer and in a relatively short time interval the data are transmitted automatically to the data storage internet space via GSM/GPRS network. From the data storage space and through a File Transfer Protocol (FTP) authorized users can upload all the monitoring data in file format ready for further analysis and post-processing.

4 USE CASES AND RESEARCH PROJECTS

4.1 Vassiliko Energy Centre's (VEC) Flagship Project

The flagship project was created to focus on the Vassiliko Energy Centre's (VEC) onshore and coastal/offshore operations and facilities, which constitute a key national and private energy infrastructure for the country. The goal of EMERGE, since the inception of the flagship project, is to provide a framework for multiple research activities that aimed at improving the VEC's safety, efficiency, environmental protection, and long-term viability. The intensive development of the Vassiliko Energy Centre (VEC) reflects the rapid growth of the Oil and Gas (O&G) industry in Cyprus. Apart from the strategic location of Cyprus in the Eastern Mediterranean Sea, which renders the country as an important energy interconnection node, this growth has considerably been stimulated by the discovery of significant gas reserves in the country's Exclusive Economic Zone, as well as the recent establishment of major O&G operations by global companies in the area. A substantial number of major energy infrastructure facilities is currently established at the VEC, while many others – including liquefied natural gas infrastructure units – are under study or development.

The concept of digital transformation of the VEC is driven by the need for advancing efficient holistic management solutions through the digitization of the various activities involved in such a highly-concentrated and high-risk industrial area. The ultimate objective is to provide through research, technological development and innovation (RTDI) a holistic solution for improving asset, environmental and operational conditions in the VEC and the wider energy sector. Such potential solutions should fully align with current technological trends and capabilities, and more specifically the advancing steps of the energy sector towards the 4th industrial revolution through “digitization”. The potential digitization solutions will aim at satisfying the following needs:

- Secure the structural integrity of key energy infrastructural assets of national significance, aiming at ensuring the safe and unobstructed import, storage and use of oil and gas in the VEC.
- Improve the resilience of existing ageing energy supply infrastructure.
- Safeguard the environment and ensure the safety of operators and the wider community.
- Optimize future infrastructure design and operation, including supply chain management and proactive maintenance activities.
- Develop effective links and synergies among all interested stakeholders through a systematic, user-driven, co-creation approach integrating research, innovation and implementation processes.

4.2 Machine learning based wave modeling of VEC coastal area

Significant work has been undertaken in the area of advanced wave modeling. The key incentive for the undertaken research work stems from the keen interest of major energy stakeholders in the accurate prediction and forecasting of significant wave heights. In this regard, the work on wave modeling is divided in two main areas:

- i) The development of advanced machine learning models that capitalize on data recorded from meteorological as well as structural monitoring systems and
- ii) Advanced machine learning models that capitalize on the concept of hierarchical classification for improving their prediction accuracy.

Importantly, both of the studies have yielded significant and very promising outcomes which have been already disseminated to the scientific community via their publication in top-tier journals. The studies proved that indeed machine learning models developed on both structural and meteorological data can improve significantly the performance of wave models. These results highlight the potential of tapping into the untapped pool of structural data for significant wave height prediction, paving the way for new research to be undertaken in this direction but most importantly generate value for the energy stakeholders involved in marine operations. The effort is guided in the following direction; to improve the wave predictive performance of current methodologies by utilizing, for the first time, readily available data gathered from structural condition monitoring systems present on coastal and offshore infrastructure. As a vehicle towards this direction, the classification performance of the developed networks is examined for the cases of: i) artificial neural networks and decision tree ensembles for which only meteorological data are used as inputs during the network's training, and ii) artificial neural

networks and decision tree ensembles in which both meteorological and structural acceleration data are used during training.

4.3 Daily report on wave and wind conditions in Vassiliko area

Appropriate models and tools were developed by the EMERGE research team which generate an automated daily report with measured data (wind and wave) as well as a next day forecasting generated combining machine learning algorithms and analytical models. This report is stored and shared with stakeholders operating in the area automatically every day. In the report the following information are included: (a) Measured data related to wave characteristics (wave height and wave period), (b) Measured and web-based data related to wind characteristics (wind speed and wind direction), (c) One day ahead forecasting of wave characteristics based on measured data with the use of different types of numerical methods based on Neural Network and d) One day ahead forecasting of wind characteristics based on web-based data. The folder containing the reports is updated on a daily basis, and people with access to the folder are able to view the reports. The reports assist stakeholders in the area in both operational and maintenance activities. A sample of daily automated report is presented below.

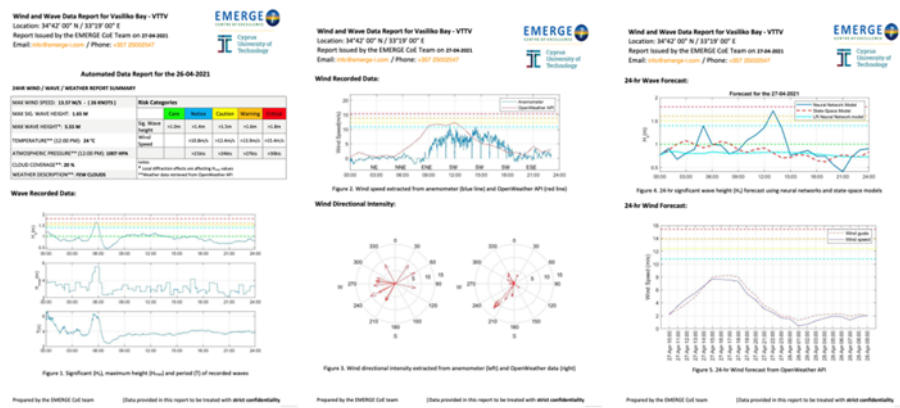


Figure 2 Daily automated report generated with use of the monitoring system in Vasiliko, Cyprus

4 CONCLUSIONS

The creation and installation of in-field monitoring laboratories in cooperation with industry stakeholders has been a key strategic element of the EMERGE CoE's actions, which in turn provides a strong foundation for digitisation and proactive management of coastal and offshore infrastructure and environment. Two initial operational monitoring systems for measuring the response of marine infrastructures and environmental factors at two distinct marine locations in Cyprus have been developed through the EMERGE CoE. Valuable data collected through these in-field laboratories provide a strong base for relevant use cases and research studies.

The development and establishment of EMERGE aims to provide significant added value by transitioning from an unfocused and fragmented level of knowledge and capability which is created from various independent actions in this area, to an integrated, systematic, and high-quality framework provided by EMERGE. The continuing actions of the development and strengthening of the capability within the EMERGE CoE aims to gradually facilitate various actions with a focus towards the use of smart technologies in marine engineering science and technology.

References

- Demetriou D, Michailides C, Papanastasiou G, Onoufriou T (2021). Coastal Zone Significant Wave Height Prediction by Supervised Machine Learning Classification Algorithms, *Ocean Engineering*, 221, 108582.
- Demetriou, Michailides, Papanastasiou G, Onoufriou (2022). Nowcasting significant wave height by hierarchical machine learning classification, *Ocean Engineering*, 242, 11013.

A case-study for the water renewal in the Rio Castle moat in Greece

G.A. Leftheriotis^{1*}, I.A. Chalmoukis¹, A.A. Dimas¹

¹Department of Civil Engineering, University of Patras, Patras, 26504, Greece

*Corresponding author: gletheriot@upatras.gr

Abstract

The Rio Castle in Greece is located at the coast, and originally its moat was connected to the sea both eastwards and westwards. Over the years, the western inlet was blocked due to coastal sediment accretion, and nowadays the moat functions as a semi-enclosed hydrodynamic system with weak seawater circulation and renewal. The objective of this work is to assess the present situation and demonstrate that the placement of a culvert to connect the western part of the moat with the sea will greatly improve hydrodynamic circulation and water renewal. The study is based on numerical simulations of wind and wave forcing using the commercial software DHI MIKE 21/3. The results verified the weak hydrodynamic circulation and water renewal in the present situation and showed that the placement of a culvert in the western side of the moat induces a dominant flow path with strong currents in the moat and achieves a significant improvement of the water renewal rate.

Keywords Rio Castle moat, Water renewal, Residence time, Hydrodynamic circulation.

1 INTRODUCTION

The Rio Castle is located at the northwestern coast of the Peloponnese peninsula in Greece, and specifically at the Rio-Antirio Strait between the Gulf of Patras and the Gulf of Corinth. The layout of the Rio Castle is approximately triangular; its northern corner coinciding with the tip of the peninsula (Figure 1). The moat separates the Castle from the land at its southern side, and it has an average width of 25 m. Its shape follows the Castle precinct, forming an angle of about 90 degrees at its southernmost point. Two triangular bastions (B1, B2 in Figure 1) of about 1500 m² each exist in the moat. The moat is about 350 m long, and its average depth is 1 m with a maximum depth of 1.8 m. It covers an area of about 15000 m² (0.015 km²), and its water volume is about 15000 m³. The moat was initially connected to the sea both to the west (Gulf of Patras) and to the east (Gulf of Corinth). In time, the western opening of the Rio Castle moat was filled with sediments due to wave-induced accretion, and it remains blocked to the present day (Figure 1). As a result, the moat is now connected to the sea only at its eastern side by a single culvert 6.5 m long, 2.5 m wide and 2 m high, leaving 0.75 m water depth, which is not adequate to facilitate significant seawater exchange with the open sea. The reduced water circulation has created eutrophication phenomena, leading to large population of insects (mosquitoes, flies, etc.), stench, contamination, and a feeling of a suffocating atmosphere for the visitors. In Figure 1 (top right) clear signs of eutrophication are visible at the surface and the banks of the moat where the western opening used to be.



Figure 1. Left: Panoramic view of Greece (top left corner) with indication of the study area. Right: Aerial photograph of the Rio Castle with the current situation of the western blocked opening (top right corner).

In the present work, a case-study of the Rio Castle moat is presented and investigated numerically. First, the focus is on the water renewal of the moat at its present condition. It is demonstrated that the numerical results predict accurately the moat hydrodynamics at its present situation. Then, it is numerically investigated if it is possible to improve the moat flow circulation and water renewal rate, by using a culvert to connect the western side of the moat to the sea.

2 METHODOLOGY

2.1 Hydrodynamic formulation

The effect of waves and wind-generated currents on hydrodynamics and water renewal in the moat was investigated by coupled numerical simulations of wave propagation and wave- and wind-generated current flow using the MIKE 21/3 software (DHI, 2022). In particular, the following specific modules of the software were used: MIKE 21 Spectral Waves (SW) for wave propagation, MIKE 3 Flow Model (FM) for wave- and wind-generated currents, and MIKE 3 Transport (TR) for the water renewal. MIKE 21/3 software has been used in the literature for the numerical investigation of water renewal and the estimation of residence times in lagoons and bays (Cavalcante et al., 2012, Mahanty et al., 2016, Ranjbar and Zaker, 2018, Fourniotis et al., 2018, 2021).

2.2 Wind and wave data

Regarding wind forcing, the mean wind data from the meteorological station of the Hellenic National Meteorological Service at Lepanto were used, which is located at latitude 38.39 N and longitude 21.84 E. The data were recorded in the period 1977-2011. The main wind directions that affect the study area are: eastern (E), northeastern (NE), northwestern (NW) and western (W). Two scenarios, in terms of the wind intensity, were examined for each wind direction: one with a mild wind speed that occurs frequently during the year, and one with a return period of 1 year ($T_r = 1$ yr) and, thus, stronger wind speed. A moderate wind of 3 Bf was selected for the mild scenario; such winds are observed for a total duration of about 27 days per year in the study area. Based on the mean annual wind data, the U_{10} wind speed with $T_r = 1$ yr was also determined. The corresponding wind and deep-water wave parameters for the dominant wind directions are given in Table 1 for both wind-intensity scenarios. Since no wave measurements exist, a hindcast method was used to obtain the wave characteristics based on the existing wind data. First, the fetch length, for each dominant wind direction, was calculated and then, the SMB-Wilson methodology, according to OCDI (2009), was applied to calculate the corresponding deep-water wave height and period for both wind intensities (Table 1).

Table 1. Wind and deep-water wave parameters in the study area, corresponding to two wind-intensity scenarios (mild and $T_r = 1$ yr) for each of the dominant wind directions.

Direction	Fetch (km)	Wind speed (Bf)	U_{10} (m/s)	H_s (m)	T_s (s)
E	6.45	3	4.4	0.2	1.66
		5	10.30	0.55	2.51
NE	8.38	3	4.4	0.22	1.76
		8	18.90	1.21	3.53
NW	15.44	3	4.4	0.27	2.01
		5	9.32	0.71	3.01
W	26.81	5	9.32	0.71	3.01
		6	12.99	1.31	4.08

The effect of the four dominant winds, E, NE, NW, and W with mild intensity (3 Bf) and intensity of $T_r = 1$ yr, was extensively analyzed in conjunction with the corresponding wind waves (Table 1) for the existing moat condition and the proposed solution. The current condition of the moat was examined using the winds and waves with $T_r = 1$ yr to demonstrate the bad water circulation situation even under the most favorable loading. On the other hand, the assessment and evaluation of the proposed solution was examined using the milder wind conditions to demonstrate the effectiveness of the proposed solution to the water renewal even under the least favorable loading. The bathymetric data were obtained using bathymetric measurements provided by the Region of Western Greece. The computational domain includes the moat area and the coastal waters surrounding the Rio Castle (Figure 2). Note that the

western opening (red circle) does not exist in the present moat condition, but it corresponds to the proposed solution. The spatial grid resolution ranges from 1 m in shallow waters to 5 m in deep waters, whereas the grid discretization in the moat, and especially around the bridges and its openings (existing and proposed), was particularly dense with a cell resolution of less than 0.5 m (Figure 2). Overall, a grid of approximately 37,000 unstructured triangular cells in the horizontal plane was used.

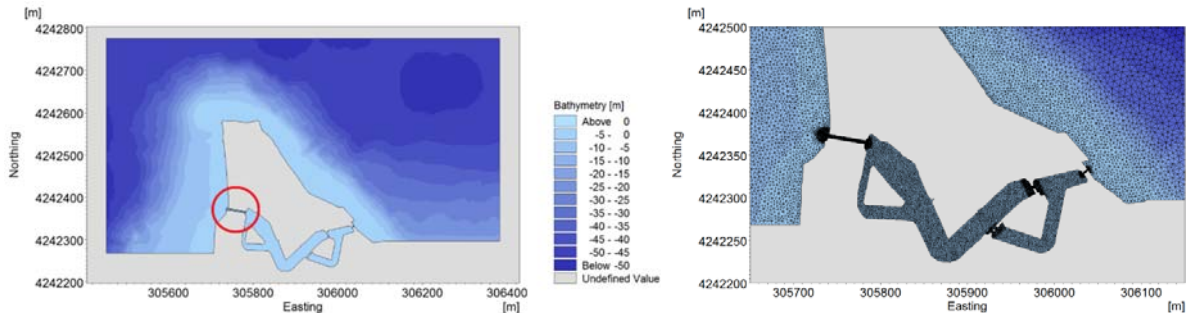


Figure 2. Left: The computational domain with the bathymetry around the Rio Castle. The proposed opening is highlighted with the red circle. Right: The numerical grid with dense discretization in the moat and its openings.

3 RESULTS

3.1 Hydrodynamic study of the present moat condition

In this chapter, the wind and wave action in the present condition is examined. In all cases, it was observed that, in the moat, the current field is very weak and the water renewal rate is very small. For brevity, only two of the four wind cases with $T_r = 1$ yr are presented in detail; the ones that correspond to the most (NE) and the least (NW) favorable wind directions in terms of water renewal. Furthermore, based on the wind data, these two wind directions have the highest occurrence frequency in the area. The poor water renewal in the moat for the present situation is evident in Figure 3, due to the action of NW and NE winds. The most favorable situation corresponds to the NE winds, where the tracer concentration has been reduced to 50-60% of its initial value in the proximity of the eastern opening. However, the rest of the moat remains almost unaffected (concentration levels > 0.7), even though, locally, the current velocity is significant (0.4 m/s around the western bastion). This is explained because the water is entrapped at the western side of the moat. The high current velocity values induce a water circulation around the western bastion (B1 in Figure 1) but no water renewal is achieved, since the inflow from the opening does not reach the western side. The least favorable situation corresponds to the NW winds (Figure 3), where the entire moat seems unaffected after 24 hours. Only a small area around the opening seems to be mildly affected with concentration levels of 0.8-0.9.

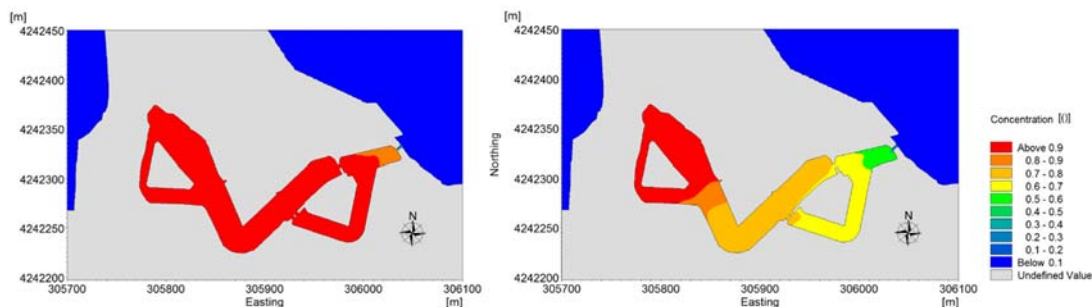


Figure 3. Depth-averaged distribution of the tracer concentration in the moat (present situation) after 24 hours due to the action of NW with $T_r = 1$ year and 5 Bf (left) and NE winds with $T_r = 1$ year and 8 Bf (right).

Based on the above, the Rio Castle moat in its present condition acts like a closed hydrodynamic system due to the presence of a single opening in the eastern side, even for the strong winds. Water renewal is minimal, as well as wind- and wave-generated flow recirculation development at the existing opening and in the moat. This result is in accordance with the stagnant waters and eutrophication problems that

are observed presently in the moat and serves as a confirmation for the validity of the numerical models used.

3.2 Hydrodynamic study of the proposed solution

To overcome the above problems, the construction of a new western opening is proposed, which should be consistent with the geometric dimensions of the eastern one. Thus, a double (twin) rectangular culvert is proposed with the following dimensions for each channel: 2 m width, 1.5 m height and 55 m length. The bottom of the culvert is located at a depth of -1 m from the mean sea level (MSL), leaving a freeboard of 0.5 m to reduce the risk of clogging and facilitate maintenance. In Figures 4 and 5, the tracer concentration is presented in the moat with the additional western opening, due to the action of the NE and NW winds, respectively. After the addition of the western opening, the moat acts as a flow-through hydrodynamic system, resulting in an increase of the water circulation within the moat. To better understand the tracer advection, the action of NE and NW winds is presented at four different time instants.

Regarding the NE wind, a significant amount of fresh seawater has entered the moat from the sea through the eastern opening after only one hour of simulation (Figure 4a). At the same time an equivalent amount of water has exited the moat from the western opening since the moat functions as a flow-through hydrodynamic system. After two hours, the eastern side of the moat has been almost fully replenished, apart from a few areas where water has been entrapped (Figure 4b). The tracer concentration in these areas is considerably reduced during the next two hours (Figure 4c), until eventually the water of the moat is almost fully renewed after eight hours (Figure 4d). The only area where low concentration levels are still observed (less than 0.4), is at the southern side of the western bastion. From the depth-resolved results (not shown here due to space limitations), it was observed that the entire volume of water in the moat is completely renewed after approximately eighteen hours.

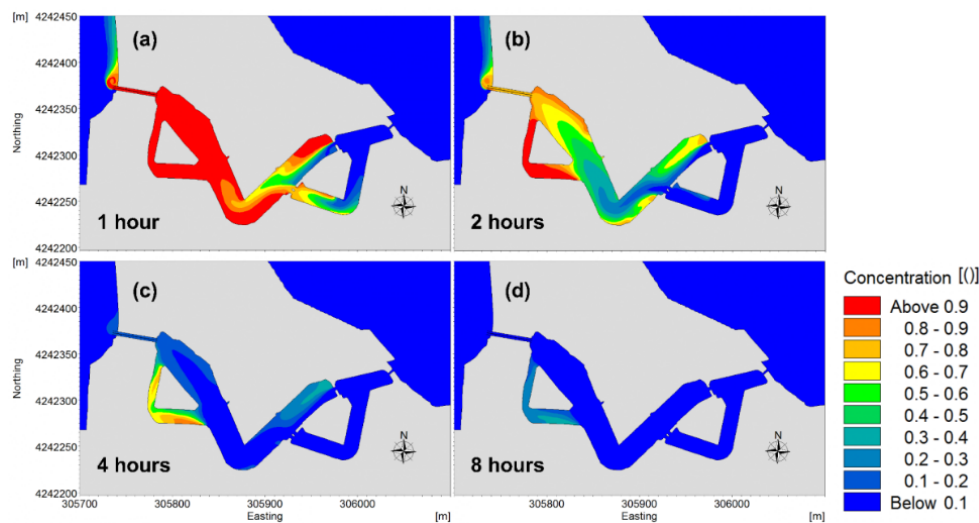


Figure 4. Depth-averaged distribution of the tracer concentration in the moat (proposed solution) due to the action of NE winds (3 Bf), corresponding to 1, 2, 4 and 8 hours after the beginning of the simulation.

Concerning the NW wind, significant water volume has entered the moat from the western opening and the main western body of the moat has been almost renewed (tracer concentration lower than 0.2) after only one hour (Figure 5a). Simultaneously, considerable amount of water has exited the eastern opening. After two hours, the western side of the moat has been almost replenished, except for the southern side at the western triangular bastion, where water has been entrapped again (Figure 5b). During the next two hours, the tracer concentration at the eastern side of the moat is significantly reduced (Figure 5c), until the renewal of the entire water of the moat after eight hours (Figure 5d). The only area that presents high concentration levels (approximately 0.7) is the southern side of the western triangular bastion. The water in the moat is completely renewed after about 24 hours.

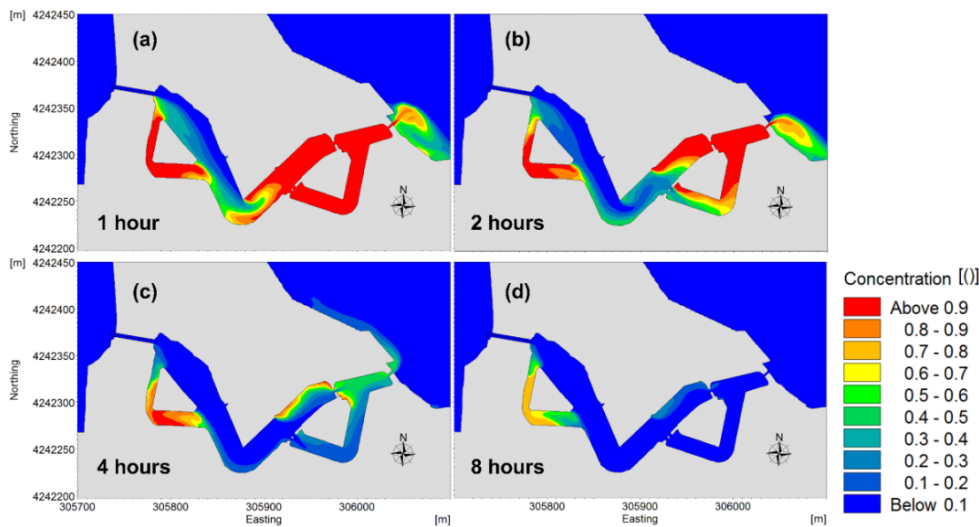


Figure 5. Depth-averaged distribution of the tracer concentration in the moat (proposed solution) due to the action of NW winds (3 Bf), corresponding to 1, 2, 4 and 8 hours after the beginning of the simulation

4 CONCLUSIONS

In the present work, the case study of the Rio Castle is investigated, where the western connection of the moat to the sea has been clogged over the years. The reconstruction of the western opening is proposed and investigated numerically to ensure the improvement of the hydrodynamic circulation and the satisfactory water renewal rate in the moat. The proposed solution includes the excavation of the western connection and the installation of a concrete rectangular culvert. Due to the relatively large length of the culvert (55 m), and in order to facilitate construction and installation procedures, a double (twin) culvert is proposed, i.e., two parallel culvert branches of the same cross-section. The dimensions of the new cross section should be consistent with the eastern opening, so a total width of 4 m and a water depth of 1 m were chosen. Based on the numerical results, the moat, in its present condition, functions as a closed hydrodynamic basin, characterized by negligible water replenishment. After the implementation of the proposed solution, the moat behaves like a flow-through hydrodynamic system, which is characterized by a dominant flow path with strong currents and enhanced water renewal rates and small residence times.

References

- Cavalcante GH, Kjerfve B, Feary DA (2012) Examination of residence time and its relevance to water quality within a coastal mega-structure: the Palm Jumeirah Lagoon. *J Hydrol* 468, 111–119. doi:10.1016/j.jhydrol.2012.08.027
- DHI, 2022. MIKE 21 Spectral Waves, User Guide.
- DHI, 2022. MIKE 3 Flow Model FM, Hydrodynamic Module, User Guide.
- DHI, 2022. MIKE 3 Flow Model FM, Transport Module, User Guide.
- Fourniotis NT, Horsch GM, Leftheriotis GA 2018. On the Hydrodynamic Geometry of Flow-Through versus Restricted Lagoons. *Water* 10, 237. doi:10.3390/w10030237
- Fourniotis NT, Leftheriotis GA, Horsch GM 2021. Towards enhancing tidally-induced water renewal in coastal lagoons. *Environ Fluid Mech* 21, 343–360. doi:10.1007/s10652-020-09776-0
- Mahanty M, Mohanty P, Pattnaik A, Panda U, Pradhan S, Samal R (2016). Hydrodynamics, temperature/salinity variability and residence time in the Chilika lagoon during dry and wet period: measurement and modeling. *Cont Shelf Res* 125, 28–43. doi:10.1016/j.csr.2016.06.017
- OCDI (2009) Technical Standards and Commentaries for Port and Harbour Facilities in Japan. The Overseas Coastal Area Development Institute of Japan, Tokyo, Japan
- Ranjbar MH, Zaker HN (2018) Numerical modeling of general circulation, thermohaline structure, and residence time in Gorgan Bay Iran. *Ocean Dyn* 68, 35–46. doi:10.1007/s10236-017-1116-6

A preliminary study of water renewal in a flow-through lake in Western Greece

N.Th. Fourniotis^{1*}, G.A. Leftheriotis²

¹Department of Civil Engineering, University of the Peloponnese, 26334 Patras, Greece

²Department of Civil Engineering, University of Patras, 26500 Patras, Greece

*Corresponding author: nfou@uop.gr

Abstract

In the present paper, we present the basic hydrodynamic characteristics as well as the water renewal parameters of Lysimachia Lake, one of the most important lakes of Western Greece. Water renewal parameters such as the residence time of the lake and the outflow discharge via the "Dimikos" channel to the Acheloos River were simulated numerically, while the hydrodynamic regime of the lake such as flow currents, gyres formation due to local topography, as well as the effect of inflow waters from the Ermitsa stream and the Trichonida lake, via the connecting channel "Alabey", were analyzed in a time period of approximately 2 months. The numerical predicted results for the water renewal were found in good agreement with those found in literature. More specifically, the Lysimachia Lake seems to be replenished by the inflow waters from Trichonida lake as well as the Ermitsa stream and surface waters from the catchment area approximately 13 times per year, i.e. every 28 days.

Keywords Lysimachia Lake, Water renewal, Flow-through system, Hydrodynamic circulation.

1 INTRODUCTION

In recent years, many water bodies have been affected by natural and anthropogenic factors, leading to alterations in their physical, chemical and biochemical parameters. The concentration of the corresponding substances in these water bodies is generally dependent on hydrodynamic circulation and water renewal time or the ability of the hydrodynamic system to achieve a significant flushing rate. Thus, renewal time remains a crucial factor for decisions regarding the design of water bodies' restoration and management actions, aiming at the improvement of environmental conditions. The water renewal of a water body is achieved via different mechanisms. In the marine environment water renewal is mainly achieved under the combined action of the wind and the tide. Regarding the fresh water bodies, i.e. lakes or reservoirs, the water renewal remains nearly seasonal, due to the rivers or streams inflow that fed the water body. The generation of flow-through conditions in these water bodies can substantially affect the water renewal giving rise to a fast replenishment mechanism.

Based on the above mentioned, in this paper a three dimensional (3D) hydrodynamic and transport model has been applied for the calculation of the flow field and the renewal time in the flow-through monomictic lake Lysimachia (also referred to, below, as "Lake", for brevity), located in the region of Aitoloakarnania in western Greece. The lake has a surface area of 11-13 km², corresponding to +12.5 ~ +14.5 m surface elevation and a water volume 52-57x10⁶ m³. The lake a relatively large catchment area (314 km²), and communicates with other larger and much deeper water bodies that seem to determine its flow field and the water renewal. It is affected mainly by the waters from the deepest and largest Lake Trichonida (via a constructed connecting channel), as well as by the inflow waters from the Ermitsa stream, at the northeasterly part of the lake, while it drains its flood waters to Acheloos River. It shows large seasonal fluctuations in water level, while during the winter it often overflows. The lake is of particular environmental and hydraulic-hydrologic significance, since, after a series of technical hydraulic works, it has been turned into a regulating water reservoir. Regarding the water renewal, the worst case scenario for the Lake includes minimal inflow from Lake Trichonida and zero inflow from Ermitsa stream under windless conditions.

2 MATERIALS AND METHODS

2.1 The study area

Lysimachia Lake is located to the south of Aetoloakarnania prefecture in Western Greece and is approximately 5 km away from the city of Agrinio. More specifically, it is fed by the Ermitsa stream which outflows at the northeastern of the lake and constitutes the main freshwater input. Lysimachia is only 2 km away from the largest and deeper Lake Trichonida, as they are only separated by a strip of land. It is also linked to Lake Trichonida by a connecting channel (~ 2.7 km), which gets excess water and with which and the greater lake they constitute a single ecosystem. Surplus of water, i.e. flood winter waters from Trichonida, is drained via the connecting channel to Lysimachia and subsequently channeled by Dimikos channel to Acheloos River, in the west of the lakes ecosystem. It has a nearly elongated shape with low banks. Maximum length is 6 km and its width is about 3 km, while its surface has an area up to 13 km². Its maximum depth is around 7.5 m. The lakeside area is smothered in reeds and among the, species of birds find shelter in winter, while there are endemic fish species in its waters.

2.2 Simulation set-up

The numerical simulations have been performed using the commercially available CFD (Computational Fluid Dynamics) numerical model MIKE 3 Flow model FM (where FM stands for flexible mesh), developed by the Danish Hydraulic Institute (DHI). The MIKE 3 FM Hydrodynamic Module (HD) is used for the simulation of unsteady 3D flows taking into account density variations, bathymetric data and external forcing. For the spatial discretization, a cell-centered finite volume approach is followed, using an unstructured mesh approach in the horizontal direction, while a structured mesh is used in the vertical direction. MIKE 3 FM Transport Module (TR), also used in the specific work, simulates numerically the spreading and fate of dissolved or suspended substances in the aquatic environment under the influence of the fluid movement and the associated diffusion processes. More specifically, the advection and diffusion of a conservative tracer, applied in the Lysimachia Lake, is simulated utilizing the TR Module. The details of the codes can be found in DHI (2018a, b) and the specific choices selected in the runs described below can be found in Fourniotis et al. (2018, 2021). The simulations were based on the numerical solution of the 3D Reynolds averaged Navier–Stokes (RANS) equations for unsteady, incompressible flow, with the assumption of hydrostatic pressure. The free-surface is taken into account using a sigma-coordinate transformation approach. Concerning the turbulence closure it is achieved by means of an eddy viscosity concept. A standard k- ϵ model (Rody, 1984) is used for the vertical eddy viscosity, while the model proposed by Smagorinsky (1963) is used for the horizontal eddy viscosity.

2.3 Computational domain and grid

The suitable locations to be chosen as inflow fresh water boundaries for the simulations are the main inflows from Lysimachia Lake, one of which, i.e. the eastern open boundary, is close to the outflow of the connecting channel between the two lakes. The second inflow boundary is located at the northeastern part of the Lake where the Ermitsa stream outflows. Furthermore, two outflow open boundaries are chosen, one at the western part of the lake, close to the outflow of drainage channel "Dimikos" to Acheloos River. The second outflow boundary is located at the south of the lake where the Lysimachia tunnel outflows. The numerical domain for the 3D simulations covers the entire Lake system. Specifically, a truncated computational domain was formed covering the entire Lysimachia Lake and the adjacent open boundaries. Further, in the vicinity of the freshwater inlets/outlets, i.e. northeasterly and easterly (inflow from the Ermitsa stream and the connecting channel) and westerly and south (outflow to the Acheloos River via "Dimikos" channel and the Lysimachia tunnel) a much finer grid is required for adequate simulation of the freshwater plume propagation from the stream or connecting channel to the Lake's body. Thus, a non-uniform computational mesh was generated (Figure 1). In the vicinity of the open boundaries, i.e. inlets and outlets of the lake, the area is consisted of cells, the characteristic dimension of which is ~ 10 m, gradually increasing outwards. Adjacent to this area lies a greater zone covering the Lake's body where the grid size increases gradually from ~ 10 m near shore to ~ 50 m inside the lake. The overall number of horizontal cells in the whole domain is 14416 (7738 nodes). The specific discretization keeps the computational cost at a reasonable level, while trying to enhance, the accuracy of the simulations. In the vertical plane 10 layers over depth have been used.

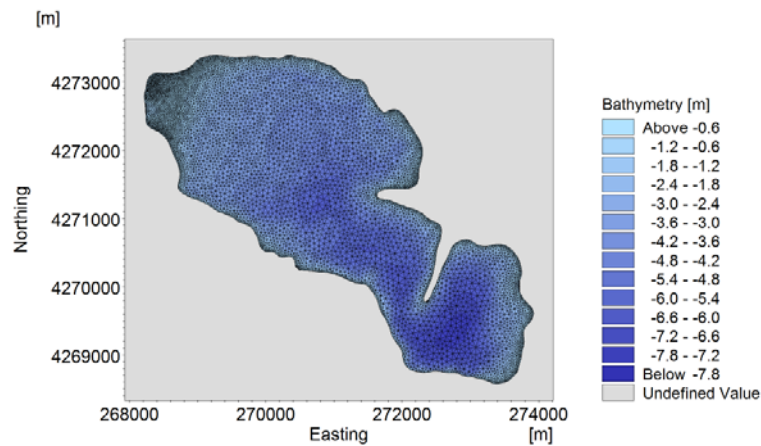


Figure 1. The computational domain with the bathymetry of Lake Lysimachia

2.4 Boundary and initial conditions

In all simulation cases the bank of the Lake has been defined as an impermeable boundary with zero normal velocity, while the bottom is a no-slip (via wall functions), impermeable boundary. With respect to the Lysimachia Lake, mean values of inflow and outflow discharge that resulted from the literature were used as open boundary conditions in the following simulations. The inflow forcing, i.e. the discharge from the connecting channel between the two Lakes as well as fresh water inflow discharged from the Ermitsa stream are imposed as a specified discharge value which is constant along the open boundary. More specifically, a mean value of $\approx 22 \text{ m}^3/\text{s}$ is considered for the eastern open boundary, while the fresh water discharge from the Ermitsa stream is imposed equal to $\approx 1.5 \text{ m}^3/\text{s}$. In the south open boundary, where the Lysimachia tunnel is considered, a mean outflow discharge of $\approx 18 \text{ m}^3/\text{s}$ is considered while in the western boundary of the Lake free outflow condition is taken into account. The roughness height of the bottom was set equal to 0.01 m and special care was taken to ensure that the geometry of the bottom cell was compatible with the requirement of fully rough flow, assuming the minimum flow depth equal to 0.2 m. Concerning the initial conditions, all simulations were initiated from the state of rest. Furthermore, it should be noted that the simulations were performed considering barotropic flow.

2.5 The numerical tracer

In this section we present the method applied to numerically estimate the residence time of the Lysimachia Lake ecosystem. Various transport time scales have been used in the literature to quantify the renewal of waters in natural systems (Monsen et al. 2002). For the purposes of the calculation, we define as residence time the time needed for the concentration of a conservative, passive tracer to fall to $1/e$ ($\sim 37\%$) of its initial value (Ranjbar and Zaker 2018, Fourniotis et al., 2021). By defining the initial concentration of the conservative numerical tracer to be equal to 1 inside and 0 outside the Lysimachia Lake, we are able to calculate the residence time everywhere inside the Lake by following the evolution of the concentration of the tracer as determined by the conservation equation. This information should be useful in the analysis of the very complex problem of the water renewal of the Lake, as well the estimation of areas inside the Lake where low water renewal exists. We note, however, that the e -folding value is a mere convention and that in different applications the use of different cut-offs may be in order. This is especially true for research concerning the causes of the complex environmental problems which can arise in Lake waters.

3 RESULTS AND DISCUSSIONS

The horizontal geometric lengthscale of Lysimachia Lake basin is in the order of $5 \times 10^3 \text{ m}$. The Rossby number (Ro) value of the fresh water plumes generated flow as well as the wind-induced flow is expected to be less than 1, approaching a value of 1 for strong winds, so that Coriolis force is expected to influence the flow. However, the Lake is restricted with variable depths, mainly in the central part of

the basin due to the Ermitsa stream outflows. Thus, the effect of rotation is expected to be reduced with increasing wind speed. More specifically, the Lake consists of two sub-basins, one at the eastern part of the Lake, and the other at the west. The maximum depth of the former basin is ≈ 7.5 m and that of the latter ≈ 6 m. Thus, the formation of the shape of the Lake will be seen to play a decisive role in the renewal of the waters. Finally, another important characteristic of the basin of the Lake is that the smaller sub-basin on the east has a horizontal lengthscale of ~ 1.5 km, whereas the central part of the Lake that connects the sub-basins, a nearly restricted area due to the sedimentation from the Ermitsa stream outflows, is approximately only 1 km. Thus, the importance of the Coriolis force is expected to be suppressed in these areas, the overall value of Ro notwithstanding, and the behavior of the wind-induced flow at the central and the eastern part of the Lake seems to resemble that of a hydraulic flow rather than a geophysical flow.

All the simulations, where the flow was driven by the fresh water plumes, i.e. the outflow of the Ermitsa Stream as well as the inflow discharge from the connecting channel, were pursued up to the achievement of a steady state, in spite of the fact that, in reality, such a state is seldom approached. Based on the numerical simulations it is shown that the inflow discharge from the connecting channel causes the formation of a well formed cyclonic eddy at the eastern part of the Lake (smaller sub-basin). The eddy is already well formed and present by the end of the first 24 hours of simulation. At the northern-central part of the Lake, a smaller weak cyclonic eddy is formed. At the western part of the lake (larger sub-basin), the formation of a main flow path is observed at the north side, which is dictated by the fresh water plumes. It is noteworthy that in all cases, the sense of rotation of eddies described above is determined by the nearly strong currents dictated by the fresh water inflow and outflow in the Lake. An instance of the resulting surface flow field is depicted in Figure 2. In general terms, the salient features of the flow are survived during the steady inflow/outflow discharges in all simulations: the currents in the near field region of the fresh water inflows/outflows are substantially stronger than currents in the central parts of the Lake (i.e., open waters). Furthermore, a flow-through hydrodynamic regime is formed that substantially affects the water renewal.

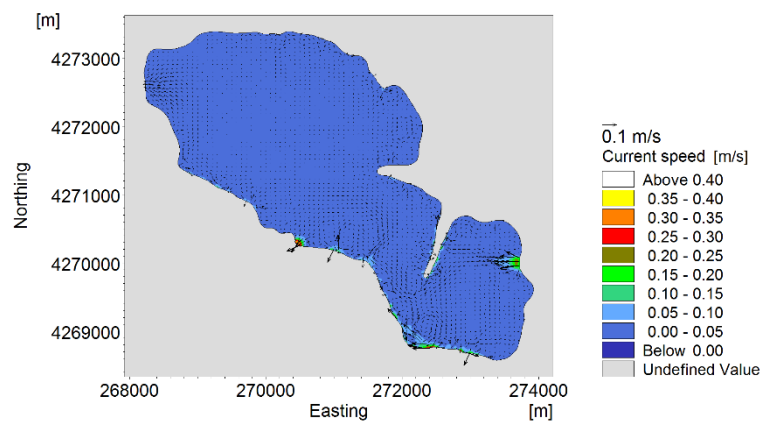


Figure 2. Surface flow field in the Lake generated by fresh water plumes, after steady state is reached

In addition, the hydrodynamic circulation of the Lake seems to be affected by the presence of a sand spit, formed at the northeastern part due to Ermitsa stream outflows, which works as a sandbar leaving waters nearly isolated at the deepest eastern part of the lake. As a result, a central gyre is formed at this area, leading to water entrapment and recirculation and eventually increased residence times. The incoming flood waters from the Trichonida Lake significantly improve the renewal of the Lysimachia waters, regardless the effect of the Ermitsa stream inflow, which is negligible. More specifically, a considerable inflow ($\sim 22 \text{ m}^3/\text{s}$) from the Trichonida Lake generates a flow-through regime from east to west, which is the main reason for the lake's replenishment. In this case the residence (e -folding) time varies from 20 days to 30 days, based on the inflow discharge (Figure 3).

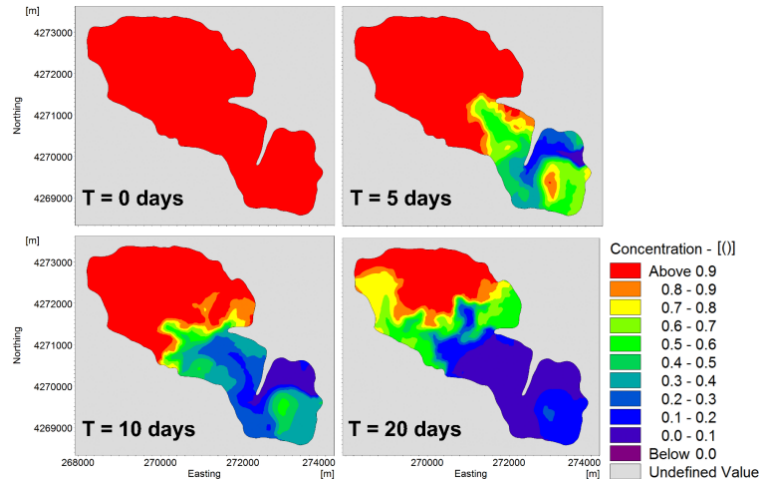


Figure 3. Distribution of the numerical tracer concentration inside Lysimachia Lake, after 5, 10 and 20 days

4 CONCLUSIONS

The present study documented, that the geometry of the Lysimachia Lake, under the fresh water inflows and outflows generates a characteristic flow-through hydrodynamic function of the water body. It has been shown that the inflow and outflow discharges, applied at different inlets and outlets of the Lake, generate a nearly unidirectional flow within the basin, the eddy formation notwithstanding, which enhances the mechanism of Lake's replenishment by creating flow-through like conditions. The resulting flow regime is considerably more efficient in terms of water renewal.

Acknowledgments

Part of this work has been supported by the Region of Western Greece under the research project "Investigation of the hydraulic behavior and suggestions for the regulation of the hydrodynamic system of Trichonida - Lysimachia lakes, in Western Greece".

References

- DHI (2018) MIKE 3 FLOW MODEL FM. Hydrodynamic Module-User Guide, DHI Software, p 138
 DHI (2018) MIKE 3 FLOW MODEL FM. Transport Module-User Guide, DHI Software, p 46
 Fourniotis NTh, Horsch GM, Leftheriotis GA (2018) On the Hydrodynamic Geometry of Flow-Through versus Restricted Lagoons. *Water* 10, 237. doi:10.3390/w10030237
 Fourniotis NT, Leftheriotis GA, Horsch GM 2021. Towards enhancing tidally-induced water renewal in coastal lagoons. *Environ Fluid Mech* 21, 343–360. doi:10.1007/s10652-020-09776-0
 Smagorinsky J (1963) General circulation experiments with the primitive equations I. The basic experiment. *Mon Weather Rev* 91, 99–165. doi:10.1175/1520-0493(1963)091<0099:GCEWTP>
 Ranjbar MH, Zaker HN (2018) Numerical modeling of general circulation, thermohaline structure, and residence time in Gorgan Bay Iran. *Ocean Dyn* 68, 35–46. doi:10.1007/s10236-017-1116-6
 Monsen N, Cloern J, Lucas L, Monismith S (2002) A comment on the use of flushing time, residence time and age as transport time scales. *Limnol Oceanogr* 47:1545–1553. doi:10.4319/lo.2002.47.5.1545

Ground penetrating radar for inspecting the core and base of coastal sand dunes

J.D. Alexopoulos^{1*}, I.K. Giannopoulos¹, G.S. Mitsika¹, V. Gkosios¹, A. Konsolaki¹, E. Vassilakis¹
S.E. Poulos^{1,2}

¹Faculty of Geology & Geoenvironment, National and Kapodistrian University of Athens, Panepistimiopoli,
Zografou, 15784, Attiki

²Institute of Computational Mathematics, Foundation for Research and Technology, 100 Nikolaos Plastira,
Vasilika Vouton, 70013 Heraklion, Crete

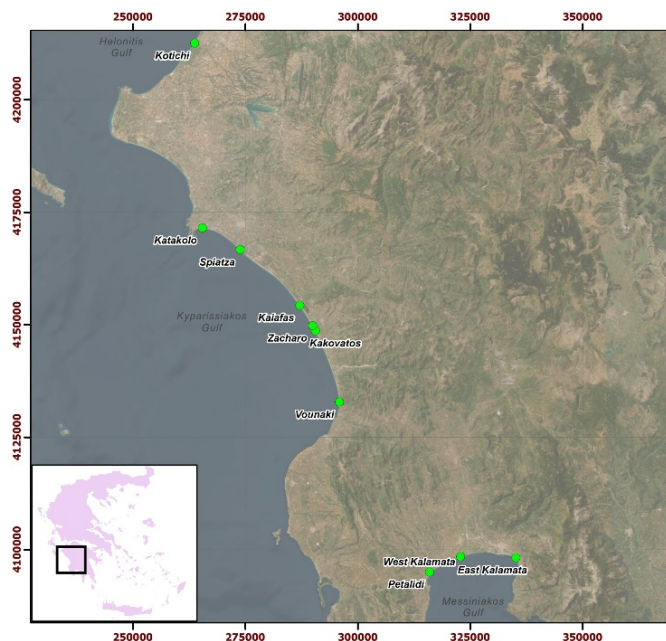
*Corresponding author: jalexopoulos@geol.uoa.gr

Abstract

The coastal environment of the west and south coast of Peloponnesus, Greece is characterized as an essentially tideless coastal environment exposed to high wave activity. Regarding the identification, the thickness and characteristics of the uppermost substratum of the selected coastal zones, at Hellonitis, Kyparissiakos and Messiniakos Gulfs, a detailed geophysical research was carried out. The geophysical survey aims to determine the thickness and the characteristics of the upper substratum of the selected coastal area, leading to the quantification of the sediment budget; the latter is considered essential to address potential coastal erosion. For this reason, the geophysical techniques of Electrical Resistivity Tomography (ERT) and Ground Penetrating Radar (GPR) were implemented to profiles normal and parallel to the shoreline. The geophysical results reveal the presence of the interface between the dry and wet sand deposits, along with the structure and the downward extension of the coastal material.

Keywords GPR, ERT, dune field, cross-bedding.

1 INTRODUCTION



substratum of the selected beach zones.

Figure 5. Map of the investigated coastal zones

Coastal zones are often associated with the presence of near-sea dunes, which act as a reservoir of sand. No matter of the causes of coastal erosion, either by a natural process and/or human intervention, its investigation has also to consider the backshore availability of sediment (i.e. dunes). The present investigation, within the concept of the ILIDA-KIT project, that deals with coastal erosion, concerns dunes being present at beach sectors located at the west and south coast of Peloponnesus (Greece), with the combined application of geophysical techniques of GPR and ERT. (Alexopoulos et al. 2022). More specifically, the investigation aims to identify the thickness, the internal characteristics and the base of the dunes, along with the uppermost lithostratigraphic

2 METHODOLOGY

The GPR and ERT techniques were implemented to profiles normal and parallel to the shoreline at **9 coastal sites** (Table 1), the location of which is presented in Figure 1. For the GPR survey a GPR Noggin 100 system, with a bistatic 100 MHz shielded antenna was used, provided by *Sensors & Software*. The data were acquired with a 10cm trace interval. The electromagnetic pulse transmission and the distance calculation was controlled by an odometer wheel. The traces were averaged, using the unique feature of

the system, that controls the number of stacks, depending on the environment and rate of acquisition. The aquired data were processed in *EKKO_Project* software, after implementing a typical filtering procedure, with the application of dewow, background removal, bandpass filters, sec2 gain and FK migration. The ERT measurements were carried out normal to the shore using the *Syscal Pro switch 48* unit, provided by *IRIS Instruments*, with 48 electrodes. The 2D inversion of the ERT data and the attribution of the topographic relief, were performed, using the *Res2DINV* software. All geophysical data were topographically corrected through GNSS measurements, acquired with RTK-NTRIP method.

Table 1. ERT and GPR lines

Sites	No of ERT lines	ERT Total Distance (m)	No of GPR lines	GPR Total Distance (m)
Kotichi	2	329	1	100
Katakolo	2	141	4	376
Spiatza	1	70.5	1	70
Kaiafas	3	212	17	2,010
Zacharo	-	-	2	400
Kakovatos	7	994	19	6,300
Vounaki	2	314	1	94
Petalidi	1	47	2	120
West Kalamata	1	47	2	120
East Kalamata	1	47	2	164
Total	20	2,201.5	51	9,754

3 RESULTS - DISCUSSION

The processing results of both geophysical techniques, revealed the characteristics (i.e. internal structure, thickness) of the uppermost layer of the beach sites under investigation. Also provide information for the quantification of the possible erodible upper layer of sands. The GPR profile at **Kotichi** coast (Figure 2a), covering a distance of 100m provides information limited to the upper layer (about 2m thick), due to the signal attenuation, induced by the high substratum conductivity. The ERT results indicate the existance of a relatively conductive subsurface distribution (Figure 2b), similar to that depicted from the GPR results. Both techniques indicate a small thickness of the upper unconsolidated (dune) layer, which is also related to the presence of a shallow water table that inhibits the deeper signal penetration.

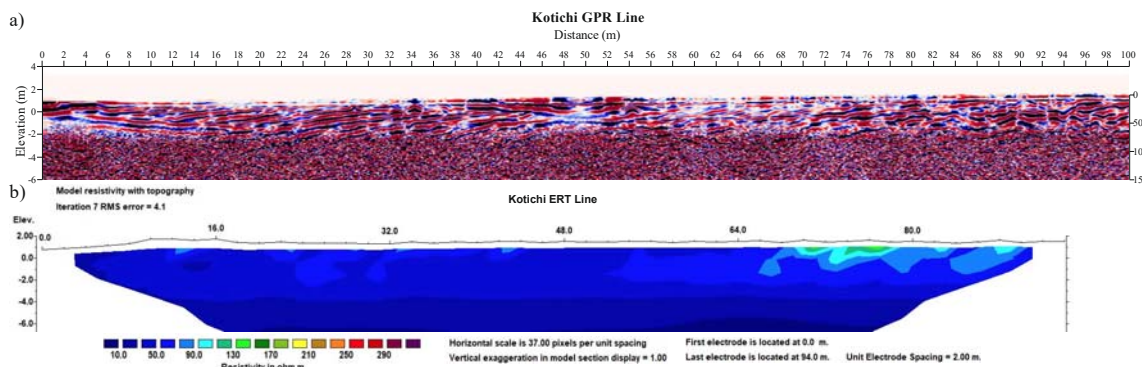


Figure 2. Geophysical results at Kotichi coast: (a) GPR profile, (b) ERT Profile

The GPR profile at **Katakolo** coast (Figure 3a), with a total length of 94m, reveals the subsurface information up to the absolute elevation of -4m. The propagation of the electromagnetic pulse at greater depths, is constrained by the increasing substratum conductivity. The above argument is strongly supported by the ERT results (Figure 3b), where high resistivity (>200 Ohm.m) areas have been investigated at the upper 3m (maximum), while in greater depths a more conductive (~50 Ohm.m) environment appears.

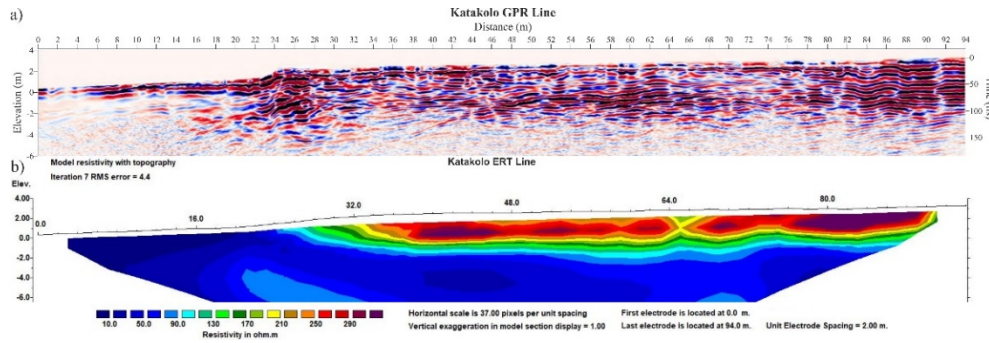


Figure 3. Geophysical results at Katakolo coast: **(a)** GPR profile, **(b)** ERT Profile

Further south, at **Spiatz** coast, although sand dunes are well developed, the GPR results are not satisfactory, due to high attenuation of the electromagnetic pulse; this is possibly related to anthropogenic activities that have affected to a great extent the natural coastal zone. The ERT results delineate the thickness of the coastal sandy sediments correspondingly to Katakolo coast.

The next selected coastal environment is located at **Kaiafas** coast (Figure 1), where the sand dune field is well-developed (Poulos et al. 2012). The combined ERT and GPR geophysical investigation, concerns the first two lines of dunes. At the GPR profile (Figure 4a), the electromagnetic pulse propagates until the absolute elevation of approx. -4.0m. A strong reflection surface prevails throughout the profile at an elevation of 0m (i.e mean sea level). This surface probably represents the interface between the dry (positive elevations) and the wet (negative elevations) sand deposits (Costas 2022). The pore water in the wet substratum may either comes from the freshwater aquifer and/or seawater intrusion. Cross-bedding is particularly profound at the 2nd dune line (distance >74 m), at the area where the basement of the second dune appears. The ERT technique, implemented along the same profile with the GPR, provides similar results (Figure 4b). More specifically, areas with high resistivities (>300 Ohm.m) are located from the distance of 18m until the end of the ERT profile and at an absolute elevation of -2 m maximum. Below this upper layer a more conductive substratum is investigated.

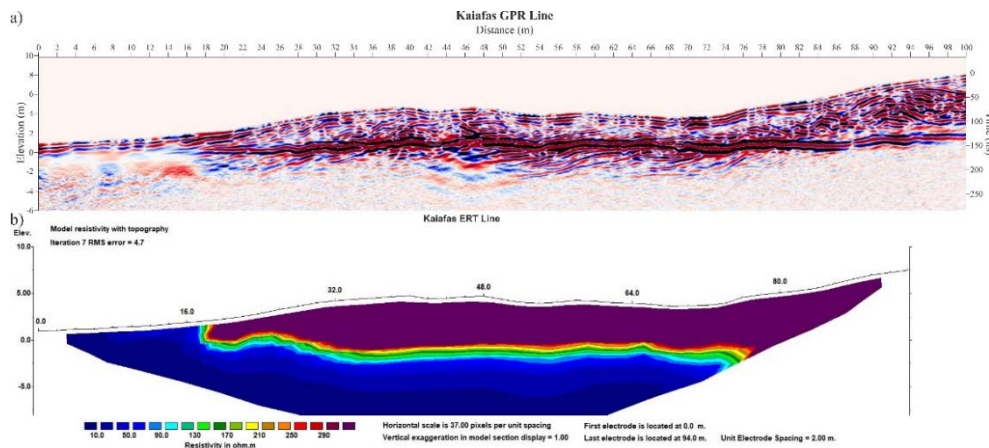


Figure 4. Geophysical results at Kaiafas coast: **(a)** GPR profile, **(b)** ERT Profile

At the coastal area of **Kakovatos** (Figure 1) where the dune field comprises of four (4) lines of dunes, the geophysical investigation based on the combined implementation of GPR and ERT techniques, covered the first two (2) series of dunes, adumbrated their internal structure and development (Alexopoulos et al. 2014). It has to be mentioned that the area between the 1st and the 2nd dune line, has been subjected to agricultural activity. The GPR profile (Figure 5a), normal to the coast, delineate the development of the first dune until the distance of 90m and at absolute elevation of no more than -3.0m, while the slack area, i.e., the plain area located between the dune ridges (90 - 110m distance), presented higher conductivity due to increased fine-grained sediments associated also to agricultural activity. This area appears at 90m to 110m distance in the GPR profile, while further inland (distance >110m) the presence of the second flattened dune is inferred, due to the structure of the subsurface medium, highlighted by the GPR technique. The presence of a strong reflection surface appears throughout the

1st dune line, at absolute elevation of 0m. It possibly represents the interface between the upper dry and lower wet deposits. Similar results are investigated by the ERT technique (Figure 5b). Areas with high resistivity values (>300 Ohm.m) are identified until the distance of 90m, which comply with the development of the 1st dune line. At the same area a rapid deterioration of the resistivity values is also observed at the level of 0 m. The slack area is also validated by the ERT results, at a distance between 90m to 110m, where a more conductive (<90 Ohm.m) environment has been investigated. The possible existence of the 2nd dune sediments is derived from high resistivity values (>300 Ohm.m) areas.

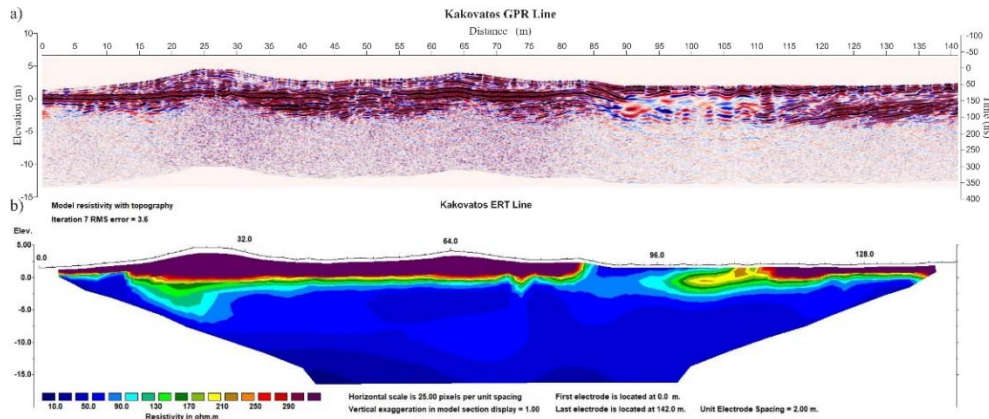


Figure 5. Geophysical results at Kakovatos coast: (a) GPR profile, (b) ERT Profile

At **Zacharo** coastal site (Figure 1) the geophysical investigation was based on the implementation of GPR technique, in two profiles. The processing results revealed the internal structure (cross-bedding), correspondingly to the Kakovatos coast.

The southern coastal sector of **Vounaki** was also investigated, with the implementation of GPR and ERT techniques. The GPR (Figure 6a) results, penetrating within the coastal sand deposits, until a maximum depth of 8.0m. Dune's internal structure (i.e., cross-bedding) has been destroyed to a great extent, most probably by human activities. It seems that the 2nd line of dunes has been artificially flattened. The ERT results, (Figure 6b), present a resistive area (>200 Ohm.m) at a distance greater than 20m. The thickness of this resistive zone increases landward, reaching its maximum (8m) at the end of the ERT profile. The ERT verifies the existence of a well-developed sand dune field in the area, which has been partially distorted by human intervention.

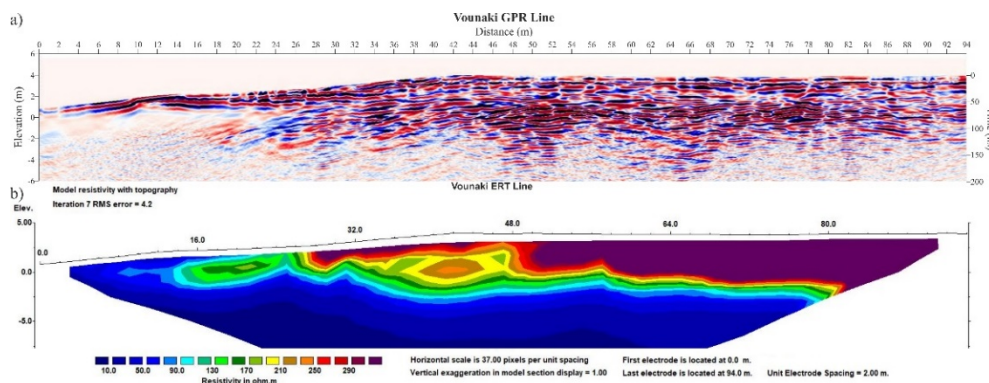


Figure 6. Geophysical results at Vounaki coast: (a) GPR profile, (b) ERT Profile

The geophysical investigation continues further south, in Messiniakos Gulf, at the coastal zones of **Petalidi and West Kalamata site**, where the sand dune environment is poorly developed and the sand deposits thickness is limited. Some lateral variations with a high percentage of pebbles are also recognized in the beach zone. The GPR results are limited to the elevation of -2.0m (maximum), due to increased conductivity of the substratum, causing the high attenuation of the electromagnetic waves. In both sites the ERT results revealed the presence of high resistive (>300 .Ohm.m) areas, with a maximum depth also of 2.0m (maximum), verifying the GPR outcome results.

The last investigated beach zone (**East Kalamata site**) was selected, due to its high percentage in coarse-grained material (i.e., pebbles and gravels). The GPR results (Figure 7a) reveal a rather conductive substratum, as the propagation of the electromagnetic pulse is limited at depths <4.0m. The dry beach sediments seem to develop to the elevation of -2.0m. This may be related to the seawater intrusion. The ERT results (Figure 7b) verify the assumption of the existence of a conductive substratum with low resistivity values (<50 Ohm.m), dominate throughout the ERT profile at elevation below 0m (absolute elevation). On the contrary, a high resistivity (>300 Ohm.m) formation, consisted by the dry coastal sediments, overlays the above-mentioned conductive environment.

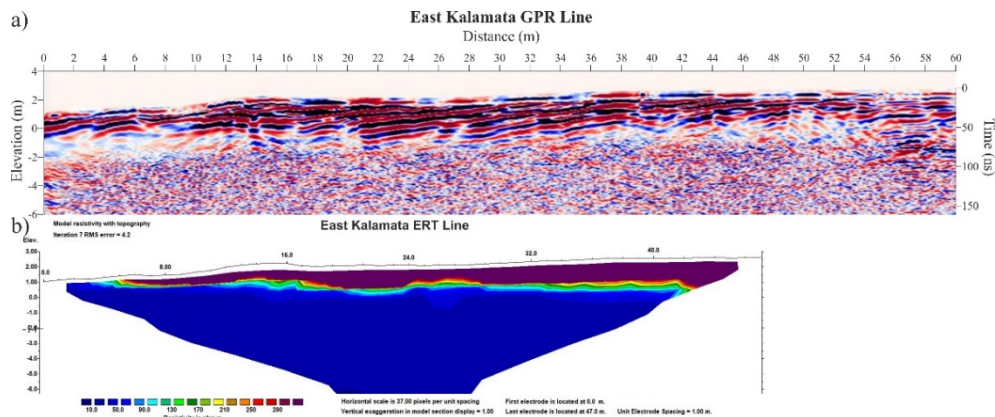


Figure 7. Geophysical results at East Kalamata coast: (a) GPR profile, (b) ERT Profile

4 CONCLUSIONS

The combined application of GPR and ERT geophysical methods in coastal environments and especially in coastal zones with sand dune fields, provide useful information on the composition, internal structure and volume of dry sediments, as well as information on the presence of an aquifer and, under certain conditions, indications of seawater intrusion. In the framework of the ILIDA_Kit tool, for the nine (9) different coastal zones, the material (sediment) most easily eroded by wave processes is restricted to the upper meters (absolute elevation >0m), where the sediments are dry. However, unconsolidated sediment is also present below the sea surface, but it appears to be saturated with water (either fresh or marine, depending on the land supply). In order to make the best use of the geophysical results in these complex and laterally variable geo-environments, sample drilling in combination with CPT, should be carried out.

Acknowledgements

This research was funded by the project “Decision-making tool for the confrontation of coastal erosion and extreme wave events in the coastal zone, in the context of climate change” (MIS 5129417), financed by the Sectoral Operational Programme «Competitiveness, Entrepreneurship and Innovation» (NSRF 2014–2020) and co-financed by Greece and the European Regional Development Fund (ERDF).

References

- Alexopoulos JD, Dilalos S, Poulos SE, Ghionis G, Mavroulis S (2014) Application of geoelectrical techniques in the investigation of a coastal sand dune field. In Near Surface Geoscience 2014-20th European Meeting of Environmental and Engineering Geophysics, 1, pp. 1-5
- Alexopoulos JD, Mitsika GS, Giannopoulos IK, Gkosios V, Konsolaki A, Vassilakis E, Poulos SE (2022) ILIDA-KIT tool: First results of near surface geophysical investigation techniques for successful management of coastal erosion. In: Bulletin of the Geological Society of Greece, 10
- Costas S (2022) Evolutionary Trajectories of Coastal Sand Barriers along the West Portuguese Coast during the Holocene. J Mar Sci Eng, 10(12), 1894. doi:10.3390/jmse10121894
- Poulos SE, Gaki-Papanastasiou K, Gialouris P, Ghionis G, Maroukian H (2012) A geomorphological investigation of the formation and evolution of the Kaiafas sand-dune field (Kyparissiakos Gulf, Ionian Sea, eastern Mediterranean) in the Late Holocene. Env Earth Sci, 66, 955-966. doi:10.1007/s12665-011-1305-4

Coastal marine steel corrosion: the environment's influence and in-situ monitoring – A review

Kassinis C.^{1*}, Onoufriou T.², and Michailides C.³

¹ EMERGE Research Centre, Cyprus University of Technology, Limassol, Cyprus

² EMERGE Research Centre, Cyprus University of Technology, Limassol, Cyprus

³ Department of Civil Engineering, International Hellenic University, Serres University Campus, Greece

*Corresponding author: christos.kassinis@cut.ac.cy

Abstract

It is without doubt that marine corrosion is of great interest and significance from various viewpoints, starting from an engineering design point of view, a safety concern view but also from an economic standpoint. At the forefront of exposure, coastal marine steel structures are exposed to the sea environment either directly in an immersed setting or in the immediate vicinity of the marine atmosphere (mist-laden sea air). Offering its contribution to understanding corrosion, this study gathers the literature's available findings in an effort to extract, in a concise and refined manner, the knowledge on the marine environment's effect on steel structures and the field monitoring of the corrosion taking place as a result of these interactions. Ultimately, it is expected that this study will form a reliable basis for further research, to be used in anticipating a realistic marine corrosion rate which will aid in avoiding over-engineering practices and properly appraising the remaining life of existing infrastructure.

Keywords: Corrosion, Marine, Steel, Monitoring.

1 COASTAL MARINE STEEL CORROSION

A naturally abundant electrolyte, the seawater stands out as an unpredictable and dynamic medium which corrodes steel either physically, chemically or even biologically. This silent degradation, as a result of the interaction of infrastructure with the sea, is globally causing a staggering annual cost of US\$2.5 trillion which constitutes around 3% of the world's GDP (Koch G., et al, 2016). The characterization of the material interactions and the environment, with the seawater being the protagonist, is crucial in understanding its impact on steel infrastructure.

1.1 The Coastal Environment

Apart from the natural annual cyclic and low sensitivity changes taking place, certain marine conditions in the shoreline's vicinity vary when compared to the open ocean. The fact that the movement of water is more constrained and the inflow of fresh water, both contribute to making the coastal waters more susceptible to physiochemical changes. Factors that are otherwise considered unchanged in the open ocean, are deviating in enclosed seas and estuaries. Other factors involved in the variation of parameters in coastal/enclosed seas is the influx of river waters, the pollution effects and the increased evaporation rate such as in the Red Sea's case. The corrosivity of coastal site seawater may thus vary significantly compared to open sea water. "Table 1" summarizes a comparison between important parameters changing from an open sea to an enclosed coastal setting.

1.2 Field Corrosion Data Availability

An otherwise excellent material of choice, steel's susceptibility to corrosion under saline conditions is a subject, in need to be studied in greater detail. Age related structural degradation is wed to corrosion and in fact it is considered to be the most important factor (Soares C., et al, 2009). An improved knowledge of fatigue performance as a result of field monitoring campaigns and a generalized sharing of corrosion data gathered from the industry is a necessity. This need for open data access and gathering of material failure information was stressed by professor Xiaogang Li in his article in Nature in 2015 (Li X., et al 2015). Forecasting mathematical models cannot be accurately constructed without the input of historic data. The better understanding of the behaviour of steel under marine exposure

will both contribute in the avoidance of overestimations and in the prevention of accidents. In addition, it will directly contribute to the great need of the industry’s Fitness for Purpose (FFP) assessments for life extension (by repairing or strengthening interventions) in structures that have reached or exceeded their design life (Nezamian A., et al 2012, Dehghani A. and Aslani F., 2019).

Table 1. Major Parameters’ Variation in Closed Vs Open Seas (Jsseling F.P., 1990, Dhanak M.R., Xiros N.I., 2016, Arias H.A. and Botte E.S., 2020, Shifler D.A. 2005)

Parameter	Coastal/Enclosed Setting Compared to the Open Seas	Explanation
Salinity	Lower/Higher	Due to Dilution by Inflowing River Flows/Due to Increased Evaporation. Depending Which Phenomenon Prevails
Nutrients	Higher Concentration	Enriched River Influx and Agricultural Runoffs/Sewage Effluents
Biological Activity	Higher	Favorable Conditions (Nutrients)
Pollution	Higher	Proximity to Industrial/Agricultural/Domestic Activity
Dissolved Oxygen	Lower	Most of The Times It Is Lower (Due to Increased Biological Activity Consuming Oxygen and Due to Increased Salinity)
Temperature	Higher	Proximity to Land Bodies and Enclosed/Minimized Circulation Environment
pH	Higher/Lower	Due to Inflowing “Hard” (Caco ₃ Containing) River Waters/Due to Acidic Pollutants
Calcareous Scale Formation	Higher/Lower Chance to Form	Due to Inflowing “Hard” (Caco ₃ Containing) River Waters/ Due to Inflowing “Soft” (Low Caco ₃ Content, Low Ph) River Waters

1.3 Marine Steel-The Material of Choice

The choice of material can greatly influence the rate at which it will deteriorate but the decision cannot be based solely on the resistance to corrosion, even though important. Carbon steel is amongst the most active metals but when combined with protective measures such as cathodic protection, coating and sacrificial thickness allowance it still remains the material of choice due to its cost effectiveness and strength properties. Other parameters such as toughness and weldability or the alloying materials choice also affect the decision-making process. In “Table 2”, primary and secondary properties for the selection are presented along with their assigned weighted factors as adopted from Charles J.A. (Charles J.A. et al, 1997) in his study on material choice for ship hulls. This multi-criteria decision making (MCDM) problem of material choice is in need of informed decision-making that takes into account all available technical characteristics in order to ensure a cost effective, failure resistant and safe optimized choice of material. Mathematical approaches and decision analyses methods such as the Technique for Order of Preference by Similarity to Ideal Solution (TOPSIS) could be used in greater extend in an effort to improve the material selection methodology.

Table 2. Marine Material Selection Properties and Weighting Factors (Charles J.A. et al, 1997, Reuben R., 1994)

Primary Properties	Weighting Factor	Secondary Properties	Weighting Factor
Strength (MPa)	20	Corrosion Rate (mm/year)	4
Toughness (MPa.m ^{1/2})	20	Weldability	3
Cost (€/kg)	10	Density (kg/m ³)	1

2 CORROSION INFLUENCING FACTORS

Several researches have studied the sea environment in an effort to conclude on the leading factors influencing the corrosion rate of steel receiving marine exposure. The complexity of this dynamic medium and the interrelation of environmental factors makes this a challenging task. Ultimately the

scope served by the gathering of these factors is the quantification on the corrosion rate based on the environment in hand and their incorporation in corrosion rate predictive mathematical models. It is thus imperative to understand their effect both in isolation but also how each relates and is affected by others. “Table 3” below has been constructed by gathering information from an extended review on published literature on this subject. The effect of the factors has been split into two generic environmental zones one being under immersed conditions and the other under an atmospheric setting. Furthermore, their importance on corrosion rate has been characterized.

3 MONITORING CORROSION

The dynamic and living character of the marine environment demands for monitoring methods that are in situ and real time in order to convey the real picture of the conditions and parameters of interest. This translates to a responsive act of intervention during environmental compromising events and to a clearer understanding of the complex interactions of, for instance, the corrosion rate and the marine environment. Furthermore, the real time facet of these technologies make automation a reality but also the capability to become part of a network of machine to machine (M2M) interaction that minimizes the need for human interference. “Table 4” consists of a snapshot of a part of the technologies analyzed in the complete review study. This includes both physical and real time electrochemical methods.

Table 3. Marine Corrosion Influencing Environmental Factors (Roberge P., 2019, Cramer S. and Covino B., 2006, Melchers R.E.,2009, Soares Guedes C., 2011, Shifler D.A., 2005, Pei Z., et al, 2021, Little B.J., et al, 2020)

MARINE CORROSION INFLUENCING ENVIRONMENTAL FACTORS	
Immersed Setting	
<i>Marine Environmental Parameter</i>	<i>Comments</i>
Temperature	Initially Doubles for Every 10°C Increase in Temperature
Dissolved Oxygen (Do)	At Initial Stages it is Rate Controlling
Microbial Organisms	(Metabolic Products of Sulphate Reducing Bacteria (SRB) Cause Corrosion, Nitrogen Is Their Limiting Nutrient (So Ammonium and Nitrates Are Vital)
Pollutants	CO ₂ , NH ₃ , H ₂ S
Salinity	Some Authors State Effect Is Negligible
Ph	Some Authors State Effect Is Negligible (No Correlation). It Indirectly Affects Calcite Buildup (Calcium Carbonate)
Flow Velocity	Can be Ignored in Calm Waters
Calcites Layer	Dynamically Dissolves/Builds Up on The Metal Surface Based on pH Changes
Atmospheric Setting	
<i>Marine Environmental Parameter</i>	<i>Comments</i>
Salinity (Cl)	Marine Chlorides Transferred in The Form of Aerosols (By Waves, Mist Etc.) Deposit on The Metal Surface and Dissolve in The Moist Film.
Moisture	(In Any Form (Relative Humidity (RH), Dew Etc.), Time of Wetness (TOW)
Temperature	Follows Same Principles as In Immersion Conditions
Wind Speed	As a Carrier of Abrasive and Corrosive Particles
Wave Height	As a Carrier of Salinity
Pollutants	Most Important Are NO _x 's And SO ₂
Rainfall	In Removing Pollutants' Buildup
Metal Orientation and Geometry	Angle of Exposure to The Horizontal and to the Direction of Winds
Dust and Soot	In Combination with Wind Speed and Pollutants

Table 4. Marine Corrosion Monitoring Technologies (Musik D., et al, 2022, Diler E., et al, 2021, Cox M.W, 2014, Lv J., et al, 2020)

Technology	Environment	Real Time Application	Field Application	Responsiveness
Corrosion Coupons (CC)	Immersion/ Atmospheric	Not Real Time	Wide Use	High if exposed for long periods
Electrical Resistance (ER)	Immersion/ Atmospheric	Real Time	Wide Use	High
Linear Polarization Resistance (LPR)	Immersion/ Atmospheric	Real Time	Wide Use	High
Electrochemical Noise (EN)	Immersion/ Atmospheric	Real Time	Medium Use	High

4 CONCLUSIONS

This study forms part of an extended research project which revolves around the subject of water quality in a coastal setting and its in situ monitoring. Enclosed seas are characterized by limited exchange of water with the oceanic bodies and are thus very responsive and sensitive to pollution events. A prime example is the Mediterranean Sea whose only connection to the oceans is through the narrow Strait of Gibraltar. The design and deployment of suitable monitoring stations is already in the initial stages of implementation and will form the backbone of data acquisition. The data processing and their final utilization will aid in monitoring environmental changes both in regards to their effect on the ecosystem and the structures found in its vicinity.

References

- Arias HA, Botte ES (Eds.) (2020) Coastal and Deep Ocean Pollution, CRC Press Taylor & Francis Group, Florida USA
- Charles JA, Crane FAA, Furness JAG (1997) Selection and Use of Engineering Materials, Butterworth-Heinemann, Oxford
- Cox WM (2014) A Strategic Approach to Corrosion Monitoring and Corrosion Management. *Procedia Engineering*, 86:567–575. doi:<https://doi.org/10.1016/j.proeng.2014.11.082>.
- Cramer S and Covino B (2006) ASM Handbook, Volume 13C, Corrosion: Environments and Industries, ASM International, Ohio USA
- Dehghani A, Aslani F (2019) A review on defects in steel offshore structures and developed strengthening techniques, *Structures*, Volume 20, 635-657, doi:<https://doi.org/10.1016/j.istruc.2019.06.002>
- Dhanak MR, Xiros NI (Eds.) (2016) Springer Handbook of Ocean Engineering, Springer, New York
- Diler E, Peltier F, Becker J, Thierry D (2021) Real-time corrosion monitoring of aluminium alloys under chloride-contaminated atmospheric conditions, *Materials and Corrosion*, Volume 72, Issue 8:1377-1387, <https://doi.org/10.1002/maco.202112302>
- Guedes Soares C, Garbatov Y, Zayed A (2011) Effect of environmental factors on steel plate corrosion under marine immersion conditions, *Corrosion Engineering, Science and Technology*, 46:4, 524-541, doi: 10.1179/147842209X12559428167841
- Guedes Soares C, Garbatov Y, Zayed A, Wang G (2009) Influence of environmental factors on corrosion of ship structures in marine atmosphere, *Corrosion Science*, Volume 51, Issue 9, 2009, 2014-2026, doi:<https://doi.org/10.1016/j.corsci.2009.05.028>
- IJsseling FP (1990) Illustrated Case Histories of Marine Corrosion, London UK, The Institute of Metals, <https://doi.org/10.1515/CORRREV.1995.13.2-4.297>
- Jeffrey R, Melchers RE (2009) Corrosion of vertical mild steel strips in seawater, *Corrosion Science*, Volume 51, Issue 10, 2009, 2291-2297, <https://doi.org/10.1016/j.corsci.2009.06.020>
- Koch G, Varney J, Thompson N, Moghissi O, Gould M, Payer J (2016) International measures of prevention, application and economics of corrosion technologies study, Houston, NACE
- Li X, Zhang D, Liu Z, Li Z, Du C, Dong C (2015) Nature, Materials science: Share corrosion data, Volume 527, Issue 7579, 441 – 442, <https://doi.org/10.1038/527441a>

- Little BJ, Blackwood DJ, Hinks J, Lauro FM, Marsili E, Okamoto A, Rice SA, Wade SA, Flemming HC (2020) Microbially influenced corrosion—Any progress?, *Corrosion Science*, Volume 170, 2020, 108641, <https://doi.org/10.1016/j.corsci.2020.108641>
- Lv J, Yue Q, Ding R, Wang X, Gui T, Zhao X (2020) The Application of Electrochemical Noise for the Study of Metal Corrosion and Organic Anticorrosion Coatings: A Review. *ChemElectroChem*, 8(2), 337–351 <https://doi.org/10.1002/celec.202001342>
- Melchers RE (2009) Long-term corrosion of steels exposed to marine environments, *European Journal of Environmental and Civil Engineering*, 13:5, 527-546, DOI: 10.1080/19648189.2009.9693132
- Musik D, Wójcik K, Sekuła-Wybańska M, Konopacki M, Rakoczy R (2022) Analysis of the Corrosion Process with the Application of the Novel Type of Coupon Installation. *Processes*. 2022; 10(12):2468. <https://doi.org/10.3390/pr10122468>
- Nezamian A, Nicolson RJ, Iosif D (2012) State of art in life extension of existing offshore structures, ASME 2012 31st international conference on ocean, offshore and Arctic Engineering, 1-10, doi:10.1115/OMAE2012-83302
- Reuben RL (1994) *Materials in Marine Technology*, Springer-Verlag, London
- Roberge P (2019) *Handbook of Corrosion Engineering*, McGraw Hill, New York USA
- Shifler DA (2005) Understanding material interactions in marine environments to promote extended structural life, *Corrosion Science*, Volume 47, Issue 10, 2335-2352, <https://doi.org/10.1016/j.corsci.2004.09.027>
- Singh R (2014) *Corrosion Control for Offshore Structures-Cathodic Protection and High-Efficiency Coating*, Oxford United Kingdom, Gulf Professional Publishing-Elsevier, <https://doi.org/10.1016/C2012-0-01231-8>

Monitoring and analysis of coastal eutrophication using remote sensing

I. Biliani^{1*}, I. Zacharias¹

¹Department of Civil Engineering, University of Patras, Rio, Patras, 26500

*Corresponding author: biliani.i@upnet.gr

Abstract

The degradation of water quality due to marine eutrophication has become a crucial issue in recent years. The number of eutrophic water sites worldwide has dramatically grown due to anthropogenic activities such as agricultural runoff, marine effluents, and intensive human activity in coastal areas. Remote sensing analysis has shown to be a quick, affordable, and nearly instantaneous method for assessing the surface quality status of many water bodies. Using remote sensing technology, this study provides an efficient method of determining the seasonal distribution of chlorophyll-a in coastal waters.

Keywords Marine Eutrophication, Remote Sensing, Seasonal.

1 INTRODUCTION

In recent years, marine eutrophication has become a major factor in water bodies' quality control. Agricultural runoff, seawater effluents and intense anthropogenic activities in the coastal areas have amplified the geographic distribution of eutrophic water sites globally (Ménesguen and Lacroix, 2018).

Climate change is also related to an increase in the number of eutrophic ecosystems. The need to retain, protect and restore water bodies' quality status has been recognised by European Member States.

The analysis of remote sensing allows the monitoring of several water bodies simultaneously, with no cost, and in near real-time. Identifying the mechanisms that influence and operate in the aquatic ecosystem and reflect climate change is achieved through water quality cartography (Poschold and Braun-Reichert, 2017). Remote sensing analysis is a fast, cost-effective, and near real-time tool to evaluate multiple-water bodies' quality status.

In this study, an effective approach is presented for determining the seasonal distribution of chlorophyll-a in coastal and inland waters.

2 METHODOLOGY

Daily MODIS Aqua Atmospherically Corrected Surface Reflectance georeferenced images were freely downloaded from NASA's LAADS DAAC website. The analysis expands over a period of almost two decades from July 2002 to 2021 for the selected study area with spatial distribution of 500m.

The selected study area for our analysis was Aitoliko Lagoon (Figure 1). Aitoliko Lagoon is situated in Western Greece and has high ecological importance because it is a wetland protected by Ramsar and Natura 2000 conventions (Gianni et al., 2012). Field measurements have resulted that Aitoliko Lagoon suffers from eutrophication and anoxic crisis during the spring season (Gianni et al., 2011, Papadas et al., 2009).

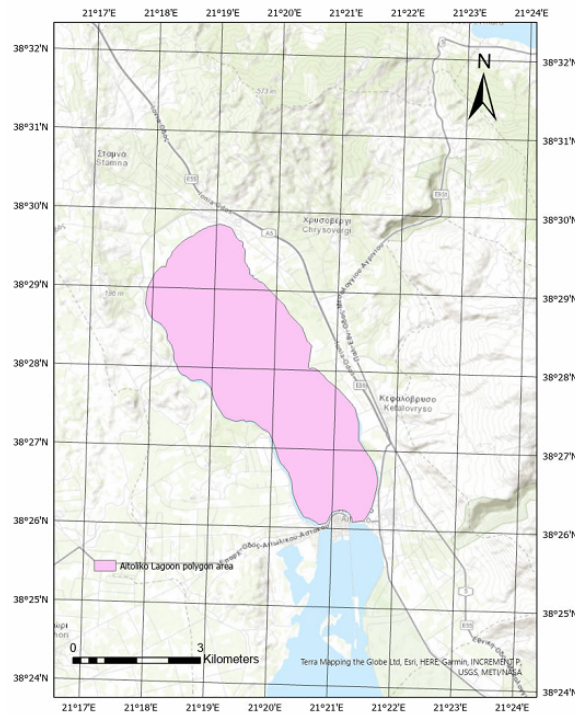


Figure 1. Aitoliko Lagoon Polygon Area

Daily georeferenced images had been downloaded, applying RStudio numerical algorithm. Then, specific point stations within the Aitoliko Lagoon were isolated and the satellite values were obtained for each spectral channel, for each point station and for a period of almost 20 years.

Statistical data processing is applied to the derived timeseries for each vector of the dataset table. The methodology used does not manually exclude possible deriving from aerosols and atmospheric particles. The extreme values are identified and attributed with the constant «c». Negative surface reflectance values with no physical meaning are also attributed with the constant «c». Therefore, the new statistical components were found for each vector of the Satellite Dataset. Then, the statistical characteristics were recalculated. Chlorophyll-a concentration is calculated from the corrected remote surface reflectance values of each point station of the study.

According to NASA's Ocean Color approach, the acquisition of chlorophyll-a's concentration requires the values of three spectral channels: red (469nm), blue (555nm) and green (655nm). Two algorithms were created: the OCx algorithm from O'Reilly et al. (O'Reilly and Werdell, 2019) when the concentrations were greater than 0.35mg/m³ and the Color Index (CI) algorithm as described by Hu et al. (Hu et al., 2019) when concentrations were lower than 0.25mg/m³. The weighted average was calculated for values between 0.25 and 0.35 mg/m³.

3 RESULTS AND DISCUSSIONS

The seasonal distribution of chlorophyll-a concentration of Aitoliko Lagoon describes a eutrophication increase in April until August. In situ measurements of Gianni et al and Papadas et al. (Gianni et al., 2011, Papadas et al., 2009) have concluded to the same result.

Aitoliko Lagoon is eutrophic since it receives wastewater from Aitoliko town and irrigation waters from the catchment (Figure 2).

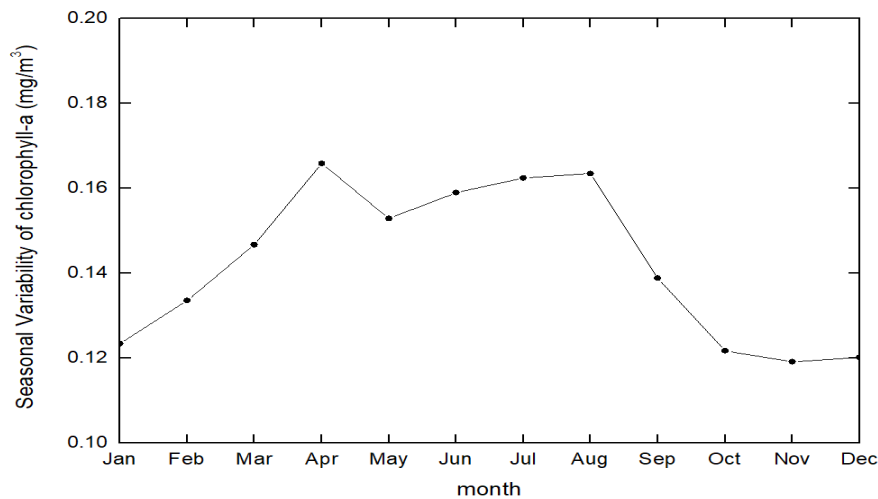


Figure 2. Seasonal variability of chlorophyll-a (mg/m³)

The results of this study could help stakeholders to identify potential months for restoration and water treatment. The sporadic in situ measurements do not offer the opportunity to evaluate the change of chlorophyll-a over time. Remote sensing chlorophyll-a evaluation offers a new tool for the management plans for coastal areas, as well as lakes and reservoirs.

References

- Gianni, A.; Kehayias, G.; Zacharias, I. (2011) Geomorphology modification and its impact to anoxic lagoons. *Ecol. Eng.*, vol. 37 (11), pp. 1869–1877
- Gianni, A.; Kehayias, G.; Zacharias, I. (2012) Temporal and spatial distribution of physico-chemical parameters in an anoxic lagoon, Aitoliko, Greece. *J. Environ. Biol.*, vol. 33 (1), pp. 107–114.
- Hu, C.; Feng, L.; Lee, Z.; Franz, B. A.; Bailey, S. W.; Werdell, P. J.; Proctor, C. W. (2019) Improving Satellite Global Chlorophyll a Data Products Through Algorithm Refinement and Data Recovery. *J. Geophys. Res. Ocean.*, vol. 124 (3), pp. 1524–1543.
- Ménesguen, A.; Lacroix, G. (2018) Modelling the marine eutrophication: A review. *Sci. Total Environ.*, vol. 636, pp. 339–354.
- O'Reilly, J. E.; Werdell, P. J. (2019) Chlorophyll algorithms for ocean color sensors - OC4, OC5 & OC6. *Remote Sens. Environ.*, vol. 229 (April), pp.32–47
- Papadas, I. T.; Katerinopoulos, L.; Gianni, A.; Zacharias, I.; Deligiannakis, Y. (2009) A theoretical and experimental physicochemical study of sulfur species in the anoxic lagoon of Aitoliko-Greece. *Chemosphere*, vol. 74 (8), pp. 1011–1017
- Poschlod, P., Braun-Reichert, R., (2017) Small natural features with large ecological roles in ancient agricultural landscapes of Central Europe - history, value, status, and conservation. *Biol. Conserv.* 211, 60–68.

Carrying capacity indicators in tourism: the case of the island of Paros coastal zone

D. Prokopiou^{1,2*}, B. Tselentis¹

¹University of Piraeus, Department of Maritime Studies, Athens, Attika, Greece

²Paros Municipality, Paros Island, Cyclades, Greece

*Corresponding author:

Abstract

Many researchers have studied the challenges concerning the carrying capacity of tourist destinations. Carrying capacity has been defined as the ability of an ecological system to sustain the development of human activities without negatively impacting the ecosystem services inherent within the system. It is a common belief that the carrying capacity approach has proved to be both significant and functionally supportive of tourist destination sustainable management. Considering the challenge of sustainable growth, it is important to emphasize that tourism causes various negative impacts that may risk long-term growth and that overlooking the interdependence between the concept of carrying capacity and sustainability of tourism growth, will most likely, exacerbate the many problems that arise in areas of unique socio-cultural and ecological value. Previous research has developed specialised measurement instruments and indicators, as well as a comprehensible methodological guide for their use, in order to estimate the carrying capacity and limits of a tourist destination. Many Greek islands and coastal areas have been studied to identify the factors influencing a tourist product and its ecological, social, and economic sub-systems, including infrastructure, environmental characteristics, and tourism entrepreneurship. The above were applied to Paros, a Greek Island in the central Aegean Sea, which hosts a many as 500.000 tourists per year, in an attempt to further involve local societies and stakeholders in addressing and understanding the impacts on existing non- renewable resources, the transport infrastructure and primary production. This endeavour aims to design a comprehensive, diverse, and socially integrated sustainable tourism strategy policy for the island of Paros.

1 INTRODUCTION

It is the purpose of this paper to apply the principles of carrying capacity assessment to Paros Island in order to address tourism development and business opportunities. In this study we have used carrying capacity indexes in order to formulate a sustainable tourism development plan for the island. The research and data collection were financed by the Municipality of Paros Island Greece [1].

Paros lies almost at the centre of the group of islands called Cyclades and is the third largest island, after Naxos and Andros. Paros is an international well- known tourist destination for summer holidays, because of natural beauty, the nice beaches, extraordinary architecture, the sun, and Mediterranean climate. Before its tourist development, agricultural and fishery were the main economic sectors in Paros, while in the recent years, vineyard cultivation and wine production experienced significant growth. The coastline is indented, with numerous small islets and two large, sheltered bays, those Paroikia in the west and Naoussa in the north. Around the island there are also several small ports that have taxi boat services to the excellent beaches of adjacent islands.

2 IN PAROS ISLAND

According to transport statistics since the operation of the new airport (July 2016), the number of passengers has increased dramatically. In 2013 the passenger arrivals at the old airport were 14,954, whereas the numbers increased to 37,872 (2016) and 86,8400 in 2017. Arrivals in Paroikia port totaled 631.000 in 2013, whereas in 2018 visitors increased to 710.000, an increase of 45%. Hotels first appeared in Paros in 1973 and by 2007 hotel rooms numbered 1000 beds. Three year later, in 2010, these increased to 6,893 beds, an increase of almost 700%. In 2019 hotel beds reached a record number of 7,148 [2]. Apart from hotels, the room-to-let business offered 14,847 beds capacity, and “air b’n'b” houses were estimated to have contributed as many as 7,000 beds, in 2019. Although these figures

indicate that as early as the 60's the island developed as a summer tourist destination and one of the most famous holiday resorts in the Cyclades islands, this increase was highly seasonal and was not accompanied by a planned tourist policy.

3 CARRYING CAPACITY INDICATORS FOR PAROS ISLAND

Carrying capacity is defined as the maximum number of people that may visit a tourist destination at the same time, without causing destruction to the physical, economic, socio-cultural environment, as well as causing an unacceptable decrease in the quality of visitors' satisfaction [3]. When estimating carrying capacity it is important to analyze the whole business as the environmental infrastructure of the region. [4-5]. Today, controlling tourism growth has become a central policy issue for the tourism trade [6] and it is noteworthy that carrying capacity assessment has become an important tool for facilitating planning and developing policy issues for the tourism industry [7]. Previous studies for other destinations [8-10] highlighted the following indices describing the Paros case [11].

The categories of the carrying capacity indices in Paros case study were: Energy and Natural Resources, Production, Environmental Infrastructure, Natural Environment and Land Use, Tourism, Coastal Zone, Transport, Health Services, Public Security and Culture. Data were collected from the Municipality of Paros, the Hellenic Civil Aviation Authority, the Hellenic Police, the Hellenic Coast Guard, the Public Electricity Board, the Ministry of Health Services, the Hellenic Public Insurance Fund (EFKA), the Archaeological Museum of Paros, the Hellenic Emergency Aid Centre, the Greek National Tourism Organisation, the Regional Government of the Aegean Sea, the Hellenic Fire Service and the Paros Hotel Union. The estimated carrying capacity indicators for Paros was 76.

3.1 Energy and natural resources

Paros electricity demands are serviced by the mainland through an underwater cable. Electricity consumption amounts to 50 MW, and energy from renewable energy sources stands at 3 MW. Electricity consumption in tourism season is 40 MW. Regarding the undergrounding of electricity networks, a large percentage of the networks are above ground, and the island is unable to accept other above ground networks. The water supply on the island of Paros is marginally sufficient in terms of quantity, while the supply network is old and in need of repair, by the municipality, creating several problems as to the quality, especially for drinking. This problem is further increased due to the fact that during the high season, the population of Paros quadruples. Water consumption is about 347.510 tons per year.

3.2 Production

Production in Paros is oriented towards the tertiary sector, processing is prosperous and primary production is low. Primary production has 337 employees (mainly in livestock, since the island accommodates a cattle population is 11.500), secondary production 1375 and 3.663 employees in tertiary production. In Paros, there are 2008 companies have sole owners, while others amount to 929. In fact, most businessmen are permanent residents of the island.

3.3 Environmental infrastructure

The waste management infrastructure is modern and well maintained, while waste recycling amounts to about 1100 tons per year. Garbage production amounts to about 10.000 tons per year. Urban wastewater amounted to 713,000 cubic meters in 2018, while about 42% (7040 to a total of 16.905) of all households and business are connected via a central sewage collection network. The island has no hazardous waste and any atmospheric exhaust emissions are mainly found around the port and on the road network, including the ring road of Paroikia. Unfortunately, no data exist concerning greenhouse gas production and the quality of air on the island, which is expected not to be impacted seriously.

3.4 Natural environment and land use

There is one protected wildlife area of 1401 acres. All over the island there is interesting bird fauna and sea mammals are found. There are also 26698,74 acres regarding the land use regulations.

3.5 Natural environment and land use

Tourism in Paros is the main economic activity. In Paros there are 24 tourists per acre of protected areas and 2,919 tourists per permanent resident. Tourist development is concentrated on the coastal zone but extends all over the island, which is connected via an extended road network connecting several major cities and villages. The distance between tourist destinations is relatively small making it easy to visit several places in a short time. For example, the distance between Paroikia and Naoussa (two main cities) is only 10.6 km. Tourist density amounts to 204 tourists per square kilometer and the estimation of maximum seasonal population was 55.000 for the month of July 2019. Based on a calculation using data of urban waste production for the same month, the population was estimated at 65.000 people.

Tourism infrastructure includes 7.148 hotels, 14.847 rooms to let and 7.000 houses (Airbnb). The total number of overnight stays is estimated at 278.140 for foreigners (2019) and 80,923 for visitors (2019), while the average stay in days is one week. The total active population of the island is 5.375 and the number of employees in the tertiary sector (mainly tourism) is 3.663. In summary, the maximum population of Paros on a daily basis is 55,000 people. With data from 2022, 65,000 people. This number is an estimate and for an island like Paros it is huge.

The amount of the active population employed in accommodation services are 994 people which represents 44% of the total population (tertiary sector employees). The percentage of the active population employed in tourism represents 60.23% of the total population of the island. The analysis of total tourist arrivals in Paros and available accommodation lead to the conclusion that there are at least more 10.000 non licensed beds, probably without license, beds that are on the market, but are not declared and registered to Greek Government. Tourism activity is mainly concentrated along the coastal zone, with the number of beaches being 36, many of which are located on the west coast. Tourism infrastructure is located in Naoussa and Paroikia. Conference halls in hotels are 4 with a capacity of 100 persons each. A theatre room is available at a technical high school.

Alternative tourism companies in Paros are 20, privately owned boats for day cruises, ecological excursions, sea sports, boat renting, sea skiing, scuba diving, fishing tourism, excursions with cars, excursions with horse carriages, horse riding and bike excursions. There is public transport for residents and tourists with 15 intercity buses and 1 city bus and 6 tourist buses. It is calculated that there are 215 tourists per kilometer of coastline. Finally, there were 17 cruise ships arrivals in 2018 with 2.476 visitors. In Paros there are 5 camping sites, 500 restaurants and 800 coffee shops. A variety of vehicles can be rented in Paros during the tourist season amounting to about 2700 cars and 500 motorbikes.

The local tourism development policy is based on the General Urban Plan of Paros. The local tourist demand is mainly from Scandinavia, Britain, France, and Germany.

3.6 Tourism destination marketing

The tourist promotion is organized by the Municipality of Paros with the assistance of partners. Participation of Paros in tourism exhibitions is an important marketing activity, by providing information and promoting Paros as a tourist destination in forums such as BIT, BOOT, Ferrien Messe, Greek Tourism Expo, ITB, Philoxenia, Salon Mondial du Tourisme, Top Resa, WTM It is believed that tourist promotion of Paros is well organized and has positive results.

3.7 Coastal zone and ports

The coastal zones are always sensitive and impacted by environmental pressures mainly human based. In total the beaches extend for about 22.5 km and the coastline is 175 km. There are 5 beaches with a Blue Flag accreditation out of a total of 36. The majority of the coast is inhabited and built. Settlements along the coast include: Paroikia, Naoussa, Voutakos, Pounta, Aliko, Gyfas, Dryose, Tserdakia, Logaras, Pisolivadi. The only port that of Paroikia, has 8 berthing areas, while only four are in use by the Port Authority. In 2018, the port of Paros received 613.847 passengers, 54.227 more than in 2017, while the arrival of privately owned vehicles amounted to was 58.088 in 2018, compared to 51,067 in 2017. There are plans to build a new port on the island in the near future, to accommodate arrivals of commercial - non-passenger ships, which amount to about 300 per year. Marine pollution cases are limited in Paros,

with only three in last decade. Paros beaches for swimming are 36 with 22,5 kilometers length as the whole coastal zone is 56. The beaches with blue flag are 5 in 2022.

3.8 Health services and public security

Paros has one health centre and 48 doctors. Regional crimes and incidents are mainly concentrated in the Naoussa region, which accounts for about 70% of the island total. About 52% of accidents occur in the regional and urban roads of Paroikia. Forest fire incidents are rare.

3.9 Culture

Paros has museums, archaeological sites, and Byzantine monuments of special interest. Archaeological excavations are being carried out in Paros in 6 locations.

4 CONCLUSIONS – PROPOSALS

Taking into account the categories of the carrying capacity (CC) indices in Paros as described above, several conclusions and proposal are reached on issues such as energy and natural Resource management, primary and tertiary production, environmental infrastructure, protection of the natural environment and land use, and coastal zone planning. Other issues highlighted from the above CC analysis were also studied and specific proposals reached on issues pertinent to both sea and land transport, health services, culture and heritage and finally public security. The findings are summarized below covering the relevant areas of interest as far as tourist policy and development are concerned.

4.1 Infrastructure and Development

The biggest problem facing Paros is wastewater and water management. In order for the place to develop, the island needs to be covered by sewage treatment plants. Water reserves must become further self-sufficient, and the water supply networks modernized and extended. The Municipality is gradually working towards resolving the problem. Water reserves are sufficient and there is an action plan to improve the network. In Paros there are further sewage networks which serve settlements that do not have biological treatment.

The city and village wastewater networks are slowly being developed in order to interconnect with new urban waste treatment plants. Regarding garbage management, the existing landfills are almost full, but the Municipality cannot take action, since this infrastructure is the responsibility of the regional government, leading to long delays. According to Greek legislation, each hotel unit is obliged to operate its own waste treatment facility.

4.2 Tourism and Habitats plus Natural Environment

Production in Paros is oriented towards the tertiary sector, processing is prosperous and primary production is low. Primary production has 337 employees (mainly in livestock, since the island accommodates a cattle population is 11.500), secondary production 1375 and 3.663 employees in tertiary production. In Paros, there are 2008 companies have sole owners, while others amount to 929. In fact, most businessmen are permanent residents of the island.

4.3 Wind Farm Electricity Power Units

The waste management infrastructure is modern and well maintained, while waste recycling amounts to about 1100 tons per year. Garbage production amounts to about 10.000 tons per year. Urban wastewater amounted to 713,000 cubic meters in 2018, while about 42% (7040 to a total of 16.905) of all households and business are connected via a central sewage collection network. The island has no hazardous waste and any atmospheric exhaust emissions are mainly found around the port and on the road network, including the ring road of Paroikia. Unfortunately, no data exist concerning greenhouse gas production and the quality of air on the island, which is expected not to be impacted seriously.

4.4 Tourism and Cycling

The use of bicycles is a very important component of the holidays as it has an ecological way of transportation that the visitor can spend his time in his vacation place.

4.5 Quarries and Tourism

Traditionally, caves and quarries are attractions for tourists and act as destinations for hikers, climbers, underwater exploration, fish fauna monitoring and other alternative tourism activities are advertised at global alternative tourism fairs. The quarries in Marathi, from where the marble was mined in ancient times, are a permanent asset. Paros is the capital of ancient marble. Its association with the majority of the great masterpieces of ancient marble sculpture, is an advantage for the place.

4.6 Cultural and Archaeological Tourism

Greek tourism is based on ancient Greek history. Traditionally, tourism in Greece began with visits to archeological sites on the mainland. Also, most of the masterpieces of Classical Antiquity were processed from Parian Marble. Paros and its rich historical reserve are the basis for the promotion of the place. The previous chapter mentions the archeological sites. The Archaeological Museum needs continuous and intense promotion.

4.7 Tourist Awareness Seminars

Tourist Consciousness is, the knowledge that we prove that we have through the professional and friendly service of the tourist who spends holidays in a place, predisposed to have a positive recreation,

4.8 Tourism and Photography

The art of photography is well respected and recognized. Everyone is photographing and being photographed. A large portion of the population is involved in artistic photography, participates in photographic groups or works individually. Many tourist destinations, especially big cities, organize photo festivals. Some of them have an international impact of global interest while some have a transnational character.

4.9 Wedding Tourism

A recent trend in marriage practices, involves couples choosing to get married in a place different from that of permanent residence.

4.10 Gastronomy and Tourism

Gastronomy is the delivery of dishes of a place, essentially the preparation of local dishes with traditional recipes of high quality.

4.11 Traditional music and island traditions

Music is a cultural heritage and connects indigenous peoples. Paros has a rich island music tradition. In the many festivals that take place in Paros, tourists become "mysteries" of the special island music culture of the island.

4.12 Health services

With over 60,000 people on an island on a daily basis, it is necessary to have a well-staffed and equipped Hospital. So as to ensure the protection of the health and life of the inhabitants. In this case, the need for transportation to the General Hospital of Syros and Piraeus is reduced. Deliveries are expensive and time consuming and can be fatally fatal.

4.13 Port infrastructure

The berths of merchant ships in Paros are 8 but the port authority gives permission for only 4. For night mooring only 1 place is offered. The construction of a new port which has been launched is a common acceptance. The port of Paros presents problems with congestion in traffic waves since, despite the existence of several parabolic and safety places, there is no ease of decongestion of traffic when they have more than 1 or 2 ships. Then the situation becomes particularly difficult despite the efforts of the port corps. The presence of merchant ships in the port of Paros aggravates the situation given the frequent arrival of trucks and tankers supplying inert materials and liquid fuels of the island. As a result, Paroikia is significantly burdened with a degree of dangerous traffic congestion, especially during the

summer months. Therefore, the need for the construction of a new commercial port outside the urban fabric is considered urgent.

Specifically, the preparation and approval of all the studies regarding the transfer of the Paroikia Commercial Port of Paros to the Kaminaki site is expected to be completed at the end of 2022, when the tender for the project will be held, with the target of immediately starting the construction work.

4.14 Cruise industry

The prospect of introducing a cruise industry in Paros is a challenge. It has many monuments and beautiful settlements, which make it a unique destination for this form of tourism. Priority is given to high-income private cruises. Carrying capacity can also be applied to the cruise, by studying ports and their services, consumption cost of cruise passengers, cruise ship mooring size and weather safety, vehicle service infrastructure, roads and parking that transport cruise tourists, sites of archaeological interest, cruise ship traffic annually, monthly and daily, the percentage for cruise passengers to permanent residents, total passenger arrivals both per day and per month, extent of cruise ship mooring docks, hops that serve cruise, catering and tourism, Environmental nuisance from cruise traffic, etc..

4.15 Traffic and vehicle safety

The ring road of Paroikia has special characteristics of traffic congestion. Accidents are often observed, especially in the summer the traffic is difficult. It is suggested, the signaling or the constant presence of a traffic warden as a temporary measure. There is an urgent need to bypass the intersection since the construction of a car. A very important problem is that of car parking in Paroikia and Naoussa. Along with the necessary traffic study, new parking spaces must be found. A regional parking lot is a rational measure. But it is long-term and brings great costs.

4.16 Support for Tourism Promotion and Creation of an Updated Promotion video for Culture and Tourism in Paros

Modern destination videos combine not only the tourism product and the tourist experience but also emphasize the culture of each place. A new documentary is needed from a search that was carried out. The parameters must be, highlighting the uniqueness of Paros. More specifically, the priorities must be: History and archeology, Ecology, Tradition and music,

4.17 Gastronomy and restaurants as well as the production of products as well as wine production

The traditional settlements and the architectural character of the accommodation, Gastronomy restaurants, Natural beauties, and the beaches as well as the coastal zones in general, Culture - festivals - events and cultural events all year round, Paths

4.18 Integrated Destination Management

The parameters of tourist destination management are: The levels of action strategy, the level of destination by service sector, the purpose set by stakeholders involved in tourism.

4.19 Fishing Tourism

Paros has the largest fishing fleet in the Cyclades. Many boats and fishermen are based in Paros. Fishing tourism is special for tourists as it combines sea cruising with fishing and gastronomy. It is another comparative opportunity for Paros.

4.20 Carrying out research on tourism in Paros.

These surveys are done with questionnaires which are distributed to tourists. Many destinations have made similar efforts. The results of these surveys of visitors are prerequisites for the tourism policy of the Municipalities, the tourist promotion, the measurement of the expenses of the visitors, the quality of the tourist product and the study of the origin of the tourist demand.

4.21 Sports Tourism

Sports Tourism is related to sports organizations such as clubs, associations, federations, national and international, confederations at local, regional, national, continental, and global levels.

4.22 Utilization of nearby areas

Despotiko Island is of special archaeological interest. The excavations reveal very important ancient monuments with a very characteristic temple of Apollo. Utilizing it as a place to visit the same day from Paros is an excellent opportunity. AntiParos is a small island adjacent to Paros, the entrance to the island is through Paros. Thousands of tourists visit it every year. Many visitors to Paros go for a swim or a drink in AntiParos. The co-operation of the two islands is an issue that needs to be addressed.

References

- [1] Prokopiou D, Research for Sustainable Tourism Development for Paros Island (in Greek), Municipality of Paros, Paros 2019.
- [2] Greek National Tourism Organization.
- [3] http://www.biodiversity.ru/coastlearn/tourism-eng/con_capacity, World Tourism Org.
- [4] UNEP/MAP/PAP, 1997. <http://www.unepmap.org>
- [5] http://ec.europa.eu/environment/iczmpdf/tcca_en.pdf
- [6] Coccosis, H. & Mexa, A., Challenge of Tourism Carrying Capacity Assessment, Ashgate 2004
- [7] Garrigós-Simón F., Narangajavana Y., & Palacios-Marqués D., 'Carrying capacity in the tourism industry': a case study of Hengistbury Head' Tourism Management 2003
- [8] Navarro Jurado E, Mtejada Tejada, F. Almeida Garcia, J. Cabello Gonzalez, R. Cortes Macias, J. Delgado Pena, F. Fernandez Gutierrez, G. Gutierrez Fernandez, M. Luque Gallego. G. Malvarez Garcia, O. Marcenaro Gutierrez, F. Navaz Concha, F. Ruiz de la Rua, J. Ruiz Sinoga, F. Solis Becerra, (2012) "Carrying Capacity Assessment for Tourist Destinations . Methodology for the Creation of Synthetic Indicators Applied in a Coastal Area", Tourism Management 33.
- [9] Blancas F.J., Gonzalez M., Lozano-Oyola M, Perez F., The Assessment of Sustainable Tourism: Application to Spanish Coastal Destinations, International Journal Ecological Indicators 10, 2010
- [10] Prokopiou D.G., Tselentis B.S, Mavridoglou G., Lagos D. Prototype model of carrying capacity in tourism: the implementations for the island of Rhodes, European Scientific Journal Sept 2014 Special edition vol.2.

Towards a digital twin for marine and maritime activities: the ILIAD project framework

G. Sylaios^{1*}, A.-J. Berre², B.L. Bye³, U. Broenner⁴, V. Kiouisi⁵

¹ Democritus University of Thrace, Department of Environmental Engineering, Vas. Sofias 12, 67100 Xanthi, Greece

² SINTEF Digital, P.O. Box 4760 Torgarden, N-7465 Trondheim, Norway

³ BLB, Oslo, Norway

⁴ SINTEF Ocean, P.O. Box 4760 Torgarden, NO-7465 Trondheim, Norway

⁵ NETCOMPANY – INTRASOFT, 19 km Markopoulou - Paianias Av., GR 19002, Attiki, Greece

*Corresponding author: Georgios Sylaios, gsylaios@env.duth.gr

Abstract

A digital twin is a digital replica of a living or non-living physical entity. The digital twins are implemented to give users tailored access to high-quality information, services, models, scenarios, forecasts, and visualisations. Digital twins rely on the integration of continuous observation, modelling and high-performance simulation, resulting in highly accurate predictions of future developments. ILIAD capitalizes on the explosion of new data provided by many different Earth Observation data sources, advanced computing infrastructures (cloud computing, HPC, Internet of Things, Big Data, social networking, and more) in an inclusive, virtual/augmented, and engaging fashion to address the related challenges. It will contribute towards a sustainable ocean economy as defined by the Centre for the Fourth Industrial Revolution and the Ocean, a hub for global, multistakeholder co-operation.

Keywords Marine and maritime activities, digital twin of the ocean, smart sensors, IoT systems, simulations, ILIAD.

1 INTRODUCTION

The concept of Digital Twin was firstly introduced in 2002 by M. Grieves from the University of Michigan, presenting the formation of a Product Lifecycle Management (PLM) center, in which all elements of the Digital Twin were introduced. Such sub-components are: the real-physical space, the virtual-digital space, the link for data flow from real space to virtual space, the link for information flow from virtual space to real space and the virtual sub-spaces. This meant that there was a mirroring or twinning of systems between what existed in real space to what existed in virtual space and vice versa. The technology of Digital Twin emerged in the framework of Industry 4.0 coupling basic IT technologies like cloud computing, Internet of-Things (IoT), Big Data, and Machine Learning (ML).

Following that concept, we may define a Digital Twin as a virtual/digital representation, serving as the real-time digital counterpart of a physical object or process. Digital twins are the result of continual improvement in the creation of product design and engineering activities. Presently, DTs are based on the following elements:

- ✓ Smart Sensors for RT data collection
- ✓ Systems for data transfer and data feeds
- ✓ Decentralized or centrally-stored data in cloud servers
- ✓ High resolution/high in accuracy simulations to virtual copies
- ✓ Interactive platforms to display RT 3D/4D spatial-temporal data
- ✓ Integrating IoT, AI and software analytics
- ✓ Augmented reality (AR) systems as visualization technologies
- ✓ Optimize machines, products, processes, services
- ✓ Monitoring, diagnostics, prognostics

Digital Twins connect the real and virtual worlds by (a) collecting real-time data from installed sensors, (b) running operational models and producing short and medium-term forecasts, (c) producing and

analyzing Big Data (external and internally-produced), (d) utilizing IoT technologies to transfer data to cloud storages (local or centralized), (e) representing a virtual copy of the performance and operation of physical assets, and (f) automating the processes and optimizing the procedures. The DTs are currently being used in several industrial sectors, like manufacturing, automotive industry, construction, utilities and healthcare. Digital Twins are not only used for product improvement, but also for failure prevention, quality upgrading, higher performance, cost reduction, shortening of time-to-market, and higher customer satisfaction.

2 THE DIGITAL TWIN OF THE OCEAN

The Digital Twin is a continuous loop of physical-to-digital processes, and vice versa. Expanding this concept to the marine and maritime activities, it becomes obvious that the physical to digital space transition is based on networks of deployed on-line sensors, the automatized execution of a ‘chain’ of operational prognostic models, the use of high-volume storage capacity to accommodate Big Data and the high-performance cloud servers employing machine learning models and AI tools. However, in a DT environment, the digital to physical transition is also required, aiming to improve operations, exert controls, optimize processes, perform diagnostic tests and advance decision-making.

Limited literature currently exists on the topic of development and implementation of Digital Twin of the Ocean (DTO). Jiang et al. (2021) developed a Digital Twin acting as a fast and accurate surrogate of the coastal ocean aiming to minimize the coastal flood risk under accelerating sea level rise. Corradu et al. (2019) proposed a data-driven DT to estimate the speed loss of a cargo carrier due to marine fouling at the hull and propeller, leveraging on the large amount of data collected from the on-board sensors. Collected data (GPS lat and lon, pitch, roll, yaw, fuel consumption, fuel temperature and density, propeller speed, ship draft (fore, aft), sea depth, wind speed and direction, sea water temperature, etc.) were fed on Deep Extreme Learning Machines to detect during real operations a deviation in the speed performances (with respect to the ones achievable with clean hull and propeller), and consequently to identify the extension of the marine fouling phenomena. Schirmann et al. (2019) presented a digital twin for ship motion and estimation of structural fatigue due to wave response.

3 THE ILIAD PILOT DTs

ILIAD is developing a series of Pilot DTs for selected marine and maritime sectors to support the fourth industrial revolution (Industry 4.0), to benefit from IoT data collection and transfer, to leverage from Big Data analysis and AI tools, and produce standardized and accredited data, in accordance to the FAIR principle. Through the implementation of the many Pilot DTs, the project seeks to support a central marketplace, enabling policy-makers, individuals, and enterprises to understand, preserve and operate in the European Oceans, supporting both the Green Deal and DestinE initiatives of the European Commission. These Pilot DTs are: Met Ocean, Coastal Sediment Transport, Plastic Pollution Monitoring, Oil Spills, Aquaculture, Fisheries, Ballast Water Monitoring, Jellyfish Swarms, Harbor Safety, Existing Offshore Wind Farms and Ocean Energy Potential, across all European oceans.

An example on the steps to be followed for a DT of an offshore wind turbines farm is given in Figure 1. The physical farm operates offshore harvesting wind energy and transforming it into electricity. During its operation, a series of sensors collect data on the conditions (meteorologic, hydrodynamic, wave, water quality) prevailing in the farm. These data are transferred in RT mode to a land-based server, in which QA/QC processes are carried out on the received level-zero datasets. Data are harmonized according to international standards and are transferred to the central cloud server for further processing. After reaching level-three, data are ready to be ingested to the platform for visualization, statistical analysis, ML and assimilation in forecasting models. A series of downscaled, high-resolution forecasting models may be applied in the wind farm area, to simulate the wind conditions at turbine hub level, the currents and waves in the pole area, the loads exerted on the various parts of each wind turbine, the corrosion rates, etc. As the digital space is built, we can then perform complex scenario analysis, optimize processes, execute diagnostic and prognostic tests and analyze risks and assess uncertainties.

At the end of this cycle, informed decisions may be reached by the operator of the wind farm, improving the real-time control and optimizing the overall performance of the system.

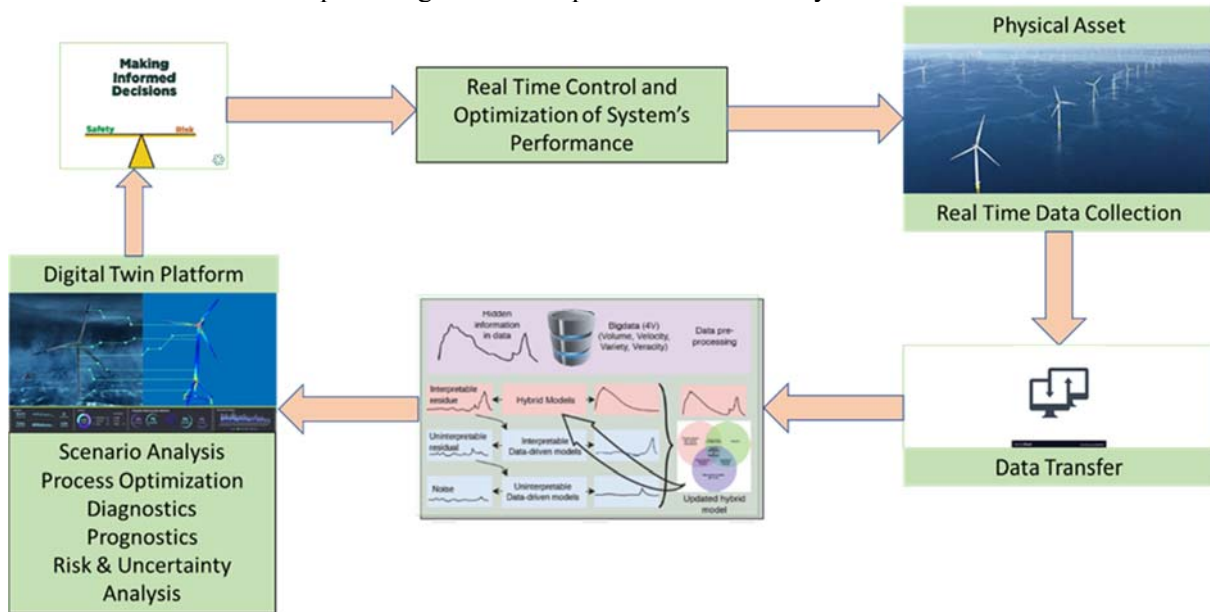


Figure 1. The conceptual framework of an offshore wind farm DT

4 PILOT DTs CLASSIFICATION

Following the loop concept of Digital Twins, and the continuous interexchange of data between the physical and the digital space, it occurs that the above pilot DTs may be classified in two basic categories: the one-way DTs, referring mostly to marine environmental and ecological DTs, in which the flow of data is one-way, i.e., from the physical to the digital space. In environmental and ecological DTs the manager is unable to complete the loop and optimize the physical space. The ILIAD DTs on plastic and micro-plastic pollution, on met-ocean data, hind-, now- and forecasts, the biodiversity assessment and insurance against extreme events for marine and maritime facilities fall within the ‘one-way DT’ class.

The second category is the well-known two-way DTs, which refers mostly to engineering, industrial maritime DTs, in which the whole loop is completed. The ILIAD DTs on wind energy, the marine renewable farms (e.g., ocean currents turbines, WECs, floating solar panels), fisheries and aquaculture, and harbor safety and marine traffic are some examples of this category.

A third DT category may include the twins with limited intervention; therefore, the loop is partly closed. The insurance of maritime facilities from extreme marine events, the response to oil spills and the aquaculture (mussel and cages) may fall in this ‘hybrid’ category. Based on Figure 1, it occurs that as we move towards the full loop DTs, the complexity of the system and the resources required to be allocated for DT implementation rise exponentially. In parallel, the business development and innovation capacity of these DTs is similarly exponentially risen.

Focusing on the individual components comprising the DT, we may find that:

- The one-way DTs, like the marine ecological DTs (e.g., biodiversity and plastic pollution), which act as Data Integrators, being characterized as DTs with rather high spatial dimensions, limited sensors and model requirements, in most cases RT data transfer and advanced data analytics are not achievable, while the policy implementation in these DTs is high.
- The hybrid DTs in which the loop is partly achieved, like the insurance from extreme events and oil spill response. These DTs act like Simulators, with increased RT data transfer and moderate citizen science engagement.

- The maritime industrial and engineering DTs, like the ports, the wind and wave farms and the aquaculture facilities, characterized by low spatial dimensions, high requirements in monitoring and modelling and limited citizen science engagement. These DTs appear as ‘two-way’ Control Systems, with a closed continuous loop, in which data are integrated and simulations play a key role in system’s performance optimization.

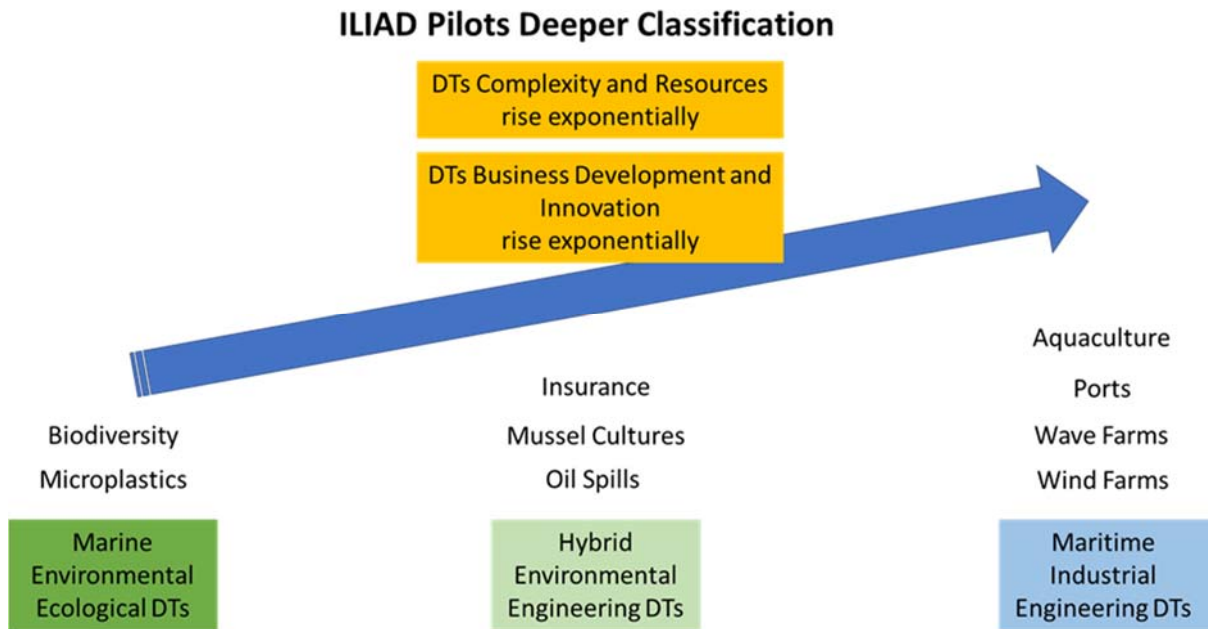


Figure 2. ILIAD Pilot DTs classification and characteristics of each category

5 COMPONENTS OF PILOT DTs

The ILIAD Pilot DTs are comprised of the following components: (a) continuous link to existing EO resources (satellite data, databases, global models), (b) a multitude of sensory systems, (c) numerical models, (d) AI algorithms, (e) Citizen Science data, (f) IoT systems, (g) DTO Platforms, and (h) Dashboards.

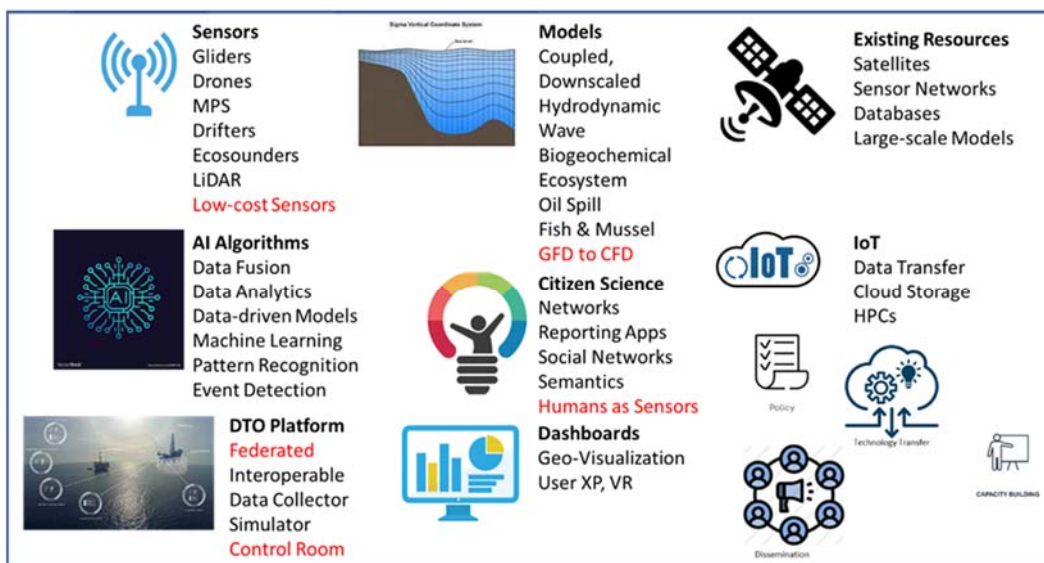


Figure 3. ILIAD Digital Twin Ingredients and Novelties

ILIAD Sensors will be built and deployed at all ILIAD pilot DTs to collect data in RT and/or NRT mode. ILIAD will build a new, novel sensor network, utilizing the emerging Internet of Underwater

Things Technology and intercalibrating Earth Observing Systems of various scales. Emphasis will be given in the monitoring of the Essential Ocean Variables, but with an initial focus on the pilot areas. Data will be transferred in RT/NRT mode utilizing state-of-the-art communication protocols (like LoRa, Iridium). ILIAD Pilots will utilize Existing Data Resources, like historic, present and forecasted data on meteorology, climate, hydrology, hydrography, biogeochemistry, environmental, biological and fishery data. Novel observations, made through several Citizen Science Apps, across many different Pilot DTs using different languages, will be shared. Data coming from different CS sources (citizen apps, social media, open sources, online encyclopedias and other resources) will be integrated into one single, coherent view in which redundancy between sources will be eliminated and where each specific information source will bring its view on the ocean. Finally, a series of forecasting models, analytics and ML algorithms will be employed to instantiate tailored analysis, forecasting and simulation services, as required by pilot DTs. These models will provide a better understanding of local (at pilot DTs) dynamics and will force other thematic, sector-targeted models, developed and implemented, that will be coupled to the operational modelling chain, like (a) the oil spill model, to aid the emergency response and the development of contingency plans for accidental surface and subsurface oil releases; (b) the wind, currents, and wave energy models to assess the potential for renewable energy at selected areas; (c) the micro- and macro-plastics transport and distribution model; (d) the coastal morphodynamics model; (e) the ecosystem status assessment model, utilizing abiotic data from the ILIAD DTO; (f) the fish and mussel farm models, focusing on individual-based and population dynamics; (g) locality-specific model for safe navigation in ports and channels, during unfavorable weather conditions; (h) the ballast water risk assessment and management model; and (i) ship-routing algorithms for estimating CO₂-optimal routes, based on operational met-ocean forecast products.

Furthermore, ILIAD will develop ML methods for pattern discovery to infer tendencies, detect seasonal patterns and find deviations and anomalies, correlating and comparing data sources to understand the root cause of outlier events, developing predictive models for the early detection in repeated events of interest. Thus, facilitating the development of decision support services for long-term planning and development of mitigation strategies and the development of services and applications that operate in near real-time. Utilizing the advances in sensing and computing simulation technologies that enable the collection and generation of massive data sets every second at different spatio-temporal scales, the ILIAD DTO will explore data streaming through IoT domains, while fusing the collected spatio-temporal, multi-scaled marine data with data from social media platforms and citizen science apps.

Finally, the ILIAD DTO Platform will be built using the GAIA-X/IDS federated architecture approach, including a Federated Data/Service Catalogue, with a Federated Identity service, using OAuth2 and X509 standards, harmonized with the NEXTGEOSS DataHub for the support of the ILIAD Marketplace. Following the decentralized approach principle, each existing platform or system will be interfaced with ILIAD interoperability space via a GAIA-X/IDSA Provider Connector. The Connector will act as a gateway that efficiently and securely transfers data from a data provider to a data consumer, while data sovereignty is technically enforced by usage constraints that govern data usage. The data-sharing infrastructure will be decentralized, whereby all data is transferred directly between a data provider and a data consumer, based on a virtual peer-to-peer network.

References

- Jiang, et al. (2021). Digital Twin Earth - Coasts: Developing a fast and physics-informed surrogate model for coastal floods via neural operators. NeurIPS 2021, Vancouver, Canada.
- Coraddu, Oneto, Baldi, Cipollini, Atlar, Savio (2019). Data-driven ship digital twin for estimating the speed loss caused by the marine fouling. *Ocean Engineering*, 186, 106063.
- Schirmann, Collette, Gose (2018). Ship motion and fatigue damage estimation via a digital twin. In: *Life Cycle Analysis and Assessment in Civil Engineering: Towards an Integrated Vision*, Caspeepe, Taerwe, Frangopol (Eds), CRC Press, 604 p.

Advancing image analysis practices for condition assessment of port infrastructure with GIS applications

C. Tsaimou^{1*}, D.G. Kagkelis¹, P. Sartampakos², V.K. Tsoukala¹

¹Laboratory of Harbour Works, Department of Water Resources and Environmental Engineering, School of Civil Engineering, National Technical University of Athens (NTUA), Zografou, 15780, Greece

²NIREAS Engineering, 1-3 Skra Str., Athens, 17673, Greece

*Corresponding author: ctsaimou@gmail.com

Abstract

Ports are challenged to maintain the performance of their infrastructure under the influence of various stressors. Powerful management strategies are required to ensure the structural and functional capacity of port infrastructure by applying monitoring and condition assessment practices. Regarding port concrete infrastructure, condition assessment encloses crack detection. Currently, there is a growing trend in utilizing Unmanned Aerial Vehicle (UAV) imagery for identifying cracks in concrete surfaces. Red, Green, and Blue (RGB) images collected by cameras mounted on UAVs are further analyzed with image processing methods to extract information about cracking. The present research seeks to advance crack detection in port concrete infrastructure by combining current practices on image analysis enhanced with tools that enable working with geospatial information. The proposed methodology involves the use of modules imported into programming languages for managing geospatial data and Geographic Information System (GIS) tools. A field test is conducted at Lavrio Port, a Greek port located at the southeastern tip of Attica to verify the robustness of the methodology. The overall analysis indicated that image processing enhanced with tools to assist in working with geospatial data enables mapping and locating detected cracks in port concrete infrastructure.

Keywords Port concrete infrastructure, Image analysis, Condition monitoring, GIS analysis.

1 INTRODUCTION

Ports serve as strategic hubs for maritime transportation, energy generation, trade, and blue economy (Langen et al. 2018). Their undisrupted operation affects the functional and structural integrity of port infrastructure. Stressors including aging, harsh marine environment, natural hazards, inadequate measures for maintenance and rehabilitation, loading conditions, and climate change impacts imperil the infrastructure serviceability (Lauritzen et al. 2019). Hence, asset owners are tasked to apply efficient practices for condition monitoring of port infrastructure.

Ports include different types of facilities such as concrete, steel, or timber structures. Regarding port concrete infrastructure, one typical distress encountered during condition monitoring is cracking, a linear separation of concrete (Heffron 2015). Nowadays, Digital Image Processing (DIP) is gathering momentum for crack detection to advance the procedures of assessing concrete condition (Gupta and Dixit 2022). Image analysis is applied with several methodologies that involve data collection, data pre-processing, and algorithms' implementation for crack detection. However, these methodologies lack providing geospatial information required to identify the exact crack location.

In light of the above, the present research seeks to advance crack detection in port concrete infrastructure by applying current practices on image analysis enhanced with tools for working with geospatial information. Such tools include: a) modules imported in programming languages for managing georeferenced images and b) Geographic Information System (GIS) applications for analyzing geospatial metadata acquired by image analysis. The proposed methodology is applied at Lavrio Port, located in the southeastern tip of Attica, Greece. The investigation is conducted by the Laboratory of Harbour Works (LHW) of the National Technical University of Athens (NTUA) and includes in-situ inspections with Unmanned Aerial Vehicle (UAV) employment, photogrammetry analyses, python coding, and GIS applications.

2 MATERIALS AND METHODS

2.1 Background and Objectives

Image-based crack detection techniques are gaining increasing interest in the field of condition monitoring of various types of structures. These techniques include processing-based and learning-based techniques (Munawar et al 2021; Gupta and Dixit 2022). Image processing-based techniques intend to detect items in the image, while image learning-based techniques are used to train models to recognize patterns. Both techniques are linked since advancing processing-based techniques assists machine learning applications (i.e. learning-based techniques) in better training the system to identify cracks.

Image processing-based techniques involve, among others, thresholding (e.g. Otsu algorithm), and morphological operations (e.g. eroding and rebuilding) methods (Gupta and Dixit 2022). These methods are carried out for crack detection in the spatial domain where images are represented by three forms: the two coordinates fixed by two axes that refer to a surface, and the amplitude fixed by a third axis (Sundararajan 2017). Following this, current practices for DIP are focused on image analysis in the spatial domain, without using the geospatial information required to map cracks within a selected coordinate system. Geospatial information is important to precisely locate the cracking pattern at a concrete surface.

The above need is further intensified considering the recent surges in condition monitoring with UAV inspections (Kim et al 2018). The employment of UAVs allows for acquiring geospatial information with photogrammetry analyses. To capitalize on the benefits of this georeferenced output, it is essential to integrate tools for working with geospatial data during image analysis.

2.2 Research Methodology

A structured methodology is proposed to enable working with geospatial data and mapping cracks in port concrete infrastructure (Figure 1). Image processing-based techniques for crack detection in orthophotos are engaged. GIS and programming tools are involved to work with georeferenced images, both represented with different colors and icons in Figure 1. Two (2) open-source software are employed for the GIS and programming processes: a) QGIS (version 3.22.11) and b) Spyder (version 5.4.2) for Python language (version 3.9.15), respectively.

QGIS is used for pre-processing the orthophotos (steps 1, 2, and 3). These analyses are required to reduce the size of the raster image without missing the geospatial information provided by the orthophotos. Achieving an optimal size for an image is significant to ensure execution without returning errors. The orthophotos are clipped based on a defined cell grid and a new raster dataset is then created.

Each raster image is analyzed with Python tools (steps 4, 5, 6, and 7). Image analysis begins with inserting the GDAL library which is essential to work with geospatial data. The procedure proceeds with converting RED, Green, and Blue (RGB) images to grayscale ones to reduce the influence of color differences. A median filter is implemented to smooth the surface (Dorafshan et al. 2016). The new grayscale image is analyzed with the Otsu local thresholding technique. Otsu algorithm allows for image binarization based on a predefined threshold value (Sundararajan 2017). The binary image is then post-processed with morphological operations to identify whether pixels are related to the observed crack or other distress and/or image noise (Dorafshan et al. 2016). This step is important to achieve eliminate small noisy items close to the crack and enhancing the connection of the crack segments.

Once Spyder analyses are completed, QGIS tools are employed again for post-processing the new binary image. The detected crack is isolated (step 8) and vectorized (step 9) for GIS-based quantification. GDAL and GRASS tools are used to represent the crack with polygons and lines, respectively. Hence, geospatial information regarding the width, length, and location of the detected crack is acquired. This output is essential for condition monitoring and assessment of port concrete infrastructure.

2.3 Case Study

The above-mentioned methodology was applied at Lavrio Port, a Greek port located at the southeastern tip of Attica (37°42'44 N, 24°3'25 E) (Figure 2). Lavrio Port is listed as a port of national importance. It serves as an essential node to assist maritime transportation, enhance trade, and support fishing and recreational activities (<https://oll.gr/en/>). The port's undisrupted operation affects the condition of its

facilities. The concrete infrastructure of the domestic ferry domain (Figure 2) is continuously exposed to loading and environmental conditions, thus threatening its functional and structural integrity. Hence, one common distress observed at the concrete slabs is cracking. To proceed with crack detection based on the proposed methodology, a field test was conducted at Lavrio Port. In-situ inspection was taken place by employing the DJI MAVIC 2 pro UAV. Further details regarding data collection can be accessed by relevant work conducted by LHW, NTUA (Tsaimou et al. 2022). The present investigation refers to the first conducted in-situ inspection (ISI-1: 2020-02-10). UAV collected data was analyzed with Agisoft software (version 1.6.4) to generate orthophotos, i.e. the georeferenced output required for the image analysis applications (Figure 2).

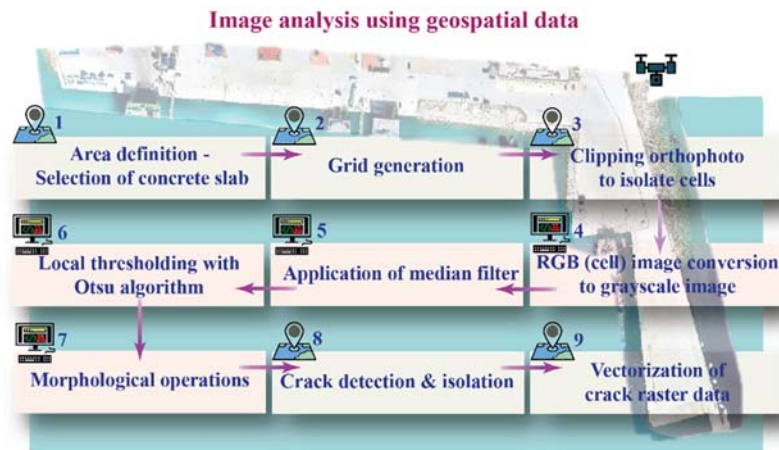


Figure 1. Image analysis methodology enhanced with tools for working geospatial data

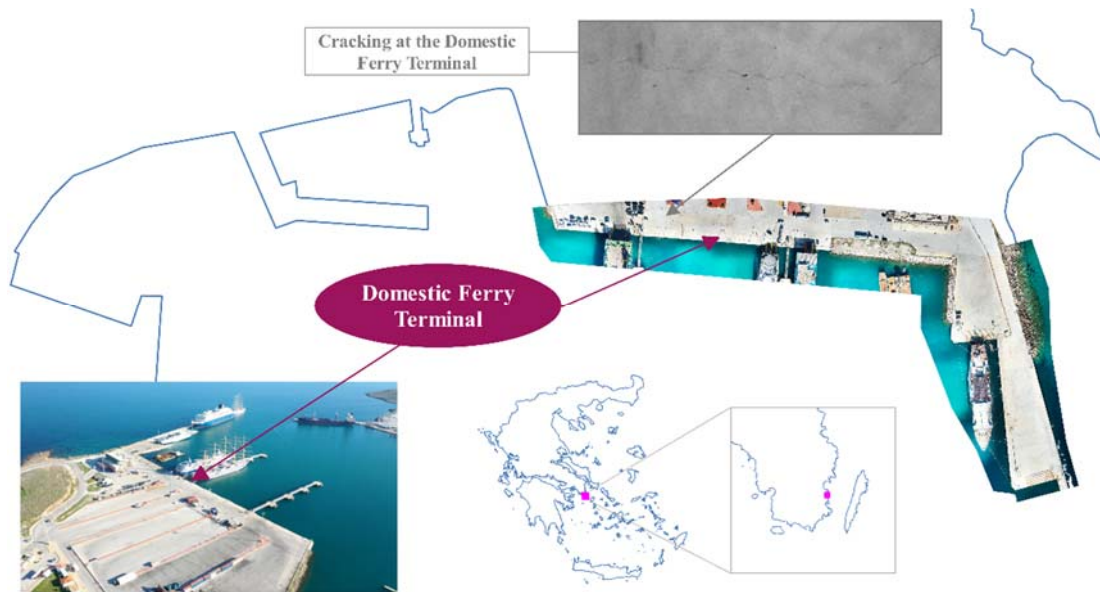


Figure 2. Case study of Lavrio Port

3 RESULTS

The proposed methodology was applied at the orthophoto of ISI-1 for a concrete slab of the domestic ferry terminal of Lavrio Port (step 1 of Figure 3). The selection of the slab was based on the absence of noise including vehicles, passengers, and shadows. Cracking and surface marks by tires and marking lines were present at the surface of the selected slab. The angle of the x-axis of the slab was 99.5° from the North. The slab was divided into cells by constructing a grid with a rotated coordinate system to match the x-axis and y-axis of the slab (step 2 of Figure 3). Twenty-eight (28) cells were defined with dimensions 2.5 m x 2.5 m, except the ones in the last column that have dimensions 2.0 m x 2.5 m. After

applying layer rendering tools in QGIS it was noticed that cubic convolution interpolation was the appropriate zoom-in option for further analysis of the selected cell (step 3 of Figure 3).

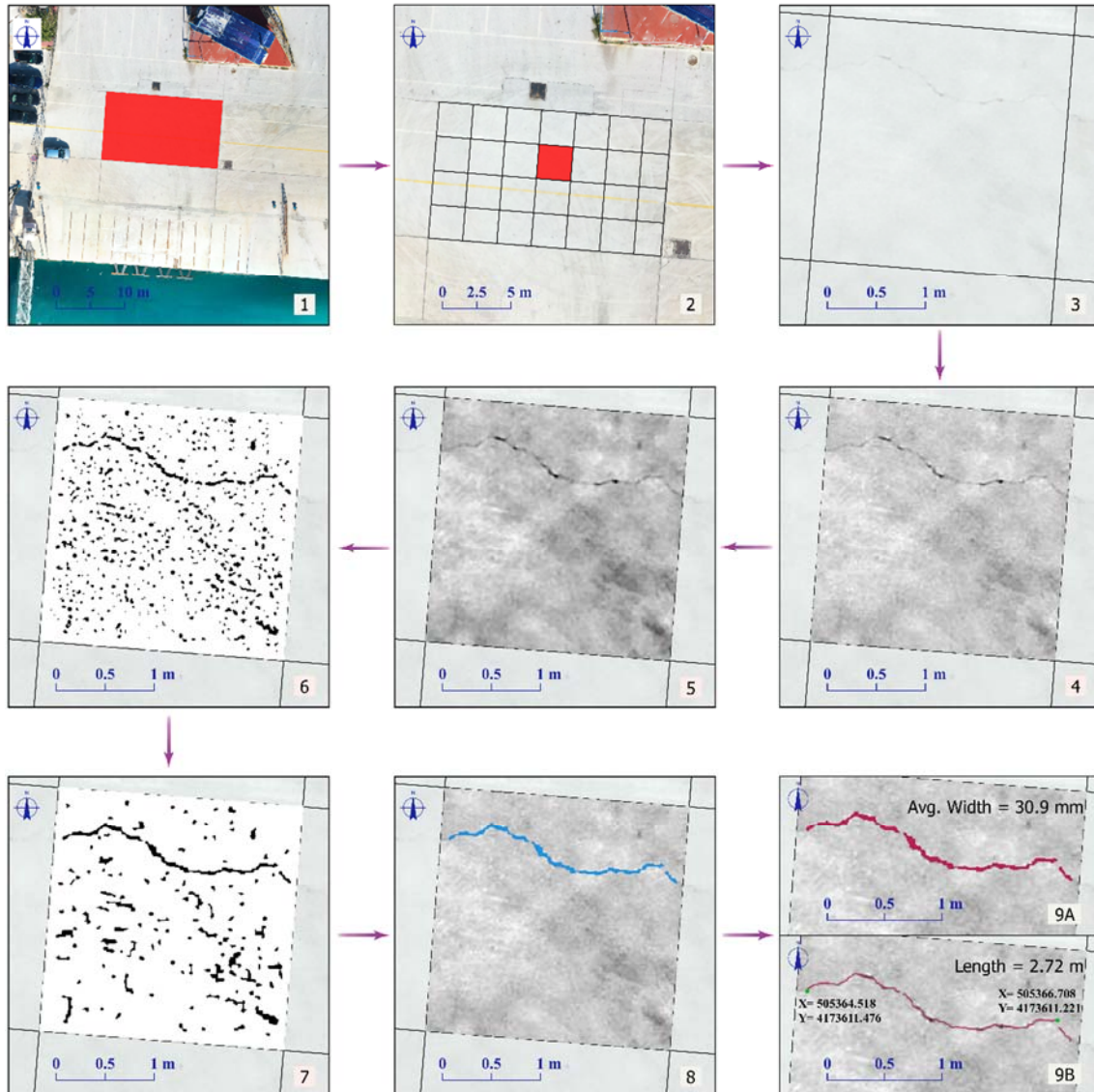


Figure 3. Results for crack detection at the domestic ferry terminal of Lavrio Port

Once the GIS-based pre-processing of the orthophotos was completed, the RGB image of step 3 (Figure 3) was converted into a grayscale image (step 4 of Figure 3). A median filter with a 3 x 3 kernel was implemented in the grayscale image to eliminate noise (step 5 of Figure 3). To convert the image into a binary raster format with local Otsu thresholding, a repeat procedure was conducted to select the optimal values of the required algorithm parameters depending on the noise and the lighting conditions of the image. The values of the parameters should be carefully determined so that they can effectively capture local variations in the image while avoiding excessive computational overhead. For the specific orthophoto of Lavrio Port, it was found that binarization of the image should be performed for a window size equal to 17 (i.e. a square-shaped area of 17 by 17 pixels) and an offset value equal to 1.1 (step 6 of Figure 3). The result of Otsu algorithm implementation shows that the pattern of the crack can be identified. However, the flow of the crack line is interrupted in some areas. Moreover, several black pixels irrelevant to the crack are present. The result of removing the small black holes and filling some gaps in the crack line by using morphological operations is shown in step 7 of Figure 3. The crack was better represented despite that some gaps are still present. Furthermore, although a significant part of the noise was removed, some black pixels irrelevant to the crack line are still present in the processed image.

To quantify cracking results, the detected crack was isolated as shown in step 8 of Figure 3. GIS vectorization allowed for defining the polygon that indicates the shape and the pattern of the crack, as well as the line that represents the crack (step 9 of Figure 3). Based on the vectorized output, the minimum, maximum, and average width values of the crack were found to be equal to 0.8 mm, 192.6 mm, and 30.9 mm, respectively. Moreover, the length of the crack was estimated to be 2.72 m. Finally, locating the crack was achievable by determining the coordinates of its points, as indicated in step 9B of Figure 3 (coordinate system: Greek Geodetic Reference System 1987, GGRS87). In light of the above, it is observed that the implementation of the proposed methodology allows for crack detection and quantification, both assisted by integrating the geospatial information required for map cracking. Hence, condition assessment of port concrete infrastructure can be achieved by monitoring crack propagation with periodic in-situ inspections.

3 CONCLUSIONS

Detecting and mapping cracks in port concrete infrastructure is a demanding task. The present work is focused on introducing the integration of tools for managing geospatial data into current practices on image analysis for crack detection. Modules imported in programming languages for working with georeferenced images and GIS applications were employed. The outcome of the overall investigation indicated that the proposed methodology enables locating and quantifying detected cracks. Information regarding the width, length, and location of the detected crack is acquired. Although the results are satisfactory, further research is required to improve the output of the image processing-based analysis to obtain higher-quality metadata for the GIS-based post-processing.

Funding

This research was supported by the Special Account for Research Funding of the National Technical University of Athens, Greece (grant number 65/219100).

References

- Dorafshan S, Maguire M, Qi X (2016) Automatic surface crack detection in concrete structures using otsu thresholding and morphological operations. UTC Report 01-2016, Utah State University
- Gupta P, Dixit M (2022) Image-based crack detection approaches: a comprehensive survey. *Multimedia Tools and Applications* 81: 40181–40229. doi.org/10.1007/s11042-022-13152-z
- Heffron RE (2015) Waterfront facilities inspection and assessment: Waterfront facility inspection committee. American Society of Civil Engineers, Virginia. doi:10.1061/9780784413579
- Kim IH, Jeon H, Baek SC, Hong WH, Jung HJ (2018). Application of crack identification techniques for an aging concrete bridge inspection using an unmanned aerial vehicle. *Sensors* 18:1881. doi.org/10.3390/s18061881
- Langen P, Turró M, Fontanet M, Caballé J (2018) The infrastructure investment needs and financing challenge of European ports. European Seaports Organisation.
- Lauritzen PN, Reichard J, Ahmed S, Safa M (2019) Review of non-destructive testing methods for physical condition monitoring in the port industry. *Journal of Construction Engineering, Management & Innovation* 2(2):103-111. doi:10.31462/jcemi.2019.02103111
- Munawar HS, Hammad AWA, Haddad A, Soares CAP, Waller ST (2021) Image-based crack detection methods: A review. *Infrastructures* 6:115. doi:10.3390/infrastructures6080115
- Slifka MK, Whitton JL (2000) Clinical implications of dysregulated cytokine production. *J Mol Med* 78:74–80. doi:10.1007/s001090000086
- Sundararajan D (2017) *Digital Image Processing - A signal processing and algorithmic approach*. Springer, Singapore. doi:10.1007/978-981-10-6113-4
- Tsaimou CN, Kagkalis DG, Karantzalos K, Tsoukala, VK (2022). Remote Sensing Synergies for Port Infrastructure Monitoring and Condition Assessment. Paper presented at the 12th International Conference on Engineering, Project, and Production Management, Athens, Greece.

Expansion of pier 6 of the port of Thessaloniki

C. Solomonidis^{1,*}, K. Papadopoulos¹, D. Pachakis², D. Fotiadis², V. Drossos³

¹Rogan Associates S.A., 5 Chatzigianni Mexi Str., Athens 11528, Greece.

²ex. Cowi A/S, Bevis Marks House, 24 Bevis Marks, London EC3A 7 JB, UK

³GR8 Geo, Dimitrakopoulou 79, Athens 11741, Greece

*Corresponding author: csolominids@roganassoc.gr

Abstract

The port of Thessaloniki is one of the largest ports in Greece. The port's land zone occupies a total area of approximately 1,550,000 square meters and spans a length of approximately 3,500 meters. It comprises a 6,150-meter-long quay, 6 piers, administrative and technical support buildings, warehouses and shed, special equipment and other installations. The geographic location of the Port of Thessaloniki and its excellent road links and train connections makes it the largest transit-trade port in the country, and it services the needs of approximately fifteen million inhabitants of its international mainland. The expansion of Pier 6 has always been considered necessary for the Port to fulfill its role.

Keywords: Pier 6, Expansion, soil improvement.

1 GENERAL DESCRIPTION OF THE PROJECT

Following the Concession Contract, Thessaloniki Port Authority S.A. (THPA S.A) holds the responsibility of completing the Pier 6 Expansion. The detailed design of this work was carried out by ROGAN ASSOCIATES, as part of the DPM's JV (Hill Intl.–Rogan Associates), in collaboration with COWI and GR8, which includes:

- Extending quay 26 of Pier 6 by 513m southwards (see Figure 6), of which 470m will have a functional berthing depth of at least -16.80m (LLW) or -17.70m (MSL).
- The superstructure equipment will include fenders and bollards, so as to cover the needs of all ships expected to berth as well as quay climbing ladders (see Paragraph 2.3 for Design Vessel).
- Additionally, the superstructure will be equipped with crane rails so as to accommodate STS (Ship - to - Shore) type cranes. The crane rails will be placed with a gauge of 30.48m between them.
- The new quay wall will be constructed with the precast floating RC Caisson technique. Caissons will be made of reinforced very high quality C45/55 concrete. At the back of the caissons a relief prism made of pumice aggregates will be placed (see Figure 7).
- The foundation caisson trench has been shaped to a great degree from a previous construction stage. Therefore, any remaining of the upper silty formation will be removed and filled with rip-rap from crushed aggregates. Additionally, along the full length and in order to reinforce the foundation further, CHS457/30mm steel pile inclusions of 22m length will be placed in four rows, in a 3.5m X 3.5m mesh.
- Construction of additional reclamation zone, 306.5m in width, including the width of the new quay wall, to the back of the old quay and longitudinally to it. The reclamation fill will be compacted with the vibro-flotation technology in order to minimize the settlements and to its susceptibility to liquefaction.
- In order for the south and eastern section of the extension to be protected from waves, the construction of a revetment made of two layers of rock armor, is required.
- For the construction of the reclamation area, a soil improvement method will be applied to improve the subgrade properties. These are: (a) excavations, removal of the surface soft clay layer and replacement with coarse-grained materials and (b) installation of prefabricated vertical drains (PVDs).
- Heavy - duty type pavement, reinforced with steel and polymer fibers and of high quality C40/50 concrete, will be constructed to accommodate the heavy machinery traffic areas of the land zone.

- Construction of the independent foundations of the second crane rail, on top of piles, so as to accommodate Ship - to - Shore (STS) type cranes with a distance of 30,48m from the seaward crane rail.
- Construction of all the complementary infrastructure, electric and mechanical installations necessary for ensuring the full functionality of the new quay wall and the corresponding land zone.
- Dredging the port channel and maneuvering in such a way as to accommodate the safe approach and mooring of the maximum size design ship at the harbor.

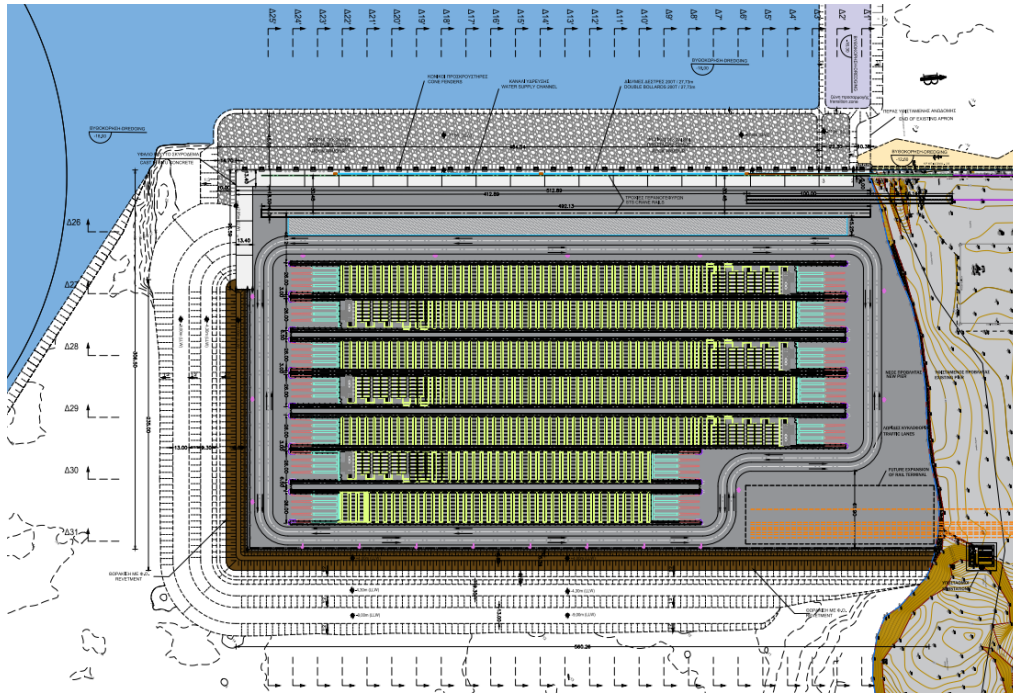


Figure 6 General layout of Pier 6 Expansion according to the approved Design

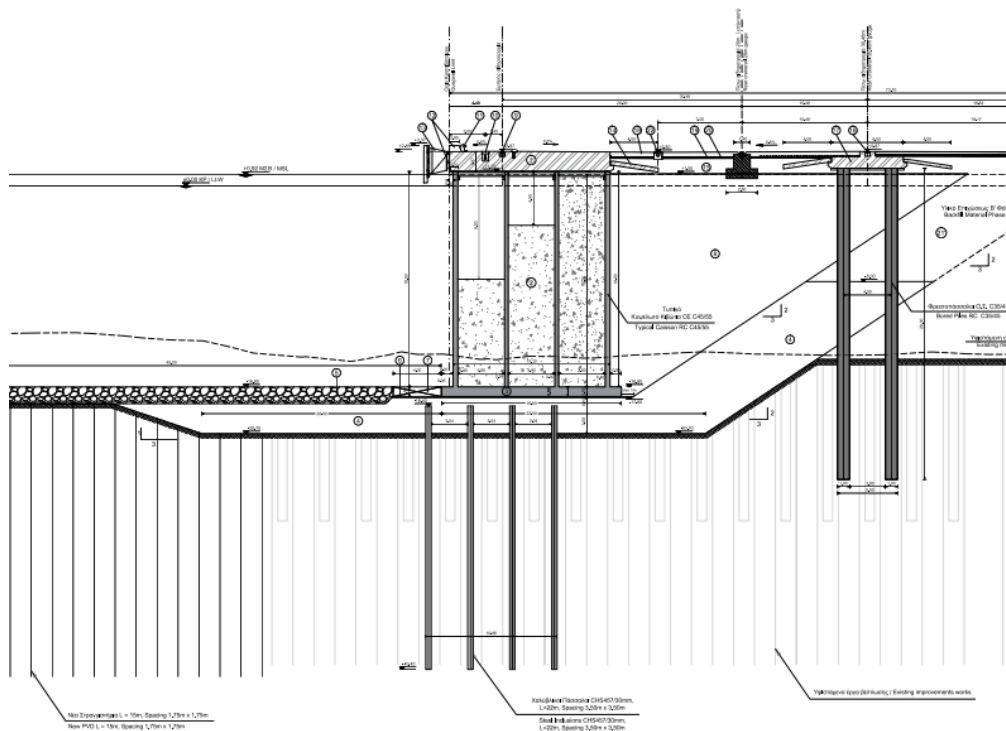


Figure 7 Typical Cross-section of the quay wall according to the approved Design

2 DESIGN PARAMETERS

2.1 Geology

Major part of the urban area from the harbor to the southeastern suburbs is located on Quaternary–Neogene formations (D.Raptakis, K.Makra 2010). Recent deposits of this particular region, covering the Neogene formation and forming an extensive plain, are Holocene deposits consisting of coastal deposits (sand, gravel), valley deposits and red clay with calcareous concretionary bodies (Institute of Geological and Mining Research, Thessaloniki Sheet). The project area has high seismic activity during recorded history. Deltas form interbedding layers of finer, cohesive material and coarser material, further interbedded with marine deposits. That is reflected in the top stratigraphy of Thermaikos Gulf, which is composed of mainly fine, very soft to firm clayey and silty material. The bedrock (metamorphic gneiss, epigneiss and green schists) is located at a larger depth, which was not reached by any of the new and existing investigations. Based on the available geological and geophysical studies for the broader project area it is estimated that very soft to firm sand/silty clays reach up to 100-150 m below seabed (D.Raptakis, K.Makra 2010).

2.2 Stratigraphy & Geotechnical Parameters

Data from previous geotechnical investigations along with additional data from a ground investigation scheme, that was carried out on September 2019, were used for the geotechnical interpretation. The new survey for the project in reference, included four (4) supplementary rotary continuous sampling boreholes, comprising three (3) offshore and one (1) on land and six (6) cone penetrometer tests (CPT). The following four main layers have been determined. The geotechnical parameters obtained for each layer is presented in Table 1.

[F] - FILL: Fill of existing reclamation works. The fill is composed of a mixture of all type of soils starting from fat clays and ending at coarse gravels/pebbles. The fill layer is up to 20 m thick in the Pier 6 project area.

[1] - VERY SOFT SILT: This layer starts at seabed and it is composed of very soft to extremely soft deltaic deposits. Black or very dark grey SILTs and clayey SILTs, locally with very silty CLAYs were encountered within this layer. Thickness of this layer in the project area varies from 2.3 to 9.5 m.

[2A] –SAND/GRAVEL LENSES: Alluvial delta deposits characterized by clayey, gravelly and/or well-graded SANDS and clayey, sandy and/or well-graded GRAVELS, typical example of delta deposits in more energetic river seasons.

[2B] PREDOMINANTLY FINE-GRAINED DELTA/MARINE DEPOSITS: This layer is represented by various mixture of fine- and coarse-grained soils such very soft to very stiff silty, sandy and locally gravelly CLAY, sandy to very sandy SILT and clayey to very clayey, silty to very silty SAND and GRAVEL. This layer is interbedded locally by the poorly graded coarse-grained deposits of layer [2A] and extends to depths below seabed larger than 60 m, which corroborates with the broader area geology.

Table 1. Geotechnical Parameters of the stratigraphy formations

Parameter	Formation		
	[1]	[2A]	[2B]
γ_i (kN/m ³)	18.0	20.0	20.0
c_u (kPa)	5	-	2.2xz(m)+25
c' (kPa)	-	-	12.0
ϕ_i' (deg)	25.0	32.0	27.5
E/Eu (MPa)	-/1.5	31/-	-
Eoed (MPa)	-	-	0.15xz(m)+3

Cc Cec	-	-	0.18 / 0.11
Cv (m ² /yr)	-	-	4.0

2.3 Design Vessel

The requirements of THPA S.A., concerning the design ships are as follows:

- Ultra Large Container Vessel (ULCV) - carrying capacity 24,000 TEU
- Smallest design ship: Feeder – carrying capacity 1,500 TEU.

2.4 Seismicity

According to the Greek Seismic Code - EAK 2000 (EPPO, 2001) and the updated Seismic Hazard Map (EPPO, 2003), the design PGA value at Thessaloniki for a 475-yr return period event is 0.16 g. More recently, the SHARE project (Giardini et al., 2014) conducted a pan EuroMediterranean probabilistic seismic hazard assessment. The hazard values are referenced to a rock velocity of $V_{s,30} = 800$ m/s. For the area of Thessaloniki, the study was coordinated by Prof. K. Pitilakis (AUTH). According to this map, the expected PGA at bedrock for a 475-yr return period event is about 0.3 g close to Pier 6. For PGA estimates, the use of the more recent studies (e.g. SHARE) are considered more appropriate. In addition, the Eurocode (EC8) spectrum is considered more reasonable than EAK's since it accounts for soil amplification effects.

3. SOIL IMPROVEMENTS CONCEPT

As mentioned in Paragraph 2.2 the ground of the design area is consisting of an upper very soft clayey Silt layer which is underlaid by very soft to very stiff silty, sandy and locally gravelly CLAY. In order to secure the soil stability due to the additional loads and to minimize the generating settlements from consolidation, improvement measures will be applied. To this direction, the superficial soft soil will be removed, and the underlying stiff clay has been improved by using prefabricated vertical drains (PVDs) and preloading. Besides, 4 rows of inclusion piles are installed below caisson to reduce the tilt of caisson and increase the global stability. There is a 3m thick layer of gravel between caisson and improved soil to transfer and redistribute load.

The above design is based on the fact that the silt-clay layer which is subject to long-term settlements has a thickness exceeding 100m and probably around 150m. This means that there is no cost-efficient way to mitigate the long-term settlements along the entire layer thickness and the only solution is to mitigate the settlements of a limited upper part of the entire layer. This upper improved layer will act as a buffer zone, where settlements will be completed before construction of the permanent top structures and operation start. This will result in the remaining long-term settlements, after project operation, to be due to the deeper non-improved silt-clay layer, which are expected to be mostly uniform with a very limited differential component. The target of this design method is that the largest part of the differential settlements will occur before port operation and the remaining settlements after that will be mostly uniform (see Figure 8). Due to the geotechnical conditions uncertainties related to consolidation rate, appropriate geotechnical & settlement monitoring programs during construction and during operation will be implemented.

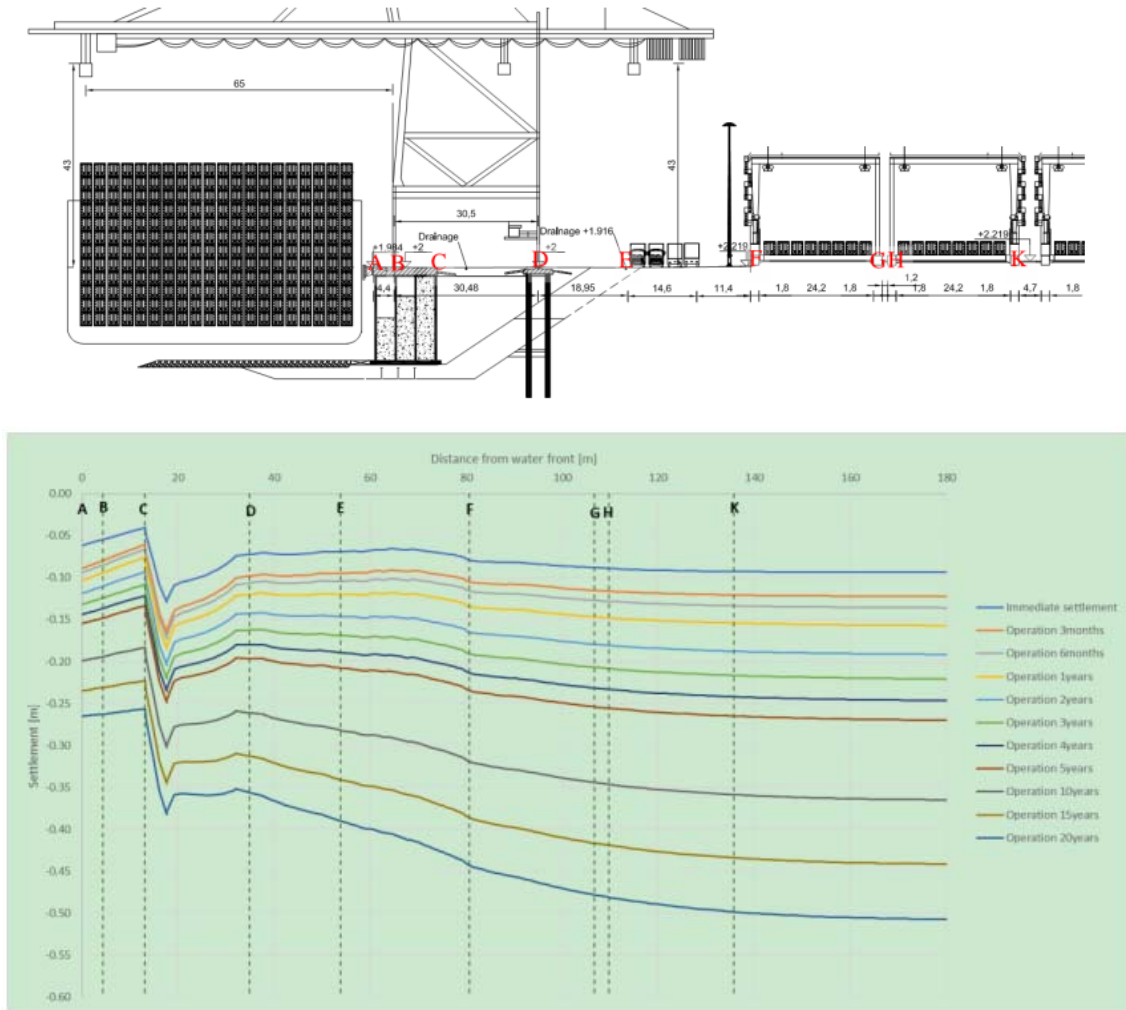


Figure 8 Settlement along ground surface in the transverse direction

4. DYNAMIC ANALYSES

Two-dimensional dynamic soil-structure interaction analyses were performed to estimate the earthquake-induced horizontal and vertical displacements of the caisson and the crane supports and kinematic demands in piles. Planned structures include a partially-infilled concrete caisson, ground improvement of the relatively weak foundation soils using a variety of techniques that result in variations in soil resistance, the use of lightweight fill in the form of a relief prism behind the caisson and a Ship to Shore (STS) crane that is supported with one rail on the caisson and one rail on support piles. The project is located in a seismically active area with significant ground shaking hazard. Since simplified techniques and pseudo-static analyses are not readily able to capture the deformation modes of such a complex structure, and given the expected highly nonlinear soil response, detailed nonlinear dynamic analyses were conducted to evaluate alternative design concepts and to estimate the potential deformations and structural forces resulting from design events on the selected concept (see Figure 9).

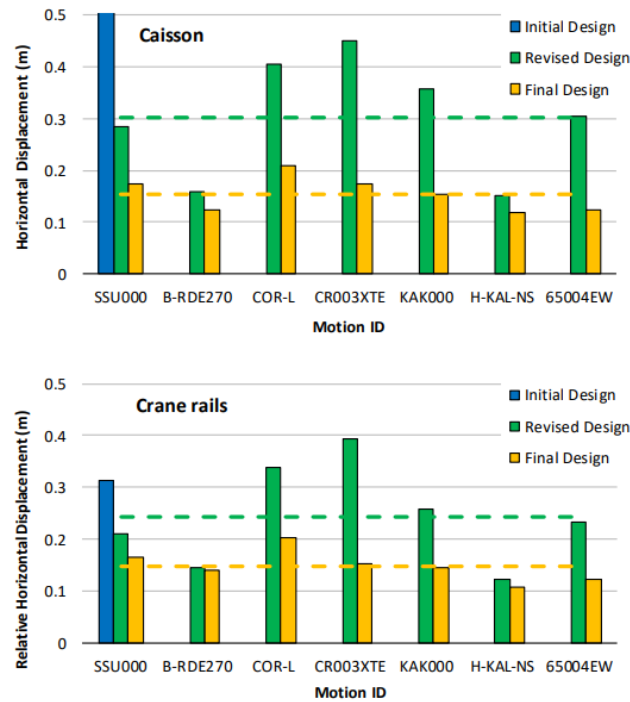


Figure 9 Comparative evaluation of analyzed designs in terms of (a) residual horizontal displacements of the caisson (upper bar chart) and (b) residual relative horizontal displacement between the crane rails (lower bar chart) for all the ground motions considered [ULS level – 475-yr return period – Load Case 2]

References

- Shear wave velocity structure in western Thessaloniki (Greece) using mainly SPAC alternative method; D.Raptakis, K.Makra, Thessaloniki University, Greece, 2010
- Anastasiadis, A., Raptakis, D., and Pitilakis, K. (2001) “Thessaloniki’s Detailed Microzoning: Subsurface Structure as Basis for Site Response Analysis.” *Pure and Applied Geophysics*, 158: 2597-2633
- EPPO (2003) New Seismic Hazard Map of Greece, Earthquake Planning and Protection Organization, July 2003 (in Greek) – ΟΑΣΠ (2003) Νέος Χάρτης Σεισμικής Επικινδυνότητας της Ελλάδας, Οργανισμός Αντισεισμικού Σχεδιασμού και Προστασίας, Ιούλιος 2003
- Giardini D, Woessner J, Danciu L (2014) “Mapping Europe’s seismic hazard”. *EOS Trans Am Geophys Union* 95:261–268. doi: 10.1002/2014EO29

Creation of a double berth Jetty for small scale LNG Carriers & barges in Revithoussa island, Greece – A multipurpose terminal

C. Solomonidis^{1*}, P. Biniskos¹, M. Aggelidis²

¹Rogan Associates S.A., 5 Chatzigianni Mexi Str., Athens 11528, Greece

²Amte S.A., 5 25th Martiou Str., Melissia 12127, Athens, Greece

*Corresponding author: csolomonidis@roganassoc.gr

Abstract

The present study constitutes the FEED Design of the appropriate harbour works for the creation of a New Small Scale LNG Infrastructure (SSLNG) at Revithoussa Terminal of DESFA, capable of accepting LNG carriers with capacities ranging from 1.000 m³ up to 20.000 m³. The proposed harbour works include the creation of a double berth jetty (cross jetty berthing arrangement) that can accommodate two Small Scale LNG Carriers simultaneously. The multipurpose character of the specific terminal is due to the fact that the accommodated LNG Carriers, can either replenish Revithoussa's tanks with LNG, or receive LNG to distribute it either to vessels that use it as a fuel (ship to ship operations) or to LNG trucks (ship to shore operations).

Keywords Liquefied Natural Gas (LNG), Harbour Works, Jetty, Dolphins.

1 INTRODUCTION

1.1 General

The present study, assigned to Rogan Associates by Asprofos, is based on the outcomes of the Conceptual Design performed in the framework of "Poseidon Med II" project.

Poseidon Med II project aimed at bringing the wide adoption of LNG as a safe, environmentally efficient and viable alternative fuel for shipping, and assist the East Mediterranean marine transportation propel towards a low-carbon future. The project, which was co-funded by the European Union, involved three countries Greece, Italy and Cyprus, six European ports (Piraeus, Patras, Limassol, Venice, Heraklion, Igoumenitsa) as well as the Revithoussa LNG terminal. The project brings together top experts from the marine, energy and financial sectors to design an integrated LNG value chain and establish a well-functioning and sustainable LNG market.

1.2 Objective

The objective of the study is the production of a FEED Design and of all appropriate documentation necessary for application, at a later stage, by an EPC Contractor who shall perform the detailed engineering, construction and pre-commissioning of a New Small Scale LNG Infrastructure at Revithoussa Terminal of DESFA, that shall be able to accommodate LNG carriers with capacities ranging from 1.000 m³ up to 20.000 m³.

2 STUDY AREA – EXISTING SITUATION

The DESFA LNG Terminal is located about 40 km West of Athens, on the Island of Revithoussa, in Megara Bay. It has been in operation since the year 2000 and it is featured to receive LNG Carriers up to 266.000 m³.

The existing terminal consists of an import jetty (located on the southern side of the isle), storage system, re-gasification equipment and send-out facilities. The terminal overall authorized storage capacity is of 225.000 m³. Storage system is composed by two (2) tanks of 65.000 m³ each plus a third one of 95.000 m³.

In the framework of "Poseidon Med II" project, a site selection process was carried out by DESFA, focusing on the selection of the most suitable location to install a new maritime infrastructure on

Revithoussa isle, that could host small scale carriers and defined as the most suitable location a coast sector located on the North-Eastern side of the isle.

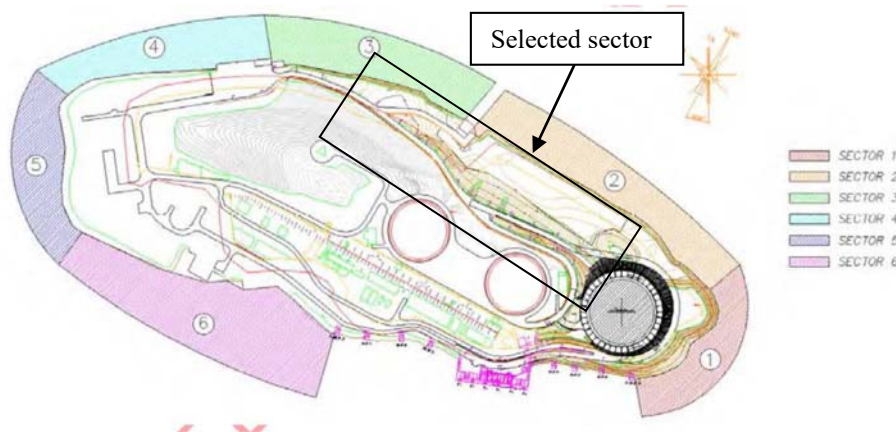


Figure 1 Site selection for the development of a small-scale LNG infrastructure

A Hazard Identification Study (HAZID) as well as a Hazard and Operability Study (HAZOP) have also been conducted in the framework of the specific project (by Lloyd's Register)

DESIGN CRITERIA

The design criteria used for the project are briefly presented below.

- A) Design Ships: LNG Carriers with Loa between 74m and 162m and draught between 4.90 and 9.30m.
- B) Winds: The wind conditions governing the marine area around the isle of Revithoussa were retrieved from the data provided by the station of the National Meteorological Service at Megara. The prevailing winds recorded are those propagating from Northwest directions, with annual frequency of occurrence equal to 42,701% and follow the ones propagating from South directions, with annual frequency of occurrence equal to 19,034%. It is noted that the selected site is exposed to winds of NW sector.
- C) Tides and currents: The tidal data were retrieved from the recording station of Piraeus. The mean tidal range recorded (range between Mean High Water and Mean Low Water), is equal to 9 cm. The maximum tidal range recorded (range between the High Water and Low Water), is equal to 29 cm. No recorded current data were available for the area of study.
- D) Waves: A dedicated Wave Study was performed making use of the MIKE 21 Spectral Waves model as well as the MIKE 21 Parabolic Mild Slope model. At the area of the proposed works, the significant wave heights reach at a maximum of up to 1m height.
- E) Geotechnical parameters: A geotechnical investigation was carried out including five offshore (Θ1-Θ3-Θ4-Θ5-Θ8) and one onshore (X1) exploratory boreholes. According to the findings of the geotechnical investigation, the presence of coarse grained layers of medium density is predominant in all boreholes. In the area of boreholes Θ3-Θ5-Θ8 (i.e., to the east), stiff to hard clayey layers are encountered deeper (approximately 6.00-14.00m beneath seabed level). However, the limestone bedrock that outcrops on Revithoussa island and was encountered in borehole X1, was not encountered up to the maximum investigated depth of 25-35m in any of the offshore boreholes. This has been attributed to the presence of a fault. Another, younger, possible fault is estimated to exist between boreholes Θ1-Θ4 and Θ3-Θ5-Θ8 within the deeper and respectively older alluvial deposits.

3 PROPOSED WORKS DESCRIPTION

3.1 Introduction

The necessary infrastructure foreseen for this Project includes the following:

1. Offshore Marine Works: Double Berth Jetty for the loading/ unloading operations of small-scale LNG Carriers and barges

2. Breasting and Mooring Dolphins

3. Cryogenic pipelines

Various E/M installations necessary for the operation of the SSLNG infrastructure.

The layout of the proposed marine infrastructure is presented in the following Figure.

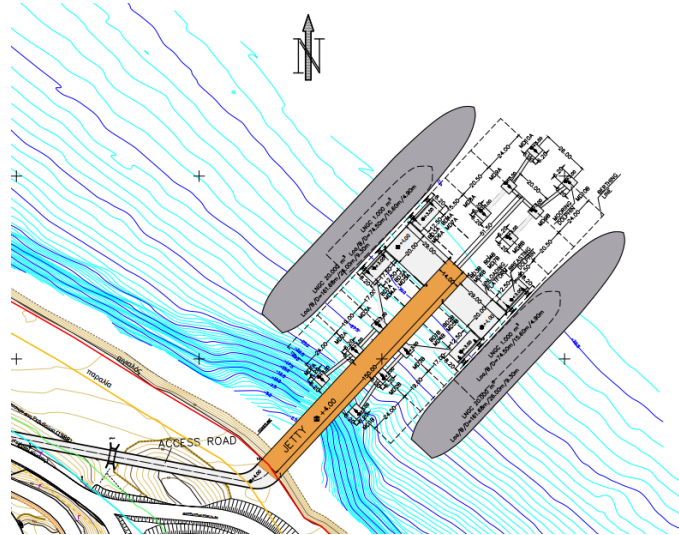


Figure 2 Layout of proposed Harbour Works

A new offshore Jetty Facility founded on piles, having an overall length of about 150m was designed along the North-East side of Revithoussa island.

The jetty will be perpendicular to the coast, allowing the berthing of two (2) LNG carriers/ barges at the same time. Minimum sea depth of 11m is guaranteed to host LNG carriers with capacity up to 20.000 m³.

The Jetty consists of a trestle on piles, of length 150m and width 14m, two (2) loading platforms, one on each side of the trestle, each of dimensions 29m X 20m, four (4) Breasting dolphins, each of dimensions 17,5m X 8,2m, and twelve (12) mooring dolphins, six (6) on each side of the jetty each of dimensions 6,20m X 6,20m.

Therefore, each berth consists of two (2) breasting dolphins, each equipped with two (2) Super Cone Fenders and two double Quick Release Mooring Hooks, and six (6) mooring dolphins, each equipped with one triple Quick Release Mooring Hooks (QRH).

3.2 Access jetty – Trestle

The width of the trestle is 14m, as it is designed to accommodate LNG piping installations to service two berths (two LNG carrier vessels) simultaneously. The deck of the trestle is divided into three “lanes” of 4,50 m width each. Each of the end lanes accommodates the pipe racks for the two berths, whereas the middle lane is dedicated to traffic access of light vehicles.

The central access jetty / trestle has a length of 150m. The deck slab is constructed by trapezoidal composite deck sheeting supported on steel girders, which are supported on built-up steel beams, of height 1,45m. The deck structure is supported on eight abutments, at spans of 20 m. The abutments consist of a reinforced concrete beam of length 22,5m and 4m width, serving also as the pile cap of a row of six steel tubular piles of diameter / thickness Ø 1422 / 25mm. The upper part of the piles is filled with reinforced concrete, to allow connection of the piles with the pile cap.

3.3 Loading Platforms

There are two loading platforms (one for each berth). The dimension of each loading platform is 29m X 20m, and its elevation is at +4,00m (above MSL).

The deck of the loading platform is constructed with trapezoidal composite deck sheeting, supported on a grid of steel girders and IPE beams. The deck is based on a grid of perpendicular tubular steel piles of diameter / thickness Ø 1422 / 25mm. The piles are located at the “junctions” of the girders. A total of 24 piles (4 X 6) are constructed to support each loading platform.

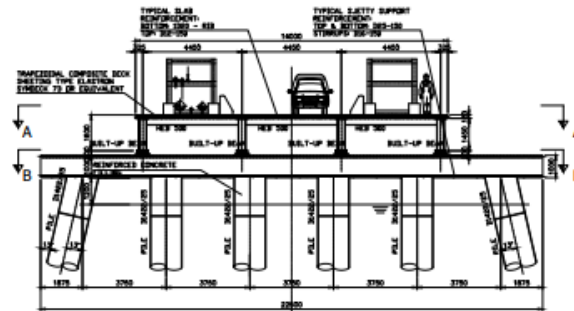


Figure 3 Trestle's typical cross section

3.4 Walkways (Catwalks)

All walkways are steel trusses, of height 2,2m and width 2m, whereas the typical span of the trusses is 2,02m. The trusses are constructed with steel beams.

3.5 Mooring Dolphins

Twelve (12) mooring dolphins are proposed to serve as mooring points for the LNG carriers. They are all equipped with one triple Quick Release Mooring Hook (QRMH). All mooring dolphins, have rectangular shaped superstructure, with plan dimensions 6,20m X 6,20m. The elevation of the upper side is at +3,00m above MSL. The height of each mooring dolphin is 2m. The pile caps are formed by precast reinforced concrete elements that serve as formwork for casting in situ concrete. The foundation of each of the mooring dolphins consists of four tubular hollow section steel piles $\Phi 1422/25$. Two of the piles are inclined (raked piles), with an inclination of 1:4.

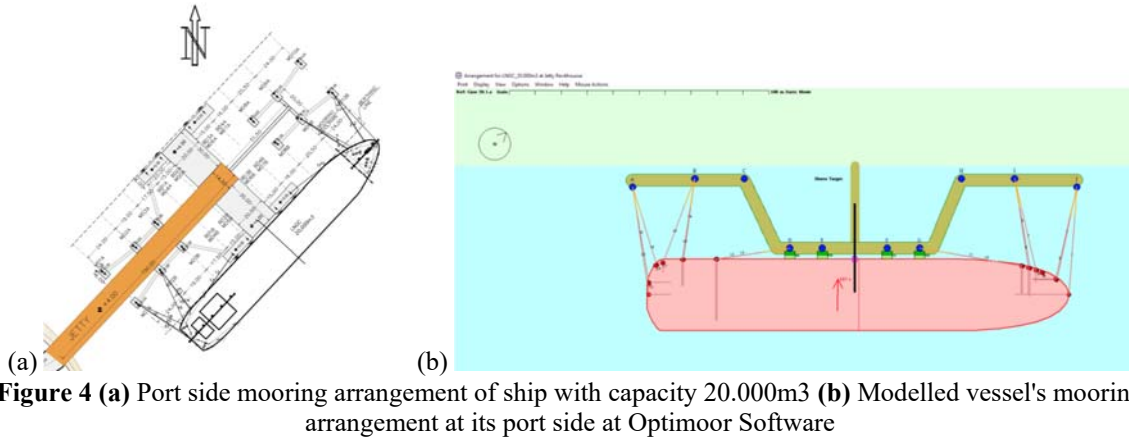
3.6 Breasting Dolphins

Four (4) Breasting Dolphins are proposed to be constructed in total. All breasting dolphins will be equipped with suitable cone fenders, which will protect the structure and absorb the kinetic energy of the berthing vessels. On their apron, they are equipped with double quick release mooring hooks, for the "spring" mooring lines of the vessels. The plan dimensions of the superstructure of all the breasting dolphins are 17,50m X 8,20m. The elevation of the upper side is at +3,00m above MSL. The pile caps will be formed by precast reinforced concrete elements that will serve as formwork for casting in situ concrete. The foundation of each of the Breasting Dolphins consists of five tubular steel piles $\Phi 1422/25$. The upper part of the piles will be filled with in situ concrete. The embedment depth of the steel piles is between -49m and -55m below MSL.

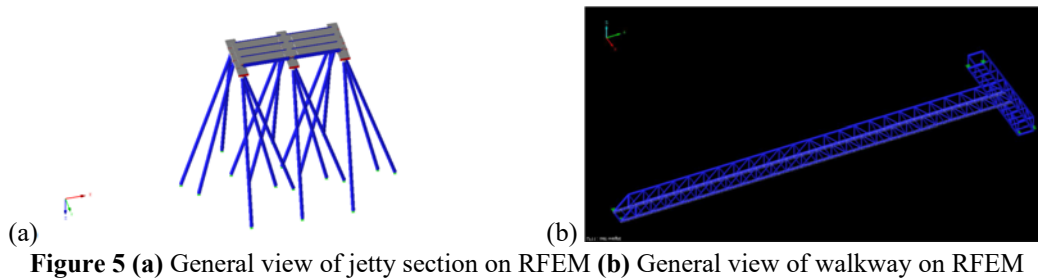
4 CALCULATIONS

The main calculations included:

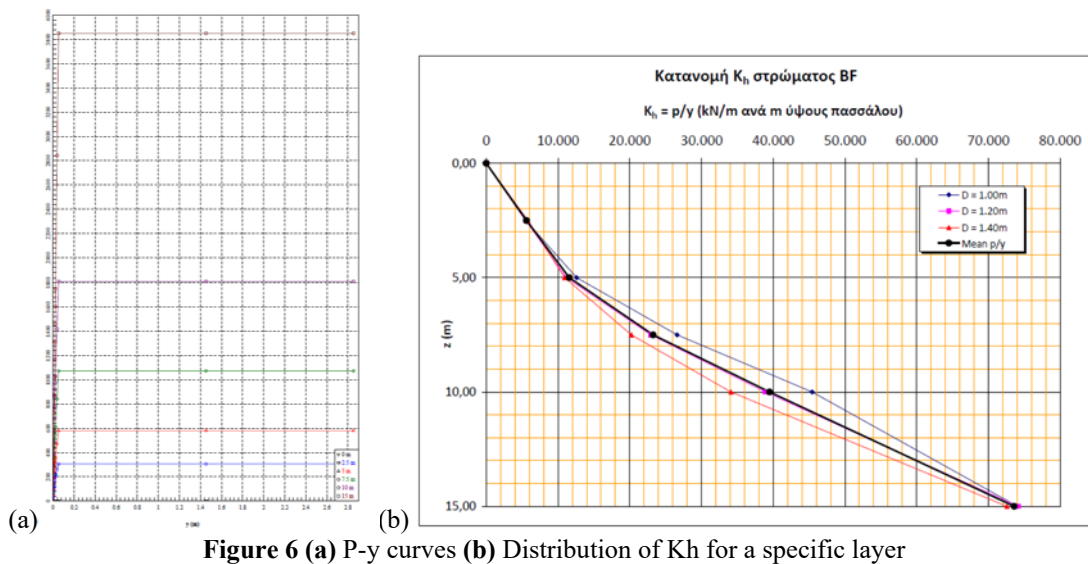
- a) The determination of the berthing loads, that were carried out in accordance with PIANC (2002) guidelines and the British Standards 6349-4 (2014). Based on the relevant results, the appropriate fendering system was defined.
- b) The determination of the mooring loads on the Mooring Dolphins. A dedicated Mooring Analysis was performed making use of the software OPTIMOOR. The analysis was carried out in accordance with OCIMF - "Mooring Equipment Guidelines". Based on the results, the Safe Working Load of the QRMHs as well as the operational limits of the terminal were defined.



c) Structural Analysis of all the marine structures making use of the software RFEM (Dlubal GmbH), a finite element analysis and design software.



d) Geotechnical calculations: A parametric estimation of axial pile bearing capacities for various pile embedment depths below sea bottom, at all borehole locations, was carried out. For the determination of the skin frictional and end-bearing resistances, the guidelines of Tomlinson (1987) were followed. The horizontal spring constants to be used for the structural analysis were determined with the aid of the software LPILE Plus.



References

- British Standards, Maritime Structures, BS 6349 Parts 1 – 6
- PIANC 2002: Guidelines for the design of fender systems
- OCIMF Mooring Equipment Guidelines 3 (MEG3)

Numerical modelling of dredged material dispersion at dredging and disposal areas

Th. Karambas^{1*}, A. Papageorgiou¹

¹Department of Civil Engineering, Aristotle University of Thessaloniki, University Campus, 54124 Thessaloniki, Greece

*Corresponding author: karambas@civil.auth.gr

Abstract

This paper presents a numerical model for simulating the advection, diffusion, and dispersion of dredged material. The wind-induced current is estimated by applying a quasi-3D hydrodynamic model. The sediment concentration is obtained by solving the 3D advection–diffusion–dispersion equation. The model is applied in both dredging (by simulating dredging-induced sediment resuspension) and disposal areas. Finally, morphology evolution in the disposal area is estimated.

Keywords Dredged material disposal, wind-induced currents, sediment resuspension, pollutant dispersion

1 INTRODUCTION

Numerical modelling using sediment transport models (coupled to hydrodynamics and wave models) can be used to predict the ecological pressure caused by dredging activities (through increases in suspended solids, sediment smothering and light reduction). During dredging operation, and the disposal of dredged sediment in open sea, the resulting turbidity plume can decrease light for photosynthesis, interfere with fish respiration and feeding, cause discoloration of normally clear surface waters, reduce oxygen levels, and release adsorbed pesticides, herbicides, toxic metals, or synthetic organic compounds into the water column. The magnitude of sediment concentration should be placed in context with other sediment resuspension events or sources, (i.e., waves, currents, river flow, etc.).

The goal of the Numerical Modelling is to improve the prediction of the transport and diffusion of dredge-generated sediments by developing an improved understanding of key physical processes that control the extent, intensity and duration of sediment plumes.

2 SEDIMENT SUSPENSION DURING DREDGING OPERATION

During dredging, in the suction area, especially when a cutting head is used, sediment re-suspended and it is transported, diffused, and dispersed in the marine environment by currents. At the same time, through the overflow water of the temporary storage tank a part of the incoming sand will not settle during loading in the hopper but will re-enter in the water column of the wider dredging area.

If a trailing suction hopper dredger is used, the net concentrations of resuspended sediments C_r (kg/m³) induced by cutterhead dredges is given by (Hayes et al., 2000):

$$\frac{C_r}{\rho 10^{-6}} = F_F F_D \left(\frac{V_s}{V_i} \right)^{2.848} \left(\frac{V_t}{V_i} \right)^{1.022} \quad (1)$$

where V_s = swing velocity at the tip of the cutter (m/s); V_i = suction intake velocity at the cutter blades (estimates based upon observed flow rates and assuming an elliptical cutterhead surface) (m/s); and V_t = tangential velocity of the cutter blades at the top of the rotation relative to the surrounding water (m/s), ρ = density of waters above the mudline (g/cm³); F_F = regression parameter that accounts for the cutter size and median grain diameter; and F_D = regression parameter that accounts for the thickness of cut relative to the cutter diameter (Hayes et al., 2000).

The cumulative concentration of suspended sediment due to re-entering varies with time: at the beginning of dredging, it is of the order of 0% of the amount of the incoming sediment, while at the end when the hopper is filled it can even reach 40% of the incoming sediment (Van Rhee, C., 2002).

3 QUASI 3D HYDRODYNAMIC AND ADVECTION-DISPERSION MODEL

A quasi-3D hydrodynamic model is used to predict wind induced current velocities. The model equations are derived from Navier-Stokes equations, after the assumption of hydrostatic pressure distribution and constant over the depth eddy viscosity. The equations are written:

$$\begin{aligned} \frac{\partial \zeta}{\partial t} + \frac{\partial(U_c(d+\zeta))}{\partial x} + \frac{\partial(V_c(d+\zeta))}{\partial y} &= 0 \\ \frac{\partial U_c}{\partial t} + U_c \frac{\partial U_c}{\partial x} + V_c \frac{\partial U_c}{\partial y} &= -\frac{1}{\rho} \frac{\partial p_a}{\partial x} - g \frac{\partial \zeta}{\partial x} + \frac{1}{h} \frac{\partial}{\partial x} \left(\nu_h h \frac{\partial U_c}{\partial x} \right) + \frac{1}{h} \frac{\partial}{\partial y} \left(\nu_h h \frac{\partial U_c}{\partial y} \right) + \frac{\tau_{sx}}{\rho h} - \frac{\tau_{bx}}{\rho h} \\ \frac{\partial V_c}{\partial t} + U_c \frac{\partial V_c}{\partial x} + V_c \frac{\partial V_c}{\partial y} &= -\frac{1}{\rho} \frac{\partial p_a}{\partial y} - g \frac{\partial \zeta}{\partial y} + \frac{1}{h} \frac{\partial}{\partial x} \left(\nu_h h \frac{\partial V_c}{\partial x} \right) + \frac{1}{h} \frac{\partial}{\partial y} \left(\nu_h h \frac{\partial V_c}{\partial y} \right) + \frac{\tau_{sy}}{\rho h} - \frac{\tau_{by}}{\rho h} \end{aligned} \quad (2)$$

where U_c and V_c are the mean over the depth current velocities, ζ is the free surface elevation, h is the total depth, p_a the pressure at the surface of the sea, τ_{sx} and τ_{sy} are the surface shear stresses, τ_{bx} and τ_{by} are the bottom shear stresses and ν_h the horizontal eddy viscosity is given through the Smagorinsky eddy parameterization.

By assuming constant over the depth vertical eddy viscosity coefficient, a parabolic over the depth horizontal velocity distribution is obtained according to Koutitas (1988). Alternatively, a parabolic distribution of the vertical eddy coefficient leads to a double-logarithmic velocity profile including both the surface and bottom sublayer (Tsanis, 1989, Wu and Tsanis, 1995). Thus a quas-3D simulation is obtained resulting to the horizontal velocities distribution $u(z)$ and $v(z)$.

Wave induced currents are also described through by including radiation stress terms.

The sediment concentration is obtained by solving the advection–diffusion–dispersion equation, which has the form:

$$\frac{\partial c}{\partial t} + u \frac{\partial c}{\partial x} + v \frac{\partial c}{\partial y} + (w - w_f) \frac{\partial c}{\partial z} = \nu_h \frac{\partial^2 c}{\partial x^2} + \nu_h \frac{\partial^2 c}{\partial y^2} + \nu_t \frac{\partial^2 c}{\partial z^2} + q \quad (3)$$

where c is the sediment concentration u , v and w are the current velocities, w_f is the fall velocity of the sediment, ν_t is the vertical diffusion coefficient, q is a source term which is used to insert the sediment into the system due to dredging, according to eq. (1).

Sediment suspension due to current and waves and deposition are introduced through bottom boundary conditions, i.e. "gradient" bed b.c. or "concentration" bed b.c.:

$$\nu_t \frac{\partial c}{\partial z} = E - D, \quad E = w_s c_e, \quad D = w_s c_{\text{bottom}} \quad (4)$$

$$c_{\text{bottom}} = \frac{0.01 D_f}{g(\rho_s / \rho - 1)} \quad (5)$$

where E , D are the erosion and depositional rates respectively, D_f is the work done by bottom friction, C_{bottom} is the bed concentration, c_e is the equilibrium concentration at the reference (bed) level and ρ and ρ_s the water and sediment density respectively.

Bed evolution in the disposal area is calculated by solving the equation of the conservation of sediment transport.

4 MODEL APPLICATION

The model is applied to Thermaikos Gulf for the prediction of for tracking of dredged material both in dredging and disposal areas.

Considering a dredging area located in the port of Thessaloniki region, the current velocity field and the suspended sediment concentrations during dredging operation area are shown in Figures 1 and 2 respectively. In Figure 2, the area of the sediment deposition on the sea bed is also shown. The wind conditions are: NW and 9Bf. Following eq. (1), the source term in eq. (3) is estimated to be $q = 500 \text{ kg/s}$.

At the dredging area the sediment plume is transferred towards the port of Thessaloniki area. Consequently, under the above wind conditions dredging operations should be avoided.

By considering that 20000 kg of sediment are disposed within 10 min, in the centre of Thermaikos Gulf, under the same wind conditions, the calculated concentration as well the sediment deposition area at the sea bed is shown in Fig. 3. No significant advection-diffusion-dispersion of the sediment plume is predicted, indicating the correct choice both the time (which could be related to the predicted wind conditions) and the disposal area.

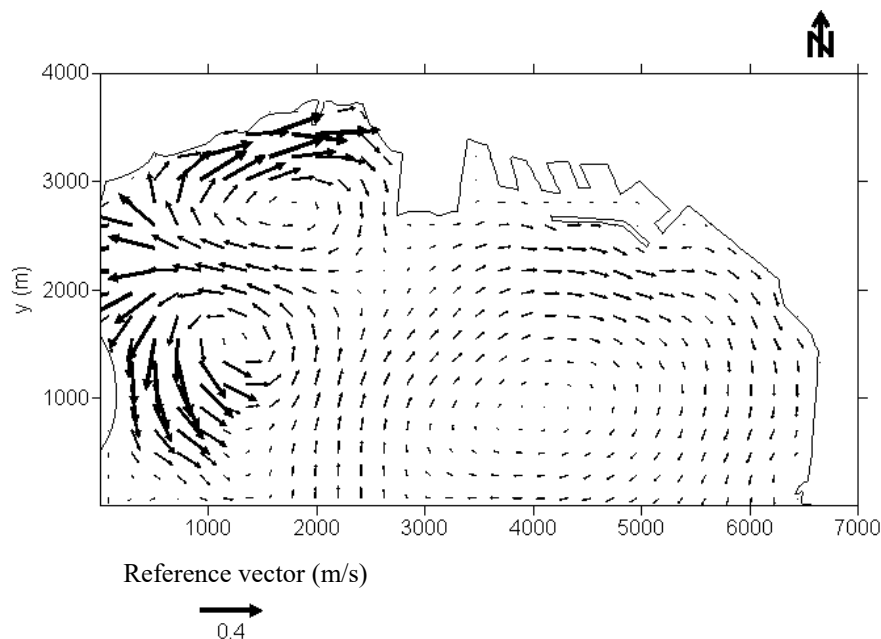


Figure 1. Velocity field in Thessaloniki Port area. The wind conditions are: NW and 9Bf

CONCLUSIONS

By using quasi-3D hydrodynamic and advection-diffusion-dispersion numerical models the time of the dredging operations as well as the time and the area of the disposal can be estimated. In this way the evaluation of the environmental impacts and the management of dredging operations could be supported.

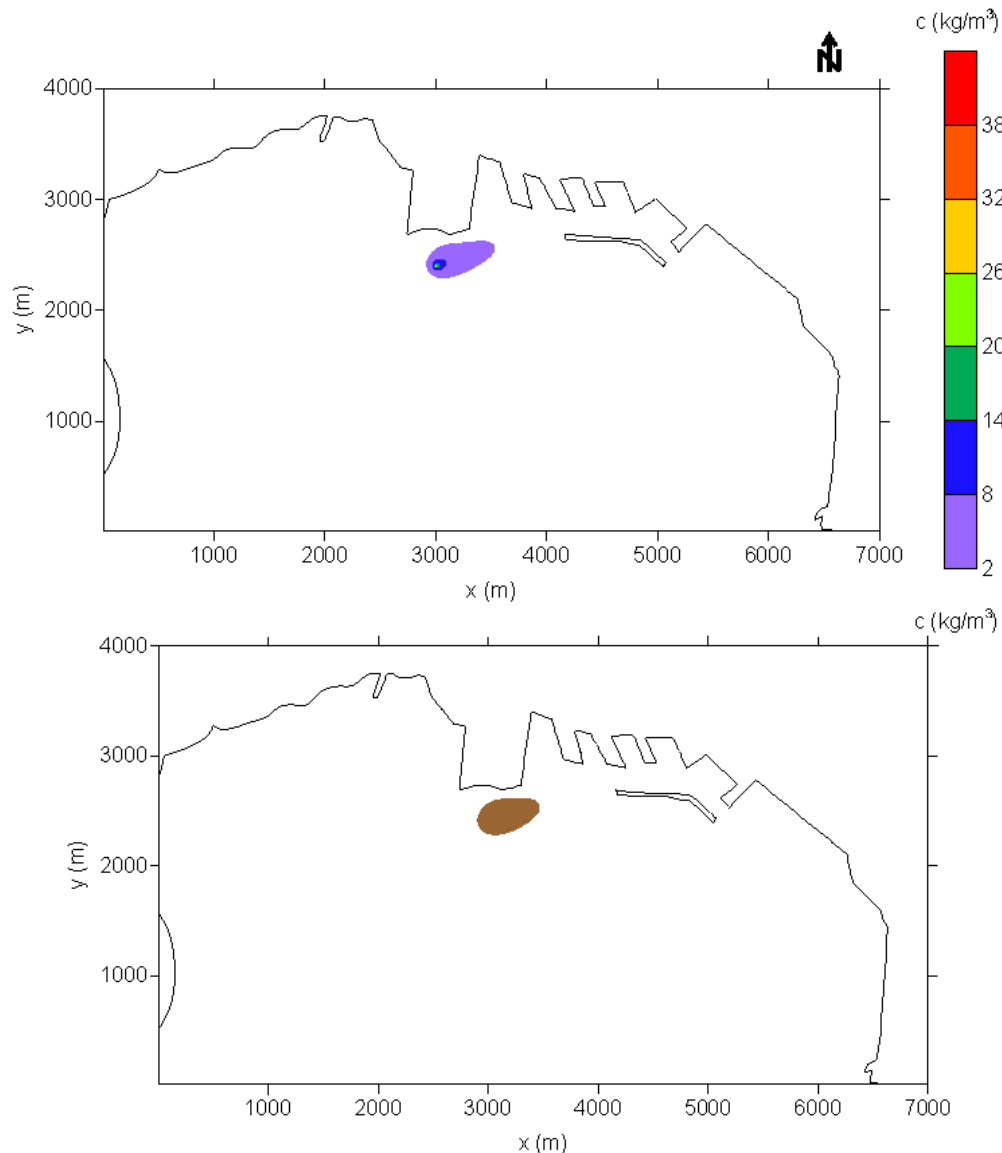


Figure 2. Suspended sediment concentrations at the dredging area (above) and area of the sediment deposition at the seabed (below)

References

- Hayes D. F., T. R. Crockett, T. J. Ward, D. Averett (2000) Sediment resuspension during Cutter-head dredging operation. *J Wat Port Coastal Oc Eng* 126 (3):153–161.
- Koutitas Ch. (1988) *Mathematical Models in Coastal Engineering*, Pentech Press Limited, London.
- Tsanis I. (1989) Simulation of wind-induced water currents. *Journal of Hydraulic Engineering (ASCE)*, vol. 115 No 8: 1113-1134.
- Van Rhee C. (2002) *On the sedimentation process in a trailing suction hopper dredger*. Doc. Thesis, Faculty of Civil Engineering, Delft University of Technology, Delft, The Netherlands.
- Wu J., I. Tsanis (1995): Numerical study of wind-induced water currents, *Journal Hydraulic Engineering (ASCE)*, vol. 121 No 5, pp. 388-395.

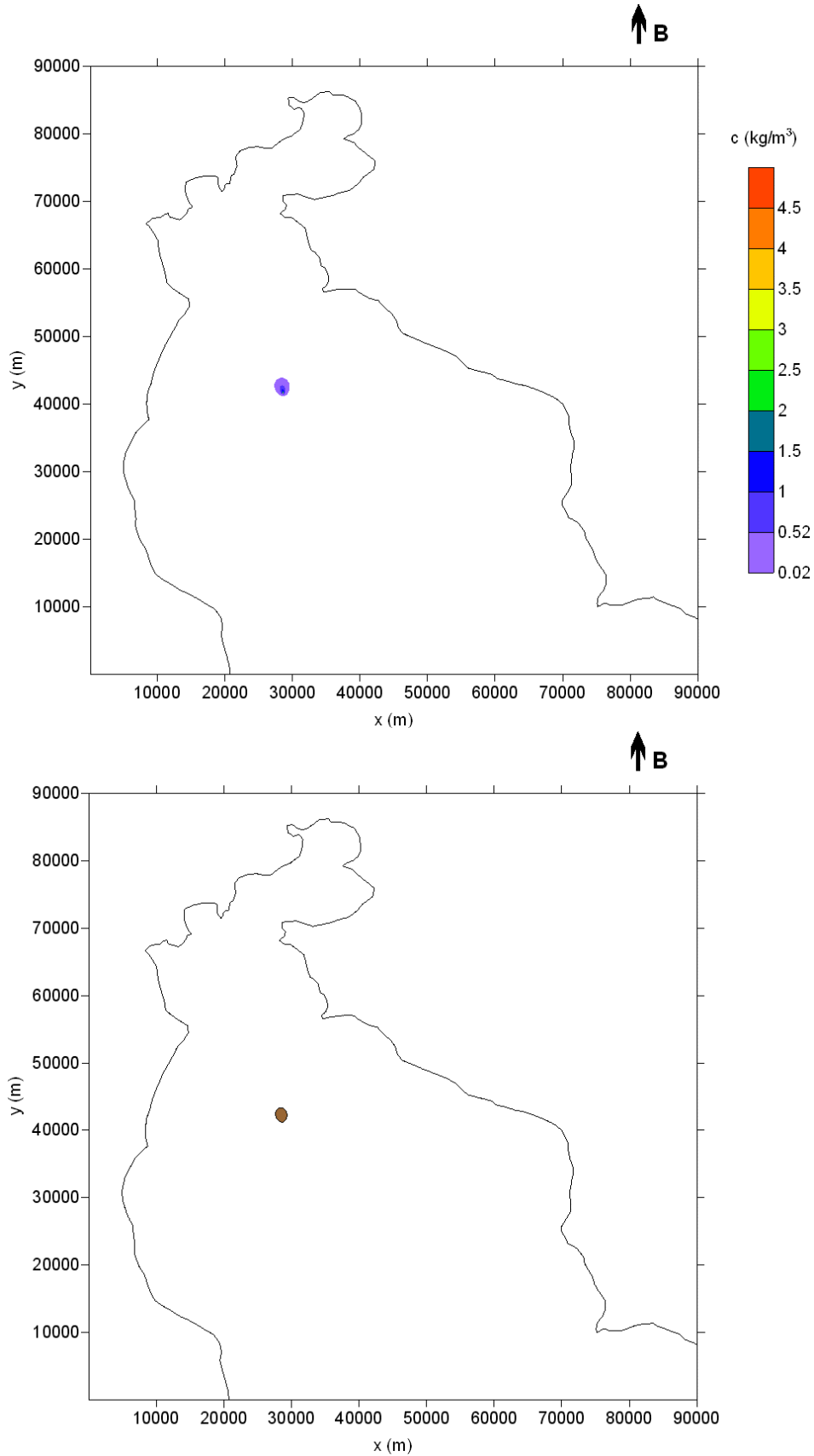


Figure 3. Suspended sediment concentrations at the disposal area (above) and area of the sediment deposition at the seabed (below)

Assessing the impact of climate change in wave agitation for the port of Piraeus

I. Kollias¹, A. Papadimitriou¹, M. Chondros¹, V.I. Chalastani¹, D. Spyrou², C.S. Laspidou³, P. Koudouri⁴, V.K. Tsoukala^{1*}

¹Laboratory of Harbour Works, NTUA, 15780, Zografou, Greece

²Piraeus Port Authority S.A., Marketing & Quality Control department, EU co-funded projects, 18538, Piraeus, Greece

³Civil Engineering Department, University of Thessaly, Pedion Areos, Volos 38334, Greece

⁴School of Economics and ReSEES Research Laboratory, Athens University of Economics and Business; Department of Technology, Management and Economics, Denmark Technical University; Sustainable Development Unit, ATHENA RC; Academia Europea

*Corresponding author: tsoukala@mail.ntua.gr

Abstract

Ports are vital links in the chain of maritime transportations and are essential for the global trading network. Ensuring low wave agitation levels inside the port basin is of paramount importance for safe port operations and economic prosperity. Climate change is expected to alter wave dynamics. However, the impact of climate change in the wave field inside port basins has not been thoroughly investigated yet. The scope of this study is to evaluate by means of numerical modelling, if the wave field in the basin of the passenger port of Piraeus, Greece is altered once the effects of climate change are considered. To ensure transparency, data are derived from open oceanographic databases. A slight increase in the projected values of wave height with respect to the prediction based on a past (historical) dataset, was observed for the “worst-case” Representative Concentration Pathway emission scenario, hence the RCP 8.5. The findings of this study have strong implications on the vulnerability of the port of Piraeus in relation to wave action and its alterations, in the context of climate change.

Keywords Climate Change, Wave agitation, Vulnerability, Wave propagation modelling.

1 INTRODUCTION

Ports are vital links in the chain of maritime transportations and are extremely valuable for the global trading network. In parallel, they constitute long-lasting and critical infrastructure. Given their crucial role, their exposure to climate change related hazards poses a considerable threat to both their infrastructure and operations. The passenger port of Piraeus in Greece is one of Europe’s largest ports of this type, handling the transportation of millions of passengers, while simultaneously being a significant draw for cruise ships. Therefore, ensuring minimal wave agitation levels and securing undisturbed loading and unloading operations is of the utmost importance for the economic prosperity of the port, especially in the coming decades. Taking advantage of the rapidly grown and publicly available metocean datasets, this study aims to investigate, by means of numerical modelling, the climate change impact on wave disturbance in the basin of the port of Piraeus. Wave heights are on average expected to decrease in the Mediterranean Sea due to climate change (IPCC 2019), whereas changes in directions, frequencies of extreme events occurrence (Tsoukala et al. 2016) and sea-level rise are expected to affect wave agitation of port basins in the coming decades. The scope of this study is to investigate the climate change impact on wave patterns in the basin of the port of Piraeus, to estimate its vulnerability regarding wave action and possible implications to the port’s operations.

2 MATERIALS AND METHODS

2.1 Past and future offshore wave climate

Offshore sea-state wave characteristics are obtained from publicly available and reliable oceanographic databases to ensure transparency and reproducibility. In particular, both historical and projected data, incorporating the effect of climate change, are extracted from the Copernicus Climate Data Store (CDS)

(<https://cds.climate.copernicus.eu/>), from the product titled “*Ocean surface wave time series for the European coast from 1976 to 2100 derived from climate projections*”. The wave characteristics are calculated using the ECMWF's Wave Model (SAW) forced by surface wind and accounting for ice coverage in polar latitudes. The SAW model is run for three (3) different climate conditions: the current climate (also termed historical), and two Representative Concentration Pathways (RCPs) that correspond to an optimistic emission scenario where emissions start declining beyond 2040 (RCP 4.5) and a pessimistic one, where emissions continue to rise throughout the century (RCP 8.5). The wave climate for these pathways is simulated using wind forcing from a member of the EURO-CORDEX climate model ensemble. The datasets that are taken into account in the present study are given below along with their corresponding time periods:

- HISTORICAL dataset for the time period 1976-2015.
- RCP 4.5 dataset for the time period 2041-2100.
- RCP 8.5 dataset for the time period 2041-2100.

The wave data extraction point, from the CDS database, is shown in Figure 1, in relation to the location of the passenger port of Piraeus. In the same figure, the computational bathymetry of the study area is also illustrated.



Figure 1. Passenger port of Piraeus, Greece, offshore wave data extraction point and computational bathymetry.

Given the orientation of the port entrance, waves approaching from the S, SSW, WSW, and W sectors are able to generate wave agitation inside the port basin and consequently interrupt port operations. Hence these sectors are of significant importance and will be further investigated in the present study. The aforementioned datasets were statistically analyzed to derive the mean annual offshore wave climate for each of the three (3) considered datasets. The wave characteristics were grouped in 30-degree directional bins (i.e., 12 sectors in total) and in equally spaced wave height groups with a step of 0.5 m. The resulting mean annual frequencies of occurrence per each wave height group and sector are given in Table 1, Table 2 and Table 3 for the HISTORICAL, RCP4.5 and RCP8.5 datasets respectively.

It is observed that the cumulative frequencies of occurrence per each sector are comparable and of the same magnitude between the HISTORICAL, RCP4.5 and RCP8.5 datasets. It is worth mentioning that in both pathways an increase in the occurrence of extreme events from the SSW, WSW and W directions is observed (these frequencies are highlighted with red color in Tables 2 and 3). This trend can consequentially lead to an increase in future wave agitation levels, since waves coming from the SSW and WSW sectors are entering almost undisturbed in the port basin, albeit with a low frequency of occurrence.

Table 1. Mean annual wave frequency of occurrence per height group and sector for HISTORICAL dataset.

H_s [m]	Sectors				
	S	SSW	WSW	W	other
(0.0-0.5m]	16.473%	5.627%	3.558%	6.310%	47.134%
(0.5-1.0m]	3.807%	1.088%	0.436%	1.137%	10.930%
(1.0-1.5m]	1.307%	0.177%	0.060%	0.184%	1.064%
(1.5-2.0m]	0.391%	0.029%	0.006%	0.011%	0.109%
(2.0-2.5m]	0.097%	0.004%	-	-	0.014%
(2.5-3.0m]	0.024%	0.001%	-	-	0.003%
(3.0-3.5m]	0.008%	-	-	-	0.001%
(3.5-4.0m]	0.003%	-	-	-	0.001%
(4.0-4.5m]	0.001%	-	-	-	-
(4.5-5.0m]	0.001%	-	-	-	-
(5.0-5.5m]	0.004%	-	-	-	-
total	22.117%	6.926%	4.060%	7.641%	59.256%

Table 2. Mean annual wave frequency of occurrence per height group and sector for RCP 4.5 dataset.

H_s [m]	Sectors				
	S	SSW	WSW	W	other
(0.0-0.5m]	15.300%	5.433%	3.563%	6.228%	47.990%
(0.5-1.0m]	3.683%	1.148%	0.483%	1.157%	11.658%
(1.0-1.5m]	1.214%	0.222%	0.067%	0.168%	1.055%
(1.5-2.0m]	0.331%	0.039%	0.008%	0.015%	0.106%
(2.0-2.5m]	0.077%	0.004%	-	-	0.019%
(2.5-3.0m]	0.022%	0.001%	-	-	0.003%
(3.0-3.5m]	0.003%	0.0004%	-	-	0.001%
(3.5-4.0m]	-	-	-	-	-
(4.0-4.5m]	-	-	-	-	-
(4.5-5.0m]	-	-	-	-	-
total	20.630%	6.848%	4.121%	7.568%	59.256%

Table 3. Mean annual wave frequency of occurrence per height group and sector for RCP 8.5 dataset.

H_s [m]	Sectors				
	S	SSW	WSW	W	other
(0.0-0.5m]	15.149%	5.239%	3.381%	6.184%	47.990%
(0.5-1.0m]	3.617%	1.022%	0.52%	1.098%	11.658%
(1.0-1.5m]	1.134%	0.214%	0.071%	0.161%	1.055%
(1.5-2.0m]	0.341%	0.040%	0.010%	0.017%	0.106%
(2.0-2.5m]	0.090%	0.004%	0.001%	0.001%	0.019%
(2.5-3.0m]	0.023%	0.001%	-	-	0.003%
(3.0-3.5m]	0.009%	0.0004%	-	-	0.001%
(3.5-4.0m]	0.001%	-	-	-	-
(4.0-4.5m]	0.001%	-	-	-	-
(4.5-5.0m]	-	-	-	-	-
(5.0-5.5m]	-	-	-	-	-
total	20.364%	6.519%	3.965%	7.462%	59.256%

2.2 The Maris HMS wave model

In order to simulate the wave penetration inside the port basin, the Maris HMS model (Scientia Maris 2022), an advanced nonlinear irregular wave propagation model for port and coastal areas, is implemented. It is based on the hyperbolic approximation to the mild slope wave equation and it is capable of accurately simulating all the dominant phenomena that take place in such areas, i.e., partial or total reflection, diffraction, shoaling, refraction, energy dissipation due to breaking and bottom friction. The governing equations of the model are the continuity (Eq. 1) and the momentum (Eq. 2) equations:

$$\zeta_t + \frac{c}{c_g} \nabla \frac{c_g}{c} Q_w = -\frac{D}{E} \zeta_t \quad (1)$$

$$U_{w,t} + \frac{c^2}{d} \nabla \zeta = v_h \nabla^2 U_w - f_b \sigma U_w \quad (2)$$

where ζ is the surface elevation, $U_w = (U_w, V_w)$ is the mean velocity vector, ∇ is the horizontal gradient operator, d is the depth, $Q_w = U_w h_w = (Q_w, P_w)$, h_w is the total depth ($h_w = d + \zeta$), c is the phase celerity, c_g is the group velocity ($c_g = (gd)^{0.5}$), v_h is the horizontal eddy viscosity coefficient coping with (partial or total) wave reflection, D denotes energy dissipation due to wave breaking, E is the wave energy, σ is the intrinsic angular wave frequency and f_b denotes energy dissipation due to bottom friction, and the subscript t denotes time derivative. More details on the discretization numerical scheme and the boundary conditions can be found in Chondros et al. (2021) and Papadimitriou et al. (2022).

2.3 Methodology to assess wave agitation levels in the port basin

Having determined the offshore wave climate (Tables 1-3), numerical simulations are performed to assess the wave agitation in the port basin. The methodology adopted is based on the following steps:

- For each wave height group, associated with a non-zero frequency of occurrence (f_i) a mean value of significant wave height ($H_{s,i}$), peak wave period ($T_{p,i}$) and mean wave direction (MWD_i) are calculated from the respective dataset. In this manner, 25 incident wave scenarios are determined for the HISTORICAL dataset, 22 for RCP 4.5 and 26 for RCP 8.5.
- Subsequently, the bathymetric grid is constructed based on hydrographical charts of the wider area and on bathymetric data from recent surveys and then numerical simulations for each of the aforementioned scenarios of wave characteristics are carried out.
- For each dataset (i.e., HISTORICAL dataset, RCP 4.5, RCP 8.5) a weighted average value of the significant wave height, $H_{s,m}$, is calculated at each computational grid cell through Eq.3

$$H_{s,m} = \frac{\sum f_i H_{s,i}}{\sum f_i} \quad (3)$$

To quantify the wave agitation levels considering the impact of climate change, the results of the weighted averaged significant wave height from the HISTORICAL dataset are considered as the baseline prediction and a percentage difference in wave height levels is calculated for the two (2) RCP scenarios through Eq.4:

$$Per. Diff = \frac{H_{s,m}(RCP) - H_{s,m}(HISTORICAL)}{H_{s,m}(HISTORICAL)} \quad (4)$$

3 RESULTS

The results of the percentage change (increase or decrease) between the RCP datasets and the HISTORICAL one, are presented in Figure 2. A decrease of wave agitation levels on average is observed, for the RCP 4.5 dataset, with an average percentage decrease of 5.6% in the port basin, with respect to the baseline wave height values obtained from the HISTORICAL dataset. In general, the RCP 4.5 dataset encompasses less energetic waves, compared to the HISTORICAL dataset, especially for waves propagating from the dominant S direction. Nevertheless, an increase in specific berths is observed, which can be attributed to the increase of the frequencies of occurrence of energetic waves

propagating mostly from the SSW and WSW sectors. The latter may be responsible for potential hinderance in port operations. Regarding the RCP 8.5 dataset, a mean percentage increase, about 3.3%, in the port basin is observed in the agitation levels. This increase is more intense in the outer berthing positions of the port and can be attributed to the increase of occurrence of extreme events from the SSW, WSW, and W sectors, which are more harmful for the port's surface tranquility.



Figure 2. Percentage difference of the weighted averaged between the results of the HISTORICAL and RCPs datasets: (a) RCP 4.5, (b) RCP 8.5.

4 CONCLUSIONS

In light of the abovementioned results, a slight decrease in the annually averaged wave agitation levels is observed for the RCP 4.5 dataset, and a slight increase for the RCP 8.5 dataset. The main cause for the increase of agitation levels for the RCP 8.5 dataset is the more frequent occurrence of extreme events from wind directions that generate waves which enter almost undisturbed in the port, hence increasing the wave height levels in the port basin. The results have strong implications on identifying accurately vulnerability elements, which will allow to determine proper adaptation actions to reduce the effects of the climate change in the passenger Port of Piraeus.

Acknowledgments

The work described in this paper has been conducted within the project ARSINOE. This project has received funding from the European Union's Horizon 2020 Innovation Action programme under Grant Agreement No. 101037424 ARSINOE.

References

- Chondros M, Metallinos A, Karambas Th, Memos C, Papadimitriou A (2021) Concerted nonlinear mild-slope wave models for enhanced simulation of coastal processes. *Appl Math Model* 91: 508-529. doi: 10.1016/j.apm.2020.08.027
- IPCC (2019) *Special Report on the Ocean and Cryosphere on a Changing Climate: Summary for Policymakers: Oceans & Cryosphere*, Cambridge University Press, Cambridge, UK and New York, NY, USA, pp. 3–35
- Papadimitriou A, Chondros M, Metallinos A, Tsoukala VK (2022) Accelerating predictions of morphological bed evolution by combining numerical modelling and Artificial Neural Networks. *J of Mar Sci and Eng* 10:1621. doi: 10.3390/jmse10111621
- Scientia Maris (2022) *Maris HMS User Guide*, Athens, Greece
- Tsoukala VK, Chondros M, Kapelonis Z, Martzikos N, Lykou A, Belibassakis K, Makropoulos Ch (2016) An integrated wave modelling framework for extreme and rare events for climate change in coastal areas – the case of Rethymno, Crete. *Oceanologia* 58: 71–89. doi: 10.1016/j.oceano.2016.01.002

Contemporary types and models of private sector involvement in ports

Chlomoudis K.¹, Tozidis M.²

¹Dept. of Maritime Studies, University of Piraeus, Grigoriou Lampraki 21, Piraeus, Athens, 18533, Greece

*Corresponding author: mtozidis@gmail.com

Abstract

A changing economic environment produced by the globalization of production and distribution, changing forms of cargo transportation, technological breakthroughs, and many more issues, ended a long period of state - controlled (public) port governance models in most countries. To adapt to the new context, many governments entered a period of port reform, changing applicable governance structures. Private sector participation in ports has been increasing continuously ever since either through privatization or, most commonly through public-private partnerships (PPP). Public authorities are embracing PPP to overcome budgetary constraints, to compensate for their lack of expertise in operations, to boost economic growth and to attract foreign direct investments (FDIs). This paper aims to discuss the reasons behind the implementation of Public-Private Partnerships as well as the various forms in which these partnerships have taken place within the port industry. A detailed analysis will be presented regarding the characteristics and applications of each PPP model with emphasis to concession agreements.

1 INTRODUCTION

Globalization of complex industrial production processes has increased the importance of seaports in the global supply chain. (Munim & Schramm, 2018). Ports are dynamic entities serving as crucial links between the local and global economies. The ownership and governance of ports have gone through profound transformations over the past decades. A port is a kind of organic system in a national socio-economic-political system as well as the globalized economic system. Therefore, port devolution and port governance would be understood in the context of structural changes of the overall systems. (Lee & Lam 2016). This does not necessarily mean that the state withdraws entirely from investing in its ports sector. Indeed, to believe so would be to misunderstand the very nature of port investment (long term payback, high capital cost, limited potential for full cost recovery, public good aspect, and wider social and economic benefits). Nevertheless, pressure to reduce the burden of port investment on the public sector has resulted in a need to bring in private sector investment; not to replace the state as such, but to bring about a partnership between the public and private sector. These partnerships have become known as Public Private Partnerships (PPP). The purpose of this paper is a presentation of the prevailing forms of private sector participation in the port industry. To that end data from two surveys from ESPO and World Bank were analyzed, and the results are presented below.

2 PUBLIC PRIVATE PARTNERSHIPS

OECD defined Public Private Partnerships (or using its acronym, PPPs) as an agreement between the government and one or more private sector partners (which may include operators and financiers) whereby private partners provide the service in such a way that the objectives for service delivery are aligned with the profitability objectives of the private sector partners and where the effectiveness of the alignment depends on an adequate transfer of risk to the private partner (OECD, 2008). PPPs have also been described as “a long-term contractual arrangement between the public and private sectors” while Van Ham and Koppenjan (2001) defined PPPs as “a partnership between public-private entities in which the cooperating entities jointly develop products and services and share the risks, costs, and resources associated with those products and services” (Garvin and Bosso, 2008). Public Private Partnerships are conducted through various forms: Design-Build-Finance-Operate-Maintain (DBFOM), Design-Build-Finance-Operate (DBFO), Design-Construct-Manage-Finance (DCMF), Concessions, Private Finance Initiative (PFI), Operations and Maintenance (O&M), Affermage, Management Contract (World Bank 2022).

3 PUBLIC PRIVATE PARTNERSHIPS IN THE PORT INDUSTRY

As PPPs in the Port Industry, we can define a Public-Private Sector relationship that includes the management and organization of ports as well as the production of the port product in such a way as to align these entities with private law and economic criteria. The result of this new public-private sector relationship should be to fairly distribute business risks to both the public and the private partner. In a survey conducted by ESPO (72 port managing bodies from 20 EU Member States and Norway) it was found that while most port managing bodies in Europe are publicly owned (compared to the last edition (2016) the share of public ownership has risen from 87% to 93%) most port services to ships (Table 1) and services to cargo (Table 2) are provided by private operators (ESPO 2022). The widespread use of the Public Owned Private Operations model (POPO) strengthens the conclusion that Public-Private Partnerships have become predominant in the global port industry.

Table 1. Provision of port services to ships

	Port managing body	Government	Private operator	Other
Pilotage outside the port area	9%	40%	49%	8%
Pilotage inside the port area	20%	29%	51%	7%
Towage outside the port area	7%	7%	92%	4%
Towage inside the port area	13%	4%	89%	1%
Mooring	35%	4%	76%	3%
Waste reception facilities	51%	1%	63%	-
Onshore power supply	69%	2%	38%	-
Bunkering	3%		94%	3%

Source: (Reshaped data from ESPO 2022)

Table 2. Provision of services to cargo

	Port managing body	Government	Private operator	Other
Cargo handling on board ship	10%	-	96%	1%
Cargo Handling ship-shore	19%	-	90%	1%
Cargo handling shore-inland transport	7%	1%	97%	1%
Logistic services	11%	-	99%	1%
Warehousing services	16%	-	94%	1%
Road haulage	1%	1%	97%	1%
Rail operation	8%	14%	91%	6%
Inland barging	3%	3%	98%	3%

Source: (Reshaped data from ESPO 2022)

Another survey that demonstrates the continuous use of PPPs is from World Bank (2021). In this survey, that was conducted in 75 countries outside the EU and North America, we see that in a period of 30 years (1991-2021) 640 Public Private Partnerships were made (World Bank 2022).

Table 3. Subtype of PPP

Subtype	Number	Percentage
Build, lease, and transfer	8	1,25%
Build, operate, and transfer	208	32,5%
Build, own, and operate	17	2,7%
Build, rehabilitate, operate, and transfer	87	13,6%
Full	11	1,7%
Lease contract	26	4,1%
Management contract	13	2,0%
Merchant	18	2,8%
Partial	26	4,1%

Rehabilitate, operate, and transfer	221	34,5%
Other	1	0,2%
Not Available	4	0,6%
Total Number of PPPs	640	100,0%

Source: (Author's elaboration using processed data from World Bank 2022)

As we can see from table 3 the vast majority of PPP are concession agreements (82,4%). In Table 4 we see that most common financial model of concession agreements are BOT (39,6%) and ROT (42,1%) schemes.

Table 4. Subtype of concession agreement

Subtype	Number	Percentage
Build, Lease, and Transfer	8	1,5%
Build, Operate, and Transfer	208	39,6%
Build, Rehabilitate, Operate, and Transfer	87	16,6%
Rehabilitate, Operate, and Transfer	221	42,1%
Total	524	100%

Source: (Processed data from World Bank 2022)

There are several financial models under which concessions can be implemented which differ depending on whether it is a greenfield development (the terminal operator is required to build the facilities and manage them) or a brownfield development (the facilities already exist, and the terminal operator is required to improve and manage them).

- Build-Operate-Transfer (BOT). In case of the BOT technique, a government or public authority grants a concession or a franchise to a private company to finance and build or modernize a specific port facility. (Notteboom 2006; Notteboom et. al. 2022)
- Build-Lease-Operate (BLO) The government or port authority leases the construction and operation of the whole port or part of it to a private company through a long-term concession. The private company constructs facilities such as berths and terminals. In turn, the port authority controls the rights throughout the concession period and receives an annual lease payment. (Notteboom 2006; Notteboom et. al. 2022)
- Rehabilitate-Operate-Transfer (ROT) The government or public authority grants a concession to a private company to finance and rehabilitate or modernize a specific terminal or an entire port. (Notteboom 2006; Notteboom et. al. 2022)
- Build-Rehabilitate-Operate-Transfer (BROT) The government or public authority grants a concession to a private company to finance, build, and rehabilitate or modernize a specific terminal or an entire port. (Notteboom 2006; Notteboom et. al. 2022)
- Build-Operate-Share-Transfer (BOST) BOST is similar to BOT, when a government grants a concession or a franchise to a private company to finance and build or modernize a specific port/terminal for a designated period of time. The revenue obtained from terminal operations is shared with a designated public authority throughout the concession period. (Notteboom 2006; Notteboom et. al. 2022)

Table 5. Segment of PPP

Segment	Number	Percentage
Channel Dredging	7	1,1%
Channel Dredging and terminal	40	6,3%
Freight and passenger, Terminal	1	0,2%
Terminal	585	91,4%
Other	5	0,8%
Not Available	2	0,3%

Total	640	100%
-------	-----	------

Source: (Processed data from World Bank 2022)

In Table 5 we see that 91,4 % of the PPPs regarded terminals while in Table 6 we see that the most common form of terminal PPPs are concessions (83,9%). The most common financial model of terminal concession agreements is BOT (42,3%) and ROT (38,2%) schemes.

Table 6. Terminal PPP

Subtype	Number	Percentage
Build, lease, and transfer	8	1,3%
Build, operate, and transfer	208	35,5%
Build, own, and operate	14	2,3%
Build, rehabilitate, operate, and transfer	87	14,8%
Full	11	1,8%
Lease Contract	26	4,4%
Management Contract	13	2,2%
Merchant	15	2,5%
Partial	21	3,5%
Rehabilitate, operate, and transfer	188	32,1%
Not Available	4	0,6%
Total	585	100%

4. Concession Agreements

As evident from the above reports the most common form of PPP in the port industry are terminal concessions a finding that agrees with the existing literature. In a terminal concession, a concession contract is signed between, on the one hand, a private terminal operator and, on the other hand, a port authority owner, or an authorized government body. The government or a public authority holds the ownership rights to the facilities throughout the concession period and receives lease payments for the assets. The concession/lease fees paid by the private terminal operator are used to upgrade and expand the facility. (Notteboom et. al., 2022) The most adopted terminal concession model is the landlord model in which private operators can manage port activities at their own terminals operating under a concession contract, a policy tool that allows the Port Authority to organize and regulate the port without directly interfering in commercial operations. In the owner model the PA has only a planning and management task. (Verhoeven, 2011 and Ferrari et. al. 2015) Moreover, the landlord PA has the power to conclude contracts (including concession contracts), impose standards and enforce rules and regulations in the port area. Port operations are carried out by private companies (especially cargo handling). (Notteboom et. al. 2022) Notable examples of landlord ports can be found in Europe (Italy, France, Spain, Belgium, Germany, the Netherlands), South America (Argentina, Brazil, Chile, Colombia) and USA (17 ports including New York and New Jersey, Los Angeles, and Long Beach). (USA Environmental Protection Agency 2022, Laxe et. al. 2016, Ferrari et. al. 2015) Although the basic principles remain the same landlord ports have different organizational structures depending on each country's legislation. This is evident from a survey conducted in the landlord ports of Southern Europe. Although the Port Authority status was the same (own legal entity) and the fees were autonomous different decision-making bodies and partnership models were formed. (Laxe et. al. 2016) Ferrari et. al. (2015) divided the European landlord ports in two groups (Southern Europe "Latin Tradition" and Northern Europe "Hanseatic Tradition"). According to their research southern Europe ports faced rigidity and bureaucracy problems while northern Europe ports although they were more flexible faced a possibility of having a "limited vision for the local development". (Ferrari et. al. 2015) This paper shows the importance of concession contracts which becomes even greater due to the multiple current crises (climate, energy, food, geopolitical tensions affecting world trade). Consequently, the content of the concession contracts should be enriched to cover the new needs that arise and must be covered so that the ports continue to be "engines of growth" for the local, regional, and national economy.

References

- European Sea-Ports Organization (ESPO, 2022) Trends in EU ports governance.
- Ferrari C, Parola F, Tei A (2015) Governance models and port concessions in Europe: Commonalities, critical issues, and policy perspectives. *Transp. Policy*, Vol. 41, 60-67, 10.1016/j.tranpol.2015.03.012
- Garvin M, Bosso D (2008) Assessing the Effectiveness of Infrastructure Public—Private Partnership Programs and Projects. *Public Works Manag. Policy*, Vol. 13(2), 162-178, 10.1177/1087724X08323845
- González Laxe F, Sánchez RJ, Garcia-Alonso L (2016) The adaptation process in port governance: the case of the Latin countries in South America and Europe. *J. Shipp. Trd*, Vol. 1(1). 10.1186/s41072-016-0018-y
- Lee P, T-W Lam, J S-L (2016) A review of port devolution and governance models with compound eyes approach. *Transp Rev.*, Vol. 37(4), 507–520. doi.org/10.1057/9781137514233_8
- Munim ZH, Schramm H-J (2018) The impacts of port infrastructure and logistics performance on economic growth: the mediating role of seaborne trade. *J Shipp Trd*, Vol. 3(1). doi.org/10.1186/s41072-018-0027-0
- Notteboom T, A Pallis, J-P Rodrigue (2022) *Port Economics, Management and Policy*. New York: Routledge.
- Notteboom T (2006) Concession Agreements as Port Governance Tools in Devolution. *Port Governance and Port Performance Research in Transportation Economics*, Vol. 17, 437–455.
- Organisation for Economic Co-Operation and Development (OECD, 2008) *Competition Policy and Concessions, Policy Brief*.
- USA Environmental Protection Agency (2022)
- Verhoeven P (2011) European Port Governance ‘The ESPO Fact-Finding Report’. ESPO 2011 Conference, Limassol, Cyprus.
- World Bank (2022) *Private Participation in Infrastructure (PPI) Database*, World Bank, 2022.

Smart and green ports

P.I. Boudouris^{1*}

¹Port of Ios, National & Kapodistrian University of Athens

*Corresponding author: panagiotis_mu@hotmail.com,

Abstract

The rapid growth of world trade and the progress of digitization have led to the need for more complex infrastructures to support the increased amount of cargo and the adaptation of logistical support to the new data. At the same time, tackling climate change is one of the most important challenges the global community is facing today, and ports, which are major sources of pollution, must contribute to the protection of the environment. In this regard, smart ports, through the use of technological innovations in order to enhance port activities and services, aim to increase the competitiveness and economic viability of an area, while, at the same time, contribute to the reduction of greenhouse gas emissions and energy consumption.

The purpose of the present paper is to present the principles on which the construction and operation of a smart and green port should be based, as well as ways to make the port industry more environmentally friendly.

Keywords Ports, Smart ports, Green ports, Environment.

1 INTRODUCTION

According to a widespread definition, a port is considered as “a gateway through which goods and passengers are transported by ships to and from the land” (Goss, 1990). Ports are pillars of the economic and social development of regions and countries worldwide. They are the key points of transition from one mode of transport to another and are of vital importance to the flow of international trade. In today's globalized environment, the port industry faces constant challenges, arising from social, economic, and technological developments, in order to ensure the possibility of maintaining a competitive advantage in the market. Structural changes in trade patterns, natural disasters and terrorist attacks combined with the pursuit of environmental protection and sustainable development, as well as the rapid development of information and communication technology have led to the need to modernize port infrastructure and operations.

In this context, emerged the concept of smart and green ports. Smart ports depend on the use of new technologies to improve the overall efficiency and competitiveness of their operations, while green ports have low energy consumption and pollution reduction as their main objective. Green development, flexibility, personalization, collaboration, intelligence and liberalization are the key aspects of the development of a smart and green port.

In general, the two concepts are complementary, since on the one hand green development is an important aspect of a smart port and on the other hand the application of technological innovations of a smart port is the key means to achieve the goal of a green port. The mutual development of the two concepts contributes to the enhancement of the competitiveness between ports and the achievement of sustainable development.

1.1 Importance of a Port

The easy access offered by the seas and oceans combined with the economic and energy efficiency of shipping have made ports a hub for trade (Alexandersson & Norström, 1963), while at the same time they are vital points to the connection between sea and land transport (COM, 1997). According to the European Commission, 80% of the world trade is carried out by sea (COM, 2009).

In addition, port activities contribute directly to the increase in employment, the attraction of new investments and the increase in GDP. At the same time, ports and port facilities form the basis for multiple economic activities (maintenance and exploitation of marine infrastructure, exploitation of

ships and their services, land transport, logistics services, cargo services, etc.), contributing even more to the economic development and social welfare at local and supra-local level.

2 EVOLUTION OF PORTS: PORT GENERATIONS

Several attempts have been made in the literature to classify ports into typologies and analyze their role and functions, without however a commonly accepted framework, due to the complexity and heterogeneity of ports. In 1992, the first systematic attempt to categorize ports is made at the United Nations Conference on Trade and Development (UNCTAD) in Genoa. It is a comprehensive approach to the characteristics and evolution of the port industry that led to the classification of different types of ports into categories called "Port Generations".

The UNCTAD approach was based on the fact that certain dominant characteristics of ports could be associated with distinct time periods, resulting in the distinction of ports into three port generations. Over the years, globalization and continuous changes at social, economic and political level created a highly competitive environment, characterized by high levels of uncertainty. The need to adapt to this new environment led port authorities and administrations to adopt a new logistics approach based on agility. At the same time, the formation of port networks allowed ports to improve their competitive advantage in the global economic market. Thus, in 1999, UNCTAD proposed the arrival of the fourth generation port (Paixão & Marlow, 2003).

In the modern environment, where the port industry sector faces continuous challenges, such as structural changes in the trade pattern, natural disasters, terrorist attacks etc., while at the same time the pursuit of environmental protection and sustainable development and the rapid development of information technology dominate (Lee et al., 2018), the framework of the four port generations is not sufficient to reflect the functions of ports required by the needs of their users and the community (Flynn et al., 2011). The fifth generation ports integrate the service functions of the ports of the previous four generations, while, at the same time, adapting to the innovative trend of smart and green technology, emphasizing in the integration of advanced IT and telecommunication technology systems and environmental protection (Chen et al., 2019).

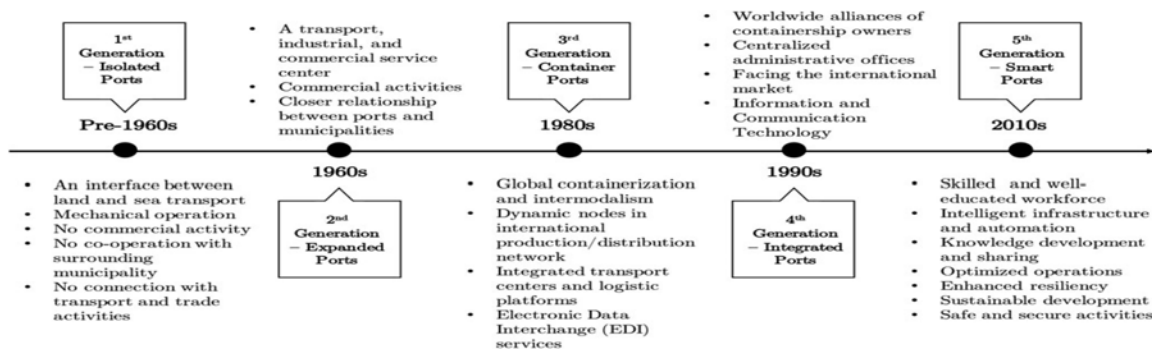


Figure 1. Evolution of ports over the years (Molavi et al., 2020)

3 SMART PORTS

A smart port, as part of a smart city, aims to use technological innovations to enhance port activities and services and provide a socio-economic boost to cities and regions with improved international trade competitiveness, while minimizing energy consumption and traffic. Moreover, a smart port brings together specialized and highly trained personnel, smart infrastructure, and automation, aiming to facilitate the development and exchange of knowledge, optimize port operations, strengthen its resilience, achieve sustainable development and ensure safe operations (Molavi, Lim, & Race, 2020).

In other words, a smart port achieves results without creating new challenges internally or elsewhere in the supply chain ecosystem, minimizes the negative impact of its activities on the natural environment and strengthens surrounding communities economically and socially. The benefits of the new technologies allow a smart port to:

- improve its efficiency in order to gain a competitive advantage,
- increase its resilience to economic shocks or disruptive forces,
- achieve maximum value extraction from physical assets,
- develop new revenue streams based on digital value propositions,
- increase employee engagement and well-being,
- achieve its environmental commitments.

2.1 Digital Technologies

The rapid development of technology has significantly contributed to the formation of the modern environment. The development of advanced information and communication technologies and automated systems provides significant advantages in all stages of the production and trading of goods, as well as an important tool for managing issues related to environmental protection, energy management and safety of ships, workers and all stakeholders in a modern port.

Smart ports are designed to operate with full use of smart technologies and automations. Big Data and Blockchain technologies, Artificial Intelligence, the Internet of Things and 5G networks are main pillars for the development and operation of a smart port.

3 GREEN PORTS

A green port is a port of sustainable development, which not only meets environmental requirements, but also brings significant economic benefits. The economic and social development of ports should not exceed the carrying capacity of the corresponding natural system. Therefore, the essence of creating a green port consists in the existence of balance between the environmental and economic effects resulting from its operation (Anastasopoulos, Kolios, & Stylios, 2011). The main objective of a green port is to achieve economic efficiency and environmental protection in the port complex and to ensure the leading position of the port in the modern market environment (Shao et al., 2009).

The concept of a green port essentially consists of the integration of environmentally friendly activities, operations and management, aiming at the efficient use of resources to reduce negative impacts, raise the level of management and improve the quality of the natural environment of the port area. The adoption of environmental legislation and policies that promote environmental protection, especially in the port and marine areas that are more exposed to pollution risks from shipping and navigation, the enforcement of policies to reduce gas emissions, the appropriate design of the port landscape to include trees that contribute to the absorption of noise and the reduction of pollution, the use of renewable energy sources and the enforcement of sustainable practices (e.g. recycle and reuse of materials) are essential measures that should be taken in order to create a green port.

3.1 Energy management

In recent years, energy consumption has been one of the main issues that preoccupy port administrations. By taking actions to improve energy efficiency, minimize energy consumption and save resources, significant financial benefits can be obtained, and, at the same time, the environmental footprint of ports can be reduced. In this direction, a wide range of technological solutions and operational measures addressing different processes have been implemented to further improve the current energy efficiency

of ports.

On the one hand, the use of different forms of energy, such as renewable energy sources (wind energy, solar energy and different forms of energy of the oceans – e.g. wave and tidal energy), Cold ironing systems and alternative fuels (LNG, biofuels, methanol, hydrogen and low-sulphur fuels), should be considered so as to reduce the environmental burden caused from the power and fuel currently used in ports (Bjerkkan & Seter, 2021). On the other hand, in terms of maritime activities, reducing the speed of ships during their approach and minimizing the waiting time in the port can contribute to the improvement of the port's energy efficiency.

At international level, a number of measures have been established by the IMO to limit SO_x and NO_x emissions from ships, such as:

- Drafting of regulations, for example the MARPOL 73/78 Convention.
- Designation of Emission Control Areas (ECAs) in cooperation with national governments, mainly in the Baltic and North Seas, as well as around the Atlantic and Pacific coasts.
- Establishment in 2013 of the Energy Efficiency Design Index (EEDI) and the Ship Energy Efficiency Management Plan (SEEMP) for CO₂ emissions for ships over 400 tons.

In conclusion, the promotion of technologies and environmental practices contributes to the increase of the competitiveness of the port, while, at the same time, has a positive impact on the local and regional community.

4 SUGGESTIONS

In the coming years, seaports will have to be able to face several challenges in order to remain competitive. Globalization, the increasing demand for goods, the ever-increasing volume of ships and goods and the proper use of energy resources are some of the issues that port authorities should be able to deal with. The transition to a “smart and green port” model, with the application of digital technologies and green policies in all infrastructure and operations within the port, is now necessary for all ports worldwide.

Greece, a country that has several ports of various sizes, should not be an exception. Despite the fact that is the main gateway for people and goods to south-eastern Europe and the eastern Mediterranean, the Greek ports are quite behind in smart systems and green development practices. In this regard, the following interventions could be applied in the Greek ports, in order to become competitive in the European and the global shipping industry.

- Elaboration of studies a full costing for the installation of the necessary smart systems in all Greek ports, for the better planning of the central government in finding financial resources and tools.
- Immediate installation of an early warning system for extreme weather events in all port facilities.
- Equipment with modern marine pollution risk assessment systems.
- Shift to digital innovation using technologies, such as artificial intelligence, big data and blockchain.
- Training the human resources of ports in the new digital technologies.
- Formation of the necessary conditions so that all Greek ports gradually receive EMAS or ISO 14001 certification for their proper environmental management.
- Drawing up plans to deal with marine pollution and waste management in all ports, in order to be able to implement the existing legislations.
- Drawing up plans to monitor and improve air quality inside and outside ports, with the installation of air pollution monitoring, sampling and reporting stations.
- Establishment of policies for the sustainable development of ports.
- Better connection with other means of transport, especially with the railway network, for the channeling of containers both in our country and others.
- Establishment of a scientific research group for the preparation of a study on alternative marine fuels.
- Construction of infrastructure for the supply of electricity from land (Cold Ironing) and facilities for alternative fuel supply (hydrogen).

- Installation of solar panels on land facilities and wind turbines in unused port areas (e.g., breakwaters) in order to cover part of the port's energy needs.

5 CONCLUSIONS

Ports have always played a pivotal role in societies, providing them with many social and economic benefits. In recent years, the port industry has faced continuous changes due to social, economic and technological developments in the modern globalized environment. This fact has led to the need to modernize port infrastructure and operations in order to ensure their ability to maintain a competitive edge in the market. In this direction, port administrations are turning to the adoption of new methods to ensure economic efficiency and, at the same time, protection of the environment.

Several ports worldwide have turned to smart technologies, in order to become more efficient in the global shipping industry. In addition, the need for environmental protection and sustainable development are an immediate priority for the port industry in order to deal with the climate change and the energy crisis that takes place on a global scale.

Greece is a country with many ports of various sizes that is a commercial crossroad in the Mediterranean, yet Greek ports are far behind in the use of smart technologies and environmental protection. However, the location and geophysical wealth of our country are important advantages that could make Greek ports important transport, trade and energy hubs. In order for this to happen, the adoption of appropriate policies and actions and the active participation of all stakeholders is considered necessary for a smooth transition to the new era with main focus on environmental protection.

References

- Alexandersson, G., & Norström, G. (1963). *World Shipping: an Economic Geography of Ports and Seaborne Trade*. New York: John Wiley and Sons.
- Anastasopoulos, D., Kolios, S., & Stylios, C. (2011). How will Greek ports become Green ports? *Geo-Eco-Marina*, 17, 73-80.
- Bjerkan, K. Y., & Seter, H. (2021). Policy and politics in energy transitions. A case study on shore power in Oslo. *Energy Policy*, 153.
- Chen, J., Huang, T., Xie, X., Lee, P., & Hua, C. (2019). Constructing Governance Framework of a Green and Smart Port. *Journal of Marine Science and Engineering*, 7(4).
- COM (1997). *Green Paper on seaports and shipping infrastructure*. Brussels: COM/97/0678 final, 10.12.1997.
- COM (2009). *Communication from the Commission to the European Parliament, the Council, the European Economic and Social Committee and the Committee of the Regions - Strategic objectives and policy recommendations for EU maritime transport until 2018*. Brussels: COM/2009/0008 final, 21.1.2009.
- Flynn, M., Lee, P., & Notteboom, T. (2011). The next step on the port generations ladder: customer centric and community ports. In *Current Issues in Shipping, Ports and Logistics* (pp. 497-510) University Press Antwerp.
- Goss, R. (1990). Economic Policies and Seaports. *Maritime Policy and Management*, 7(4), p. 257-271.
- Lee, P., Lam, J., Lin, C., Hu, K., & Cheong, I. (2018). Developing the fifth generation port concept model: an empirical test. *The International Journal of Logistics Management*, 39(3), pp. 1098-1120.
- Molavi, A., Lim, G., & Race, B. (2020). A framework for building a smart port and smart port index. *International Journal of Sustainable Transportation*, 14(9), 686-700.
- Paixão, A. C., & Marlow, P. B. (2003). Fourth Generation Ports - a question of agility? *International Journal of Physical Distribution & Logistics Management*, 33(4), 355-376.
- Shao, C. F., Ju, M. T., Yu, J. L., Hu, C. H., & Chu, C. L. (2009). The strategies and proposals for ecological port construction in China. *Journal US-China Public Administration*, 6(7).

Piraeus Port Authority S.A. and Thessaloniki Port Authority S.A. before & after the privatization

M. Voudigaris¹, Th. Giantsi^{2*}

¹Department of Business Administration, UNIWA, 250 Thivon & P. Ralli Str, Egaleo, Attica, Greece

²²Laboratory of Harbour Works, NTUA, Iron Polytechniou 5, Zografou, 15780, Attica, Greece

*Corresponding author: dgiantsi@central.ntua.gr

Abstract

The two biggest Greek Ports of Piraeus and Thessaloniki, managed by Piraeus Port Authority S.A. (PPA) and Thessaloniki Port Authority S.A. (ThPA) respectively, were privatized by transferring the majority of their shares to private companies. The procedure was undertaken and accomplished by The Hellenic Republic Asset Development Fund S.A. (HRADF). The Concession Agreement between the Greek State and Piraeus Port Authority entered into force the 10.08.2016, and Concession Agreement between the Greek State and Thessaloniki Port Authority entered into force the 22.3.2018. Both concessions had a mandatory investment plan. In the present paper were analysed volumes, revenues, and investments from both ports before and after the privatization and calculated indicators to estimate their performance. The analysis shows that sectors where the investments are directed have a better performance. As it concerns Piraeus Port, after the completion of Pier III the throughput of the container Terminal has an incredible increase, but that is not represented at the revenues. As it concerns the Port of Thessaloniki, although the investment plan is not yet completed, the performance is better, especially in the revenues.

Keywords Port Authority, Privatization, Concession Agreement, Port performance.

1 INTRODUCTION

At the end of 20th century most European Port Authorities remained publicly owned (Van Hooydonk, 2003). Later new forms appeared introducing private capital to the ports, and the landlord model can be considered as the principal function of contemporary port authorities (ESPO, 2010). In order to ameliorate the performance of their report system, port reforms were undertaken in several countries. We mention the Port Reform in France (Lacoste R. and Douet M., 2010), and the Port Reform in Italy (Ferrari et al, 2015; Parola, 2016).

In Greece also a reform was conducted during the beginning of the 21st century. In 2001-2002 the managing bodies of the two Ports became Public Limited companies (S.A.) and their shares are traded on the stock exchange with a target to become from "tool Port to Landlord Port" (PPIAF, 2007) The Concession Agreement (C.A) of Piers II and III with Cosco Pacific Ltd and PPA entered into force on 1/10/2009. Cosco Pacific Ltd will operate Pier II and will construct and operate Pier III of Piraeus Port. In 2016 under a new form of C.A. was introduced in the Greek governance system of Port by transmitting the majority of the shares and the management of the port to the beneficiary The new Concession Agreement between the Greek State and PPA included the process of a majority stake (51%) transferred to COSCO SHIPPING (HONG KONG) Limited) which was completed successfully on 10.08.2016 with a mandatory investment plan of 293.783.800 € in the first period of 5 years. An additional 16% of shares were transferred to Cosco in 2021.

The Concession Agreement between the Greek State and ThPA included the process of a majority stake (67%) transferred to «South Europe Gateway Thessaloniki (SEGT) Ltd» which was completed successfully on 22.3.2018 with a mandatory investment plan of 180.000.000 € for the first 5 years including infrastructure and equipment. Investments in equipment are in progress and the extension of Pier 6 is scheduled. In 2020 ThPA established a subsidiary dry port based in Sofia, Bulgaria, named "ThPA Sofia Ead".

For both ports, the concession fee was set as a percentage of the total consolidated revenue of each Company at 3.5%.

For the purpose of this paper statistical data from both ports were collected and analyzed. PPA revenues are from: Coastal shipping, Cruise, Car terminal, Ship Repair, Containers (Pier I), Concession (Piers II and III), and secondary sectors. Revenues for ThPA are from Containers, Coastal Shipping and Cruise, General Cargo, and land rentals.

2 DATA ANALYSIS

In the current section, the investments the revenues and the selected volumes are analyzed in order to determine the economic growth of each company and the added value of container operation especially as it is the main function of the ports.

2.1 The investment plans

The mandatory investment plan of P.P.A was of 293.783.800 € in the first period of 5 years. In this analysis is not included the mandatory investment of the first concession between PPA and Cosco, where the construction of Pier III was the main investment, which finished in 2018 with the completion of the western quay wall. We have to mention the delay observed at the construction of the cruise terminal, caused mainly by legal/administrative issues from the Greek State. The Thessaloniki's mandatory investment plan of 180.000.000 € started later. During some years that concerns only equipment, and the expansion of Pier 6 is associated with other, external to port infrastructure (of the train). Figure 1 presents from 2017-2022 from both Ports Authorities, (PPA, 2023), (ThPA, 2023), and Figure 2 presents the cumulative investment evolution for the port of Piraeus (PPA, 2023).

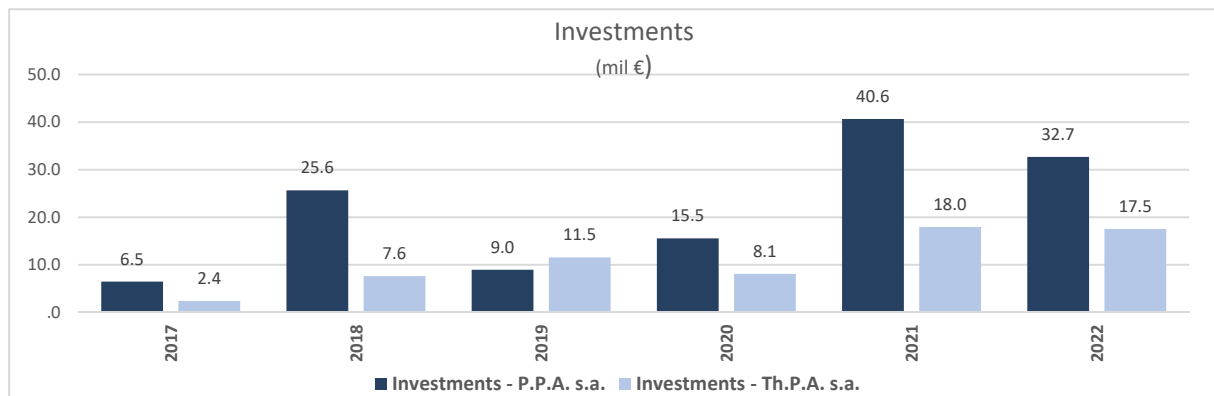


Figure 10. PPA & ThPA investments (mil €) 2017-2022, source: companies' annual financial statements

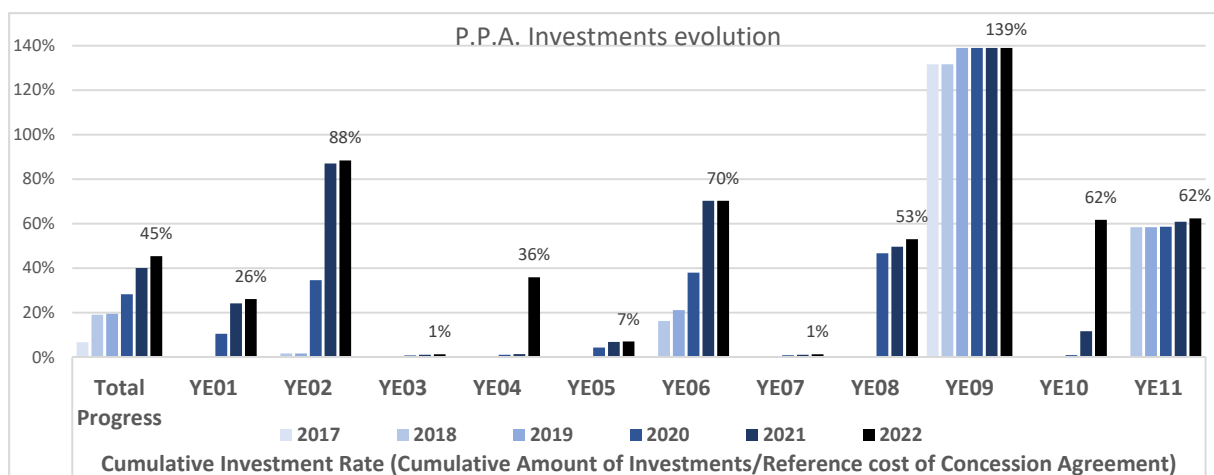


Figure 11. PPA cumulative investment rate evolution 2017-2022 (YE01: Cruise expansion, YE02: Pier I repair, YE03: Cruise passenger terminal, YE04: Logistics - Car terminal link, YE05: Maintenance & repairs of port infrastructure, YE06: Equipment, YE07: Central port dredging, YE08: Studies, YE09: Liquid bulk terminal, YE10: Car terminal expansion Irakleous, YE11: Ship repair infrastructure), source: companies' annual financial statements

2.2 Revenues

PPA's total revenues up to 2021 never overpassed the 171,35 mil € (2007 revenues). Although this changed last year (2022), when PPA announced 194,58 mil € total revenues. The revenues' compound annual growth rate (cagr) for the 15 years period (2007-2021) is -0,7012%. Additionally, the revenues' cagr for the period 2007-2022 (16 years) is 0,7975%, due to the last's year 26,19% revenue annual growth (2021-2022). Respectively, the revenues' compound growth rate for the period 2003-2007 (5 years) is 3,77%. The ThPA's revenues cagr for the period 2003-2007 was 10,50% a lot higher referred to 2007-2021 period (0,9943%). Figure 3 presents total revenues from PPA, PCT, ThPA respectively.

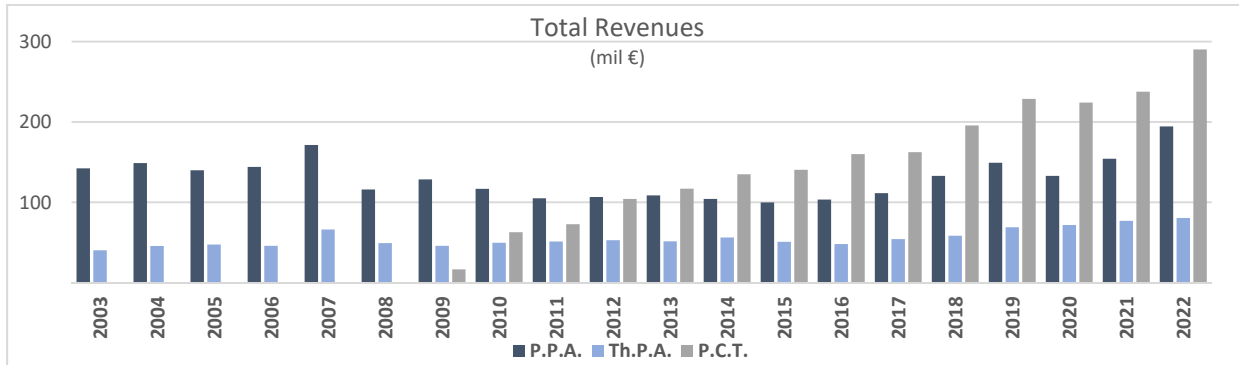


Figure 12. PPA, PCT & ThPA total revenues (mil €) 2003-2022, source: companies' annual financial statements

The dynamic five years growth of the two companies (2003-2007) could allow them to resist better to the economic crisis of Greece during the period 2010 to 2015, but the duration of the privatization process, which lasted 8+ years (from 2007- to 2016 & 2017), policies and the selected PPP model, didn't let them grow; Instead, the two companies' revenues growth was negative for many years after 2007. For both ports, the more effective sector is the container terminals.

2.3 Traffic measures: throughput

In this paragraph, the annual throughput, and the throughput as a share of the global throughput of each company were analyzed (for PPA the throughput was calculated as a summary of PPA & Piraeus Container Terminal s.a.-PCT- container throughput - as Piraeus) (see Figures 4 and 5).

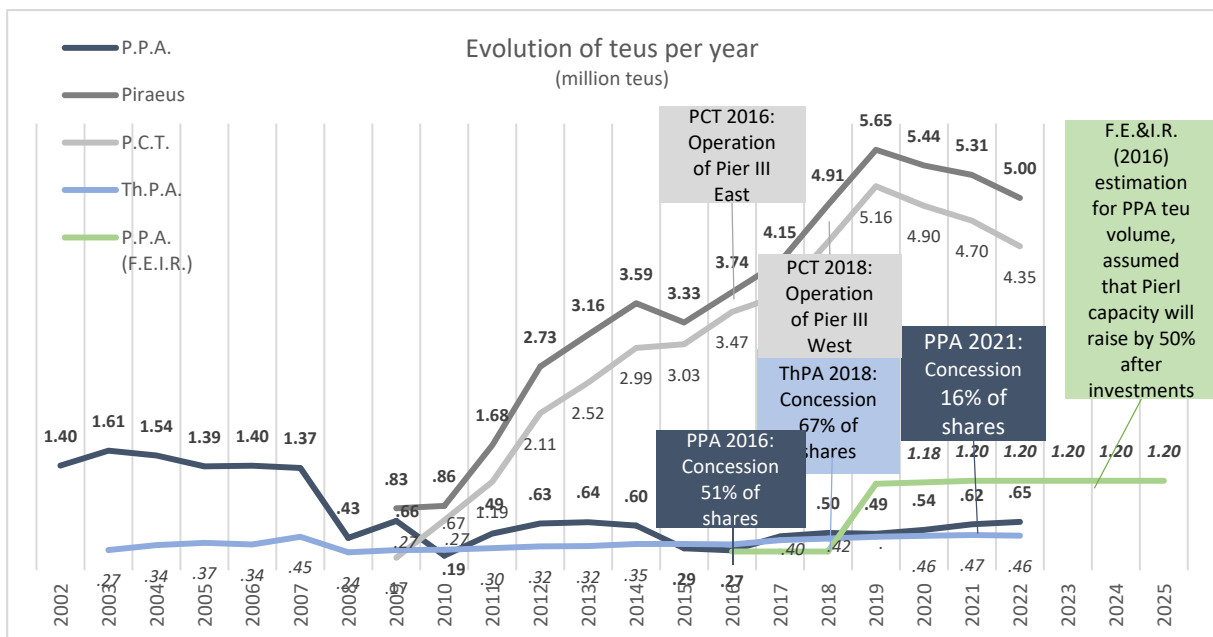


Figure 4. Port of Piraeus, PCT, PPA & ThPA container throughput teus per year (2002-2022, source: companies' annual financial statements, Cosco Ports, Foundation for Economic & Industrial Research (F.E.&I.R.) authors

The lack of investments in both companies, the privatization’s duration process, the PPP model selected, the economic crisis, and the smaller capacity Pier I container terminal of PPA, caused a significant decrease in throughput in PPA after 2008. ThPA also lost almost 50% of the throughput in 2008, after the unions of both companies’ dynamic reaction to the privatization policy, for the years after 2008 and up to 2016. The lack of train network in Greece also affects the hinterland transport chains (Van der Horst, M. and De Langen, P., 2007)

So, this decrease in both companies’ throughput, needs many factors to be considered. The result was PCT took a huge advantage, as she had the tension, capital & flexibility to invest and the bigger container terminal (Piraeus Pier II) in the country. In this race, it was obvious who will be the leader since then.

PPA operating in Pier I since 2010, achieved 0.63 & 0,64 mil teus throughput in 2012 & 2013, which was the best after the concession of Pier II container terminal, up to 2022 (0,65 mil teus). The best year was 2019.

ThPA had a throughput cagr of 5% since 2008 (up to 2021) and overpassed the throughput of 2007 (0,45 mil) in 2020 (0,46 mil teus). Although the throughput’s growth for the period 2007-2021 is only 0,3% per year.

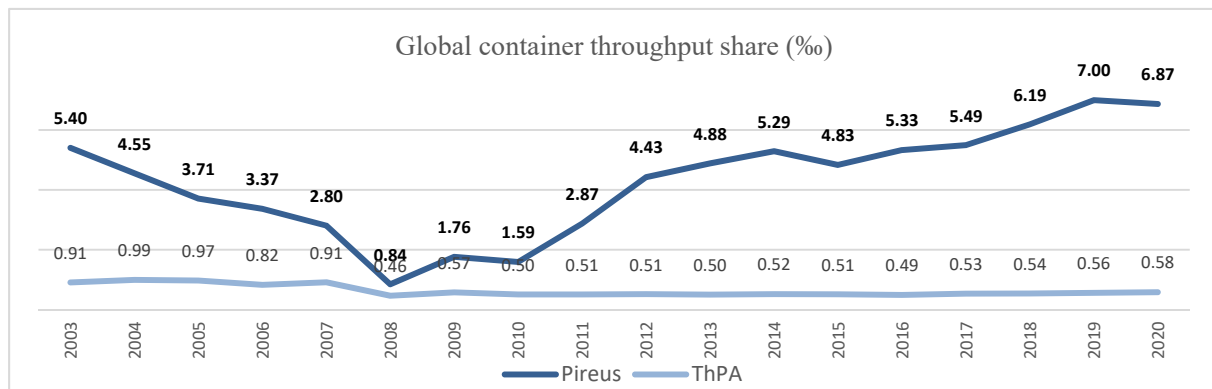


Figure 5. PPA & ThPA container throughput global share per year, source: companies’ annual financial statements, authors, World bank

The global throughput cagr 2003-2020 is 5,6%. The global port throughput was valued at about 300 mil teus in 2003; This value raised up to about 810 mil teus in 2019, before covid crisis. In 2020 the global throughput was about 792 mil TEUs. The share of Piraeus container terminals in 2003 was 5,40 teus per mille. This share was decreasing during the years up to 2008 and reached the same share in 2017 which was the year of the operational start for the east Pier III of the container terminal and after the PCT’s investments. Additionally, the share of ThPA kept steady up to 2007, due to the regional role of the port and decreased in 2008. Since then, the share cagr is 1,78% up to 2020; Lower than the global throughput growth, caused by many factors contained and the lack of investments. For a container terminal, a way to keep a steady or raising global share is to invest in container terminal: technology, machinery, and space, as much as the global throughput raises.

3 RESULTS

To compare the effectiveness of the three companies PPA, PCT, and ThPA, the revenue per TEU was calculated and presented in Figure 6. From Figure 6 it is obvious that the two ports have different tariff policies over time, on par contrary PPA and PCT have almost the same tariff policy. ThPA had higher tariffs than PPA even before the privatization and increased the tariffs (from 90 €/TEU in 2018 to 115 €/TEU in 2022) after the privatization. PPA and PCT are about 50% cheaper than ThPA and only in the last year 2022 PPA presents an increase (from 44 €/TEU in 2017 to 63€/TEU in 2022) the container handling fees. For that reason, this year is the first year that the PPA revenues are higher than the revenues of 2007 even with a decrease in volumes from 2022 to 2021 (for all port’s container terminals). Although the revenue also depends, from the type of cargo (import, transit, or transshipment).

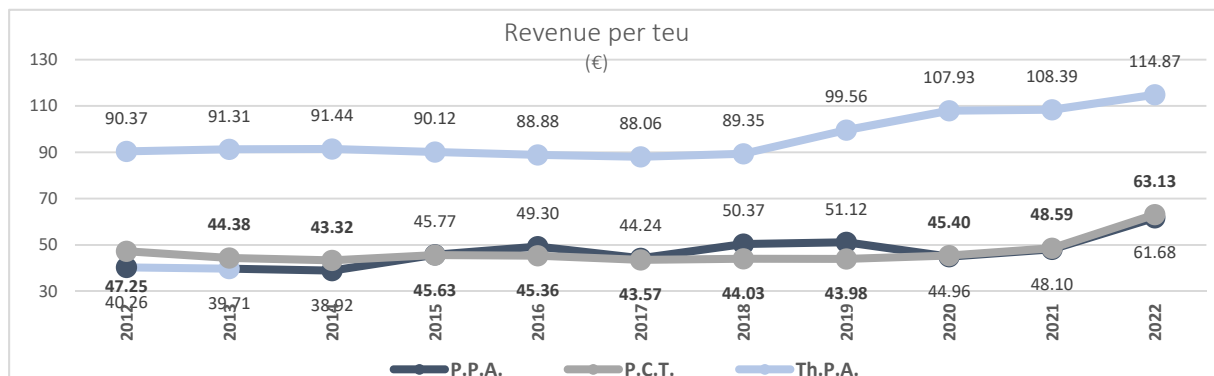


Figure 6. PPA, PCT & ThPA revenue per teu per year, source: companies' annual financial statements, authors

4 CONCLUSION

In this paper is presented the performance of PPA, PCT and ThPA in the container sector. Further analysis is needed at the other sectors like cruise, ship repair, etc. in order to achieve the correct conclusion about the performance of the ports.

Investments are essential for the growth of the ports, but also the correct tariff policy is necessary in order to obtain the maximum gain.

At Piraeus Port the significant growth during the last years is the result of the construction and utilization of Pier III by PCT, which makes Piraeus Port the biggest Greek Port. Thessaloniki Port has a better tariff policy that maximizes the benefits, not only for the company but for the society also.

References

- ESPO, (2010), European Port Governance, REPORT OF AN ENQUIRY INTO THE CURRENT GOVERNANCE OF EUROPEAN SEAPORTS
- Ferrari C., Tei A. and O. Merk O.,(2015), The Governance and Regulation of Ports. The Case of Italy , Discussion Paper 2015-01 OECD,
- Lacoste R. and Douet M., (2010), «The French ports reform of 2008», proceedings of WCTR Lisbon July 11-15, 2010
- Parola F., (2016) Italy reframes its port governance. PortEconomics.eu
- Piraeus Port Authority s.a., (2023), Financial statements 2002-2023 - <https://olp.gr>
- Piraeus Container Terminal s.a., (2023), Financial statements 2009-2022 - <https://thpa.gr>
- PPIAF. World Bank (2007) Framework for port reform. In: Port Reform Toolkit, Module 1– second edition, World Bank,1818 H Street NW, Washington, DC 20433, USA, fax 202-522-2422, e-mail pubrights@worldbank.org, p 1-20
- Thessaloniki Port Authority s.a., (2023), Financial statements (2003-2022) - <https://thpa.gr>
- Vaggelas, G.K. & .Pallis A.A. (ed.) (2023), P&S Advisory, – Report on Greek Ports, Piraeus
- Van der Horst, M. and De Langen, P. (2007), Coordination in hinterland transport chains: a major challenge for the seaport community, Proceedings of the 2007 IAME Conference, Athens
- Van Hooydonk, E. (2003), The regime of port authorities under European law (including an analysis of the port services directive), in Van Hooydonk, E. (ed), European seaports law: EU law of ports and port services and the ports package, Maklu, Antwerpen / Apeldoorn, 79-186.
- World Bank (2023) - UINCTAD Statistics. <https://data.worldbank.org/indicator/IS.SHP.GOOD.TU>. Accessed 03 Apr 2023

Revisiting port regulatory governance & substance: Towards a holistic supply chain approach

C. Chlomoudis¹, P. Pallis^{1*}, T. Styliadis¹

¹Department of Maritime Studies, University of Piraeus, Gr. Lampraki 21 & Distomou, Piraeus, Greece

*Corresponding author: ppallis@unipi.gr

Abstract

The evolution and integration of ports in global logistics chains has altered their traditional role while has initiated restructuring processes in many ports worldwide. While most of the research addresses this issue by highlighting the need for re-positioning and redefining the role of the port within the supply chains, not much attention has been given to the structure, scope and reach as well as to the tools of regulation that competent authorities could exploit in order to avert potential abusive actions of global powerful actors along the containerized transport chain, that would affect the competitive functioning of distinct segment or the integrity of supply chains. In this context, we propose the reconceptualization and reinforcement of the regulatory governance structures of ports on a national and international level as well as the extension of the scope of ports' regulations along the supply chain to counterbalance the globalization, consolidation, and integration of containerized transport actors.

Keywords Ports, Concentration, Supply chain integration, Regulation.

1 INTRODUCTION

In the context of globalization and of dispersed production and consumption, modern maritime transport along with ports are the backbones of international trade, as well as a key contributing factors in the economic growth and development of countries around the globe. To adapt to the novel characteristics of the industry (containerization, lack of public funds etc.), liberalization of the port industry and introduction of competition was promoted as the solution which would allow more integration along the transport chain and would render the production of the port product and services more efficient and more effective.

The port devolution wave that followed on a global scale (Baltazar and Brooks, 2001), through various privatization schemes led eventually on the one hand to the establishment of various novel port governance models while on the other to the shift of power from the public to the private sector. While ports became prominent fields of private investment, port managing bodies, i.e., port authorities in the majority of occasions remained public, however their functions as well as their roles within the port were reconfigured (Verhoeven, 2010).

The globalization of players within the port industry and the concentration of more and more terminals in the investment portfolios of a handful of operators, as well as the interconnection of the latter through subsidiaries, both with liner carriers as well as with companies providing hinterland and value-added services (Notteboom and Rodrigue, 2012), brought about a reorganization of the port services market while reshaped the relations and integration amongst the members of the supply chain (Van de Voorde and Vanelander, 2010). More particularly, such evolutions have led to the formulation of an intricate market environment of robust inter-firm relationships (Parola et al., 2014) where the boundaries of competition and cooperation, amongst market players, are very often blurred.

Especially, while these organizational developments did not initiate the necessary changes to upgrade the regulatory framework within which ports and in extension supply chains operate, they have rendered the existing framework rather ineffective and outdated. As such, it has been increasingly challenging and difficult for port regulatory agents (either Port Authorities or Independent Port Regulators) to implement and enforce effective tools to regulate global and interconnected players solely at a local port level; Such lack of competent regulatory structures is thus posing a potential threat to the competitive functioning of the supply chain markets and in extension of international trade. In this context, we argue

that both at the port level and at the level of the supply chain as a whole, issues for the re-examination of the role and effectiveness of the regulatory function should be raised and revisited both by academia as well as by policy makers.

The remainder of the paper is structured as follows. In section 2, we revisit ports' regulatory governance, proposing the reinforcement of port regulatory structures as well as the extension of their regulatory reach along the supply chains while section 3 summarizes the conclusion of the paper.

2 REVISITING PORT REGULATION

The deregulation of the port industry facilitated the insertion of private capital in container terminals and motivated investment risk assumption. On top of that however, as ports were amongst the few remaining sectors within the transport industry sheltered from competition, reform also enabled the establishment of an entirely competitive door-to-door supply chain. Containerization and the subsequent standardization it provided along with advancements in telecommunications i.e., logistics revolution and in intermodal technologies, led to enhanced prospects for supply chain integration while transformed ports from simple nodes to major intermodal distribution centres, service providers and critical coordinators of freight flows along supply chains (Rodrigue and Notteboom, 2009).

Amidst this transitional stage for the port industry, port governance models along with the roles and functions among the public and the private sector were reconfigured. On the one hand, with concessions becoming the "dominant design" for awarding container terminals, port managing bodies (i.e., Port Authorities), withdraw from terminal operations while, retained their functions as landlords and regulators of the port. However, while many Port Authorities were also corporatized re-orienting themselves towards the market, they focused more on developing profitable roles as landlords, cluster managers, facilitators and/or even entrepreneurs (Verhoeven, 2010), rather than on their regulatory responsibilities and/or the establishment of a sector-specific framework for the monitoring the competitive functioning of the port market.

On the other hand, private terminal operators (stevedores, liner shipping companies, financial holdings) taking advantage of the massive devolution wave and the opportunities occurring across the world, initially opted to scale up their operations expanding their terminal portfolios, thus internationalizing and consolidating their operational status in the global market. Subsequently, the enhanced possibilities of further integration along the post deregulated and fully competitive door-to-door transport chain, allowed terminal operators as well as other market players to vertically expand their activities to gain greater control over the total door-to-door movement of freight (Heaver, et al, 2000).

In the absence of a regulatory framework specifically designed to accommodate the operational dynamics within the port industry and the complexity, interconnectedness and specificities of the distinct transport markets that build-up the containerized transport chain, an increasing proportion of container shipping, handling and distribution capacity ended up in the hands of fewer, larger companies. With the rise of market concentration, port authorities, saw their bargaining power and negotiation position diminish against the emerging global transport actors, making them more vulnerable to the dispositions and market power of these incumbent transport groups. In addition, despite the fact that market actors expanded along the chain, operating as a single unit which is simultaneously integrated in multiple transnational hyper-networks (terminal operator's networks, supply chain network), port regulations remained confined within the premises of the port, making it rather challenging and difficult for port authorities to enforce effective tools (for effective price gauging, service bundling, raising rival's costs in upstream and downstream markets monitoring) to regulate global and vertically integrated players solely at a local port level.

In this context, as it is likely that the consolidation trend will continue for the foreseeable future, the danger of competition distortions, market dominance and abuse is becoming more eminent. As such, if ports do not want to further remain local spectators with limited influence over the market-driven processes, a reconceptualization of the structures and scope of ports' regulatory governance and substance is necessitated.

2.1 Reinforcing ports' regulatory governance and substance: Towards a holistic supply chain approach for ports

Every regulatory system is comprised by two core dimensions, (a) the “who” of regulatory governance i.e., which entity assumes the role of the regulator, and (b) the “what” i.e., the essence and content of regulation (World Bank, 2006). However, these dimensions appear to be increasingly at odds in the particular case of the port industry.

Port authorities neither have the capacity and resources as port regulators, nor the mechanisms, and the tools to monitor the competitive functioning of the market and assess the local, national, and international implications introduced by incumbent market actors (terminal operators and liner shipping companies) within the development framework of ports. In addition, while supply chains extend across the globe and transport actors increasingly operate along them as a unified unit, regulators should ought to do so too, by expanding the regulatory reach and the scope of regulations, beyond the port's perimeter.

Ports due to their position amidst the waterside and hinterland transport segments could evolve into the regulatory “stronghold” of the supply chains. However, since the competency and the suitability of the average port authority to implement and enforce regulations within the supply chain network is questionable; alternative and complimentary modes of regulatory governance should be assessed. As such, to restore the center stage position and bargaining power of port authorities within supply chains, it is arguing that port's regulation could be reinforced by novel structures and additional layers of governance (regional, international).

Following the paradigm of network industries such as energy and telecommunications (Abbott & Ma, 2013), which are governed by national as well as international independent regulatory agencies with explicit regulatory competencies across the network's segments; regulation of the port as well as of the entire supply chain could be devolved (in part or in whole) from the port authority to an independent national regulatory authority which would in turn be complemented and assisted by a respective international/regional regulatory body. The rationale behind the aspect of independence is also manifold. The first argument lies in the fact that task specialization results in efficiency gains (Hood, 1991). Gains in terms of credibility and efficiency are also highlighted in Maggetti (2010); while the performance-oriented management and innovative behavior of independent authorities is assessed in Verhoest et al. (2007). Thatcher (2005) in turn, argues that independent authorities are considered less bureaucratic, more independent of political influences, and able to safeguard interests of customers.

Similar examples on an EU level, include the Council of European Energy Regulators (CEER), the Agency for the Cooperation of Energy Regulators (ACER), and the Body of European Regulators for Electronic Communications (BEREC) which are the voice of Europe's national network industry regulators. Respectively, on a national level as international practice has shown (Angelopoulos et al., 2019), apart from the Greek independent Regulatory Authority for Ports, other countries have turned to the establishment of similar agencies with explicit port economic regulatory competencies. According to the authors, while differences in the organizational and institutional approaches as well as in the scope, regulatory reach (tools) and efficiency of those agencies exist, port economic regulation, provides a more coherent and holistic framework in the process of enhancing the credibility and the quality of regulatory results, and hence of competition.

Thus, the adoption of a similar multi-level regulatory governance approach could be seen as part of a broader initiative towards a model of “network governance regulation” (Coen & Thatcher, 2008). A model which could foster greater cooperation, coordination, and harmonization among the different tiers of regulatory governance and port authorities (Figure 1), with regards to the regulatory procedures, the measures adopted and the mechanisms to effectively regulate globalized and interconnected players in a manner which enhances the integrity and competitive functioning of the supply chains.

The overall purpose of the proposed reconfiguration and reinforcement of regulatory structures is to enhance and promote more integrated supply chains, as well as a monitored and transparent transport network which safeguards public interest, fair rates, and a limitation of abusive behaviors from incumbent market actors.

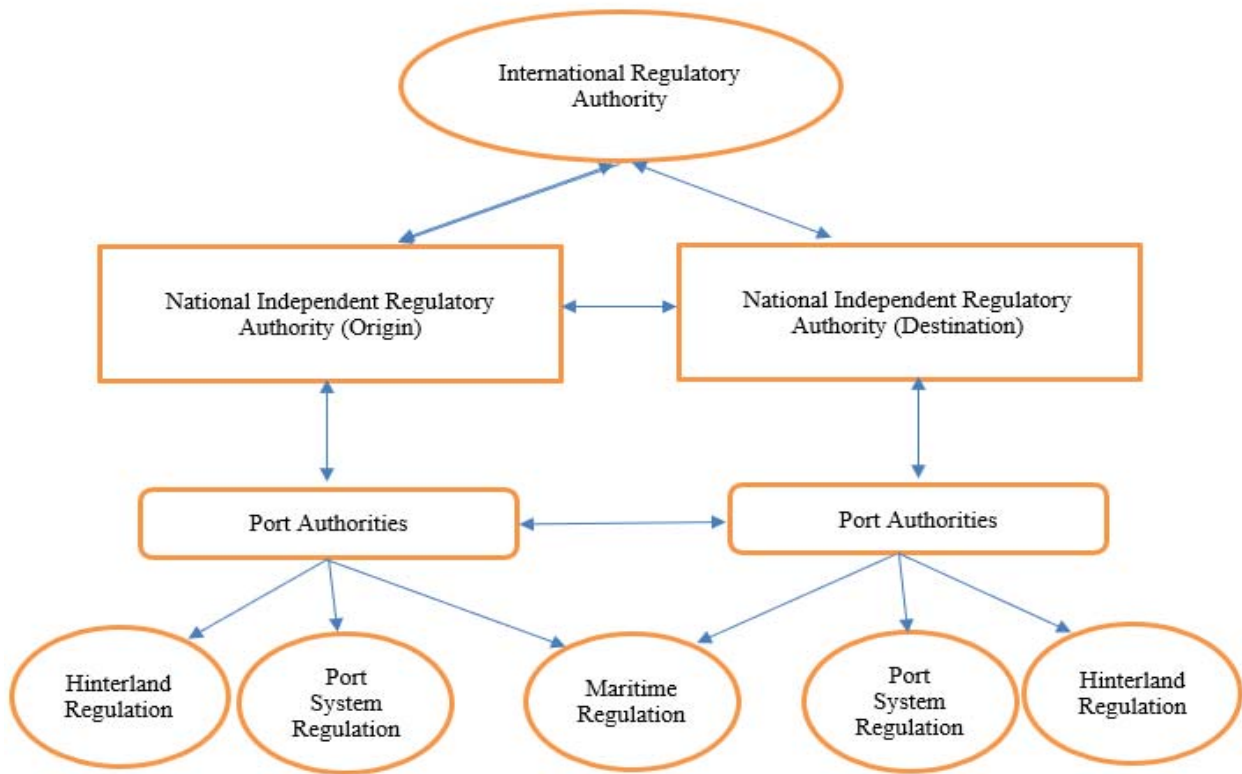


Figure 13: International, National & Local Tiers of Regulatory Governance within Supply Chains

3 CONCLUSIONS

The formation of an oligopsonistic and oligopolistic market structure in terminal operations and liner shipping respectively, has undermined the capacity of port authorities to efficiently regulate global players within the context of the port system.

As our analysis indicates, in order to regulate the globalized and powerful port actors, rethinking and repositioning the port system in today's complex supply chains will not be enough. If ports want to regain control over such global actors, they must enhance, adapt, and invent new tools to face today's challenges. To do so, appropriate updating of the regulatory function should be coupled by the re-invention of the role of the regulator on a national and international level as well as by the extension of the regulatory reach beyond the port context and throughout the supply chain network.

Paradigms from network industries (CEER, 2015) could be creatively utilized, with respect to their approach to governance of regulation and provide a base for institutional reform within the port sector. We argue that an institutional restructuring based on the delegation of regulatory function to independent authorities of national and international competence, can restore the center-stage position of economic regulation in the port and supply chain network, allowing for policy convergence and, consequently, for the creation of a common network-wide regulation framework along the supply chain, whose stronghold and epicenter will be the port node.

References

- Abbott, M., & Ma, X. (2013). The regulatory governance of the telecommunication and electricity industries in small, island nations. *Utilities Policy*, 26, 7-16.
- Angelopoulos, J., Chlomoudis, C., Flegkas, C., Leonardou, P., & Vrysagotis, V. (2019, June). Uncharted waters-independent regulation for port concessions. In IAME 2019 Conference, June 25th–28th, Athens, Greece.

- Baltazar, R, Brooks, M R (2001, July). The governance of port devolution: A tale of two countries. Paper presented at World conference on transport research, 22-27.
- Coen, D, & Thatcher, M (2008) Network Governance and Multi-level Delegation, European Networks of Regulatory Agencies". *Journal of Public Policy*, Vol.28 No.1, pp. 49-71.
- Heaver, T, Meersman, H, Moglia, F, & Van de Voorde, E (2000) Do mergers and alliances influence European shipping and port competition? *Maritime Policy & Management*, 27(4), 363-373. <https://doi.org/10.1080/030888300416559>
- Hood, C (1991) A Public Management for All Seasons. *Public Administration* 69(1): 3-19.
- Maggetti, M (2010) Legitimacy and Accountability of Independent Regulatory Agencies: A Critical Review. *Living Reviews in Democracy*, Vol.2
- Notteboom, T, Rodrigue, J P (2012) The corporate geography of global container terminal operators. *Maritime Policy & Management*, 39(3), 249-279. <https://doi.org/10.1080/03088839.2012.671970>
- Parola, F, Satta, G, & Caschili, S (2014) Unveiling co-operative networks and 'hidden families' in the container port industry. *Maritime Policy & Management*, 41(4), 384-404.
- Rodrigue, J P, & Notteboom, T (2009) The terminalization of supply chains: reassessing the role of terminals in port/hinterland logistical relationships. *Maritime Policy & Management*, 36(2), 165-183. <https://doi.org/10.1080/03088830902861086>
- Thatcher, M. (2005). The third force? Independent regulatory agencies and elected politicians in Europe. *Governance*, Vol. 18 No.3, pp. 347-373.
- Van de Voorde, E, Vanelslender, T (2009) Market power and vertical and horizontal integration in the maritime shipping and port industry. OECD Statistics Directorate. OECD/ITF Joint Transport Research Centre Discussion Papers, 67-96. <https://doi.org/10.1787/9789282102619-en>
- Verhoest, K., Verschuere, B., & Bouckaert, G. (2007). Pressure, Legitimacy and Innovative Behavior by Public Organizations. *Governance: An International Journal of Policy, Administration, and Institutions*, Vol.20, No.3, pp. 469-496.
- Verhoeven, P (2010) A review of port authority functions: towards a renaissance? *Maritime Policy & Management*, 37(3), 247-270. <https://doi.org/10.1080/03088831003700645>
- World Bank, (2006) Handbook for Evaluating Infrastructure Regulatory Systems. Washington: International Bank for Reconstruction and Development / The World Bank.

Expectations and risks for Greek ports from the upcoming new EU regulation for the Trans European Transport Network (TEN-T)

Th. Giantsi*

¹School of Civil Engineering, National Technical University of Athens, Zografou, Attika, TK 15780, Greece

*Corresponding author: Theodora Giantsi dgiantsi@central.ntua.gr

Abstract

Regulation 1315/2013 on Union guidelines for the development of the Trans-European Transport Network (TEN-T) aims to promote the development of a comprehensive and interconnected transport infrastructure network in all of Europe. This Regulation is under revision and the new Regulation will be published by the end of 2023. According to two proposals of the European Commission, the TEN-T will be expanded. At the present paper will be discussed the consequences of this expansion, especially for maritime navigation in Greece and the neighbouring countries. Nowadays 25 Greek ports belong to the core and comprehensive network, under the new Regulation we are expecting 41 Ports. For Greece, the ports are not only playing an updated role in the new energy supply chain but are a crucial element of the country's cohesion, growth, and survival. Obligations, benefits, and existing issues of the Greek port policy affect the expectations and the risks. The European existing financial tools, especially for port infrastructure are not enough to promote the expected update of them in Europe generally and in Greece more specifically.

Keywords Trans-European Transport Network (TEN-T), Sea Ports, Maritime Navigation

1 INTRODUCTION

According to the European Treaty, a Trans-European Network had to be developed in three sectors: Transport, Energy, and Telecommunication. The sector of transportation includes all the transport modes (roads, rail, maritime navigation, inland navigation, and air transport). After a long period of negotiations, EU Regulation 1315/2013 “on Union guidelines for the development of the Trans-European Transport Network (TEN-T)”, OJEC (2013), was ratified and inserted into force, with the obligation to be revised in ten years. At the annexes of Regulation 1315/2013 are presented the corridors and the nodes of the Trans-European Transport Network (TEN-T). These annexes have been amended several times by means of delegated acts adopted by the European Commission.

1.1 The EU Regulation 1315/2013

The scope of Regulation 1315/2013, is described as “The trans-European transport network comprises transport infrastructure and telematic applications as well as measures promoting the efficient management and use of such infrastructure and permitting the establishment and operation of sustainable and efficient transport services”.

Two networks, the core and comprehensive were established with 9 corridors under the rules of a strict methodology (European Commission, 2013). As it concerns maritime navigation, the ports were nodes of the networks and the Motorways of the seas, the maritime pillar of TEN-T. The criteria for joining the comprehensive network by a port, were: a) 0,1% of the average total European cargo volume in the three last years, b) 0,1% of the average total passenger volume in the three last years, c) the location of an island in NUTs 3 region and d) the location in an outermost region or a peripheral area, outside a radius of 200 km from the nearest other port in the comprehensive network. They were no specific criteria for the core network. These total volumes are the latest available three-year average, based on the statistics published by Eurostat.

According to the EU Regulation 1315/2013, the core network consists of 104 Sea Ports and a comprehensive of 225 Ports, a total of 329 European ports in a sum of ~ 1200 Commercial European

Ports. As it concerns the Greek ports, 5 ports joined the core network and 20 ports the comprehensive, a total of 25 ports.

The program Motorways of the Seas (MoS) is coming to finance projects via TENT and CEF (Connecting Europe Facility) funding tools.

1.2 The Long Way till the New Regulation

The new Regulation must be in accordance with the *European Green Deal* and the *Sustainable and Smart Mobility Strategy*. Based on evaluation studies results, (European Commission, 2021a), the European Commission presented a proposal for a Regulation of the European Parliament and of the Council, on Union guidelines for the development of the trans - European transport network, amending Regulation (EU) 2021/1153 on 14.12.2021 (European Commission, 2021b)

Including suggestions and amendments of the Council of European Union, the European Commission presented on 27.2.2022 an amended new proposal (European Commission, 2022). The European Parliament, via (3) three at least commissions, introduced 1872 new amendments. The Council General Approach of The Council of European Union on 5.12.2022, again, proposed new amendments including the spaceports in the field of air transport. The latest till today evolution in the procedure for the final vote by the European Parliament and the Council of European Union is the voted Report by the European Parliament Committee of Transport and Tourism, (European Parliament 2023), on 13.4. 2023. In this Report, new amendments were introduced including the connection a) *Sofia-Skopje -Durres – Igoumenitsa (road, rail freight and rail passengers, for the entire section)* and b) *Port of Durres*.

At these proposals, the corridors are extended including also infrastructures in neighboring countries. They set new deadlines to finalize the projects of common interest of the core, the extended core and the comprehensive network by the end of 2030, 2040 and 2050 respectively.

A new criterion, for the seaports, will be added, the total cargo volume must exceed 500.000 tonnes and its contribution to the diversification of EU energy supplies. 41 Greek Ports meet now the new criteria, 16 more than in Reg. 1315/2013. One of them (Agioli Theodoroi), who is an industrial (Refinery) port, will join the core network and 15 will join the comprehensive network. Between them, the Port of Alexandroupolis is finally included. The main benefit for those ports is the possibility of European funding via CEF according to Reg.1153/2021, OJEC (2021a).

2 THE UNDER REVISION TRANS-EUROPEAN TRANSPORT NETWORK (TEN-T)

2.1 The Structure and the Governance of TEN-T

The main objective of the Trans-European Transport Network policy is the development of coherent, efficient, multimodal, and high-quality transport infrastructure across the EU. It includes railways, routes and roads linking urban nodes, inland waterways, short sea shipping, maritime and inland ports, airports and terminals.

The Commission proposes, at the first legislative proposal of December 2021, to be integrated the nine core network corridors with the eleven rail freight corridors into nine European Transport Corridors. Two horizontal priorities were proposed, the European Rail Traffic Management System (ERTMS) and Motorways of the Sea. These 11 sectors (9 Corridors and 2 priorities) were managed by (11) Eleven European Coordinators who act as “facilitators” of the TEN-T policy and they are responsible for the implementation of the TEN-T policy. So, eleven Work Plans were established by the European Coordinators, to evaluate the existing conditions and to give the priorities.

In order to better coordinate and support the TENT-T, an Information System was set up by the Commission the TENtec. TENtec has two pillars: a) Policy-related funding/, like CEF and b) Grant management for Innovation like INEA/ CINEA (European Climate Infrastructure and Environment Executive Agency)

Finally, two (2) more legislative acts were coming to facilitate and endorse the TEN-T policy.

- The Streamlining Directive, OJEC (2021b), was adopted to facilitate the administrative processes for permitting procedures of cross-border infrastructure.

- The Action Plan on Military Mobility 2.0, (European Commission 2022), in order to facilitate the movement of military personnel and equipment.

2.2 The Greek network in TEN-T and Mos

Greece is an important part of the TEN-T network, as it is located at the crossroads of Europe, Asia, and Africa, and serves as a gateway to the Balkans and the Mediterranean. As it concerns the road and rail corridors in Greece, the situation does not change significantly compared to the existing Regulation. Even existing roads are not included. The western part of the country is neglected in the initial proposal. On the contrary, in the neighboring countries, a dense network will be developed, including countries non-EU members. In some cases that will facilitate Greek Network but, in some cases, that will transpose flows from East to the North, ignoring the South. The responsibility for that part of TENT-T belongs to the Ministry of Infrastructure and Transport (MIT).

The maritime sector of TENT-T shall consist of 41 Greek ports, the following: a) core network: Piraeus, Thessaloniki, Igoumenitsa, Patra, Herakleion and *Agioli Theodoroi*, b) comprehensive network: *Aegina, Alexandroupolis, Argostoli, Chalkida, Chania, Chios, Faneromeni Salaminas, Elefsina, Gavrio, Kavala, Kerkyra, Kos, Kyllini, Larymna, Lavrio, Lixouri, Mykonos, Mytilini, Naxos, Paloukia Salaminas, Paros, Poros Kefallinias, Poros Trizinias, Preveza, Rafina, Rethymno, Rodos, Samos, Santorini, Sitia, Skiathos, Skyros, Syros, Thassos, Tinos, Vathy Samou, Volos, Zakynthos*. Two Ports shall exclude Kalamata and Katakolo. This sector is under the Ministry of Maritime Affairs and Insular Policy (MMAIP). Most of these ports have waste reception and handling plans, approved by the MMAIP which is an obligation to be part of TEN-T. Only six ports need re- approvalment of their Plans by the Ministry.

The European Union's Motorways of the Sea (MoS) initiative is a program designed to promote the development of maritime transport within Europe, particularly for freight transport. The program is coming to finance projects via TENT and CEF (Connecting Europe Facility) funding tools.

2.3 TEN-T and Mos Financing

The main tools for financing the TEN-T's projects were mostly the Program CEF (Connecting Europe Facility), and other grants managed by CINEA. At Table 1 are presented the number of ongoing projects today, by subprogramme, and the contribution of the EU to the EU participants, for the European Union and Greece respectively, according to data provided by CINEA. Notice: The contribution concerns all the participants of the projects. Some of the Projects are of common interest between more than one country.

Table 1. Ongoing Projects financed by European Union.

Subprogramme	EU on No of projects	EU on par EU contribution (€) X10 ⁶	GR on No of projects	GR on par EU contribution (€) X10 ⁶
Totals	3,166	43,907	569	1,201
CEF Energy	39	4,690	1	35
CEF Transport	880	26,161	40	775
EMFAF	86	93	16	4
Horizon Clean Energy Transition	139	255	39	10
Horizon Climate	134	891	47	28
Horizon Energy	511	3,531	178	148
Horizon Transport	356	2,469	141	114
Innovation Fund	53	3,036	53	3,036
LIFE Clean Energy Transition	71	119	24	7
LIFE Climate	218	563	20	24
LIFE Environment	314	735	34	27
LIFE Nature	365	1,364	29	32

During the first period of CEF (2014-2017) only 4% of the financing was going to European ports with 72% directed to the rail. At the same time, 74% of the total European freight transport is imported by

ports. Of the total given amount, only 0.03% went to Greek Ports. In the next period (2018- today) some Greek Port Authorities participate in pilot projects concerning mostly energy and no infrastructure. Greek ports did not benefit significantly from the MoS programs. Data from Mos studies show that the Greek Ports had the following project budget till 2022, Thessaloniki € 0.4 M, Igoumenitsa € 7.2 M, Patra € 4.0 M, Kyllini € 0.2 M, Piraeus € 15.3 M and Iraklion € 10.3 M. At Table 2 are presented some indicative projects from Greek Ports, financed by CEF mainly about energy.

Table 2. Indicative Greek Ports Projects financed by European Union

A/A	PROGRAM	PORT	TOTAL COST (€)	EU CONTR.	SITE
1	ALFION	IGOUMENITSA	1.080.000,00	50%	https://www.alfion.gr/index.php/el/
	CIPORT	PIRAEUS	1.376.000,00	50%	https://www.olp.gr/en/environmental-protection/
	CENTAVROS	VOLOS	1.900.000,00	85%	
	ELEMED	PIRAEUS-KILLINI			https://ealingproject.eu/
	EALING	16 EU PORTS (PIRAEUS, RAFINA)	6.960.240,00	50%	https://WWW.PORT-VOLOS.GR
	ELECTRIPORT	HERAKLION	1.447.440,00	85%	https://portheraklion.gr/

According to Reg.1153/2021, the budget of CEF, in the broader context of the Multiannual Financial Framework, MFF 2021-2027, is EUR 1 384 000 000 (in 2018 prices). Most of them shall be used for the completion of missing major cross-border railway links between cohesion countries. For the completion of the OEM MS projects is needed an amount of € 80.9 billion. For the maritime sector, the amount is estimated at € 6.6 bl. (8.2%). The cost allocation for Greece is estimated (for all projects) in the amount of € 8.64 million. The amount disbursed to OEM MS through the Recovery and Resilience Fund (RRF) for Greece, is € 2.310 million for grants and € 1.650 million for loans.

3 EXPECTATIONS AND RISKS

It is obvious that Greece didn't take enough advantage of CEF during the periods of MFF 2007-2013 and 2014-2020, especially for the maritime sector. At the present period, more ports can be beneficiaries. Some thoughts about the new list are expressed. From the presented list of ports, there are missing port facilities that could be incorporated, like other Greek Refineries or Revithousa island that meet the new criterion for energy nodes. For them, that could be a new opportunity for funding. The whole area around Elefsina could be updated to the core network in order to establish a multimodal node. On par contrary, in some areas, are many port facilities included in the network, with very small infrastructure and under a Municipal / or State Port Fund, without experienced staff who can participate in an EU project. We have to pay attention that Katakolo (maybe due to covid 19, and lack of Cruise) and Kalamata Ports don't meet the criteria of the new TEN-T. In the next revision of the Regulation, many small Ports shall be excluded without any benefit. Until 2030 the priority shall be at the core corridor financing by CEF of the comprehensive network ports shall be difficult. In reality, the Greek ports, after the economic crisis, need at least maintenance. Also, it wasn't easy/possible the financing infrastructure projects with European Funds. For that, the RRF in accordance with CEF can play a significant role taken account the following issues: a) limited time for the project's completion for FFR projects (end 2026), b) limited mature projects and approvals due to non-existing studies and to bureaucracy, c) limited capacities of the construction industry, due to limited existing companies with lack of experienced technical staff. d) Lack of employees at the state institutions, including Port Funds, Municipalities, Ministries, etc, in order to supervise and accelerate the procedures, e) Unsecure financing resources, and f) Insufficient port governance system. The possibility to open new Motorways of the Sea from the Ionian and Aegean Seas to North Africa and to the Eastern Mediterranean must be more carefully studied.

4 CONCLUSION

At the upcoming New Regulation for TEN-T, 41 Greek ports shall have the privilege to have to be eligible to become beneficiaries of EU programs. At the same time, RRF is coming to facilitate the financial resources. They exist issues to be solved by the government and not only, in order to take advantage of these opportunities. More European financial resources, with easier access, right now, should be allocated to small port infrastructure and to the connections with the other networks for a resilient, coherent, sustainable, smart, and seamless Trans - European Transport Network. Bottleneck problems with the other transport modes must be solved and new Maritimes connections must be established to enhance Short Sea Shipping.

Acknowledgement

I would also like to thank Professor J. Prousalidis, who provided us with data about the Greek Ports Projects financed by CEF, and Th. Mexis from MMAIP who provided us with data about the approval of waste reception and handling plans for TEN-T Greek ports.

References

- European Commission, 2013, COMMISSION STAFF WORKING DOCUMENT The planning methodology for the trans-European transport network (TEN-T) Accompanying the document Communication from the Commission Building the Transport Core Network: Core Network Corridors and Connecting Europe Facility
- European Commission, Directorate-General for Mobility and Transport, (2021a) “Support study for the evaluation of Regulation (EU) N° 1315/2013 on Union guidelines for the development of the trans-European transport network, final report”. Publications Office.
- European Commission, (2021), Proposal for a REGULATION OF THE EUROPEAN PARLIAMENT AND OF THE COUNCIL on Union guidelines for the development of the trans-European transport network, amending Regulation (EU) 2021/1153 and Regulation (EU) No 913/2010 and repealing Regulation (EU) 1315/2013
- European Commission, (2022a) Amended proposal for a REGULATION OF THE EUROPEAN PARLIAMENT AND OF THE COUNCIL on Union guidelines for the development of the trans-European transport network, amending Regulation (EU) 2021/1153 and Regulation (EU) No 913/2010 and repealing Regulation (EU) 1315/2013
- European Commission, (2022b), JOINT COMMUNICATION TO THE EUROPEAN PARLIAMENT AND THE COUNCIL Action plan on military mobility 2.0
- European Parliament, Committee on Transport and Tourism, (2023) REPORT “on the proposal for a regulation of the European Parliament and of the Council Guidelines for the development of the trans-European transport network, amending Regulation (EU) 2021/1153 and Regulation (EU) No 913/2010 and repealing Regulation (EU) 1315/2013”
- OJEC (2013) ‘Regulation (EU) No 1315/2013 Of the European Parliament and of the Council, of 11 December 2013, guidelines for the development of the trans-European transport network and repealing Decision No 661/2010/EU’.
- OJEC (2017) ‘Regulation (EU) 2017/352 of the European Parliament and of the Council of 15 February 2017 establishing a framework for the provision of port services and common rules on the financial transparency of ports’.
- OJEC (2021a) Regulation (EU) 2021/1153 of the European Parliament and of the Council of 7 July 2021 establishing the Connecting Europe Facility and repealing Regulations (EU) No 1316/2013 and (EU) No 283/2014
- OJEC (2021b) Directive (EU) 2021/1187 of the European Parliament and of the Council of 7 July 2021 on streamlining measures for advancing the realisation of the trans-European transport network (TEN-T)
- Tsamboulas D., Lekka A.M. and Rentziou A. (2015), Development of Motorways of the Sea in the Adriatic region, *Maritime Policy & Management*, 42:7, 653-668.

Boomer sub-bottom profiler: also valid for distinguishing habitat boundaries during port geological surveys? – An example from Armenistis coastal zone in Ikaria Island

A. Poulos¹, O. Andreadis¹, I. Petsimeris¹, K.N. Chtouris¹, T. Hasiotis^{1*}, A. Kokoromytis²,
D. Karamaniolas²

¹Department of Marine Sciences, University of the Aegean, Mytilene 81100, Lesvos isl., Greece

²Geoefarmoges, Metamorfosi 14452, Attica, Greece

*Corresponding author: hasiotis@aegean.gr

Abstract

This contribution aims to examine the feasibility and efficiency of using a Boomer sub-bottom profiler for mapping the general distribution of habitats in the context of a port geological survey in Armenistis (Ikaria Island). The results are compared with the precise habitat mapping obtained from a side scan sonar. The Boomer was initially set up to achieve high resolution profiles so as to address the potential coastal geo-hazards, but the profiles' surficial echo acoustic characteristics were found to be valuable also for the discrimination of the different seafloor habitats (*p. oceanica*, rocks, sand). The comparison of the habitat distribution as observed and mapped from the Boomer profiles and the high resolution side scan sonar demonstrated that nearshore rocky areas were almost accurately mapped, whereas *p. oceanica* and sand boundaries were reasonably plotted. Thus, it seems that Boomer sub-bottom profilers, which are often utilized during marine surveys for port and other coastal works, if appropriately set up and the obtained data are carefully interpreted (although with few limitations), then they can be also used for a general habitat distribution.

Keywords Boomer sub-bottom profiler, Habitat mapping, Geomorphological mapping, Ikaria Isl.

1 INTRODUCTION

The distribution of protected habitats is a key parameter during environmental surveys for port construction studies. Most of the time this scope accompanies bathymetric and marine geological surveys for the detection of geo-hazards (gas in marine sediments, weak layers, instabilities, faults, outcrops etc.) that may affect construction activities. Depending on the size of the project and if multi-beam echo-sounder data are not available, habitat distribution relies on side scan sonars or, occasionally, habitat echo-sounders.

On the other hand, Boomer sub-bottom profiler is a widely known instrument for mapping sub-seafloor stratigraphy and geological structures and is commonly used in marine geophysical surveys and geotechnical investigations (Ramsay and Miller 2010; de Souza 2022). The system is frequently utilized in port surveys since it enables penetration in coarse sediments usually found in shallow environments. However, the potential of this technology in distinguishing habitat boundaries during port surveys remains largely unexplored. This study aims to investigate the feasibility of using the Boomer sub-bottom profiler to map the general distribution of habitats in the context of port geological surveys and evaluate its efficiency. As a case study, the coastal zone of Armenistis in Ikaria Island (central Aegean Sea) is examined (Figure 1a, 1b). The survey took place in the framework of an applied project in order to examine the subsurface distribution and outcropping of granite, the main bedrock formation found onshore, and other potential geohazards for the construction of a small port. The wider area onshore consists mainly of a big granite intrusion (namely "Raches") that occupies the western part of Ikaria Island (Ring 2007; Laurent et al 2015), and of Low Pliocene conglomerates, sand, and clays together with limestones and Quaternary deposits.

In order to verify the Boomer data analysis and examine its efficiency for the general mapping of habitat distribution, the results are compared with a side scan sonar (SSS) data set, which is considered as a more relevant and reliable tool for habitat mapping (i.e., Tecchiato et al 2019).

2 METHODOLOGY

The study was carried out in 2022 using a vessel of opportunity for the seismic survey and a supporting 4.8 m inflatable boat for the SSS survey. In the absence of valid bathymetric data, initially a Humminbird Helix 10 multi-parametric sonar was used for the acquisition of bathymetric and seabed morphological information along a grid of dense crossing lines (Figure 1c). This is a low-cost sonar able to provide high resolution data for bathymetry (180-240 kHz) and seabed morphology (455 kHz - Chirp technology side scan sonar). SonarWiz 7 was used for post-processing, analysis, and mosaicking of the collected sonographs. A van-veen grab was used for surficial sampling (14 samples) and a drop camera for sonar ground-truthing (24 stations). The sub-bottom profiler (SBP) was an Applied Acoustics, consisting of a CSP-D 700 Joules energy source, a AA251 Boomer plate mounded on a CAT-200 catamaran and a 12-element hydrophone. The Boomer system was initially tested in order to define the appropriate settings for the survey. The sweep-length was set at 100 ms and for some lines at 50 ms and the trigger interval at 200 ms so as to detect the surficial sediments with the highest possible resolution. The boomer catamaran layback was 20 m and 10 m only for the along-shore (in very shallow waters) lines, and it was applied to the navigation (GPS) data. A total length of about 20 km of seismic profiles were collected (Figure 1c) using the SonarWiz acquisition software. During the survey the research vessel speed was maintained at about 3 knots. Navigation and positioning were supported by the Humminbird Helix 10 with a position accuracy of ~ 3 m. In the laboratory, grain size analysis was performed by dry sieving due to the coarse sediment texture (Folk 1980). Statistical parameters were calculated using the Gradistat software (Blott and Pye 2001). All data were imported and processed in QGIS in EGSA87' for mapping purposes.

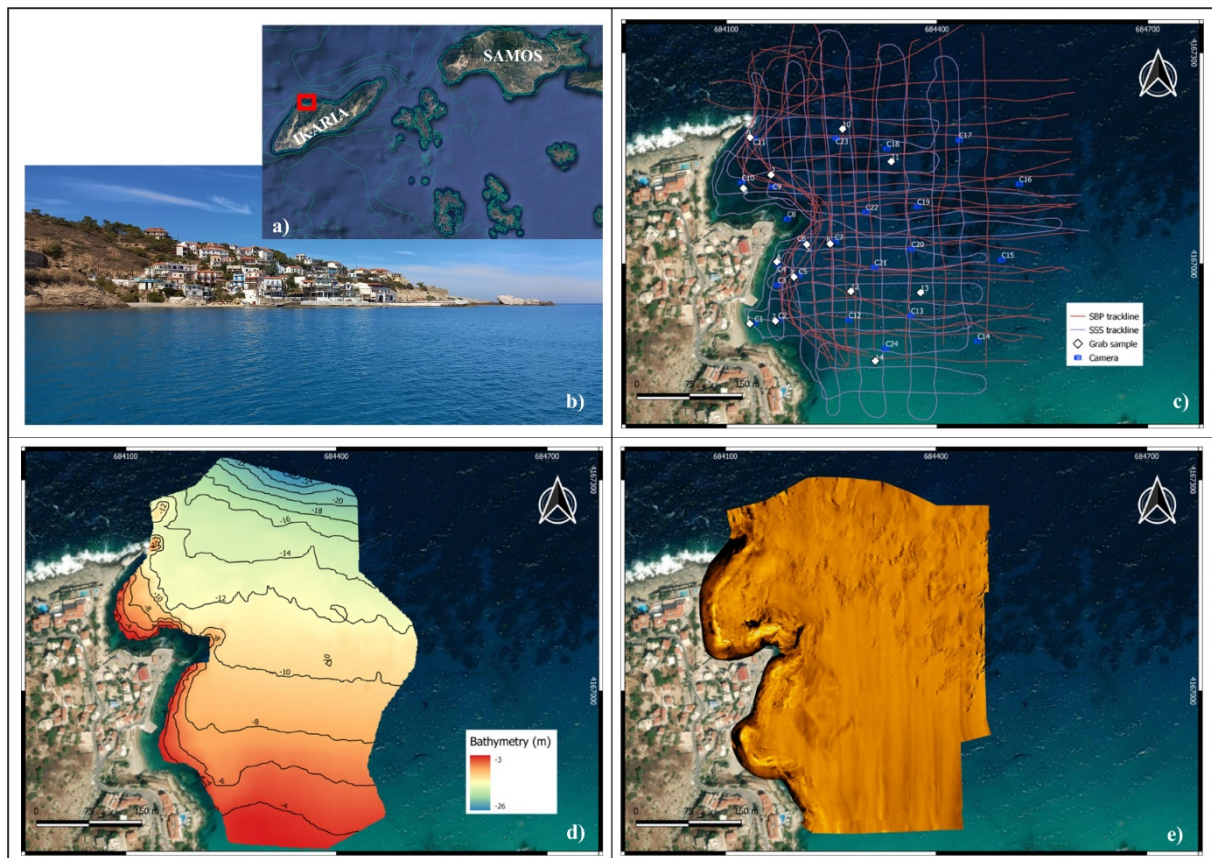


Figure 1 (a) Map showing the location of the study area (red box), (b) photo of the survey site, (c) field data collected over Armenistis coastal area, (d) bathymetry map deeper than ~ 2 m and (e) SSS mosaic

3 RESULTS AND DISCUSSION

The bathymetric data (Figure 1d) revealed relatively steep slope inclinations and an irregular relief to the west, shallower than ~8-9 m, attributed to bedrock outcropping and also an uneven relief deeper than ~10 m ascribed to seagrass (*p. oceanica*) banks and meadows.

The SBP data showed 3 main seismic facies (SF) (Figure 2). The surficial SF1 has few faint to medium intensity internal reflections and locally a semi-transparent acoustic character and can be separated into two sub-facies. The first develops shallower than ~14 m, consists of a thin veneer of loose sediments, which overlies older and denser sedimentary deposits, and probably corresponds to Holocene-Pleistocene deposits. The thickness of this unit varies, locally exceeds 8 m, and decreases sharply towards the west, where the rocky relief emerges (SF3, see below). The second sub-facies extends deeper than 14 m (to the north) with a distinct prograding depositional (oblique tangential reflections) sequence of layers covered by a thin veneer of loose sediments. The main characteristic of SF1 is the slightly undulating, locally irregular and intermittent surficial echo attributed to the relief of *p. oceanica* banks reaching 1.5 m in height (Figure 2). Penetration under the *p. oceanica* banks generally reduces and the sub-bottom echoes often exhibit chaotic patches/zones. Drop-camera verified the presence of *p. oceanica* and sand patches in various depths, whilst surficial sampling from the patches revealed sandy to gravelly sediments. The intermediate SF2 shows parallel to sub-parallel continuous to discontinuous and of varying intensity reflections, locally with acoustically chaotic pockets, which are attributed to denser material of varying granulometric composition deposited over a wider geochronological and environmentally varying period in relation to SF1 (probably during the Pliocene-Lower Pleistocene). Finally, the lower SF3 is separated by a clear unconformity from the overlying SF2 (Figure 2), and consists of very strong continuous to discontinuous reflections, often exhibiting overlapping hyperbolas that correspond to the acoustic basement (hard granitic bedrock), which towards the west appears on the surface and presents a highly irregular relief. No major geo-hazards were encountered in the study area.

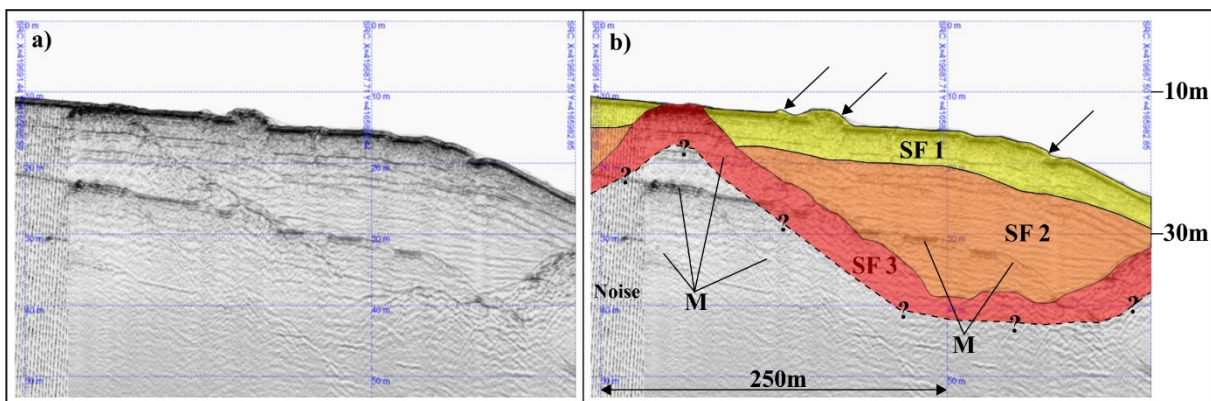


Figure 2 (a) Boomer profile showing the observed three seismic facies in Armenistis coastal area and (b) its interpretive sketch. (M: multiple, arrows: *p. oceanica* banks and meadows)

The study of the SSS images and mosaic (Figure 1e) revealed three main reflectivity types (Figure 3), which are related to the main seafloor habitats. The first has a high reflectivity, locally an uneven pattern and patches of lower reflectivity and corresponds to the *p. oceanica* and intervening sand patches. The second appears a high reflectivity with acoustic shadows of varying width and is related to the irregular relief of the rocky (granite) outcrops towards shallower waters to the west. The third has a medium to high reflectivity, it is characterized by rhythmically alternating bands of higher and lower intensity and corresponds to rippled sandy sediments. Locally, a lower reflectivity area is also related with sandy but un-rippled sediments, as it was verified by sediment sampling.

Due to specific acoustic return pattern of the Boomer SF1 surficial echo, its acoustic characteristics were compared with the observed SSS habitats for a specific area of 146600 m² (Figure 4), in order to evaluate the efficiency of the SBP in the discrimination and manual mapping of the seabed habitat boundaries. *P. oceanica* banks and meadows formed a slightly mounded and/or a step-like morphology and locally

caused interruption of the surficial echo in the Boomer profiles. Locally, this morphology alternates with flat segments of seabed where penetration increases, suggesting sediment patches. This pattern was found to develop mainly in deeper waters in the central to northeastern part of the surveyed zone. Manual junction of the limits of these patterns between the adjacent SBP survey lines delineate an area that covers approximately 67110 m². Following the same method, the outcropping boundaries of SF3 shape an area of 18390 m². The remaining area is obviously related to the sandy sediments that are distributed over an area of 61100 m². However, when the detailed mapping using the SSS images is performed, either automatically in SonarWiz or manually (the latter giving better and more reliable results), the spatial extent of the habitats presents variations, becoming 41600 m² for *p. oceanica*, 17180 m² for the rocky areas and 87820 m² for the sandy sediments. A 7% over-estimation of the rocky area from Boomer profiles is deemed reasonable, especially considering the worst-case scenario that must be employed in order to reduce uncertainties during port design and construction activities. On the other hand, a ~61% increase in the *p. oceanica* appearance could arise environmental issues. Though, this includes areas of sand patches within the meadows and also towards the shallow limit, the latter easily discernible in satellite images (i.e., Google Earth). Apparently, sand opposites *p. oceanica* distribution, found to be ~44% underestimated in the Boomer profiles.

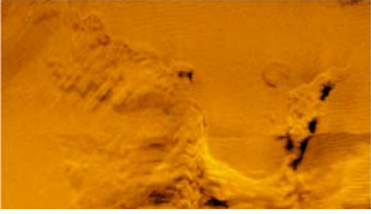

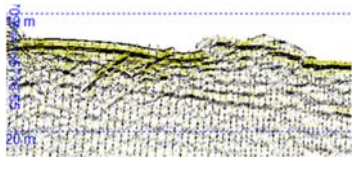
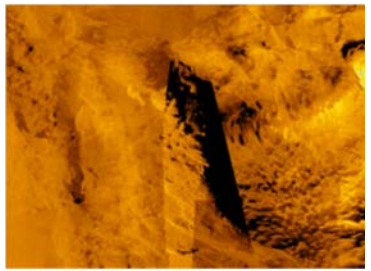

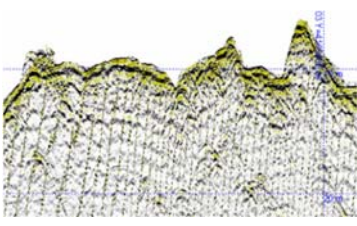


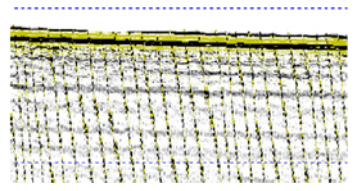
RT	SSS record	Camera (ground truth)	SBP profile
1			
2			
3			

Figure 3 SSS records and camera images (ground-truthing), together with representative SBP profiles of the main habitats observed during the survey

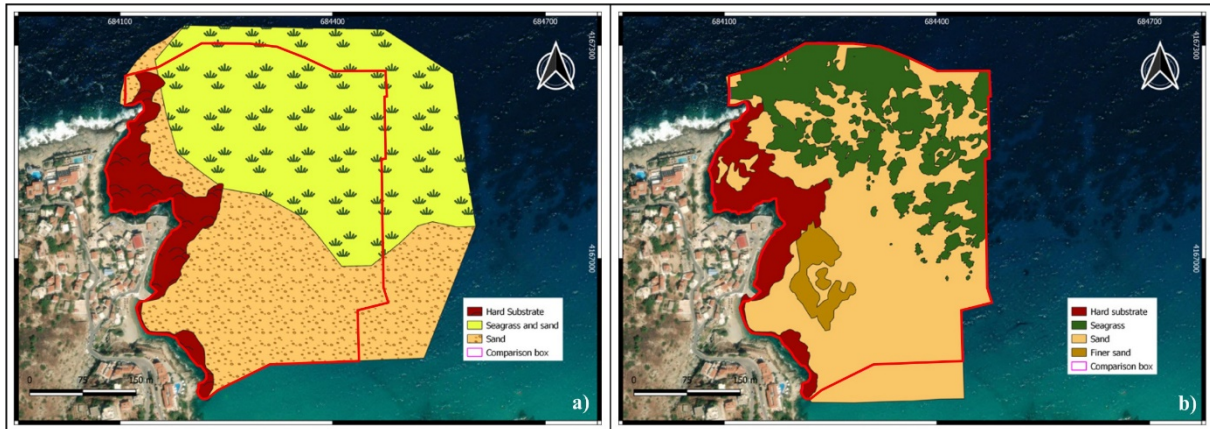


Figure 4 Comparison (red boxes) between the habitats mapped using (a) the Boomer and (b) the SSS data

Although differences in habitats' spatial extent exist between the precise distribution raised by the SSS mapping and the Boomer profiles, it is considered that (i) the accuracy of the extent for a potential geohazard (rock outcropping) but also for the hard substrate habitat is acceptable and (ii) the general boundaries of the observed habitats using Boomer profiles can be reasonably drawn. It is rational to expect that if a higher resolution SBP system is to be used (i.e., chirp) then the acoustic characteristics of the surficial echo would be sharper, and the consequent habitat boundary mapping and habitat extent would be more precise. Thus, even if high-resolution SSS systems or multi-beam echo sounders for shallow waters could be the essential tools for reliable habitat mapping, it seems that Boomers, although with few limitations, can also support preliminary habitat distribution. The results of this study help not only to understand the utility of the Boomer sub-bottom profiler in mapping habitat boundaries, but they can also inform and supplement future research and management strategies for coastal surveying during port and other nearshore technical works planning and construction activities.

References

- Blott SJ, Pye K (2001) Gradistat: A Grain Size Distribution and Statistics Package for the Analysis of Unconsolidated Sediments. *Earth Surf Proc Landf* 26:1237–1248
- De Souza L (2022) Shallow-water sub-bottom investigation. A multi-frequency approach (2022) *Brazilian Journal of Geophysics*, 40:1-8
- Folk R (1980) *Petrology of Sedimentary Rocks*. Hemphill Publishing Company, Austin, Texas
- Laurent V, Beaudoin A, Jolivet L, Arbaret L, Augier R, Rabbilart A, Menant A (2015) Interrelations between extensional shear zones and synkinematic intrusions: The example of Ikaria Island (NE Cyclades, Greece). *Tectonophysics*, 651-652:152-171
- Ramsey P and Miller W (2010) Multibeam and sub-bottom profiling surveys for major port expansions. Position IT, March, 29-33
- Ring U (2007) The geology of Ikaria Island: The Messaria extensional shear zone, granites and the exotic Ikaria nappe. *Journal of the Virtual Explorer* 27(3):1-33. doi:10.3809/jvirtex.2007.00171
- Tecchiato S, Buosi C, Ibba A, Del Deo C, Parnum I, O'Leary M, De Muro S (2019) Geomorphological and sedimentological surrogates for the understanding of seagrass distribution within a temperate nearshore setting (Esperance Western Australia). *Geo-Marine Letters* 39:249-264

The social acceptance of autonomous merchant ships in Greek ports

C. Politopoulou*, A-F. Papathanasiou, T. Giantsi

Department of Civil Engineering, National Technical University of Athens, Athens, Zografou, 15780, Greece

*Corresponding author: politopoulou@outlook.com

Abstract

Some of the levels of automation have successfully permeated all of the prevailing trends and tendencies in modern life. As in many transport industries, automation has been introduced in shipping, leading to the development of fully autonomous ships (AS), which can operate themselves unmanned. The present study aims to investigate the social acceptance of autonomous merchant ships in Greek ports. Social acceptance is often a significant obstacle to the approval of new technologies, while at the same time dealing with the replacement of human resources with robotic systems or the modification of the profession with advanced requirements. The introduction of AS promises to increase navigational and maritime safety. After completing a questionnaire, the main observations that emerged were that most of the respondents are cautious regarding the long-term operation of AS in Greek ports, while most appreciate the benefits of AS operation for shipping companies. More than half of them considered it feasible to modernize and train personnel to operate AS successfully. More than 50% of the participants deemed it feasible to upgrade and provide training to personnel for the effective operation of AS.

Keywords autonomous merchant ships, social acceptance, automation

1 INTRODUCTION

The Greek coastline exceeds 13,676 km, which is the longest in the Mediterranean basin. The country's location makes it maritime competitive. Ports are virtual places within an operating system where network connections start and end. Approximately 100 of them are pinpointed in Greece and represent international and regional vital hubs for passengers and freight, while being one of the main sources of the country's economy. In Greece, there are more than 25 important commercial ports, while EU has identified 5 of them as ports of strategic attention and main maritime interfaces of the Orient/East-Med Corridor (OEM). Shipping contributes a great deal to the Greek economy. Specifically, for 2019 it constitutes 7% of the total Gross Domestic Product (GDP). Greeks own more than 12% of ships and the Greek-owned merchant fleet is the largest in the world, about 16% of the global fleet in dead tonnage (assets). One of the main passenger and cargo ports of the Mediterranean is Piraeus. Provides fast, frequent, and lower cost connections to Far Eastern ports, compared to Northern European ports. This made Greece a significant maritime gateway for Europe. Piraeus is a rapidly developing port and is the largest in the Mediterranean and one of the largest in the world. In the 2019-2020 period, it ranked 4th among European ports in total container traffic despite the pandemic (assets). Overall, Greek ports contribute significantly to the domestic economy and European trade. Due to their importance, this study investigates the acceptance of automated ships in domestic ports.

2 LITERATURE REVIEW

In 1983, the development of automation began to develop. In recent years, autonomous technology provides remarkable economic and environmental benefits. The initial idea for the development of the automated systems was the striving for ease in shipping costs by reducing personnel. Additionally, it seems that safety at sea could be increased if humans were moved away from ships. Due to EMSA's annual overview of marine casualties and incidents for the year 2022 year, 2,637 marine casualties and incidents are reported (EMSA, 2022). According to the literature, more than 80% of maritime accidents are related to the anthropogenic factors (Navas de Maya et al., 2018; Coraddu et al., 2020). Human error is a departure from acceptable or desirable practice on the part of an individual or group of individuals that can result in unacceptable or undesirable results (IMO, 1999). Human errors can be either random or systemic (Allal et al., 2017). In the case of system, it is reported that several accidents are caused due

to limited visibility (Coraddu et al., 2020), attention deficit (Burmeister et al., 2014), fatigue, lack of communication and decisions based on meagre information, inadequate technical training or knowledge of the ship's system operation (Rothblum, 2000), deviation from Standard Operating Procedure (SOP) (Coraddu et al., 2020) or vague practice in extreme conditions (Kum & Sahin, 2015), poor automation design, insufficient maintenance and faulty standards, policies or practices (Rothblum, 2000). In addition, fire or explosion accidents are often caused by technical failures due to insufficient crew maintenance (Wróbel et al. 2017). The absence of a crew would increase safety by reducing these forms of accidents studied the influence of unmanned system on safety. They found that the majority of ship collisions they studied could have been avoided if AS were in operation. According to the research of de Vos et al. (2021), which uses shipping casualty records, most shipping accidents and most lives lost involve general cargo/multipurpose vessels. Most fatal accidents come from collisions. AS could reduce shipping accidents and save lives (Vos et al., 2021). Considering the above as well as the technological evolution, the operation of AS is expected to increase. A fully autonomous vessel of approximately 10 meters in length is already in operation for specialized work. In 2022, a 220m long Japanese autonomous car-ferry ship was tried for its maneuverability and navigation capabilities successfully (Negenborn et al., 2023). This study is about fully AS, which corresponds to the latest (Four) degree of autonomy, according to IMO scale defined as follows: 'The operating system of the ship is able to make decisions and determine actions by itself' (IMO, 2021). Although AS are capable of operating unmanned in deep water, when approaching shallow water, navigation and mooring are handled by the crew (Burmeister et al., 2014). It is expected that future AS won't have deckhouse and will be capable to moor without assistance (Allal et al., 2018). According to the estimate of Kooij et al. (2018), GPS will be accurate enough to moor the ship unaided between 2030 and 2058. Any ship should provide at least the same degree of safety, security, and environmental protection as a conventional ship of the same purpose or design (Bureau Veritas Marine & Offshore, 2019). One of the main advantages of AS is increased safety at sea and reduced operating costs compared to conventional ones (Wróbel et al., 2017). Collision avoidance systems work well even if a group of other ships coexist simultaneously (Hinostroza et al., 2021). Human absence on board could be a cause for concern (Wróbel et al., 2017). Any necessary human maintenance that might occur when the AS are in deep water could be done with the human approach of the AS by helicopters (Munim et al., 2019). Intelligent maintenance processes should be developed that monitor components, identify, diagnose, and repair faults remotely (Negenborn et al., 2023). For small ships, crew is a significant cost (de Vos et al., 2021). The implementation of AS will have a great impact on saving energy and reducing greenhouse gas emissions. AS won't have a crew, so no specific facilities and equipment will be needed. This leads to reduced weight, energy consumption and greenhouse gas emissions. Allal et al. (2018) concluded that the energy savings that could be achieved with automated container and general cargo ships amounts to 74.5%. A vital barrier is interpreting the benefits that come with AS and the profit that shipping companies could reap. Furthermore, there is still no legal framework for AS. The hint above suggests that it will take a few years for AS to become a sustainable solution (Van Hooydonk E, 2013). As mentioned above, in this study when the term AS is mentioned, it refers to the last level of automation, in which AS can operate in the deep without a crew on board.

3 METHODOLOGY

This report presents a brief literature review and aims to explain the contribution of AS and examine whether they can be expected to become socially acceptable in Greek ports. Automation is investigated because it is considered to constitute an innovative breakthrough, promising and with valuable advantages. Social acceptance is a major obstacle to the implementation of this modern technology in the transport system, as required for the successful operation of AS. The interaction between humans and automated technology is based on trust (Lee and See, 2004). Trust is often mentioned to be a strong predictor of adoption intention by other authors. Social trust has a significant role in shaping people's attitudes toward technology (Siegrist, 1999, 2000). The level of trust people has in emerging technology is often affected by their trust in the government. Particularly, people without social trust tend to be more sensitive to the risks and less to the benefits of technology (Siegrist, 1999, 2000). Due to Pande & Taeihagh (2021), similar surveys on the acceptance of automated cars did not include trust in the government as a variable that could affect the intention to use autonomous systems, but in general,

studies have shown that trust in the government has a positive impact on the adoption of new technology. Considering the aforementioned reasons, the present study takes into consideration human perception. The survey was conducted using a questionnaire, which was distributed to people associated with the topic, including port officials and employees, shipping companies, ship owners, seafarers, relevant ministries, researchers, students, and people with a high education level.

4 RESULTS

The present research focuses on capturing the technological revolution and ship automation through an online questionnaire, consisting of 10 mandatory questions, and administered in Google Drive format. This questionnaire was distributed to a sample size of 120 participants from Greece, who were either relevant to the aim of the study or had a high educational level. Participants were given the opportunity to express their opinions through various question formats, including linear scales, check-box grids, checkboxes and multiple choice questions. In addition, a paragraph-style question was incorporated to allow participants to freely express their thoughts and opinions.

Of the total of 120 respondents, 68% were male and 32% female. The majority of respondents were between the ages of 26-35 (35%), followed by 36-45 (28%), 18-25 (16%), 46-55 (12%), 56-65 (8%) and more elderly (2%). Furthermore, 93% of respondents held a bachelor's degree or higher. In terms of employment, 72% and 17% of respondents were employed in the private and public sectors, respectively, while 8% were students, 3% unemployed or seeking for employment, and 1% retired. Lastly, 31% of participants are related to the port sector, 28% to shipping, 3% to para-maritime and 39% from other industries. First of all, 44% of all respondents stated that they didn't know the intention to operate AS before completing the questionnaire. Of all those informed, 76% were men. Also, the higher the respondents' level of education, the more they knew about the intended operation of AS. Only 25% of respondents believed that AS would remain confined to a research and experimental context. The results show that the average number of respondents who are related to the sector are more optimistic about the development of automated ships (79%), compared to those who are not (68%). They assessed their level of optimism for the successful long-term operation of merchant AS in Greek ports using a five-point Likert scale ranging from "strongly disagree" to "strongly agree". The responses were as follows: 13% strongly disagree, 31% disagree, 35% remain neutral, 14% agree, 8% strongly agree. According to Kyriakidis et al. (2015), safety or and security affect mostly the use of automated vehicles. The denial to accept comes from their association with risk and lack of control. In this study about vessels, the majority of responses (25%) identified safety as the primary obstacle to AS implementation. Social rejection followed with 15%, while security was considered by 14%. This is followed by legislation (12%), initial investment costs (12%), operation and maintenance expenses (7%), risk of coexistence with conventional ships (7%), insurance issues (6%), 1% other reasons and 1% of the responses indicated that there will be no obstacles. According to Kooij et al. (2018), AS technology is more expensive than conventional ones, making the economic problem more critical than the technological problem. In this study, participants ranked this obstacle 4th and 5th. Participants were asked to rate their perception of the future benefits of AS using a five-point Likert scale, as before. Specifically, they were asked to rate whether AS will work or function effectively in the future. Of the respondents, 5% strongly disagreed, 18% disagreed, 33% remained neutral, 28% agreed and 17% strongly agreed with the statement. The results indicated that a greater number of participants agreed with the benefits of AS, compared to those who disagreed. Although the majority appeared pessimistic about the operation of merchant AS in Greece, most of the participants seem to appreciate the benefits of AS. Women seem to recognize slightly more these benefits, as the response rate was slightly higher in the case of this gender. This statement indicates the gender gap in acceptance of AV technology. Participants were asked to rate their beliefs about the potential benefits of merchant AS for shipping companies using a five-point Likert scale ranging from "not at all beneficial" to "extremely beneficial". The results showed that 4% strongly disagreed, 6% disagreed, 23% were neutral, 39% agreed and 28% strongly agreed. Overall, the majority of participants believed that shipping companies would benefit from the use of merchant AS. A lack of knowledge can lead people to believe that they are unable to directly assess the risks and benefits associated with a technology. It is obvious that once AS are operational, the training requirements will modify. At the question about the job diversification, only 29% believed that it was not feasible to modernize and properly train personnel, while 6% refrained

from answering. Between remote ship-navigation from land and on board seafarer work, 33% preferred the former and 67% the latter mode of work, respectively. Of those who preferred to work on board, 26% were men and 8% were women. Notable the heterogeneity of samples appears to play a role in shaping the diversity of trust level observed across age groups (Jing et al., 2020). From the processing of the results, it appeared that as the level of education increases, the willingness to work on board decreases. Specifically, the trend line describing the results was exponential with a r^2 0.9. Overall, 68% of respondents believe that after AS, jobs will decrease, 8% believe they will increase and 15% that they will remain the same. The remaining 9% avoided to answer this question. According to the final score of the responses for each ship-type category, the study revealed that the preference ranking for automation was as follows: container, general cargo, bulk carriers, towing/auxiliary ships, tankers and finally passenger vessels. There were some optimistic views that for merchant AS, it would be a great economic benefit to degrade the staff, also piracy could be reduced. Automation may downscale accidents in maritime. Considering how the human factor affects accidents and environmental pollution, under certain conditions merchant AS could make a positive contribution to modern society. The shipping industry is very profitable and therefore controls a huge percentage of the world economy. Some people think that the operations of a ship can be automated to a very large extent. It is possible that in the coming decades AS will operate mainly in short-distance shipping. Merchant AS are intended on the condition that the ports and the entire evolved zone is also updated. Some of the concerns identified from the respondents' comments are that the lack of ship-crew is dangerous to deal with damages, it is more difficult the ship function without technicians (e.g. engineers) against captain, the cost of new technology and specialized human trainings will be increased, there is possibility that the ports of economically weaker countries with a low level of expertise and technology would face problems, while special attention and examination of safety is required. Those who expressed a negative opinion regarding the AS state that in a country like Greece that does not provide safe human means of transport, it will not be able to support this level of technology. The alteration of the profession, staff and salary reduction is undesirable. Limited automation is preferable. Captains also are proud and gloat over their role. It was also mentioned that the strong safety rules that exist will not allow AS function.

5 CONCLUSION

The purpose of this research study is to determine whether the respondents are optimistic and positive about the introduction of ship operation, as this intention is influenced by social acceptance. As previously mentioned, the research was primarily shared to people who are either had a direct connection to the subject matter or held a high level of scientific knowledge and education. According to other researchers the latter group have the ability to recognize more the benefits than the risks that technology entails. The development of increasing levels of autonomy must be addressed to ensure safety and allow the law to be maintained. Guidelines for operations are required for vessels categorized under the four levels of autonomy. Future research could expand on the necessity for a workforce with enhanced skill sets, in light of emerging technologies. Providing incentives such as better working conditions and financial rewards can enhance crew acceptance. Besides, a main concern for the future is the potential replacement of personnel by technology. It is worth noting that the crew will not be completely absent but will be transferred to a remote operations center. This can potentially lead to unspecified hazards and risks. Moreover, to advance future research, it is recommended to enhance research efforts at lower educational levels to capture the impact on responses.

References

- Allal AA, Mansouri K, Qbadou M, Youssfi M (2017) Task human reliability analysis for a safe operation of autonomous ship. Paper presented at the 2nd International Conference on System Reliability and Safety. IEEE. doi:10.1109/ICSRS.2017.8272800
- Allal AA, Mansouri K, Youssfi M, Qbadou M (2018) Toward energy saving and environmental protection by implementation of autonomous ship. Paper presented at the 19th IEEE Mediterranean Electrotechnical Conference. IEEE. doi:10.1109/MELCON.2018.8379089
- Bureau Veritas Marine & Offshore (2019), Guidelines for Autonomous Shipping, https://erules.veristar.com/dy/data/bv/pdf/641-NI_2019-10.pdf. Accessed 10 Feb 2023

- Burmeister HC, Bruhn WC, Rødseth ØJ, Porathe T (2014) Autonomous unmanned merchant vessel and its contribution towards the e-Navigation implementation: The MUNIN perspective. *International Journal of e-Navigation and Maritime Economy* 1:1-3. doi:10.1016/j.enavi.2014.12.002
- Burmeister HC, Bruhn WC, Rødseth ØJ, Porathe T (2014) Can unmanned ships improve navigational safety?. Paper presented at the Transport Research Arena 2014. Paris.
- Coraddu A, Oneto L, de Maya BN, Kurt R (2020) Determining the most influential human factors in maritime accidents: A data-driven approach. *Ocean Engineering* 211:107588. doi:10.1016/j.oceaneng.2020.107588
- de Vos J, Hekkenberg RG, Banda OA (2021) The impact of autonomous ships on safety at sea—a statistical analysis. *Reliability Engineering & System Safety* 210:107558. doi:10.1016/j.ress.2021.107558
- EMSA. Annual overview of marine casualties and incidents 2022. <https://safety4sea.com/emsa-annual-overview-of-marine-casualties-and-incidents-2022/>. Accessed 20 Mar 2023
- Greece – International Freight Center (2017) https://assets.ey.com/content/dam/ey-sites/ey-com/el_gr/topics/logistics-/logistics-survey-en.pdf. Accessed 15 Feb 2023
- Hinostroza MA, Xu H, Soares CG (2021) Experimental results of the cooperative operation of autonomous surface vehicles navigating in complex marine environment. *Ocean Engineering* 219:108256. doi:10.1016/j.oceaneng.2020.108256
- IMO (1999) Amendments to the Code for the Investigation of Marine Casualties and Incidents. Available via IMO. [https://wwwcdn.imo.org/localresources/en/OurWork/MSAS/Documents/Res.MSC.255\(84\)CasualtyInvestigationCode.pdf](https://wwwcdn.imo.org/localresources/en/OurWork/MSAS/Documents/Res.MSC.255(84)CasualtyInvestigationCode.pdf). Accessed 10 Mar 2023
- IMO (2021) Outcome of the regulatory scoping exercise for the use of Maritime Autonomous Surface Ships (MASS). Available via IMO. <https://wwwcdn.imo.org/localresources/en/MediaCentre/PressBriefings/>. Accessed 15 Jan 2023
- Jing P, Xu G, Chen Y, Shi Y, Zhan F (2020) The determinants behind the acceptance of autonomous vehicles: A systematic review. *Sustainability* 12:1719. doi:10.3390/su12051719
- Kooij C, Colling A, Benson C (2018) When Will Autonomous Ships Arrive? A Technology Forecasting Perspective. Paper presented at the INEC Conference 2018
- Kum S, Sahin B, (2015) A root cause analysis for Arctic Marine accidents from 1993 to 2011. *Safety science* 74:206-220. doi:10.1016/j.ssci.2014.12.010
- Kyriakidis M, Happee R, de Winter JC (2015) Public opinion on automated driving: Results of an international questionnaire among 5000 respondents. *Transportation Research Part F: Traffic Psychology and Behaviour* 32:127-140. doi:10.1016/j.trf.2015.04.014
- Lee JD, See KA (2004) Trust in automation: Designing for appropriate reliance. *Human factors* 46:50-80. doi:10.1518/hfes.46.1.50_30
- Munim ZH (2019) Autonomous ships: a review, innovative applications and future maritime business models. In *Supply Chain Forum: An International Journal* 20:266-279. doi:10.1080/16258312.2019.1631714
- Navas de Maya B, Kurt RE, Turan O (2018) Application of fuzzy cognitive maps to investigate the contributors of maritime collision accidents. Paper presented at the 7th Transport Research Arena 2018.
- Negenborn RR, Goerlandt F, Johansen TA, Slaets P, Valdez Banda OA, Vanelslander T, Ventikos NP (2023) Autonomous ships are on the horizon: here's what we need to know. *Nature* 615:30-33.
- Pande D, Taeihagh A (2021) Investigating User Acceptance of Autonomous Systems: A Singapore Perspective on Governance using a modified UTAUT, Paper presented at the 5th International Conference on Public Policy. Barcelona. Spain
- Rothblum AM (2000) Human error and marine safety. In *National Safety Council Congress and Expo*
- Siegrist M (1999) A causal model explaining the perception and acceptance of gene technology. *Journal of Applied Social Psychology* 29:2093–2106. doi:10.1111/j.1559-1816.1999.tb02297.x
- Siegrist M (2000) The influence of trust and perceptions of risks and benefits on the acceptance of gene technology. *Risk Analysis* 20:195–203. doi:10.1111/0272-4332.202020
- Siegrist M, Cvetkovich G (2000) Perception of hazards: The role of social trust and knowledge. *Risk Analysis* 20:713–720. doi:10.1111/0272-4332.205064

- Van Hooydonk E (2014) The law of unmanned merchant shipping—an exploration. *The Journal of International Maritime Law* 20:403-423
- Wróbel K, Montewka J, Kujala P (2017) Towards the assessment of potential impact of unmanned vessels on maritime transportation safety. *Reliability Engineering & System Safety* 165:155-169. doi:10.1016/j.ress.2017.03.029
- Xu Z, Zhang K, Min H, Wang Z, Zhao X, Liu P (2018) What drives people to accept automated vehicles? Findings from a field experiment. *Transportation Research Part C: Emerging technologies* 95:320-334. doi:10.1016/j.trc.2018.07.024

Performance of a system of detached breakwaters on the South Corinthian Gulf

E. Papafotiou^{1*} and Th Giantsi.²

^{1,2} Laboratory of harbour Works, NTUA, Iroon Polytechniou 7 Zografou 15780

*Corresponding author: papafotiuev@central.ntua.gr

Abstract

The shoreline of the South Corinthian Gulf faces erosion, causing major problems to the inhabitants. The first signs of the problem appeared in Seventies. Later in 1990 a research project was conducted by the Laboratory of Harbour Works (LHW), NTUA, to investigate the problem. Main result of the project was the classification of the eroded areas according to the risk of land loss. 19 Areas were eroded. Three areas among them were selected to be protected by coastal structures. Among these three areas the area of Kiato, Korinthia, is included, where a system of detached breakwaters was proposed, protecting the whole area up to the fishing retreat of Kiato. The area southwest of Kiato, Korinthia has experienced many problems due to erosion. The erosion phenomena were so severe that the adjacent houses began to show signs of collapse. This paper examines the performance of these breakwater using MIKE 21 by DHI. Two main scenarios are simulated. The first scenario uses as a forcing power the equivalent waves in each direction and the second scenario uses as a forcing power the wind that has been measured in the area. Finally, the results, concerning the evolution of the coastline, of the simulation for the two main scenarios are presented, as well as the topographic measurement that took place in July 2017.

Keywords Coastal erosion; monitoring; detached breakwater; MIKE21.

1 INTRODUCTION

The study area is the South Corinthian gulf. More specifically, the study area starts inside the city of Corinth at the east and terminates at Mavra Litharia Evrostinis on the west. Many parts in the study area have experienced the consequences of intense and chronic erosion. In the past some scientific programs have evaluated erosion in the study and measures have been proposed to confront the erosion and classified each subarea based on the intensity of the phenomena. A part of the proposed measures were the breakwaters that were constructed in Kiato, Korinthia.

In the area around the breakwaters, erosion was so intense that part of the adjacent estuary of Asopos river, located southeast of the breakwaters, was destroyed. Moreover, part of the road located northwest of the estuary was collapsed. Before the construction of the breakwaters, dealing with the phenomena of coastal erosion in the area included the placement of armor rocks in front of the houses and the road. The sediments in the area are mostly sand and sand-gravel. These breakwaters were constructed in 2009 when the sea reached the yards of the houses.

2 CHARACTERISTICS OF THE AREA OF THE BREAKWATERS

2.1 Bathymetry

The gradient of the seabed around the breakwaters is mild. There are not sudden changes of depth, and the depth contours are mostly parallel to the coastline. Therefore, the solution of breakwaters was something feasible for this area.

2.2 Sediments

In the context of the past research program of the Laboratory of Harbour Works a sediment analysis in the area was conducted. The places from where the sediment was taken were specific and the sediment was taken on two different dates. Following that, a granulometric analysis took place and the granulometric curves of the sediment were designed.

2.3 Wind data in the study area

The most common winds in the area do not surpass 5 Bf, therefore, the winds here are characterized as mild.

For a better capture of the wind climate in the area to be considered, wind data were received from the National Observatory of Athens. This wind data consists of the speed and the direction of the observed wind. The time step of this time series was 10 minutes. We received the observations that cover the time between the construction of the breakwaters until the end of 2016. Two time series were received. The first one was the time series of the weather station of Isthmus and the second one was the time series of the weather station of Kiato. The time series of Isthmus contained data which covered the years between 2009-2014. The time series of Kiato contained data which covered the years 2015-2016. This happened because the weather station of Kiato started operating in 2015, therefore, there were not past data from this area, or other weather station closer to Kiato. Following that, a statistical analysis was conducted, and the wind frequency table was formed only for the Isthmus station. We chose that because the observations of the Kiato station were low in number to conduct a statistical analysis of the wind climate in the area.

3 SIMULATION SCENARIOS

The simulation of the wave field, the current field, the sediment transport as well as the coastline evolution of the breakwaters area were conducted using two different scenarios. The first scenario was the scenario using constantly variable wind as a forcing power. In this scenario the observations of the Isthmus weather station were used for the years from 2009 to 2014 and the observations of the Kiato weather station were used for the years 2015-2016. The initial time series had a time step of ten minutes. Due to the great number of the observations a refinement in the number of observations took place by changing the time step of the observations to twelve hours.

The second scenario was the forcing using the equivalent deep-water waves. That is, for every main direction of wind (north, east, south, west), the characteristics (height, period) of the equivalent deep-water wave were computed from the wind speeds and these waves are used as boundary conditions.

Moreover, three different sub-scenarios were used. Each scenario represented a different diameter of sediment grain. Three different grain diameters were chosen (0.20 mm, 0.25 mm, 0.50 mm) as a sensitivity analysis. The closest to the actual grain diameter size is the size of 0.25mm. All the scenarios and sub-scenarios can be seen in the following table.

Table 1. Simulation scenarios

Scenario	Sub-scenario	Forcing power	Grain diameter
S.1	S.1.1	Equivalent deep-water waves	0.20 mm
	S.1.2	Equivalent deep-water waves	0.25 mm
	S.1.3	Equivalent deep-water waves	0.50 mm
S.2	S.2.1	Variable wind	0.20 mm
	S.2.2	Variable wind	0.25 mm
	S.2.3	Variable wind	0.50 mm

3.1 Equivalent deep-water waves

For the equivalent deep-water waves to be computed, the effective fetches in every main direction were computed. Subsequently, using Jonswap formulae, the wave characteristics for every main direction were computed.

Then using the Borah and Ballofet (1985) formulae (1,2) the characteristics of the equivalent deep-water waves were calculated.

$$T_e = \frac{\sum T_i f_i}{\sum f_i} \quad (1)$$

$$H_e^2 T_e = \frac{\sum H_i f_i}{\sum f_i} \quad (2)$$

H_i = Deep waters wave height

T_i = Deep waters wave period

f_i = Appearance frequency of waves

The characteristics of the equivalent deep-water waves can be seen in the following table:

Table 2. Equivalent deep water waves characteristics

DIRECTION	T_i	H_i
NORTH	$T_e = 1.803$ s	$H_i = 0.360$ m
EAST	$T_e = 1.880$ s	$H_i = 0.320$ m
SOUTH	$T_e = 0.819$ s	$H_i = 0.075$ m
WEST	$T_e = 0.828$ s	$H_i = 0.058$ m

3.2 Variable wind

In the second scenario the actual wind observation was used as a forcing power. These observations arose from the time series of the wind stations of Isthmus and Kiato. However, using a time step of 10 minutes on the model would be computationally heavy, therefore a refinement took place. We used the observations corresponding to 12 hours' time step, thus leading us to a time series of 6575 observations with time step of 12 hours. The time step in the program was adjusted to 43200 sec.

4 SIMULATION RESULTS AND PRESENT-DAY SITUATION COMPARISON

The program used for the simulation was Mike 21 by DHI. To obtain the present-day coastline as a comparison reference point, a topographical mapping of the coastline was conducted on 22/7/2017. By using a topographical G.P.S. we were able to capture the coastline position of that day and plot it in a drawing. For comparison purposes in the same drawing the initial coastline position before the construction of the breakwaters was plotted as well. Finally, the simulation results for each different scenario were plotted in the same drawing for comparison purposes. Finally, for comparison purposes, a drawing containing the original coastline, the mapped coastline as well as the two different scenarios (with common grain diameter) coastlines was created.

In the following figures the coastline evolutions resulting from each scenario are visible, as well as the comparison of the two scenarios in the same figure.

In all the following comparisons we will make use of the same three zones:

- Upstream of the first breakwater (K1 in the figures), where erosion is expected
- Behind the first breakwater (K1 in the figures), where accretion is expected
- Behind the second breakwater (K2) in the figures, where accretion is expected

We will not make use of the zone downstream the second breakwater because the estuary of the river is close to this zone, thus it alters the geomorphologic conditions in this zone.

4.1 Coastline evolution results of Scenario 1

By comparing the three sub-scenarios in each zone the following conclusions are made:

- In the zone upstream of the first breakwater, the expected erosion appears in the sub-scenarios S.1.2 and S.1.3. In sub-scenario S.1.1, in this zone, some accretion appears, a phenomenon which is not expected in this zone. Maybe this appears due to the action of the currents of the coastal zone or because the grain diameter size is smaller than the actual grain diameter size of the area. In this zone the closest to reality simulation is the simulation of S.1.2. In this sub-scenario the grain size diameter is the closest to the actual grain size in the area.

- Behind the first breakwater where accretion is expected, in S.1.3 and S.1.2 the expected accretion appears. In S.1.1, in this zone, both erosion and accretion appear. The erosion in this zone is not expected. Moreover, S.1.1 overestimates the accretion that appears in this zone. In this zone the closest to reality simulation is the simulation of S.1.2.
- Behind the second breakwater accretion is expected. In all the three sub-scenarios accretion appears but this accretion is overestimated. In this zone the closest to reality simulation is the simulation of S.1.1.

In overall, the Scenario 1 simulates the coastline evolution satisfactorily. The biggest problems appear behind the second breakwater, where the expected accretion is overestimated in all sub-scenarios. In total the sub-scenario in which mistakes do not appear (unexpected accretion or erosion) is the sub-scenario S.1.2.

4.2 Coastline evolution results of Scenario 2

By comparing the three sub-scenarios in each zone the following conclusions are made:

- The expected erosion upstream of the first breakwater is present in all of the three sub-scenarios. The closest to the reality sub-scenario in this zone is the S.2.3.
- At the beginning of the zone behind the first breakwater, in all the sub-scenarios accretion appears. However, in the continuation of this zone, in the scenarios S.2.1 and S.2.3, unexpected erosion appears. Sub-scenario S.2.2 simulates the expected accretion satisfactorily in this entire zone. The closest to reality sub-scenario in this zone is the S.2.2.
- Behind the second breakwater, in all the three sub-scenarios, accretion is present. The closest to the reality sub-scenario in this zone is the S.2.2.

In overall, the Scenario of variable wind, S.2, simulates the coastline evolution with very good results. However, unexpected erosion appears in the sub-scenarios S.2.1 and S.2.3, in the zone behind the first breakwater. Only the sub-scenario S.2.2 simulates the expected accretion in this zone. In the zone behind the second breakwaters all sub-scenarios simulate the coastline evolution satisfactorily.

In total, the simulation of the sub-scenario S.2.2 is the closest to the reality in this Scenario.

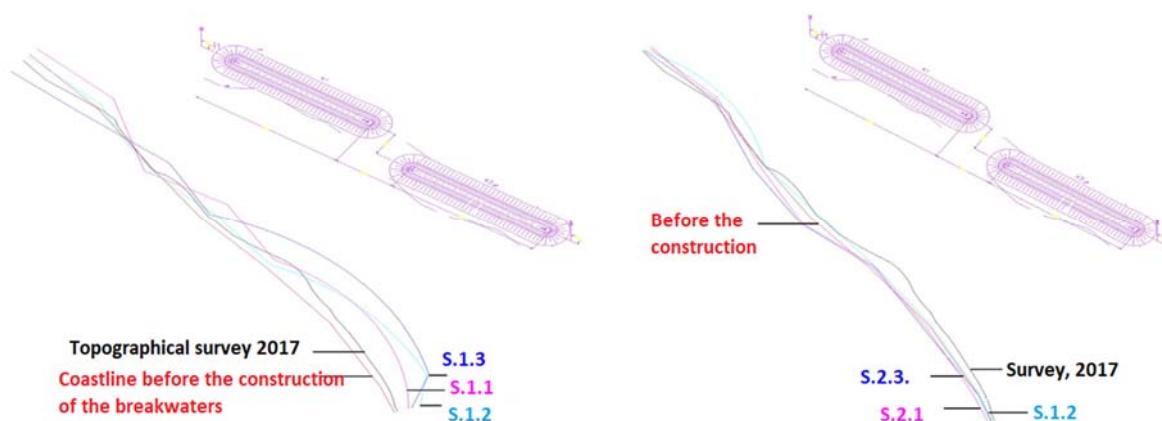


Figure 1. Coastal evolution results of Scenarios 1,2

4.3 Comparison of the coastline evolution of the two sub-scenarios S.1.2 and S.2.2.

To compare the coastline evolution computed by the two basic scenarios, we selected a common sub-scenario, that is sub-scenario 2. This sub-scenario is the closest to the reality in both basic scenarios.

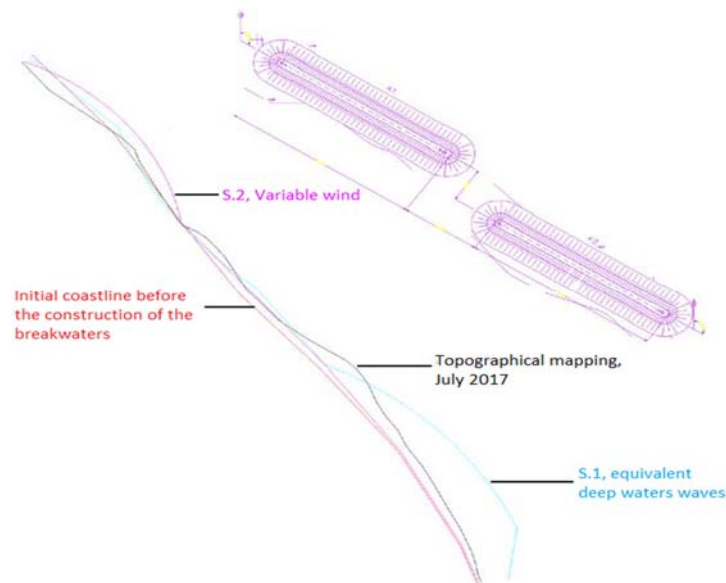


Figure 2. Comparison between the simulation and actual coastline evolution

By comparing the three sub-scenarios in each zone the following conclusions are made:

- The expected erosion upstream of the first breakwater is present in the two basic Scenarios.
- In the zone behind the first breakwater, Scenario S.2 tends to underestimate the expected accretion. In Scenario S.1 the expected accretion is present, however overestimated.
- In the zone behind the second breakwater, Scenario S.1 is at first close the actual present-day coastline but then overestimates greatly the expected accretion. On the contrary, Scenario S.2 underestimates the expected accretion, although, it is very close to the actual present-day coastline.

5 DISCUSSION AND CONCLUSIONS

Following this comparison of the results, it is evident that the approximation of variable winds is the one that calculates more accurately the coastline evolution in this area. This is expected, because the variable wind approximation approaches better the reality of the wind climate of the area. The approximation of equivalent deep waters waves remains merely a statistical approach to the observed waves in the area and may not be suitable for evaluating the coastline evolution. In S.1 the expected areas of accretion and erosion are correct, albeit with great deviations from the reality.

Acknowledgements

At this point we would like to thank DHI and its representative in Greece, Mr. Elias Mousoulis for the concession of the academic license of Mike 21.

References

- Lagouvardos, Kotroni, Bezes, Koletsis, Kopania, Lykoydis, Mazarakis, Papagiannaki, Vougioukas (2017) 'The automatic weather stations NOANN network of the National Observatory of Athens: operation and database'
- LHW, 1998, Research program 'Erosion of the coastline of the South Corinthian Gulf', L.H.W. N.T.U.A
- Papafotiou E., 'Coastal zone management in the south Corinthian gulf – Numerical computation of the performance of Kiato breakwaters', Master thesis
- Borah D.K. and Balloffet A. (1985), 'Beach evolution caused by littoral drift barrier', J. of Waterway, Port, Coastal and Ocean Eng., ASCE, vol 111, no4, 645-660

Kinematic perturbations in submerged breakwaters under waves

E. Repousis^{1*}, N. Diplarakos¹, I. Roupas¹, C. Memos¹

¹Laboratory of Harbour Works, School of Civil Engineering, National Technical University of Athens, Zografos, 15780, Greece

*Corresponding author: elpirep@hotmail.com

Abstract

Permeable submerged breakwaters (SPBs) can be successful in abstracting wave energy in micro-tidal coastal regions of up to average wave exposure. In parallel they may behave similarly to natural reefs in attracting marine life. To assess this latter function, development of the hydrodynamic field inside their body is predicted with respect to pore pressure and orbital velocities, which are the core hydrodynamic parameters playing a key role on marine life habitation. Basic aim of this study is to focus on the relation of turbulence levels to mean values of the parameters of interest, to provide a better understanding of SPBs' permeability effect on them and assess the need of considering wave kinematic perturbations when investigating the level of marine life support in SPBs. To do so, laboratory measurements for a series of physical models of SPBs under scale were analysed to quantify deviations from average values of the hydrodynamic parameters mentioned, due to turbulence phenomena. In most relevant studies researchers tend to discard the turbulent component but data analysis showed that fluctuations due to turbulence are significant and should be considered when examining the potential of an SPB to function as an artificial habitat.

Keywords Submerged breakwater, Hydrodynamic turbulence, Orbital velocity, Pore pressure.

1 INTRODUCTION

As environmental awareness gradually increases, submerged breakwaters have become a shore protection alternative to their emerged counterparts, aiming at confining the adverse environmental impact of the latter that includes low level of water renewal, degradation of the aesthetic value of the landscape, occupation of relatively large seabed areas, etc. Beyond the basic role of such structures in stabilizing the coast in micro-tidal regions, it has been deduced that especially rubble mound submerged permeable breakwaters (SPBs) may function similarly to natural reefs in attracting marine life. The response of marine organisms to the presence of SPBs has not yet been investigated in-depth. However, hydrodynamic parameters as pore pressures and orbital velocities, inside their permeable body, have been observed to be significant factors in supporting marine life within and around these bars, in terms of, for example, distribution-species biodiversity and abundance (e.g. Siddon & Witman 2003). It has been stressed so far that acquiring information on the hydrodynamic field, including maximum wave-induced forces as well, directly related to pore pressures, is important in order to assess SPBs' ecological potential (e.g. Kontaxi & Memos 2005, Moschella et al. 2005). Vital parameters in forming tolerable and proper living conditions for each species may be different but at this point it can be reasonably argued that water velocities and pressures correlated with hydrodynamic forces, are the key hydraulic factors governing marine habitation levels (e.g. Siddon & Witman 2003, Hammond & Griffiths 2004). What is to be noted is that in addition to mean velocities and pressures, extreme values are equally important in governing those levels (e.g. Siddon & Witman 2003).

Although several studies on processes around submerged breakwaters can be found in the literature, the kinematics inside a SPB is a field of relatively less research. This study aims at giving quantitative information on parameters useful to marine scientists for accessing the ecological potential of SPBs on marine life focusing on the relation of turbulence levels to mean values of the crucial parameters of particle velocities and hydrodynamic pressures. Due to the turbulent nature of the hydrodynamic field associated with wave propagation inside and around an SPB, significant deviations from the average values are expected to be developed. However, most numerical models deal with mean quantities, due to the complexity of the phenomenon that makes numerical simulation a very difficult, if not currently

impossible, undertaking. A few models predicting the hydrodynamic field under wave propagation inside a SPB have been proposed in terms of mean values (e.g., Losada et al. 1995, Lara et al. 2006, Chan et al. 2007, Metallinos et al. 2014) but their verification with “non averaged” experimental data is still limited. Systematic research on porous flow through rubble mounds, including measurements of velocity and its turbulent component for oscillatory streaming flow conditions, yielded a model proposed by Van Gent (1995), claiming to be suitable also for SPBs under wave action. However, in this work the porous models were restrained into a U-tube channel and turbulence produced should be considered as restricted to smaller scales as compared to an SPB physical model under wave action.

This study focused on data analysis of detailed experimental measurements for quantifying the turbulence levels for both pore pressures and orbital velocities developing inside a series of SPBs physical models and thus providing an overall view and quantitative information on estimating turbulence and its relation to mean values of these parameters.

2 EXPERIMENTAL SET-UPS

Within this work, the hydrodynamic field inside SPBs under regular breaking and non-breaking waves is studied through experimental data analysis of the turbulence levels of both the hydrodynamic (pore) pressure component and the orbital velocities. To this end timeseries were used of the total values of these parameters evolving inside physical SPB models under scale around 1:10.

2.1 Hydrodynamic pressure

2.1.1 TU Delft experiments

The first set took place at TU Delft’s Laboratory of Fluid Mechanics of Civil Engineering and Geoscience Department (Roupas 2019). It was conducted in a wave flume of 42 m length, 0.8 m width and 1 m height. Two physical models of submerged breakwaters of porosity equal to 0.4 were made, namely SPB1 and SPB2. Both structures were made of uniform natural stones of mean diameter d_{50} around 0.1 m, sloping 1:1.5 at both sides and height equal to 0.5 m. Crest width for SPB1 was 0.4 m and for SPB2 0.65 m. Two sea depths were tested of 0.65 and 0.7 m giving free boards of 0.15 m and 0.2 m, respectively. In regard to SPB geometry and water depth, in total four different sections of SPBs were formed and tested. The structures were tested for regular waves with incoming height (H_i) ranging from 0.06 m to 0.23 m and wave period (T) ranging from 1.0 s to 2.5 s. Pressure gauges were placed at the level of seabed on the projected center of both the upstream and downstream slopes through small holes. Thus two measurement locations were considered, while the recording frequency was 100 Hz.

2.1.2 NTUA experiments

The second set of experiments was conducted in the Laboratory of Harbour Works, National Technical University of Athens, in a 27 m long, 0.60 m wide and 1.53 m high wave flume (Metallinos et al. 2014). One physical model of submerged breakwater of porosity equal to 0.5 was made, namely SPB3. Specifically, the height of the physical model was 0.40 m and the crest width 1.0 m. The structure’s material was natural stones of $d_{50} = 0.08$ m and sloping 1:2 at both sides. Two sea depths were tested of 0.45 m and 0.5 m giving free boards of 0.05 m and 0.1 m, respectively, resulting in two different cross-sections of SPBs. The SPB3 was tested for regular waves with H_i ranging from 0.04 m to 0.107 m and T ranging from 1.3 s to 2.1 s. Two measurement locations were considered from the acquired primary data through pressure gauges at the seabed level on the projected center of both the upstream and downstream slopes, likewise for SPB1 and SPB2. The recording frequency used was 200 Hz.

2.2 Orbital velocities

For this experimental session, the same experimental layout at TU Delft’s Laboratory was used as presented for hydrodynamic pressures (see Sect. 2.1.1). Thus, measurements for orbital velocities for SPB1 and SPB2 were acquired (Diplarakos 2018). An Acoustic Doppler Velocimeter was used that recorded the three orbital velocity components. Two measurement locations were considered, each one on the center of the upstream and downstream slopes and higher by around 0.15 m than the flume bed.

2 DATA ANALYSIS

3.1 Hydrodynamic pressure

Firstly, the time series of the hydrodynamic pressure were filtered to remove the (quite limited) noise from the pressure gauges. To do so, the Savitzky-Golay (1964) Finite Impulse Response smoothing filter was used. Then to estimate turbulence levels, phase averaging over the pressure records was applied. Finally, an Extreme Value Analysis of the pressure fluctuations was performed using the “Peaks-Over-Threshold” approach to assess the probability of extreme events. Records of about 50s duration were used throughout.

3.2 Orbital velocities

Before performing any analysis, the collected data of the velocities were filtered to remove the spikes that commonly appear in Acoustic Doppler Velocimeter records. To do this, the 3-D Phase-Space Despiking method proposed by Goring and Nikora (2002) was employed. Following this process, phase averaging likewise for pore pressures was carried out. Extreme value analysis was then implemented as for hydrodynamic pressures. The Reynolds stress involving horizontal and vertical velocity components was also put under the same Extreme Value Analysis method.

4 RESULTS AND DISCUSSION

Data analysis as described previously was carried out for sea states and structures’ geometries covering a wide range of SPBs applications. Due to space limitations only a representative sample of results are presented in the following. In order to present in a uniform way, the turbulent component of the hydrodynamic parameters in relevance to the exceedance probability of extreme events, a relative wave height, i.e. the ratio of incident wave height to free board (H_i/FB), was considered for each wave test. These values were then sorted in three regions, those below 0.8 with waves tested providing an average value 0.6, between 0.8 and 1.2 with an average of 1.0 and greater than 1.2 with an average of 1.5. From the physical point of view, this three values’ classification can relate to non-breaking, breaking, and broken wave conditions, respectively. The Extreme Value Analysis results of the pressure fluctuations (p'), horizontal velocity fluctuations (u'), and Reynolds stress per unit density $|-u'w'|$ are presented in the following figures correspondingly (Figures 1, 2, and 3).

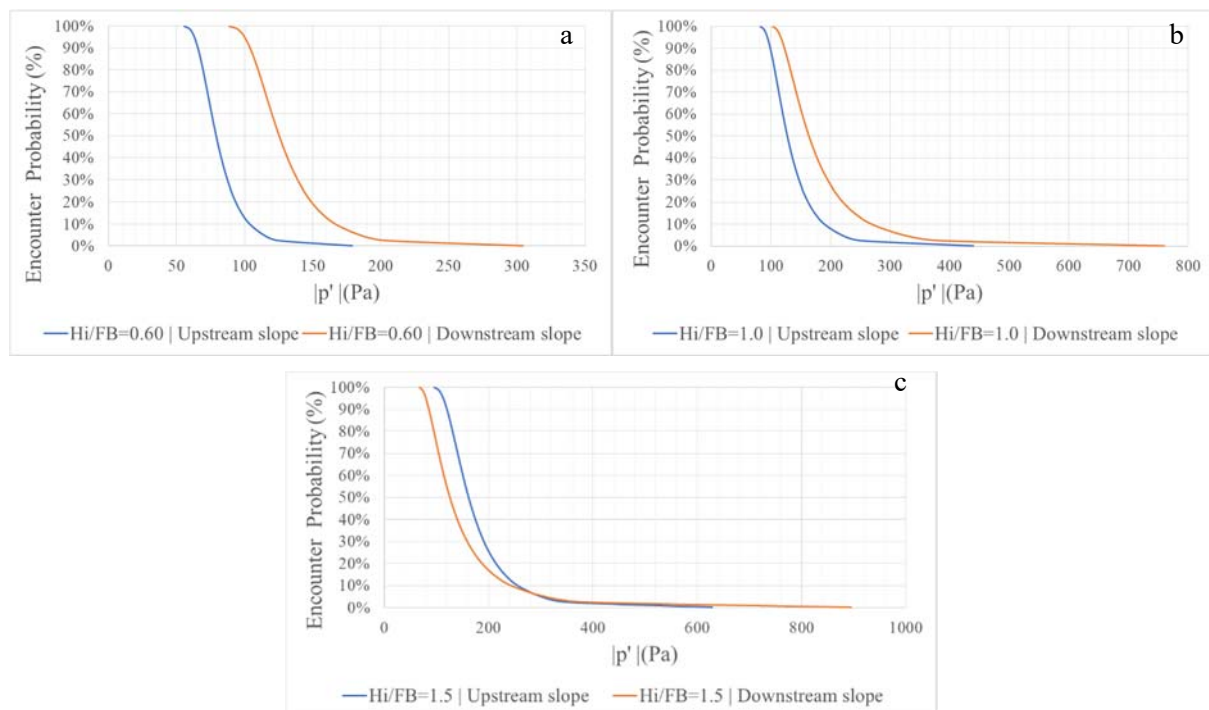


Figure 1. Encounter probability of pressure p' for H_i/FB : **(a)** 0.60, **(b)** 1.0, **(c)** 1.5

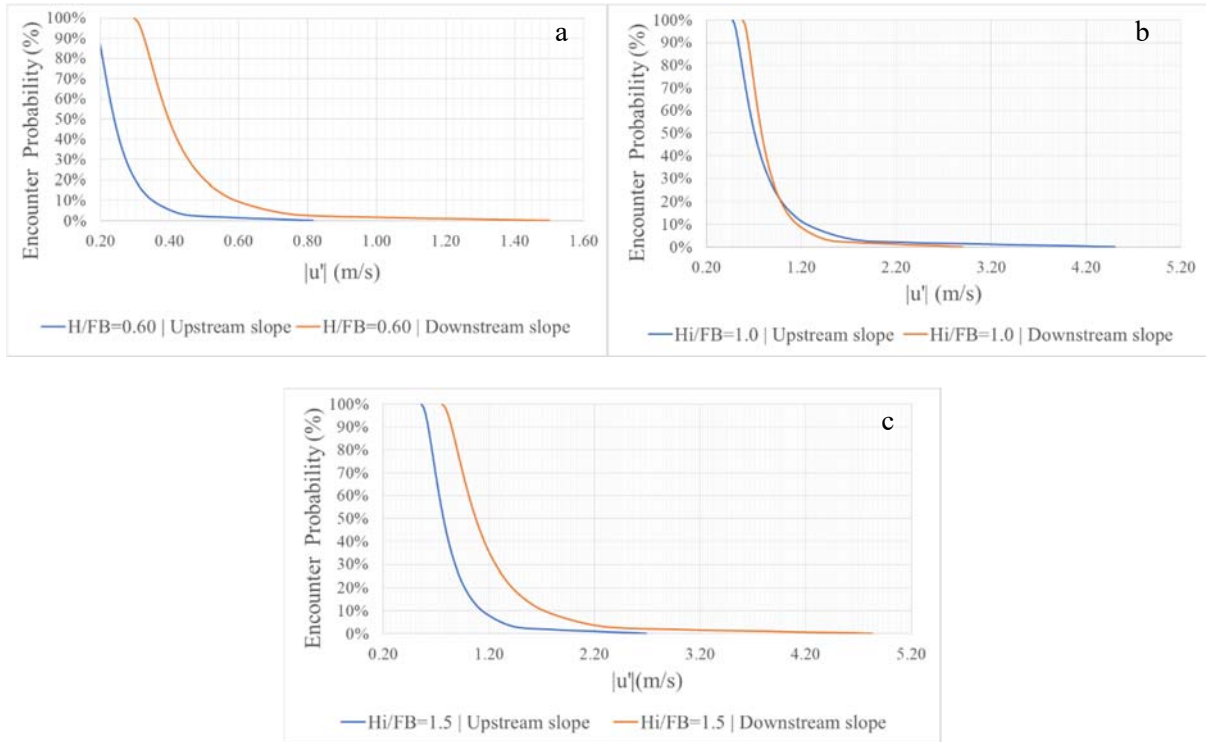


Figure 2. Encounter probability of horizontal velocity u' for H_i/FB : **(a)** 0.60, **(b)** 1.0, **(c)** 1.5

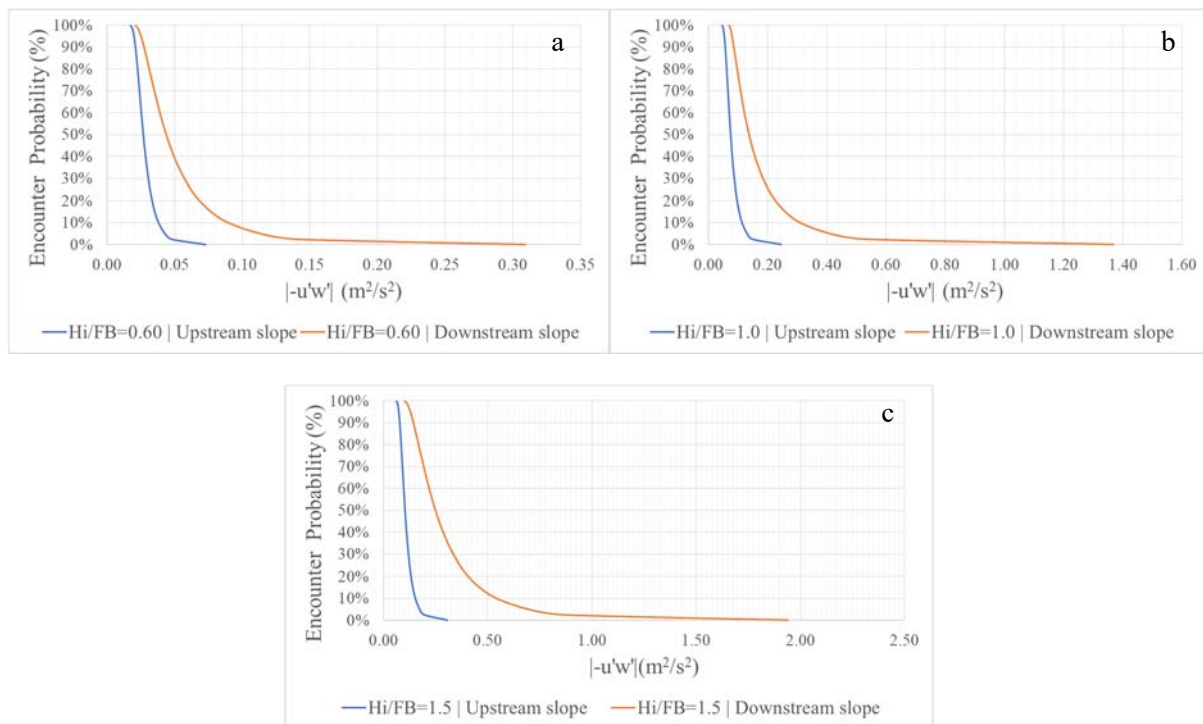


Figure 3. Encounter probability of Reynolds stress $|-u'w'|$ for H_i/FB : **(a)** 0.60, **(b)** 1.0, **(c)** 1.5

In general, for most cases tested, turbulence levels of the velocity-related parameters studied are expected to be greater at the leeward than at the seaward slope of SPBs, although the former is an area protected from waves more than the latter. This is because flow produced by waves develops not only outside but also inside the porous medium of an SPB, releasing there, due to the rough boundaries

present, a significant amount of their energy generating turbulence. Additionally, a residual part of that turbulence tends to enrich more the downstream rather than the upstream region (Figure 2, panels a and c). Of course, the said process is at an interplay with the location, in relation to the mound, and the type of wave breaking, an action that normally releases a high amount of turbulence; see, e.g., Figure 2, panel b, where this interplay produces a balanced result.

Regarding the actual turbulence levels, the overall obtained results showed that horizontal orbital velocities present significant fluctuations from mean values, while perturbations level in pore pressures is lower but still not negligible. Indeed, comparison with the corresponding mean values showed that on average, hydrodynamic pressures may present maximum fluctuations of up to 10% of their mean values, while for horizontal orbital velocities turbulence seems to be more energetic with mean fluctuations ranging between 70% and 180%, with an average close to 100%, of the mean horizontal velocity. If we focus on rare events, fluctuations can increase considerably. However, in real life these values are expected to be lower due to scale effects that enhance turbulence in reduced models. None the less, the above results show that when estimating hydrodynamic parameters during an SPB design, turbulence contribution is not to be overseen, especially when assessing the marine habitation merits of the structure.

Acknowledgements

Thanks are due to the heads and staff of the relevant TUDelft and NTUA Laboratories for making available their installations for this experimental work, and to H J Verhagen for co-supervising the Delft experiments.

References

- Chan HC, Leu GM, Lai CJ (2007) Velocity and turbulence field around permeable structure: Comparisons between laboratory and numerical experiments. *J. Hydraulic Research*. 45(2), 216-226.
- Diplarakos N (2018) Turbulence at Submerged Permeable Breakwaters, MSc Thesis, NTUA (in Greek)
- Goring G and Nikora V (2002) Despiking Acoustic Doppler Velocimeter Data. *Journal of Hydraulic Engineering*, doi: 10.1061/(ASCE)0733-9429
- Hammond W and Griffiths ZCL (2004) Influence of wave exposure on South African mussel beds and their associated infaunal communities. *Marine Biology*. 144, 547-552.
- Kontaxi C and Memos CD (2005) Submerged breakwaters as artificial habitats. Proc. 31st IAHR Congress, Seoul, 3967-3975, J. Byong-Ho, I.L. Sang, S.I. Won, C. Gye-Woon, eds. IAHR, Madrid, Spain.
- Lara JL, Garcia N, Losada IJ (2006) RANS modeling applied to random wave interaction with submerged permeable structures. *Coastal Engineering*. 53(5-6), 395-417.
- Losada IJ, Losada MA, Martin A (1995) Experimental study of wave-induced flow in a porous structure. *Coastal Engineering*. 26(1-2), 77-98.
- Metallinos AS, Emmanouilidou MA, Memos CD (2014) Wave-induced pore pressures in submerged rubble mound breakwaters simulated by a compound Boussinesq model. *J. Hydraulic Research*. 52(1), 24-35.
- Moschella PS, Abbiati M, Aberg P, Airolidi L, Anderson JM, Bacchiocchi F, Bulleri F, Dinesen GE, Frost M, Gacia E, Granhag L, Jonsson, PR, Satta MP, Sundelof A, Thompson RC, Hawkins SJ (2005) Low-crested coastal defence structures as artificial habitats for marine life: Using ecological criteria in design. *Coastal Engineering*. 52(10-11), 1053-1071.
- Roupas I (2019) Study of turbulent pressures and wave transmission coefficient at submerged permeable breakwaters, MSc Thesis, NTUA (in Greek).
- Savitzky A and Golay MJE (1964) Smoothing and Differentiation of Data by Simplified Least Squares Procedures. *Analytical Chemistry*. 36 (8): 1627-39.
- Siddon CE and Witman JD (2003) Influence of chronic, low-level hydrodynamic forces on subtidal community structure. *Marine Ecology Progress Series*. 261, 99-110.
- Van Gent MRA (1995) Wave Interaction with Permeable Coastal Structures. PhD Thesis, Delft University of Technology.

Coastal protection works of Liopetri's river "Potamos", Cyprus

S.M. Gouloumis^{1*}, M.G. Karas²

¹Civil Engineer, N.T.U.A., Papaflessa 31 str, T.K. 15772 Zografou, Greece

² Civil Engineer, MSc, University of Southampton, Ammochostos, Paralimni, 5285, Cyprus.

*Corresponding author: spirosxls@gmail.com

Abstract

The Republic of Cyprus Services have undertaken the formation of a fishing port in Liopetri's river 'Potamos' on the SE coast of Cyprus. Nowadays there is a need for 35 berths to accommodate professional fishing boats and 79 berths for amateur boats. During the last decades, illegal building of usually plain sheds and huts on the river's banks, has increased drastically, widening the river, and transforming it into a fishing port, while banks' erosion has also been noted. Due to ongoing construction works, a variety of about 1000 piles of any kind and other structures have been found into the river's banks and bed. The piles have been removed, avoiding disturbing the river's bank. New stainless-steel columns have been installed into the river's banks to support new superstructure to service the fishermen and extra measures have been taken to ensure the banks' protection.

Keywords Riverbanks, protection, erosion, steel columns.

1 GENERAL DESCRIPTION

Town Planning and Housing Department of the Ministry of Interior of the Republic of Cyprus in cooperation with the Department of Fisheries and Marine Research have undertaken the formation of a fishing port at Liopetri's river Potamos on the southeast coast of Cyprus. During the initial phase of the project, an Environmental and Educational Nature Park has been designed respecting the natural environment of the river area, resulting to the smooth operation of the Fishing Shelter, transform it to an important, alternative tourist attraction (1st DMPCO, 2019).

In recent years, many fishing boats have been berthed on the deforested banks, while nowadays there is a need of 35 berths to accommodate professional fishing boats and 79 berths for amateur boats. The river is 630 m long, and its width raises from 15m to 40m, while the width of the estuarine measures up to 110 m. During the last decades, illegal building of usually plain sheds and huts on river's banks has been severely increased, widening the river even more. Banks' erosion has also been noted.

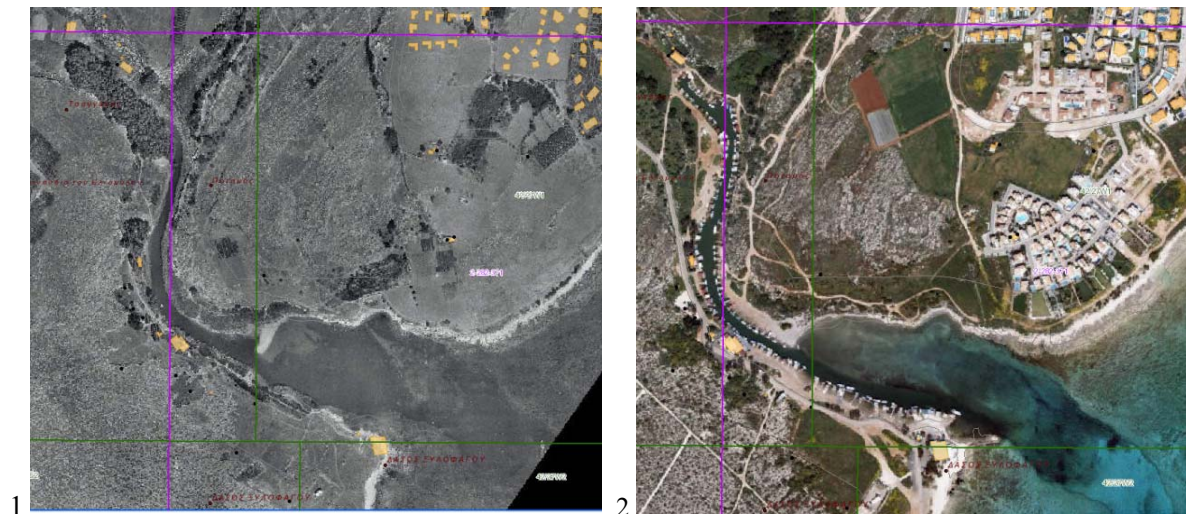
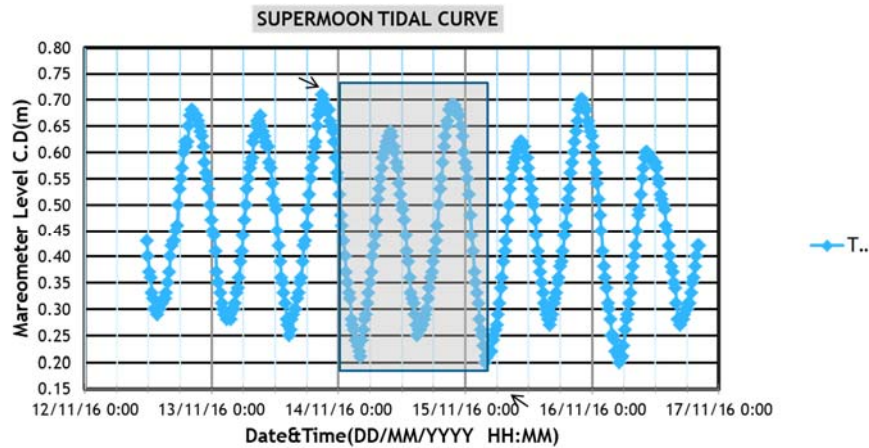


Photo 1. Photographic map of the river (1963). The banks are grown, while only a few structures are visible.
Photo 2. At the newest orthophoto map of 2014, the banks of the river are crowded by numerous structures of any kind and boats, while vegetation is mostly absent

2 WEATHER CONDITIONS

The natural formation of an extended shallow area at the inlet of the river, significantly reduces wave propagation upstream. Sea tide that is rather intense at the Eastern Mediterranean basin, constantly affects the river and its estuary, since surface fluctuation of water constantly alternates the river’s flow, direction, and velocity. It has been noticed by local fishermen that in case of intense winds blowing from south directions coinciding with the maximum tide, total water elevation could possibly exceed 50cm or more in rainy conditions, causing high velocity of river’s flow. As seen below, high tide measured at Ayia’s Napa marina mid November 2016, resulted to intense river flow on low tide.



3 EXISTING STRUCTURES REMOVAL

Special attention was paid to the removal of all existing structures founded into the banks and river’s bed, made of different piles from any kind of material. During the initial phase of the project, every shed or hut was removed by hand and using light machinery and cranes, preventing any demolition, and spread of debris into the river.



Photo 3. Structures made from local fishermen on the riverbanks had to be removed by hand and light machinery

The removal of the foundation piles supporting the sheds and huts, was a challenging task. About 1000 piles had been used throughout the decades, including plain wooden piles, iron piles, plastic or asbestos pipes filled with concrete, barrels filled with stones or concrete and even circular foundation slabs resting on the banks. Barrels and slabs were just founded on the surface of the banks and could easily be lifted off and disposed, while piles and pipes were “nailed” into the soil down to unknown level, acting as deep consolidation of the river’s banks, avoiding soil erosion.



Photo 4. Several platforms were supported on different kinds of piles on the banks of the river

The most suitable and safe way to deal with the removal of existing foundation, proved to be the use of special hydraulic disks operated by skilled divers, who cut off the piles at the level of the river’s bed. Only the asbestos pipes had to be totally removed and safely disposed of, because of the environmental restrictions applied.



Photo 5. Clear cut of wooden and steel piles using hydraulic disks by divers

3 CONSTRUCTION WORKS

As soon as the river was free from old structures, we had to investigate the thickness of the soil upon the rocky background. Since there were no geological data of the riverbanks’ soil, we record the penetration rate of several steel piles hammered along the banks, testifying the stiffness of the soil. It became clear that the rocky background was appearing deeper near the rivers’ estuary.

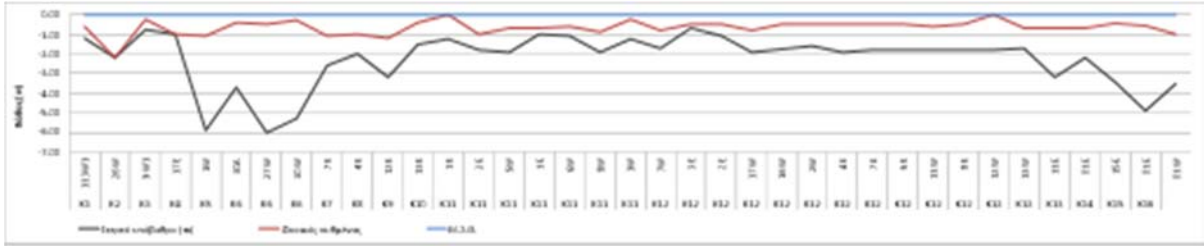


Figure 1. The rocky background level in black line under the red line of the soil, where the blue line stands for the Mean Sea Level. The rocky background level is deeper at the entrance of the west and the east bank

Until now, most of the new piles have been hammered into place and banks' protection is on the way. The upstream river's banks are mostly covered with clay and silt scattered with medium size stones, while the east bank is partly rocky. The soil near the estuary is very soft and becomes sandy when reaches the sea. Since there is ongoing fluctuation of the water surface causing river flow as mentioned before, the banks had to be protected from erosion. Gabion baskets filled with stones had to be placed between the piles on the banks where the soil was soft. The gabions baskets are fully submerged in order to prevent corrosion. Natural rock armor was also placed to fill gaps and to cover the gabions.



Photo 6. Rock armor is placed on the banks to protect the soft soil, after steel piles' hammering and before any superstructure is installed



Photo 7. Steel piles have been hammered in place and gabions placed between. Rock armor covers all, matching with the natural environment

The stone protection designed, will be finally merged into river's unique environment.

The light eco-friendly superstructures will be placed on the steel piles, withstanding any water flow and tide level. A slipway is going to be built on the west bank along with a special platform to the service of fishermen and the boats. Also, a small bridge will be constructed to join the banks.

References

COASTAL AND ARCHITECTURAL STUDY OF THE FISHING PORT ON THE ESTUARINE OF LIOPETRI'S RIVER "POTAMOS", CYPRUS, Paper presented at the 1st International Scientific Conference on Design and Management of Port Coastal and Offshore Works, Athens, Greece, 8-11 May 2019

Coastal engineering study for the rehabilitation of the beachfront at the fire-struck area of Mati, eastern Attica

C. Solomonidis¹, G. Fotis¹

¹Rogan Associates S.A., 5 Chatzigianni Mexi Str., Athens 11528, Greece

*Corresponding author: csolomonidis@roganassoc.gr

Abstract

The present study is part of a wider study of the “Urban planning & design implementation”, and constitutes a marine and coastal engineering investigation, aiming at rehabilitating the coastal front of the fire-struck area of Mati, located at the eastern part of Attica. Beach nourishment along with coastal protection works are proposed to counteract erosion and improve coastal cliffs’ stability.

Keywords: Coastal Engineering, Numerical Modelling, Coastal Protection Works, Cliff erosion.

1 INTRODUCTION

1.1 General

The present study concerns a Coastal Engineering Study / Investigation with numerical simulation of the coastal processes in the area of Mati, in order to determine the wave generated hydrodynamic processes’ regime and to understand the mechanisms that drive morphological change. Moreover, the aim of study is the assessment of suitable alternatives, and the proposal of coastal protection works to provide sufficient beach width which is required almost along the entire coastal front in the area of study.

1.2 Objective

The main objective of the study is to investigate the prevailing coastal processes in the area of interest in order to propose substantiated coastal engineering works to counteract further erosion. The proposed works will upgrade the existing condition of the foreshore. The beach nourishment is intended to provide a sufficient beach width which will in turn prevent further scouring and landslide of the coastal cliffs evident along the coastal front of interest but will also assist in creating a wide and safe refuge for the residents of the area, in case of extreme events, like the fire of 2018.

2 EXISTING SITUATION – AREA OF STUDY

The area of study covers a coastal stretch of approximately 3.5km, located at the eastern coast of Attica, in the fire-struck area of Mati. Based on a preliminary coastal investigation, the study area can be subdivided into four sub-areas which form distinct coastal cells (the cell boundaries delineate the geographical area within which the budget of sediment is balanced, providing the framework for the quantitative analysis of coastal erosion and accretion). The four coastal cells, which are examined separately, are illustrated in the figure below (**Figure 1**).

1. Kokkino limanaki & Akti Irinis
2. Argyra Akti
3. Rocky coastal stretch
4. Coastline north of N.A.O.M.

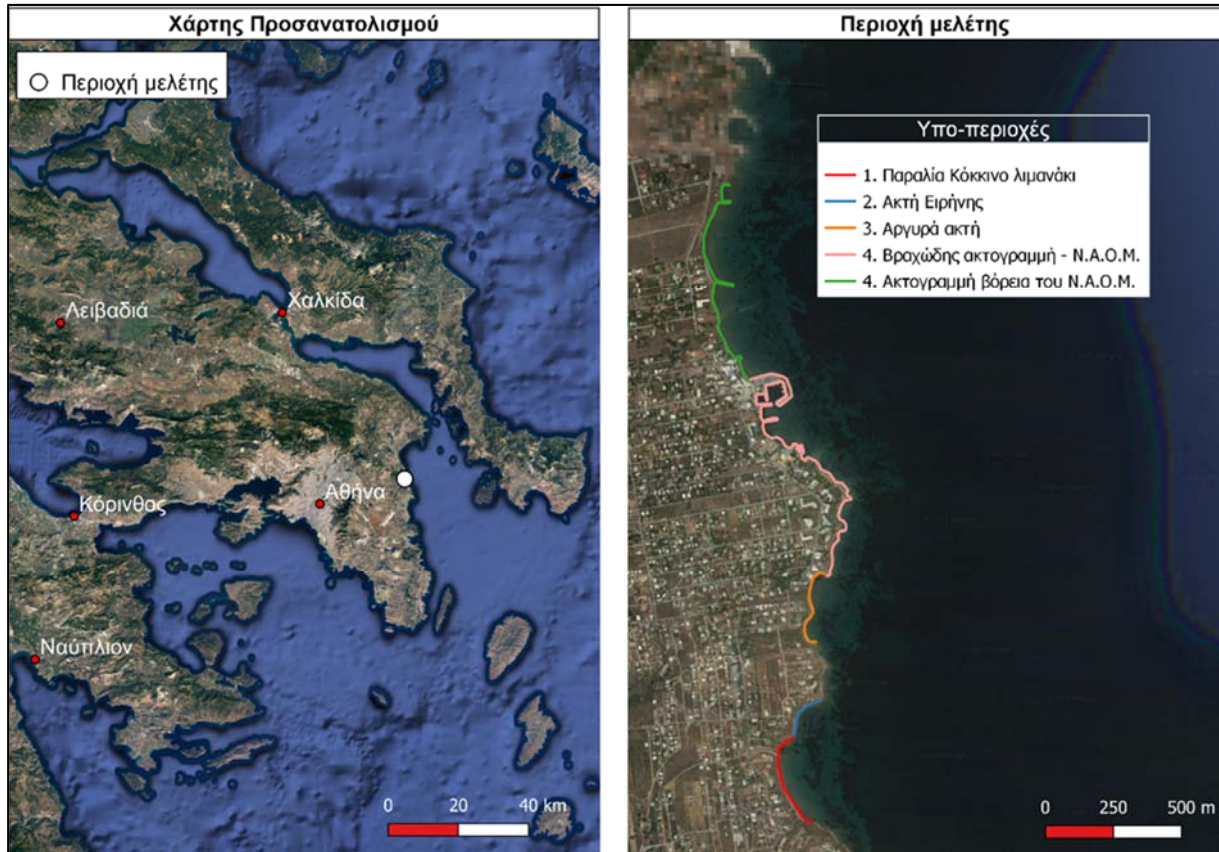


Figure 1. (a) Map of Greece – Area of Study (left), **(b)** Area of Study and sub-areas (right)

3 PRELIMINARY COASTAL ASSESSMENT

This chapter constitutes a preliminary coastal assessment, conducted prior to the coastal engineering study using mathematical modelling, that aims to identify the main coastal features, such as areas of sedimentation and erosion, existing river mouths, pipeline/stream outflows, landslide zones, etc. in each coastal cell.

The analysis undertaken is summarized below:

- Identification of main coastal features
- Photographic documentation
- Historic coastline evolution

The overall conclusions drawn following the analysis above can be summarized as follows:

- Based on the historic coastline evolution study, it appears that there is sediment movement (wave-induced sediment transport) along the coast, however no significant changes of the coastline are observed over the years of analysis. Therefore, it is concluded that the coast is in dynamic equilibrium.
- Judging from the limited beach width, it is concluded that sediment supply is very limited in the area.
- Due to the limited beach width, coastal cliff scouring is apparent along the vast area of study, as the foot of the cliffs is located within the wave run-up zone.

4 METHODOLOGY APPLIED

The following steps outline the methodology of the study procedure applied:

1. Assessment of the offshore wave climate.
2. Calculation of the nearshore wave field using numerical modelling of the Wave Transformation in the nearshore area.

3. Calculation of the wave induced circulation in the coastal area using a Hydrodynamic Numerical Model.
4. Calculation of the sediment transport rates due to wave induced circulation by using numerical model.

The numerical models of Mike 21 by DHI were used for the simulations.

Steps [2] to [4] were carried out for a number of wave cases, and for a number of alternative layouts which were considered as coastal protection schemes.

4.1 Offshore wave climate

Based on the orientation of the coast, the area of study is exposed against waves coming from the North, Northeast, East, Southeast and South direction.

The determination of the offshore mean annual wave climate in the study area, is facilitated by calculating the effective fetch length and the storm duration and subsequently applying the mathematical routines from the ACES system (Automated Coastal Engineering System) of the Coastal Engineering Research Center of the U.S. Dept of Army. In this way, the three-dimensional distribution of the significant wave heights, peak periods and mean wave directions is determined. The calculation, as described above, is based on the mean annual wind data of the meteorological station of Rafina and Syros.

The largest effective fetch length is apparent from the Southeast while the highest wind velocities are apparent from the North direction. As a result, waves coming from the Southeast and North direction are generally the highest in the area of study.

4.2 Numerical model - Prescribed boundary conditions

For the simulations, the equivalent wave characteristics were used for the most critical directions (N, NE, E, SE, S). To achieve a reduction in the number of simulations, waves from neighboring sectors were merged. In more detail, waves coming from the North were merged with the northeasterly while waves coming from the East were merged with the southeasterly. This is a common practice since waves approach the coast with similar angle of incidence, due to the orientation of the coastline and the bathymetric contours. Therefore, the set of wave cases to be simulated are the following three:

1. North-northeast (NNE)
2. East-southeast (ESE)
3. South (N)

Table 1. Wave cases for numerical simulation

MWD		Hs (m)	Tp (sec)	f
12°	N	1.42	4.30	20.08
	NE			
130°	E	2.05	5.03	1.685
	SE			
150°	S	1.89	4.93	3.71
TOTAL				25.475

Where: Hs : Significant wave height (m)

Tp : Period (sec)

f: Average annual frequency of wave conditions

5 NUMERICAL SIMULATION OF EXISTING SITUATION

Based on the results of the numerical simulation, carried out using MIKE 21 Coupled model (i.e., Spectral, Hydrodynamic, Sediment Transport), the following conclusions are drawn:

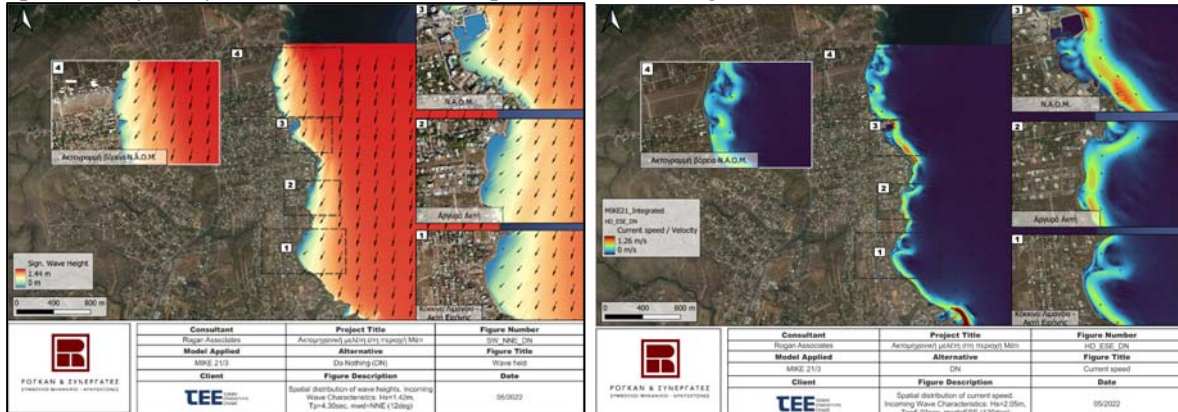


Figure 2. (a) MIKE SW results for DN (left), (b) MIKE HD results for DN (right)

5.1 Kokkino Limanaki, Akti Eirinis, Argyra Akti

- Alternating trends of erosion and deposition are observed which suggest that the coast is in a dynamic equilibrium.
- At Kokkino Limanaki, the erosion pattern that is apparent from the middle of the beach to its southern end, is due to the wave action from the NNE direction
- Erosion is evident along the entire stretch of Akti Eirinis beach, which is due to waves coming mainly from the ESE and S direction.
- Argyra Akti is exposed primarily to waves coming from the ESE and secondarily from the S direction. As a result of the wave action, erosion is observed along the coast located in the north gulf of the beach as well as at the middle of the south gulf.

5.2 Rocky coastal stretch, Coastline north of N.A.O.M.

- This rocky coastal stretch is predominantly affected by waves coming from the NNE while the coastline north of N.A.O.M. is mainly exposed to waves from the ESE and S direction.
- Alternating trends of erosion and deposition are observed which suggest that the coast is in a dynamic equilibrium.
- Erosion and deposition patterns are evident windward and leeward of the existing groynes respectively.
- Along the rocky coastal stretch beach rock acts like an armour to the beach preventing erosion
- Successive patterns of erosion and siltation are evident along the coastline north of N.A.O.M. while erosion is apparent from the middle of the beach to the north end which is due to the action of the waves coming from the ESE

6 ALTERNATIVE LAYOUTS

Three (3) alternative layouts were considered in concept and their efficiency was tested via numerical simulation. The technical works proposed in each of the alternatives are briefly described below:

1. **W1** combination of submerged detached breakwaters, groynes and nourishment
2. **W2** combination of emerged detached breakwaters, groynes and nourishment
3. **W3** combination of submerged/emerged detached breakwaters, sill (low-crested rubble mound) and nourishment

Given the complexity of the coastal system as well as the size of the study area, a single proposed alternative layout did not clearly emerge as optimal for the entire coastal front. Instead, the results of the model revealed the effectiveness of different technical solutions per sub-area. Consequently, it was considered appropriate to propose a combined solution for implementation by choosing the most effective measures for each beach as they emerged from the results of the numerical simulation (**Figure 3**):



Figure 3. Layout of proposed coastal protection works

The combined solution comprises the following works:

- Beach nourishment at all four (4) existing beaches covering a total length of about 1,65 km.
- Fifteen (15) submerged detached breakwaters, five (5) groynes, one (1) emerged breakwater and one (1) sill (low-crested rubble mound) for the protection of the rehabilitated beaches
- A coastal pedestrian walkway (promenade) of approx. 310 m long.

References

Site visit photos and satellite photos from the internet and Google Earth application.

Digital elevation models (DTM) of topography and bathymetry, including the recent topographic and bathymetry survey, undertaken in the context of this study.

The most recent Wind Data of the National Meteorological Service (hnms.gr). Specifically, 6-hourly measurements were used for the time periods 1970-1996 (M.S. Syros) and 1972-1983 (M.S. Rafina)

Bathymetric data from open databases (navionics.com) and GEBCO Gridded Bathymetric Data (https://www.gebco.net/data_and_products/gridded_bathymetry_data/)

Geospatial data provided by TEE.

A new time-dependent irregular wave propagation model

Th. Karambas^{1*}, A.G. Samaras², Ch. Makris¹

¹Department of Civil Engineering, Aristotle University of Thessaloniki, University Campus, 54124 Thessaloniki, Greece

²Department of Civil Engineering, Democritus University of Thrace, University Campus - Kimmeria, 67100 Xanthi, Greece

*Corresponding author: karambas@civil.auth.gr

Abstract

In this paper a time-dependent numerical model for the simulation of irregular multidirectional wave propagation and transformation in coastal areas, around and inside ports and harbours is presented. The model is capable of simulating the transformation of complex wave fields including shoaling, refraction, diffraction, total and partial reflection from structures, energy dissipation due to wave breaking and bottom friction in a combined way.

Keywords Wave model, Mild slope equation, Irregular waves, Port structures.

1 INTRODUCTION

The simulation of the propagation of multidirectional irregular waves (e.g., estimated by linear superposition of regular waves) in nearshore areas and inside harbours is fundamental for the design of coastal structures. Relevant models should be able to simulate not only the combined wave phenomena but also their interaction with coastal structures (e.g., diffraction, total and partial reflection, etc.) around and inside port basins (Makris et al. 2021).

2 THE 2DH MODEL

The model equations are expressed in terms of the surface elevation and the mean over the depth velocities. A wave spectrum is decomposed in N monochromatic waves. The model consists of the following pair of equations:

$$\frac{\partial \eta_i}{\partial t} + \frac{c_i}{c_{ig}} \nabla \frac{c_{ig}}{c_i} \mathbf{Q}_i = 0 \quad (1)$$

$$\frac{\partial \mathbf{U}_i}{\partial t} + \frac{c_i^2}{d} \nabla \eta_i = \nu_h \nabla^2 \mathbf{U}_i \quad (2)$$

where η_i is the free surface elevation, \mathbf{U}_i the mean velocity vector $\mathbf{U}_i = (U_i, V_i)$, d the depth, $\mathbf{Q}_i = \mathbf{U}_i d$, c_i the celerity, c_{ig} the group velocity, and ν_h is a horizontal eddy viscosity coefficient for the simulation of wave breaking. The subscript i denotes the i -th wave component. The right-hand side term of equation (2) is introduced to include breaking effects (Makris et al. 2019, 2021).

Equations (1) and (2) are solved N times separately for each wave component i . Each time step the surface elevation and the horizontal velocities are calculated from the sum of each wave component (Luo et al. 2020):

$$\eta = \sum_{i=1}^N \eta_i, \quad U = \sum_{i=1}^N U_i, \quad V = \sum_{i=1}^N V_i \quad (3)$$

The eddy viscosity coefficient is given by (Karambas and Samaras 2017):

$$\nu_h = 2d \left(\frac{D}{\rho} \right)^{1/3} \quad (4)$$

In Equation (4), D is the dissipation of wave energy expressed as:

$$D = \frac{1}{4} Q_b f \rho g H_m^2 \quad (5)$$

where H_m is the maximum wave height, ρ the water density, f the wave frequency, and Q_b the probability for a wave to break at a depth, expressed as $(1-Q_b)/(\ln Q_b) = (H_{rms}/H_m)^2$ according to Battjes and Janssen (1978). The mean square wave height H_{rms} is calculated from $H_{rms} = 2(\langle \eta^2 \rangle)^{1/2}$, with the brackets denoting a time-mean quantity (Makris et al. 2019, 2021).

3 REPRESENTATIONS OF WAVE AND RUBBLE-MOUND BREAKWATER INTERACTION AND SIMULATION OF PARTIAL REFLECTION

The energy loss due to friction effects and due to wave breaking on the slope of rubble mound breakwaters can be represented by inserting an eddy viscosity area in the computational domain instead of the structure geometry, as shown in Figure 1. This approach is based on the premise that knowing the reflection coefficient (e.g., from empirical formulae) one can calculate the value of the eddy viscosity ν_γ introduced in the momentum equation (i.e., Eq. 2 in the previous).

According to Karambas and Bowers (1996) the eddy viscosity coefficient can be calculated by solving the following equations:

$$C_r = \left(\frac{K}{k} (1 + e^{-4iKS_w}) - (1 - e^{-4iKS_w}) \right) / \left(\frac{K}{k} (1 + e^{-4iKS_w}) + (1 - e^{-4iKS_w}) \right) \quad \omega^2 - \nu_\gamma i \omega K^2 = c^2 K^2 \quad (6)$$

where K is a complex wave number, ω is the radian frequency, c is the wave celerity, $2S_w$ is the length of the area of application of the eddy viscosity coefficient ν_γ . By solving the above equations by iteration, for a given value of the reflection coefficient C_r , the value of the eddy viscosity coefficient ν_γ is obtained (Chondros et al. 2021). The reflection coefficient is given by empirical formulae (e.g., Zanuttigh and van der Meer 2007) as a function of the wave and breakwater characteristics (wave height and period, structure slope, permeability, etc.).

Figure 2 shows an exemplary result of this approach's implementation, presenting the partial wave reflection in front of a breakwater.

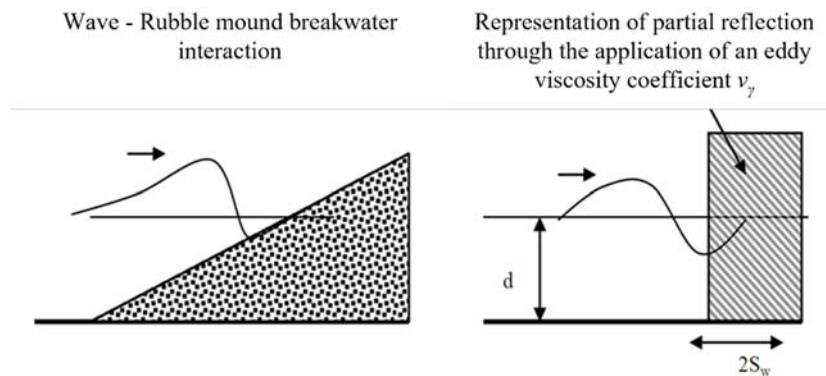


Figure 1. Realistic breakwater and representation in the model by inserting an eddy viscosity area

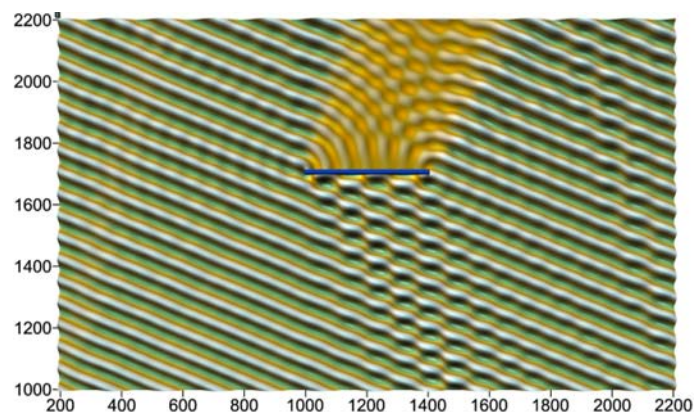


Figure 2. Partial wave reflection from a breakwater

4 MODEL APPLICATIONS AND RESULTS

Firstly, the model is applied to simulate irregular wave propagation over an elliptical shoal, reproducing the Vincent and Briggs (1989) experiments. The experimental layout and a snapshot of free surface elevation in the model's computational domain are presented in Figure 2. Wave transformation in this case is mainly due to bathymetric effects (refraction and bottom diffraction). Figure 3 shows the comparison of model results for unidirectional spectral waves against the experimental data of Vincent and Briggs (1989) along transect No. 4, which lies behind the shoal (test U3, incident significant wave height $H_i = 0.0254$ m, peak period $T_p = 1.3$ s). The comparison shows a good agreement between model results and experimental data.

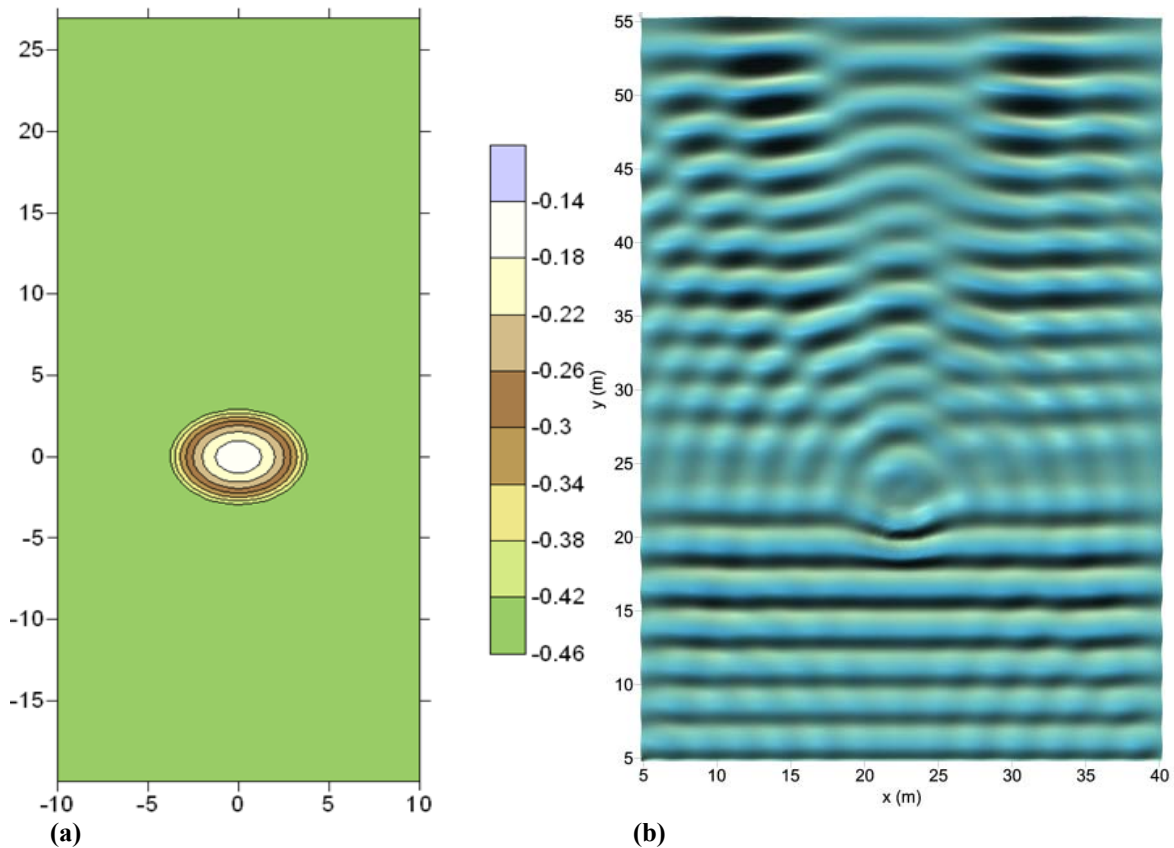


Figure 2. (a) Bathymetry (experimental layout) and (b) snapshot of surface elevation (model computation domain)

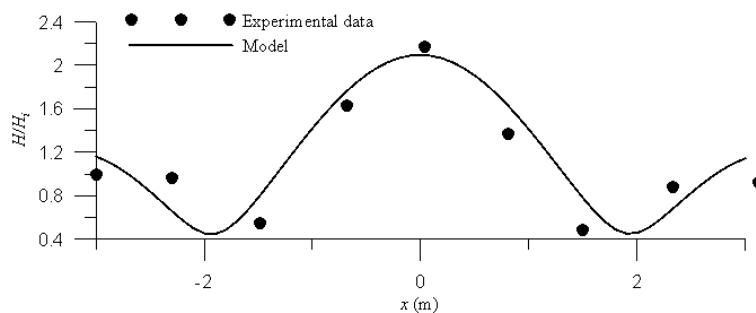


Figure 3. Comparison of model results against the experimental data of Vincent and Briggs (1989), in terms of normalized wave height H/H_i , for spectral unidirectional waves

The second set of numerical experiments concern diffraction of irregular waves passing through a breakwater gap (Li et al. 2000). The incident significant wave height for the case of unidirectional irregular waves is $H_s = 0.05$ m, the peak period is $T_p = 1.20$ s and the incident wave angle is equal to 45° . Figure 3 shows model results for the case of gap width $B = 3.92$ m and $B/L = 2$ (wave length L

corresponds to the peak period for irregular waves), in the form of a free surface elevation snapshot highlighting the diffraction effects on the irregular waves passing through the gap (left panel) and the diffraction coefficient field behind the breakwater (right panel). Figure 5 shows comparison of model results against experimental data regarding the cross-section distribution of the diffraction coefficients at a distance $y = 3L$ from the breakwater. The agreement in this second case is, again, quite satisfactory.

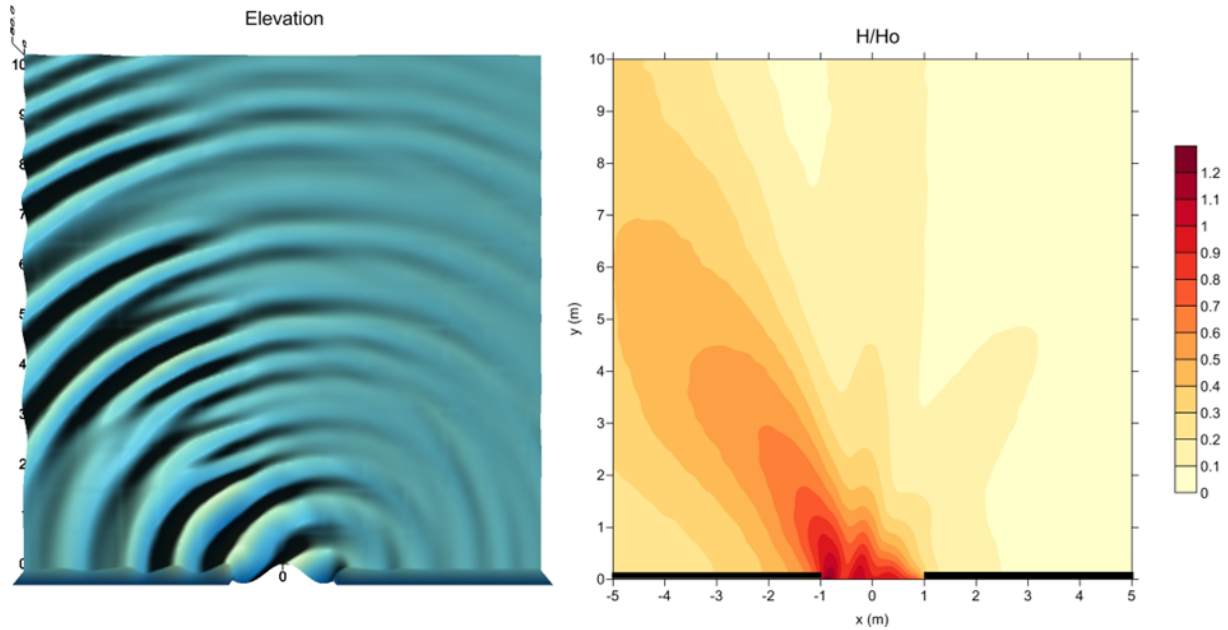


Figure 4. Diffraction of irregular waves passing through a breakwater gap: Free surface elevation snapshot (left panel) and diffraction coefficient field (right panel)

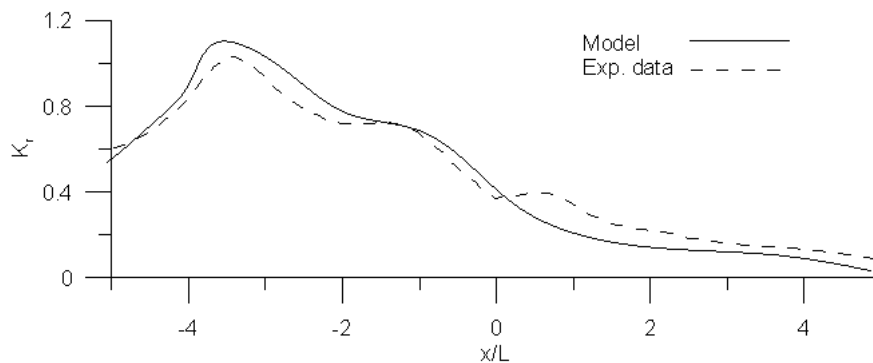


Figure 5. Diffraction of irregular waves passing through a breakwater gap: Comparison of diffraction coefficients K_D at a distance $Y = 3L$ from the breakwater between model results and the experimental data of Li et al. (2000)

Finally, the model is also applied to the real-life harbour layout of the Port of Thessaloniki (Makris et al. 2021). Indicative results for the case of South irregular waves are presented in Figure 5, as a snapshot of free surface elevation, highlighting wave-structure interactions in the harbour area. Comparisons conducted between the proposed model and a simplified mild-slope model have shown differences in wave height distribution that are considered as insignificant; in-depth analysis of this aspect will be included in future versions of this work.

5 CONCLUSIONS

This work presents an evolved version of a formerly presented time-dependent numerical model (Karambas and Samaras 2017; Makris et al. 2019) for the simulation of irregular multi-directional wave propagation and transformation in coastal areas, around and inside ports and harbours. The model is

successfully applied for wave propagation over varying topographies, behind breakwaters as well as in complicated bathymetry setups. The model is proven capable of simulating in an accurate and efficient manner the propagation of irregular waves over any finite water depth in two horizontal dimensions in the presence of coastal structures, including total and partial reflection effects.

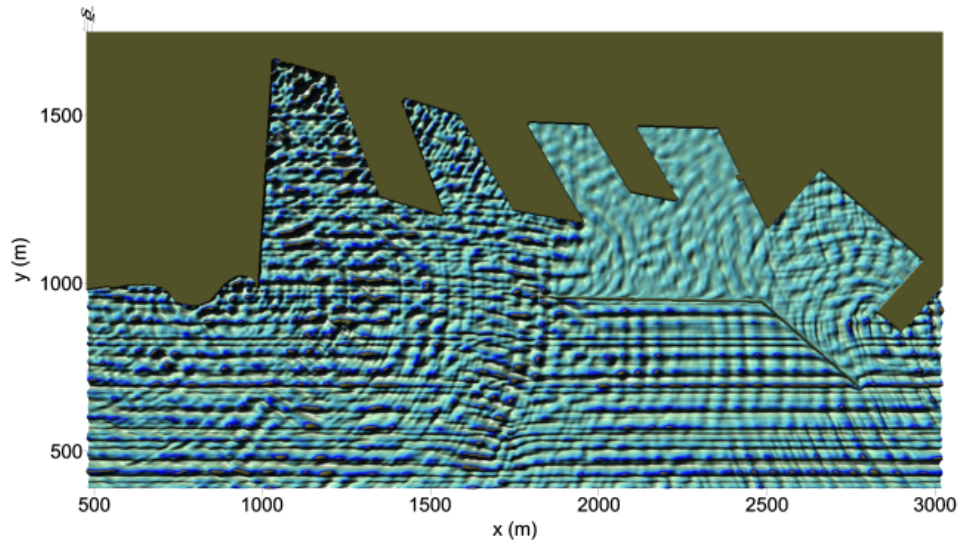


Figure 5. Model results for the Thessaloniki harbour layout: Snapshot of free surface elevation for the case of South irregular waves

References

- Battjes JA, Janssen, JPFM (1978) Energy loss and set-up due to breaking of random waves. Paper presented at the 16th International Conference on Coastal Engineering. doi:10.1061/9780872621909.03
- Chondros MK, Malliouri DI, Metallinos AS, Papadimitriou AG, Klonaris G, Karambas TV, Makris CV, Baltikas VN, Kontos YN, Nagkoulis N, Tsoukala V, Memos CD (2021) Numerical Modelling of Wave Reflection from Coastal Structures for Reliable Forecasting of Port Downtime. Paper presented at the 17th International Conference on Environmental Science and Technology (CEST2021), Athens, Greece.
- Karambas ThV, Bowers EC (1996) Representation of partial wave reflection and transmission for rubble mound coastal structures. *Wit Trans Ecol Envir*, 12: 415-423. doi:10.2495/HY960421
- Karambas ThV, Samaras AG (2017) An Integrated Numerical Model for the Design of Coastal Protection Structures, *J Mar Sci Eng*, 5:50. doi:10.3390/jmse5040050
- Li YS, Liu S-X, Yu X-Y, Lai G-Z (2000) Numerical modeling of multi-directional irregular waves through breakwaters. *Appl Math Model*, 24(8-9):551-574. doi:10.1016/S0307-904X(00)00003-2
- Luo L, Liu S, Li J, Jia W (2020) Deterministic reconstruction and reproduction of multi-directional irregular waves based on linear summation model. *Ocean Eng*, 198:106952. doi:10.1016/j.oceaneng.2020.106952
- Makris C, Androulidakis Y, Karambas T, Papadimitriou A, Metallinos A, Kontos Y, Baltikas V, Chondros M, Krestenitis Y, Tsoukala V, Memos C (2021). Integrated modelling of sea-state forecasts for safe navigation and operational management in ports: Application in the Mediterranean Sea. *Appl Math Mod*, 89(2):1206-1234. doi:10.1016/j.apm.2020.08.015
- Makris C, Karambas T, Baltikas V, Kontos Y, Metallinos A., Chondros, M., Tsoukala, V., Memos, C. (2019). WAVE-L: An Integrated Numerical Model for Wave Propagation Forecasting in Harbor Areas. Paper presented at the 1st International Conference DMPCO, Athens, Greece, 1:17-21.
- Vincent CL, Briggs MJ (1989) Refraction-diffraction of irregular waves over a mound. *J Waterw Port Coast Ocean Eng*, 115:269-284. doi:10.1061/(ASCE)0733-950X(1989)115:2(269)
- Zanuttigh B, van der Meer J (2007) Wave reflection from coastal structures. Paper presented at the 30th International Conference on Coastal Engineering. doi:10.1142/9789812709554_0364

LES of wave propagation on a beach with different vegetation characteristics

I.A. Chalmoukis^{1*}, G.A. Leftheriotis¹, A.A. Dimas¹

¹Department of Civil Engineering, University of Patras, Patras, 26504, Greece

*Corresponding author: ichalmoukis@upatras.gr

Abstract

An in-house porous medium numerical model has been implemented for the simulation of the three-dimensional, two-phase (water/air) flow induced by wave propagation over coastal vegetation (CV) fields. The model has been validated against experimental measurements of wave generation and propagation past a CV field on a horizontal bed. Then, the influence of the equivalent porosity, n_{eq} , on wave behaviour was assessed, regarding a CV field with constant plant height on a beach with constant bed slope. Results were obtained for the non-vegetated case ($n_{eq} = 1$) and for 2 vegetated cases with different n_{eq} values. It was found that decreasing n_{eq} moves wave breaking offshore at larger depths (40% increase for the case with $n_{eq} = 0.82$), while it does not affect much the breaking height (5% was the largest difference). For very high n_{eq} (0.98), wave breaking may occur at depths smaller than in the non-vegetated situation due to increased wave shoaling over the corresponding CV fields. The undertow distribution is strongly modified and increased wave setup (highest for $n_{eq} = 0.82$) is observed for all vegetated cases in comparison to the non-vegetated one.

Keywords Coastal vegetation; Porous medium approach, Wave attenuation, Large-eddy simulation.

1 INTRODUCTION

Natural coastal vegetation (CV) fields, e.g., seagrass and coral reefs, can attenuate the impact of coastal storms on beaches and coastal structures by dissipating energy of waves and currents. Furthermore, CV provides food and shelter to many organisms, and contributes to the maintenance of the quality of coastal waters and to the sustainable development of marine and coastal environments. Studies of wave interaction with CV fields are of fundamental importance to understand the effect of CV on coastal protection. The majority of experimental (field and/or laboratory) and numerical studies in the literature consider the propagation of non-breaking waves past a CV field on a horizontal bed with emphasis on the wave attenuation.

In several experimental studies (Stratigaki et al., 2011, Koftis et al., 2013, Garzon et al., 2019) the effect on wave attenuation was examined with respect to the length, L_{CV} , of the vegetation field, the density, N_v , of the vegetation plants, and the submergence ratio, h_v/d , where h_v is the plant height and d is the water depth. In terms of numerical studies, most of them are based on the use of two-dimensional horizontal models, for example based on the Boussinesq-type equations that do not resolve the depth-varying hydrodynamics. Karambas et al., (2016) used a nonlinear Boussinesq-type model where the effect of a vegetation field was taken into account by implementing a canopy flow model, and validated their model with comparisons to experimental data. Yang et al., (2018) used a nonlinear Boussinesq-type model where the effect of a vegetation field was taken into account by implementing a drag resistance term and studied wave propagation past rigid vegetation with $h_v/d \geq 1$. They found that, apart from the wave and plant characteristics, the wave height decay is also sensitive to the distribution pattern of plants in the CV field.

The main objective of the present work was to study the effect on wave propagation of a CV field on a beach with constant slope. Over a horizontal bed, wave attenuation is the sole hydrodynamic process, while over a sloped bed, wave attenuation is in competition with wave shoaling affecting wave breaking, i.e., the size of the surf zone, as well as wave setup, wave runup and wave-generated currents. An in-house 3D, LES-type, flow model was used where the effect of a vegetation field was taken into account by implementing a porous medium approach. The numerical model is based on a High Performance Computing (HPC) parallel architecture to reduce the computational cost. Results of the effect of the

vegetation porosity and the cross-shore length of the CV field on wave and depth-varying flow behaviour are presented.

2 METHODOLOGY

The combined water and air flow is modelled as one-fluid flow governed by the 3D incompressible Navier-Stokes equations based on an LES approach, and formulated appropriately to model flow in porous media (Liu et al., 2019):

$$\frac{\partial u_i}{\partial x_i} = 0 \quad (1)$$

$$\begin{aligned} \frac{1+c_A}{n} \frac{\partial u_i}{\partial t} + \frac{1}{n^2} \frac{\partial}{\partial x_j} (u_i u_j) = & -\frac{1}{\rho} \frac{\partial p}{\partial x_i} + \frac{\delta_{i3}}{\text{Fr}^2} - \frac{1}{n} \frac{\partial \tau_{ij}}{\partial x_j} + \frac{1}{n} \frac{1}{\text{Re}} \frac{1}{\rho} \frac{\partial}{\partial x_j} \left(\mu \left(\frac{\partial u_i}{\partial x_j} + \frac{\partial u_j}{\partial x_i} \right) \right) - \\ & -a_p \frac{(1-n^2)}{n^3} \frac{\nu}{D^2} \frac{1}{\text{Re}} u_i - \beta_p \left(1 + \frac{7.5}{\text{KC}} \right) \frac{1-n}{n^3} \frac{1}{D} u_i \sqrt{u_i u_i} + f_i \end{aligned} \quad (2)$$

In the above equations, x_i are the Cartesian coordinates, t is the time, u_i are the resolved velocity components in the three directions, $c_A = 0.34(1-n)/n$ is the added mass coefficient, n is the porosity, p is the total pressure, i.e., the sum of the dynamic and the hydrostatic pressure, ρ is the fluid density, normalized by the water density, δ_{ij} is the Kronecker's delta function, Fr is the Froude number, τ_{ij} are the sub-grid scale stresses associated with the LES approach, μ and ν are the fluid dynamic viscosity and kinematic viscosity, respectively, D is the characteristic dimension of solids in the porous medium, $a_p = 1000$ and $\beta_p = 1.1$ (Liu et al., 1999) are empirical coefficients and KC is the Keulegan-Carpenter number. The term f_i is associated with the Immersed Boundary method for the imposition of flow boundary conditions on the seabed (Dimas and Chalmoukis, 2020). The Navier-Stokes equations are rendered dimensionless using the characteristic water depth d_0 at the wavemaker and the gravitational acceleration g , hence, the corresponding velocities were non-dimensionalized by $(g \cdot d_0)^{1/2}$ and $\text{Fr} = 1$. The subgrid scale stresses were modelled using the standard eddy-viscosity model in Smagorinsky (1963) and the location of the water-air interface is tracked using the level-set method.

The porous medium approach is used to model the flow resistance in the CV field. Thus, an equivalent porosity, n_{eq} , is used in Eq. (2), instead of n , which depends on the combined effect of CV plant density and cross-sectional dimensions. The equivalent porosity is estimated by setting $1 - n_{eq}$ equal to the volume of the plants divided by the total volume occupied by the CV field. The specific approach has been reported to perform well in terms of simulating wave attenuation over a rigid vegetation field in Hadadpour et al., 2019. It is based on parameters of the vegetation field (plant density, height and cross-sectional dimensions), which can be easily measured and imported in the numerical model. Moreover, the approach is easily implemented in combination with the Immersed Boundary method on a Cartesian grid, which speeds up the computational time significantly, especially when implemented in parallel algorithms like the present one. Regarding pressure boundary conditions, a zero Neumann condition is imposed on the bottom and the streamwise boundaries of the domain. A Dirichlet-type condition $p = \rho g \eta$ is implemented at the top computational boundary, where η is the water surface elevation. Accordingly, the velocity boundary conditions are zero Neumann on the bottom and the right boundaries. At the wave generation boundary (left), a Dirichlet-type condition is implemented for the streamwise velocity to be consistent with the harmonic wave generation. In the spanwise direction, periodic boundary conditions are implemented for pressure and velocities.

3 RESULTS

3.1 Validation of the numerical model

The present model replicates a case in Augustin et al., (2009) where free-surface elevation data was provided for monochromatic waves propagating past a submerged vegetation field in a wave flume with

dimensions of 30.5 m length, 0.9 m width and 1.2 m depth. The incident wave height was $H = 12$ cm and the wave period was $T = 1.5$ sec at water depth $d_0 = 0.5$ m. The experimental validation field consisted of cylindrical stems with $h_v = 0.3$ m and $D = 12$ mm. The stem density of the vegetation field was equal to 97 stems/m², which corresponds to $n_{eq} = 0.99$. A flatbed region of two wavelengths exists downstream of the wavemaker for fully-developed wave conditions to be established before reaching the elevated bed of the vegetation field. The vegetation field is placed at a distance 17.1 m onshore of the wavemaker and its length is equal to 6 m. A constant slope beach (1:12) is placed at the right end of the flume to dissipate the remaining wave energy and minimize wave reflection. The relative grid spacing was selected to be uniform in all directions with values: $\Delta x_1/d_0 = 0.05$, $\Delta x_2/d_0 = 0.025$ and $\Delta x_3/d_0 = 0.02$. The specific discretization resulted in a grid with 1300 cells in the streamwise direction, 72 cells in the spanwise direction and 100 cells in the vertical direction. An instant snapshot of the free-surface elevation is shown in Figure 1 (black line) after 10 wave periods. The numerical result is in good agreement with the corresponding result (red dots) in Augustin et al., (2009).

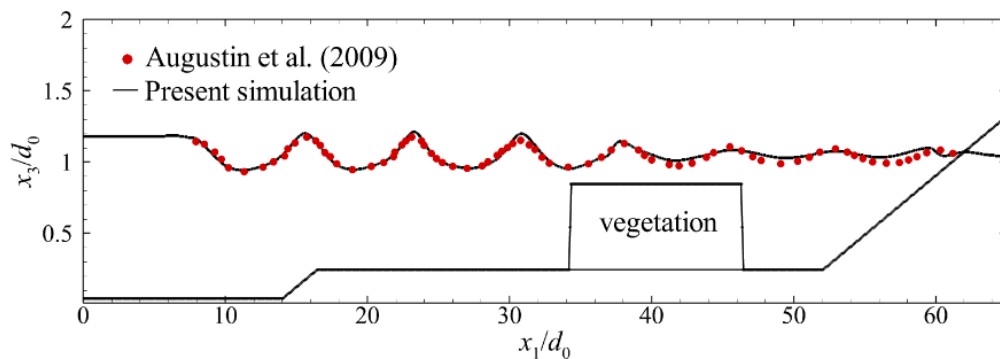


Figure 1. Free surface elevation along with the corresponding experimental result in Augustin et al., (2009).

3.2 Coastal vegetation results

Numerical simulations of wave propagation at $d_0 = 0.6$ m and breaking over a beach of constant slope $\tan\beta = 1/15$ have been performed, with and without the presence of a CV field. The CV field starts at a depth of 0.48 m, its height is equal to 0.1 m and its cross-shore length, L_{CV} , is $8.67d_0$ (5.2 m). The cross-shore length of the CV field was selected to be in the order of one wavelength, L , at its offshore depth. The CV parameters were selected to mimic observations of real meadows where CV density, as well as shape and dimensions of CV stems, vary greatly. Typical CV density ranges from 62 to 556 stems/m² or as high as 4200 stems/m², whereas *Posidonia Oceanica* density, for example, varies from sparse, 150 stems/m², to very dense, 700 stems/m² (Stratigaki et al., 2011). In nature, the shape of the stems is like a thin blade with typical dimension of 1 cm wide, 1 mm thick and up to 1 m long. In many experimental setups, the stems are constructed as long cylindrical elements with a diameter of 3 mm to 12 mm. In the present laboratory scale, a characteristic diameter $D = 1$ mm is considered. To analyse a variety of different cases, two n_{eq} values were studied (0.82 and 0.98).

The streamwise velocity field on the cross-shore vertical plane is presented in Figure 2. The porous medium model appropriately reduces velocity magnitudes inside the vegetation zone. It is interesting to note that the velocity reduction in the case of $n_{eq} = 0.98$ is almost negligible, since the porosity value is very close to unity, while with $n_{eq} = 0.82$, the velocity is significantly reduced. This highlights the importance of the correct estimation/calibration of the vegetation parameters in order to correctly model the CV effect on waves and flow.

The phase-averaged envelope of the free-surface elevation is presented in Figure 3. The wave breaking position is marked in both cases with a vertical line. The decrease of n_{eq} from 0.98 to 0.82 causes wave height reduction during shoaling over the CV field and induces wave breaking to occur more offshore. The wave breaking height for all cases is approximately the same (largest deviation is about 5%), whereas the breaking depth increases with decreasing n_{eq} (40% increase for $n_{eq} = 0.82$ with respect to non-vegetated case). As shown in Figure 4, this latter behaviour is due to the wave height reduction over

the CV field prior to wave breaking, as the breaking depth of the non-vegetated situation is towards the onshore end of the CV field.

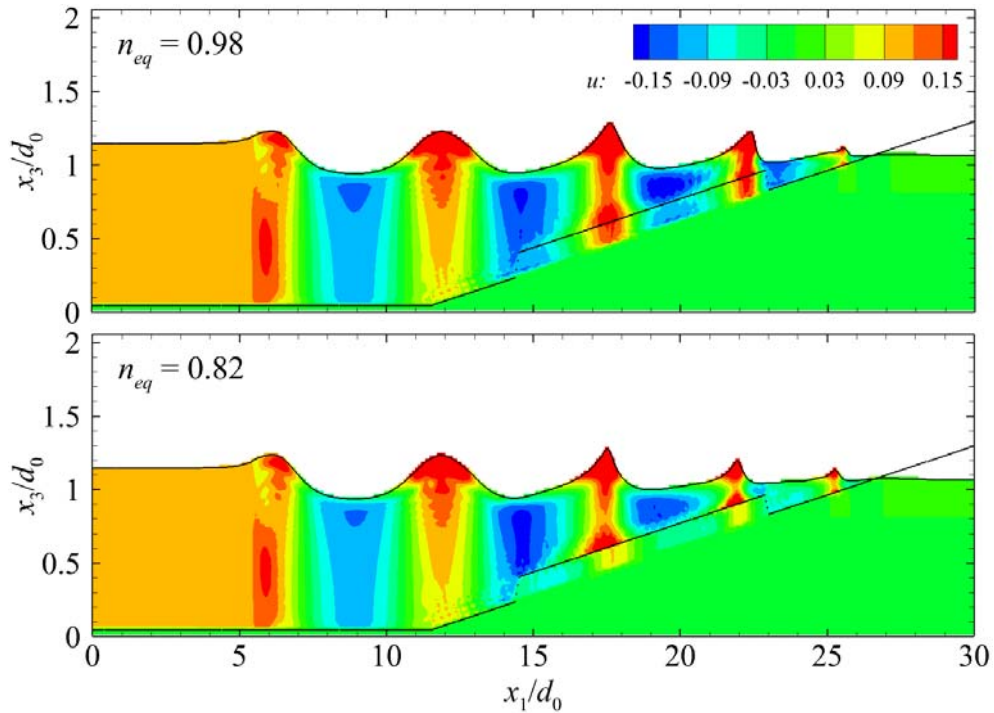


Figure 2. Instantaneous 2D vertical snapshots of the streamwise velocity induced by waves propagating over CV fields with $n_{eq} = 0.98$ and $n_{eq} = 0.82$. Note that the coordinate axes are in scale $x_1/x_3 = 0.2$ for clarity.

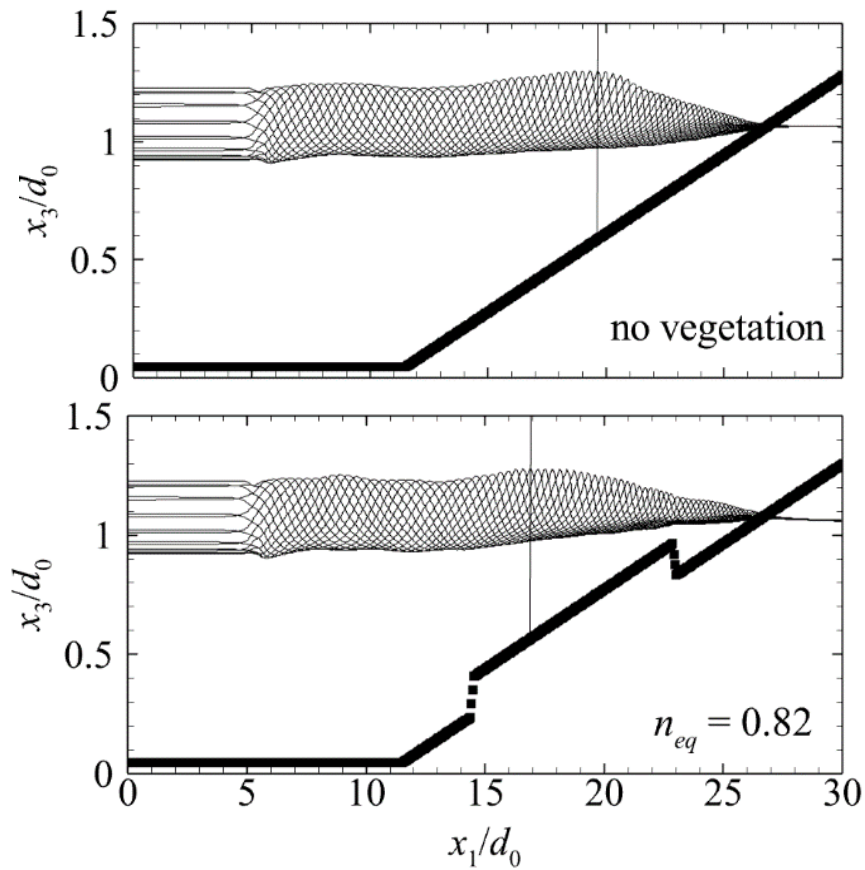


Figure 3. Phase-averaged 2D vertical envelope of the free-surface elevation of waves propagating and breaking for case of no vegetation and $n_{eq} = 0.82$. Note that the axes are in scale $x_1/x_3 = 0.1$ for clarity.

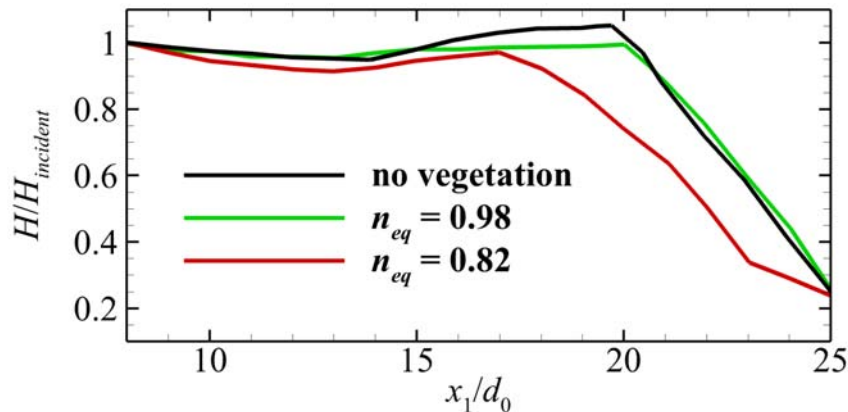


Figure 4. Wave height distribution for all cases. The sloped bed starts at $x_1/d_0 = 11.5$, the CV field starts at $x_1/d_0 = 14.4$ and ends at $x_1/d_0 = 23.1$, and the still-water coastline is at $x_1/d_0 = 26.5$.

4 CONCLUSIONS

In the present work, the effect of a vegetation field on coastal wave attenuation and breaking was studied numerically. The flow field was resolved by means of LES, and the porous medium approach was utilized to model the effect of CV. A good agreement was observed between the numerical results and findings in the literature, indicating that the present approach is a valid model to study the effect on wave attenuation and breaking of a CV field on a beach bed. Moreover, the effect of the equivalent porosity, n_{eq} , of the CV field was examined. It was found that decreasing n_{eq} moves wave breaking offshore at larger depths, while it does not affect much the breaking height. For very high n_{eq} wave breaking may occur at depths smaller than the non-vegetated situation due to increased wave height reduction during shoaling over the corresponding CV fields.

References

- Augustin LN, Irish JL, Lynett P (2009) Laboratory and numerical studies of wave damping by emergent and near-emergent wetland vegetation. *Coastal Eng* 56(3), 332–340. doi:10.1016/j.coastaleng.2008.09.004
- Dimas AA, Chalmoukis IA (2020) An adaptation of the immersed boundary method for turbulent flows over three-dimensional coastal/fluvial beds. *Appl Math Model* 88, 905–915. doi:10.1016/j.apm.2020.07.007
- Garzon JL, Maza M, Ferreira CM, Lara JL, Losada IJ (2019) Wave attenuation by *Spartina* saltmarshes in the Chesapeake Bay under storm surge conditions. *J Geoph Res Oceans* 124, 5220–5243. doi:10.1029/2018JC014865
- Hadadpour S, Paul M, Oumeraci H (2019) Numerical investigation of wave attenuation by rigid vegetation based on a porous media approach. *J Coastal Res* 92(1), 92–100. doi:10.2112/SI92-011.1
- Karambas T, Koftis T, Prinos P (2016) Modeling of nonlinear wave attenuation due to vegetation. *J Coastal Res* 32(1), 142–152. doi:10.2112/JCOASTRES-D-14-00044.1
- Koftis T, Prinos P, Stratigaki V (2013) Wave damping over artificial *Posidonia oceanica* meadow: A large-scale experimental study. *Coastal Eng* 73, 71–83. doi:10.1016/j.coastaleng.2012.10.007
- Liu PLF, Pengzhi L, Chang K, Sakakiyama T (1999) Numerical modeling of wave interaction with porous structures. *J Waterw Port Coast Ocean Eng* 125(6), 322–330. doi:10.1061/(ASCE)0733-950X(1999)125:6(322)
- Smagorinsky J (1963) General circulation experiments with the primitive equations I. The basic experiment. *Mon Weather Rev* 91, 99–165. doi:10.1175/1520-0493(1963)091<0099:GCEWTP>
- Stratigaki V, Manca E, Prinos P, Losada IJ, Lara JL, Sclavo M, Amos CL, Cáceres I, Sánchez-Arcilla A (2011) Large-scale experiments on wave propagation over *Posidonia oceanica*. *J Hydraul Res* 49, 31–43. doi:10.1080/00221686.2011.583388



Yang Z, Tang J, Shen Y (2018) Numerical study for vegetation effects on coastal wave propagation by using nonlinear Boussinesq model. *Appl Ocean Res* 70, 32–40. doi:10.1016/j.apor.2017.09.001

Coastal engineering applications in Greece from a consultant's point of view

A. Valsamidis^{1*}

¹ Aktomechanics, 38 Olympiados Street, Postcode 54633, Thessaloniki, Greece
*Dr Antonios Valsamidis : valsanton@hotmail.com

Abstract

This work aims at: briefly demonstrating the outputs of a coastal engineering project in Greece, in agreement with the standards set by the Hellenic Ministry of Infrastructure, Transport and Networks. As a case-study the Amarynthos beach on Euboea Island was chosen where a port is going to be upgraded. The scope of the current project is to examine the morphological impact of the designed new port structures on the coastal environment. To this end, three software packages were applied: a. Delft3D as a means to model the 2D wave propagations towards Amarynthos beach and the corresponding morphological evolution, considering simulation time equal to ten years. Similarly, the One-Line model UNIBEST was applied to predict the ten-year shoreline morphodynamic evolution of Amarynthos beach. Finally, the Xbeach model was used to quantify the effects of short-time storm events to beach cross-shore profiles. Therefore, the aforementioned three models provided an integrated insight to the coastal morphodynamic evolution of Amarynthos beach, as they revealed different sort of coastal processes evolving in different spatial and temporal scales. Moreover, as the beach is made of pebbles and cobbles while the smaller sandy grains have been washed away by the waves over time, it is expected that there will be negligible morphodynamic evolution, considering the prevailing mild wave climate as well in the studied area. Thus, the case of beach grain size D_{50} being equal to 1mm was taken into account to identify the local physical mechanisms of coastal evolution.

Keywords Beach erosion, One-Line Model, Delft3D, Xbeach.

1 CASE-STUDY AND AVAILABLE FIELD DATA

Amarynthos is a town near the sea, with a current population of about 5000 inhabitants. It is located on Euboea Island, in the South Euboean Gulf, very close to the well-known ancient city of Eretria, in an area which is highly regarded for its touristic value.



Figure 1. (a) The arrow points to the location of Amarynthos beach, in the South Euboean Gulf; (b) The extended area westwards of the port (in the yellow rectangle) where the shoreline was derived from a Google Earth image

1.1 The proposed port project

The fishing port of Amarynthos is going to be improved by adding the following port structures: (a) a 58 m leeward breakwater to increase berth positions inside the port, (b) a 92m wharf to make easier the

processes of ship loading and unloading, and (c) a 25 m groyne inside the port basin to separate the natural beach from the proposed wharf. The aforementioned structures are illustrated in Figure 2:

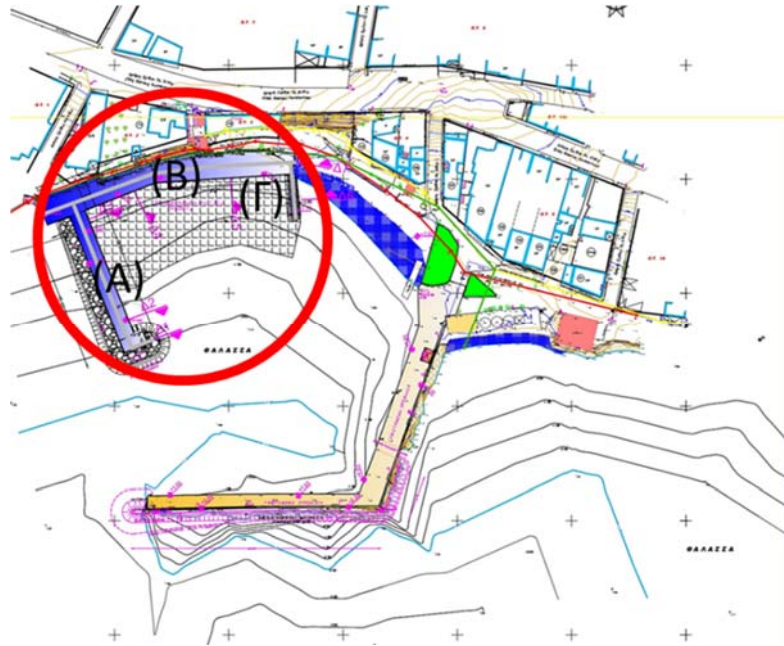


Figure 2. The red circle denotes the area where the new port elements are going to be constructed: A. the leeward breakwater; B. the wharf; and Γ. the groyne

1.2 Bathymetric data

A bathymetric survey was conducted in 2014 in the area illustrated in Figure 2. In an attempt to expand the morphodynamic analysis to a larger area, the coastal section on the west side of the port up to 500 m away was considered, and the corresponding coastline was derived from a Google Earth image (Figure 1b).

1.3 Wave data

Wave field records do not exist in the vicinity of the studied area. To this end, wind data from the Chalcis wind station were used as input-data to an empirical model, namely the JONSWAP spectrum, to derive the corresponding wave events for SE (135 deg), S (180 deg) and SW (225 deg).

1.4 Sediment data

Generally, the coastal environment of this case study starves for fine sandy sediment material as the latter has been eroded over time, thus, the beach mostly consists of pebbles and cobbles. However, given the fact that the Municipality of Eretria may decide to enrich the beach with fine sediment material, grain size $D_{50} = 1\text{mm}$ was taken into account in the modelling processes, to be in any case on the safe side.

2 MODELLING PROCESS

2.1 Application of Delft3D (Deltares 2020)

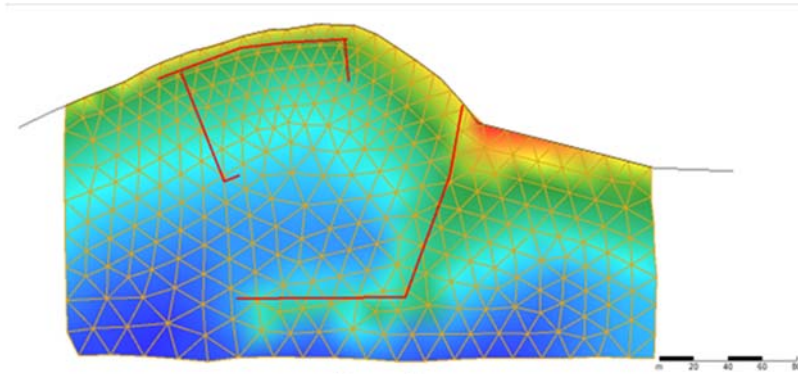


Figure 3. Construction of grid in Delft3D for the Amarynthos case study

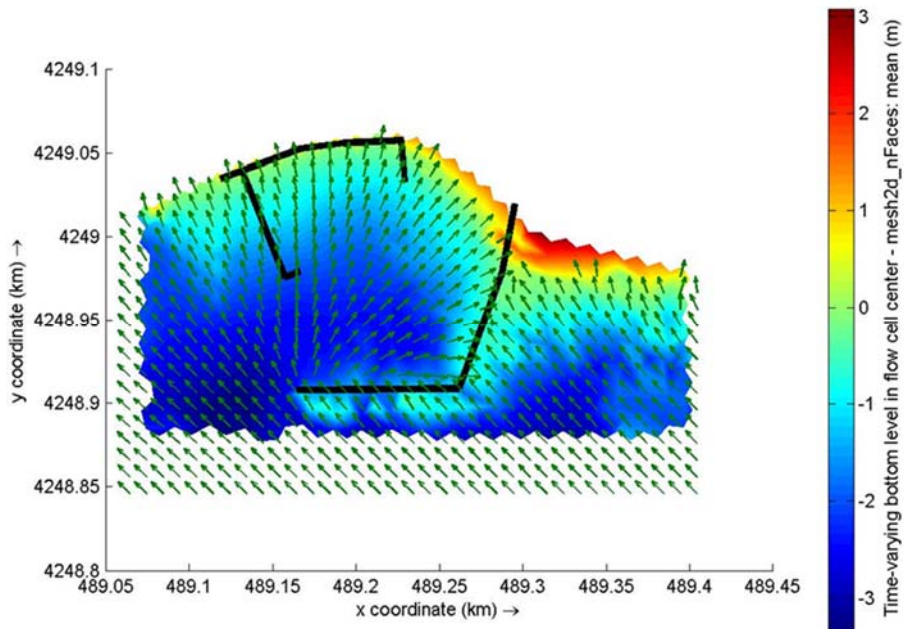


Figure 4. Modelling wave propagation towards the beach

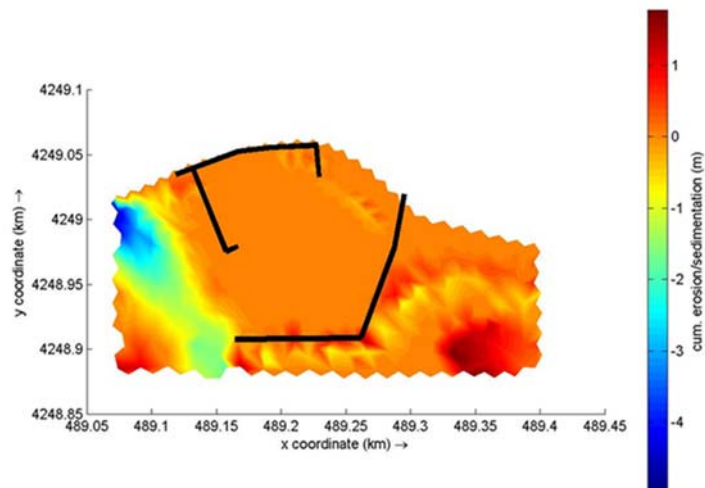


Figure 5. Modelling accumulated erosion / accretion for 10 years of simulating time

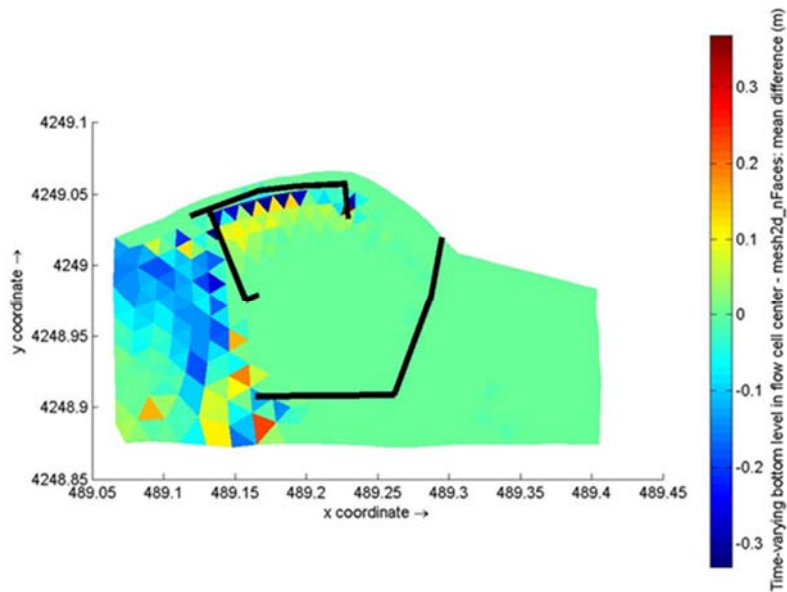


Figure 6. Bathymetric difference in the 2D space, considering as reference bathymetric map the one corresponding to the 10-year simulation of the seabed without the proposed port works, and as the final one, the bathymetric map corresponding to the 10-year morphodynamic evolution of the case study, including in the simulation process the proposed port works

The aforementioned Figure 6 shows that the construction of the proposed leeward breakwater causes 10-30 cm further erosion on its external side and moreover, in the area out of the mouth of the port, considering a simulation time of 10-years, in comparison with the expected morphodynamic evolution for the case that the proposed port facilities are not taken into account.

2.2 Application of the One-Line Model UNIBEST

Furthermore, the One-Line Model UNIBEST (Huisman and Dagalaki 2020) was applied in the area west of the port (Figure 1b), where a well-developed touristic infrastructure exists, in a beach section of 500 m. Next, a prediction of the shoreline morphodynamic evolution is presented for a 10-year simulation time:

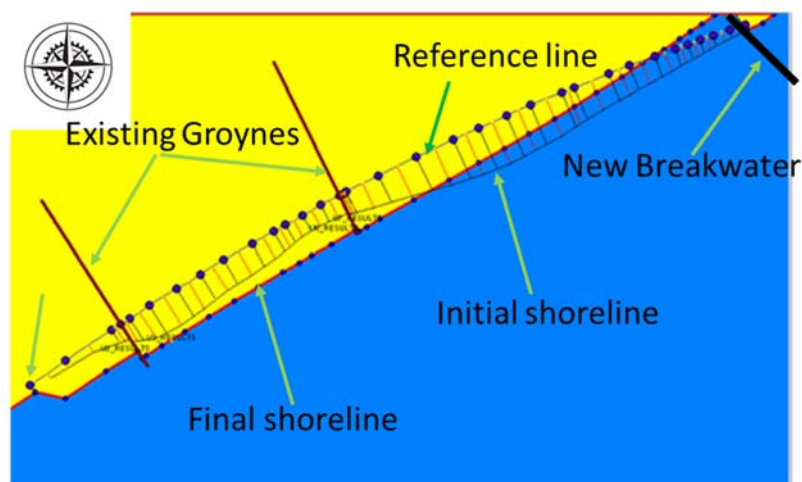


Figure 7. The initial shoreline is denoted with a thin black line while the final one identifies with the margin between the yellow (land) and the blue (sea) area. The reference line shows the general beach orientation.

2.3 Application of Xbeach

The Xbeach (Roelvink et al. 2010) application aims at showing the impact of storms on the seabed. To this end, the maximum wave event corresponding to $H=1,20$ m, $T=3,86$ sec, SE direction and duration equal to 1 hr, Results are presented in Figure 8.

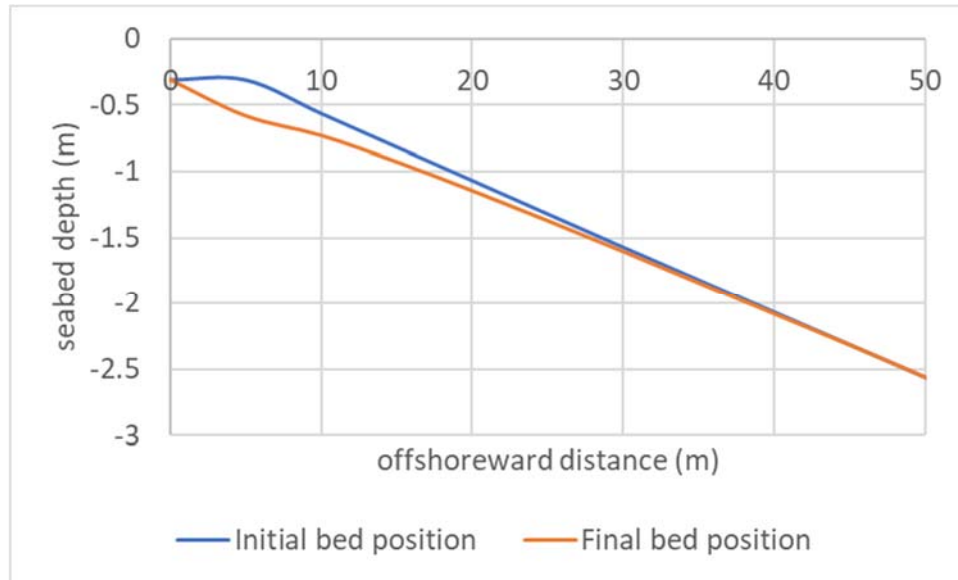


Figure 8. Erosion of a typical cross-shore profile of Amarynthos beach due to a storm event

3 CONCLUSIONS

The main conclusion of the current study is that the proposed works to the fish port of Amarynthos will not change the existing trend of morphodynamic evolution in the wider area, therefore, from a coastal engineering perspective it is considered safe to proceed to the construction phase. This is evident in Figure 6, illustrating an output of Delft3D, where the morphodynamic impact of the proposed works is shown to be negligible. The application of the One-Line model UNIBEST revealed the dominant trend of shoreline evolution which is caused by waves coming from the SE direction, consequently, mobilizing a westward littoral drift that produces erosion near the fish port of Amarynthos and accretion on the opposite side (Figure 7). Finally, the application of Xbeach showed rather small seabed erosion up to 1m water depth which can be easily restored when milder wave events prevail in the area.

It is worth noting that for the simulations via Delft3D, UNIBEST and Xbeach, the grain size of the beach was taken equal to 1mm to consider the case that coastal front is nourished, since currently the beach consists mainly of pebbles and cobbles. The latter, due to their size, but also due to the mild wave climate in the area, are expected to produce an almost negligible morphodynamic evolution, and for this reason they were not taken into account in the modelling processes.

References

- Deltares (2020) Delft3D-FLOW. Deltares, Delft
Huisman B, Dagalaki V (2020) UNIBEST user manual. Deltares, Delft
Roelvink D (P.I.), Reniers A, Van Dongeren A, Van Thiel de Vries J, Lescinski J, McCall R (2010) Xbeach Model Description and Manual. Unesco-IHE Institute for Water Education, Deltares and Delft University of Technology, Delft

Offshore infrastructures in Greece: a new era and a big challenge for marine geotechnical surveying

N.K. Chtouris, T. Hasiotis *

Department of Marine Sciences, University of the Aegean, University Hill, Mytilene 81100, Lesvos Isl., Greece

*Corresponding author: hasiotis@aegean.gr

Abstract

A large number of offshore projects in Greece are under development or planning, such as power and fiber optic cables, LNG FSRUs and pipelines and offshore wind farms. Marine geophysical and geotechnical surveys are routinely conducted to support installation of these infrastructures. Only during the last decade few geotechnical surveys are implemented through more sophisticated vibro-coring (VC) sampling and in situ measurements (piezocone cone penetration test - CPTU), mainly for the safe installation and burial assessment studies of power cables and pipelines. In light of the increasing number of planned power interconnections and other offshore construction activities, the demand for precise information on the geotechnical behavior of hosting sediments becomes paramount. This paper presents some new challenges for marine geotechnical surveying, specifically problems regarding the integration of geophysical and geotechnical information, as well as issues concerning sample disturbance, which affects data interpretation. The idea of developing a marine geotechnical data base for Greece is proposed, including the need for valid results from CPT software algorithms for the Greek marine geological conditions / environments. An example of a dataset between Evia and Skiathos is presented, with questionable shear strength CPTU profiles and VC laboratory measurements.

Keywords Geotechnical surveying, Cone penetration test, Vibro-corer, Open-digital depository.

1 INTRODUCTION - OFFSHORE INFRASTRUCTURE DEVELOPMENT IN GREECE

The Interconnected Electricity Grid (IEG) of Greece supports the highly energy-demanding Ionian and Aegean Sea Islands that are close to the mainland with submarine power cables. For non-interconnected islands, the Independent Power Transmission Operator (IPTO) considers that their connection to the IEG is a necessity. This will lead to a more sustainable electrical grid for the country as well as in the abatement of greenhouse gas emissions (Karystianos et al. 2021). Furthermore, it introduces the possibility of renewable energy sources penetration for the Aegean Islands, with offshore wind farms being a particularly promising source of energy. Moreover, Greece's anticipated role as an energy hub for southeast Europe is corroborated by a series of projects that are related to offshore natural gas facilities (LNG FSRUs and pipelines) (Peloriadi et al. 2022). Marine geophysical surveys are routinely conducted to support installations for these infrastructures. For geotechnical surveys, sampling is commonly employed with gravity-coring, usually with poor results. More sophisticated geotechnical surveying, involving boreholes or vibro-coring (VC) sampling and in situ measurements (piezocone cone penetration test - CPTU), is rare. In the last decade, few marine geotechnical surveys have applied such methodologies for the safe installation and burial assessment studies of power cables and pipelines.

In light of the increasing number of planned power interconnections and other construction offshore activities, and considering the demand for precise information on the geotechnical behavior of hosting sediments, this paper (i) refers to the challenges that must be addressed during marine geotechnical surveying, (ii) addresses the need for valid results from CPT software algorithms for the Greek marine geological conditions / environments, (iii) presents an example of a dataset between Evia and Skiathos with questionable shear strength CPTU profiles and VC laboratory measurements and (iv) proposes the idea of developing a marine geotechnical data base for Greece.

2 CHALLENGES IN MARINE GEOTECHNICAL SURVEYING

The description of prevailing sedimentary processes and marine geohazards for sites with offshore

infrastructure is dependent on geophysical surveys. When considering structure installation, however, it is imperative that sampling and geotechnical testing is conducted on surficial and deeper sedimentary layers. These are performed for engineering/designing purposes as well as for the validation of geophysical profiles. For example, burial assessment studies rely on the definition of questionable geological strata and their physical and mechanical properties. Even after geological strata have been characterized according to their geotechnical properties, uncertainty can still exist. The uncertainty is usually produced from problems associated with the physical conditions of the study area (sea state, seabed slopes and topography) and the laboratory handling of specimens. An important rule that must be respected is that no sampling method in the sea can provide massive undisturbed samples. Even though this is not a new problem, it can produce unreliable estimations of important parameters such as undrained shear strength. Experience shows that operators do not always conduct sampling properly, thus, disturbance can occur from the initial stage of operations. Disturbances also occur during transportation and laboratory treatment of specimens (Young et al. 1983; Lunne et al. 2006). For these reasons, important parameters such as bulk density, undrained shear strength, consolidation properties etc., are often questionable. Especially for undrained shear strength, differences in laboratory testing (vane test, triaxial tests etc.) can produce discrepancies in its estimation. In-situ testing, although expensive, provides more reliable results of the subsurface conditions. Nonetheless, issues in the interpretation of CPTU measurements can also arise. Specifically, software packages are employed in order to process and correct CPTU readings. Apart from the basic CPTU parameters (cone resistance, sleeve friction, pore pressure), profiles of soil parameters can also be extracted such as undrained shear strength and relative density. These profiles are based on empirical relationships between CPTU parameters and lab measurement of soil indexes, stemming from various databases. Such readings are deemed unreliable and require validation with lab tests (Powell and Dhimitri 2022). VC can assist in providing longer cores for testing, which also enables the correlation and ground-truthing of seismic data. Boreholes, on the other hand, are logistically demanding and expensive and are carried out only for big foundation projects, usually in coastal waters. The study of shear strength from a CPTU-VC dataset between Evia and Skiathos (see section 2.1) demonstrated considerable differences between the lab and CPT measurements. Shear strength (S_u) from the lab (measured by vane test) were found to be closer to the remolded undrained shear strength from CPT, while shear strength from CPT was higher, emphasizing uncertainties between measurements.

2.1 Validation of CPT Undrained Shear Strength with Laboratory Vane Tests: the Evia-Skiathos Power Interconnection

In 2020, during a geophysical and geotechnical survey for the installation of a power cable between Evia and Skiathos Islands, 32 VCs and 30 CPTUs were obtained in close proximity, in order to estimate the geotechnical properties of the subsurface sediments. From the database, 11 VCs and CPTUs were used to measure and validate S_u . From the 11 VCs, S_u was measured using a Torvane. For in-situ measurements, a Manta Heavy CPT system was used with a 3.5 m penetration rod and a 1500 mm² cone. Parameters such as cone resistance (q_t), sleeve friction (f_s) and pore pressure (u_2), (measured behind the cone) were registered to examine the subsurface. To extract CPT profiles, the corrected cone resistance (q_t) is used to calculate S_u profiles (see section 2.2). Table 1 presents the results from the physical and geotechnical analysis of the vibro-corers, which includes grain-size estimation, Plasticity Index and Water content. The classification of sediments was based on the Unified Soil Classification System (USCS).

Table 1. Summary of physical characteristics for fine-grained and mixed-composition deposits

	Fine-grained deposits	Mixed-composition deposits
Depth range (m)	95-205	54-80
Fine material (%)	80-90	50-60
Plasticity Index (%)	27-35	12-18
Water content (%)	60-80	20-40
USCS classification	Clay of high plasticity (CH)	Clay of low plasticity (CL) or silt (ML), with variable sand fraction. Occasionally gravels

2.1.1 Comparison of CPTU Undrained Shear Strength with Vane Tests

CPTU shear strength profiles were compared with laboratory Vane Shear Tests (VST). Figure 1 displays representative graphs from the fine-grained deposits (CPT01 to CPT09) and from the mixed-composition (clay to gravelly) deposits (CPT15 to CPT20). The remolded undrained shear strength from CPT is derived from sleeve friction (f_s) measurements.

For the fine-grained deposits (Figure 1), VST measurements either fall in between the shear strength and remolded strength from the CPT or align with remolded strength. In general, CPT produced overestimated readings of undrained shear strength compared to VST measurements. CPT strength readings for mixed-composition deposits are amplified probably due to the relatively lower fine-grained material present in the sediments (see Table 1). This induces more peaks in undrained shear strength, which is evident in CPT 16 and CPT 18 due to presence of gravel (SM with gravel) or higher fraction of sand (SM). In general, mixed composition cores exhibit a clay or silt composition with variable sand fraction (sandy lean clay/silt to lean clay/silt with sand), with some increases in the sand fraction (silty sand, SM) downcore (VC15, VC16). The alignment of VST measurements with remolded shear strength from CPT indicates that some level of disturbance may have been inflicted on the samples.

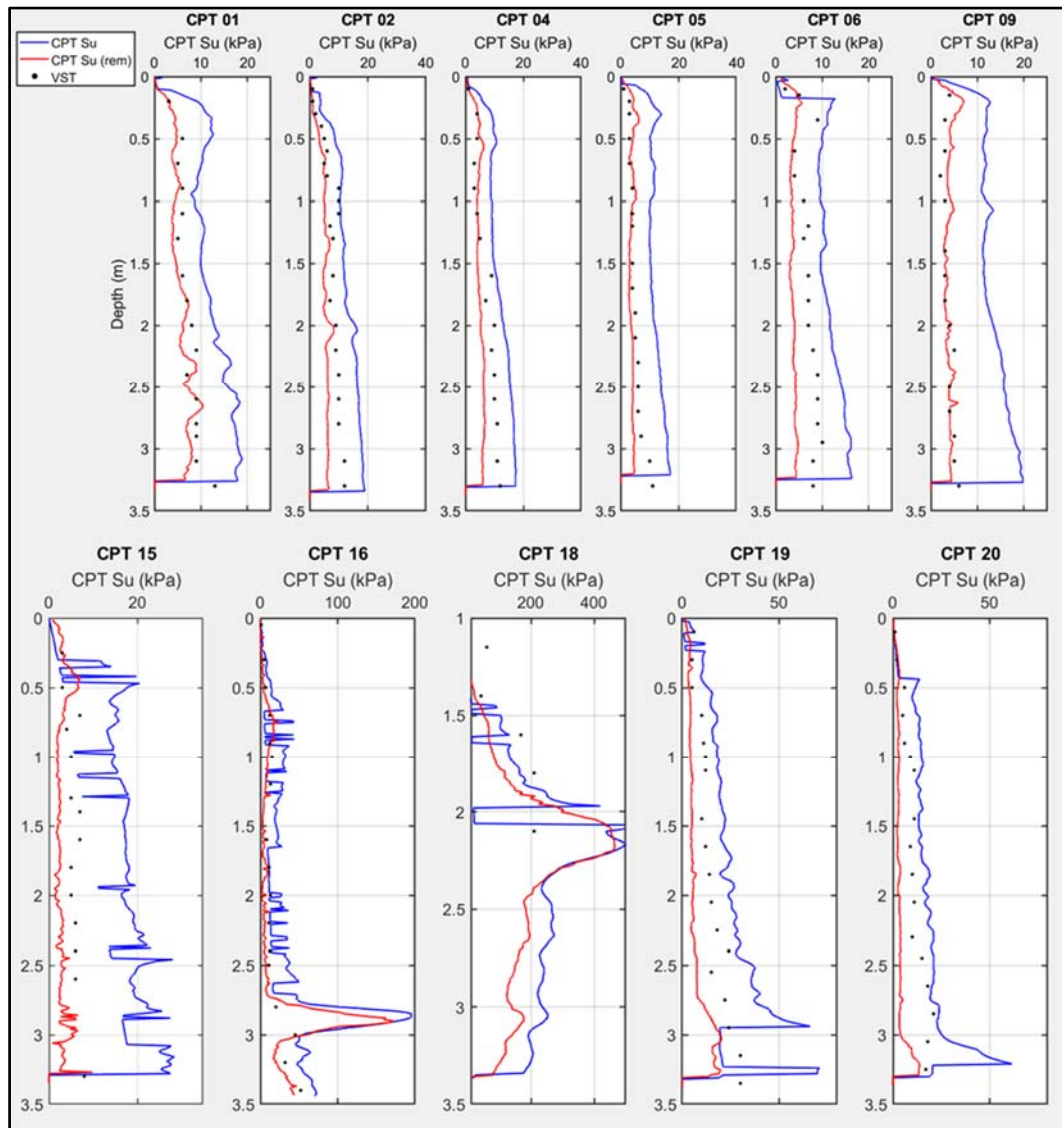


Figure 1. Profiles of undrained shear strength from CPT (blue line) and remolded strength (red line) for fine-grained deposits. VST measurements are plotted (black dots)

3 OPPORTUNITIES IN MARINE GEOTECHNICS

Offshore projects are initially based on well documented desktop and front-end engineering design studies, which rely on the availability of public or private datasets. Currently, open access to geotechnical data is not possible in Greece due to their classified status, i.e., by the companies that supervise the offshore infrastructures. This hinders researchers in their study of the Greek seafloor's sediment geotechnical behavior, as well as in the investigation of other important parameters, such as integration of geophysical data with borehole/core samples or calibration of piezocone cone penetration tests (CPTU). Regarding CPTU, no published data have been produced on the Greek seabed. For all these reasons, it is important to examine various possibilities in utilizing offshore geotechnical data based on collaboration between industry and academia. This issue becomes even more relevant in light of planned offshore projects regarding submarine cable interconnections and pipeline LNG infrastructure (Karystianos et al. 2021; Peloriadi et al. 2022).

Examples of open-access data can be found in the Netherlands, where a free-access policy has been established and has led to the development of high-quality geodatabases for the Dutch Sector of the North Sea (Peuchen and Meyer 2021). These geodatabases provide geological borehole data, seismic reflection data (2D and 3D), cone penetration test data and sample descriptions for the requirements of the hydrocarbon industry, offshore wind development, energy infrastructure (cables and pipelines) and aggregate extraction. Geotechnical information on the Dutch Sector of the North Sea is provided by a large database (BRO database), where data from other geodatabases have been collated, harmonized and processed, according to the stipulations of the INSPIRE European Directive (Peuchen et al. 2019). The concept is very similar to the EMODnet and GEMCO initiatives, where metadata are made available in order to assist researchers and surveyors (Guinan et al. 2022). The BRO database has assisted in many operations such as in the installation of monopiles, predictions of seabed mobility, development of test methods for the in-situ thermal characteristics of sediments as well as the integration of ultra-high resolution seismic reflection profiles with geotechnical data (in-situ, boreholes) (Peuchen and Meyer 2021; Peuchen et al. 2022). Moreover, the application of machine learning can also be tested using integrated data from seismic and CPT profiles, subsequently producing synthetic CPT profiles where predictions can be made for unknown soil strata (Peuchen et al. 2022). Obtaining reliable site-specific geotechnical measurements still remains a challenge, since a multitude of data measurements (seismic, CPT and borehole/core data) and high-quality lab tests are required. Within this context, measurement of undrained shear strength has become a typical example. Correlation of CPT readings with lab tests (triaxial, simple shear, vane etc.) of undrained shear strength may be better presented using large geodatabases, where trends for certain types of soils can be more easily observed (consolidated, overconsolidated etc.) (Mayne and Peuchen 2018; 2022). Based on the above, the prospect of developing a geodatabase can prove beneficial in regard to seabed geotechnical interpretation. In Greece, most of the information concerning seismic reflection data and borehole/core samples remains scattered in literature, therefore, it has not been adequately updated to assist future surveys. This also concerns research, where certain gaps in interpretation can be addressed more thoroughly through data collation and assessment from multiple datasets. Randolph et al. (2021) have provided certain examples on how collaboration between academics and industry has advanced offshore geotechnical research by addressing certain design and engineering problems. For the above reasons, it is reasonable to assume that such an endeavor can assist offshore geotechnical research in Greece by offering the following benefits: (i) enhancement of seismic stratigraphy interpretation through the use of integrated geophysical and geotechnical data, (ii) improvement of CPT soil index estimations through validated measurements, (iii) cost reduction of surveys by providing available data on sites, (iv) sustainable planning and management of offshore infrastructure, and (v) opportunities in the development of numerical and machine learning models.

References

- Guinan J, McKeon C, O'Keefe E, Monteys X, Sacchetti F, Coughlan M, Aongusha NC (2022) INFORMAR data supports offshore energy development and marine spatial planning in the Irish offshore via the EMODnet Geology portal. *Quarterly Journal of Engineering Geology and Hydrogeology* 54 (1)

- Karystianos ME, Pitas CN, Efstathiou SP, Tsili MA, Mantzaris JC, Leonidaki EA, Voumvoulakis EM, Sakellariadis NG (2021) Planning of Aegean Archipelago Interconnections to the Continental Power System of Greece. *Energies* 14, 3818. doi: <https://doi.org/10.3390/en14133818>
- Lunne T, Berre T., Andersen K.H., Strandvik S, Sjursen M (2006) Effects of sample disturbance and consolidation procedures on measured shear strength of soft marine Norwegian clays. *Canadian Geotechnical Journal*. 43: 726-750
- Mayne PW, Peuchen J (2018) Evaluation of CPTU Nkt cone factor for undrained shear strength of clays. Paper presented at the Proceedings of the 4th International Conference for Cone Penetration Testing
- Mayne PW, Peuchen J (2022) Undrained shear strength of clays from piezocone tests: A database approach. Paper presented at the Proceedings of the 5th International Conference for Cone Penetration Testing
- Peloriadi K, Iliadis P, Boutikos P, Atsonios K, Grammelis P, Nikolopoulos A (2022) Technoeconomic Assessment of LNG-Fueled Solid Oxide Fuel Cells in Small Island Systems: The Patmos Island Case Study. *Energies* 15, 3892. doi: <https://doi.org/10.3390/en15113892>
- Peuchen J, Meijninger BML, Brouwer D (2019) North Sea as geodatabase. *AIMS Geosciences* 5(2): 66-81 doi: 10.3934/geosci.2019.2.66 pp. 546-551
- Peuchen J, Meyer G (2021) Geo-intelligence from databases of offshore in-situ tests in public domain. 6th International Conference on Geotechnical and Geophysical Site Characterization (ISC2020)
- Peuchen J, van Kesteren W, Vandeweyer V, Carpentier S, van Erp F (2022) Upscaling 1 500 000 synthetic CPTs to voxel CPT models of offshore sites. Proceedings of the 5th International Conference for Cone Penetration Testing
- Powell JJM, Dhimitri L (2022) Watch out for the use of global correlations and “black box” interpretation of CPTU data. Paper presented at the Proceedings of the 5th International Conference for Cone Penetration Testing
- Randolph M, Cheng L, Lehane B, Bransby M, Hu Y, Gaudin C, Hossain MS, O’Loughlin CD, Doherty JP, Bienen B, Draper S, An H, Kim Y, Watson, PG (2021) Impact From Symbiotic Collaboration Between Industry And Academia In Offshore Geotechnics. *Australian Geomechanics*, 56 (2)
- Young AG, Quiros GW, Ehlers CJ (1983) Effects of Offshore Sampling and Testing on Undrained Shear Strength. Paper presented at the Proceedings of the Offshore Technology Conference Houston TX, OTC 4465

Satellite derived bathymetry with no use of field data

A.K. Mavraeidopoulos^{1*}

¹Laboratory of Physical Geography, Department of Geography & Climatology, Faculty of Geology & Geoenvironment, National and Kapodistrian University of Athens, Zografou, Athens, 157 84, Greece

*Corresponding author: athanasios.mavraeidopoulos@yahoo.com

Abstract

This paper experiments with the possibility to extract bathymetric information from port and coastal areas using exclusively satellite spatial data. For this purpose, very high resolution (VHR) optical imagery derived from Pleiades satellite constellation combined with data downloaded from Advanced Topographic Laser Altimeter System (ATLAS) of the Ice, Cloud, and land Elevation Satellite-2 (ICESat-2). The depths modeled using a Hybrid Bio-optical Transformation (HBT) method, together with Pleiades imagery. The relationships of the calculated IOPs and AOPs are investigated and utilized to classify the study area into sub-regions with similar water optical characteristics. The bathymetric model evaluated using surveying field data (training depths) as well as the photons measurements from ATLAS sensor. By using the abovementioned methodology, a potential revealed to model satellite derived bathymetry from coastal areas as well as performing sea-bottom investigation with a satisfactory accuracy (RMSE 1.60 – 2.62 m) for depths down to 30 m, with no use of field data.

Keywords Satellite Derived Bathymetry, Hybrid Bio-optical Transformation, Water Optical Properties, ATLAS Altimetry, Pleiades imagery.

1 INTRODUCTION

According to the official European Union demographic statistics, about 70% of the world's population lives, or lives and works up to 100 km off the coast. At the same time, EU public expenditure on protecting coastlines and coastal areas from the risk of erosion and floods amounts to € 5.4 billion per year for the period 1990-2020 **Error! Reference source not found.** However, the coastal areas including the ports are the most dynamically changing areas all over the world. One of the main reasons for this fact are the anthropogenic actions which are taking place, in such a way that impact the marine environments and ecosystems, the habitat biodiversity, and the natural resources. Bathymetry plays a significant role, contributing to the monitoring of the evolution of marine ecosystems in coastal and port areas. Researchers for more than 50 years strive to invent methodologies to describe the morphology of the 70% of the Earth which is covered by waters **Error! Reference source not found.**-[6].

Remote sensing imagery provides a mean to acquire marine environmental observations in order to understand the dynamic nature of coastal areas and its change in various temporal and spatial scales [7]-[9]. In nowadays, the satellite imagery can provide users with high resolution environmental information, such as those acquired by Pleiades sensors [10]. This issue is very critical, when scientists need to monitor bathymetry, coastline erosion, the species biodiversity and coastal productivity at small scales (spatially and temporary) as well as to undertake measures for protecting their vulnerable marine ecosystems and near shore population life quality [11]. Although coastal area mapping refers to temporal snapshots of the state of the ecosystem observed, at the time of image acquisition, bathymetry is usually a more constant parameter, since the seabed is more stable dynamically [12], [13]. The extraction (determination) of bathymetry contribute to identify and understanding the factors resulted in changes to the submerged habitats and sediment submerged transition. Speaking about passive remote sensing techniques, the accuracy of the extracted depth (height of the sea surface from seabed) related in three parameters: the accuracy of estimating the water leaving radiance or reflectance, the performance of bio-optical algorithms that related to these radiances-reflectance [14] and the accuracy of the field data used for training dataset. Should be noted that only 5-20% of radiance that propagates back to the atmosphere, derives from waters and only 1-5% originates from the seabed. In satellite extracted bathymetry techniques, most of the times, there is a requirement for performing appropriate calibration and validation procedures [15]. A crucial factor of the accuracy of the modeled depths is the quality of the field data used for the satellite derived bathymetry (SDB) model training [16]. Noticing that the in-

situ data acquisition, is a time consuming and expensive issue, especially in remote areas or in coastal areas with extended shallows.

Recent research proved that an alternative solution for SDB models fusion can be data collected through the Ice, Cloud and Land Elevation Satellite-2 (ICESat-2). NASA's ICESat2 launched in September 2018 carrying the Advanced Topographic Laser Altimeter System (ATLAS). The ATLAS LIDAR (ATL03) transmits a green wavelength lidar (532 nm), with a 10 kHz pulse repetition rate and a footprint of 17 m diameter [17]. This results to a laser footprint every 0.7 m along ground tracks. The data set of ATLAS sensor contains height above the WGS 84 ellipsoid (ITRF2014 reference frame), latitude, longitude, and time for all photons measured [18]. Latest research presents the capability to use ATLAS altimetry information for bathymetric analysis [19], [20].

The main aim of this paper/study is to model bathymetry, using High Resolution satellite data, by testing the ATLAS altimetry data in conjunction with a Hybrid Bio-optical Transformation and Very, exploiting open-source data, open-source software, taking into account the requirements for minimum manpower.

2 DATA AND METHODS

2.1 The Study Site

The geographic area selected for this research is the Laganas bay that covers a coastal area at the southern part of Zakynthos Isl., in Ionian Sea (Greece). The Bay of Laganas is very popular for its natural beauty, with blue waters, sandy beaches and wooded hills (Figure 1).

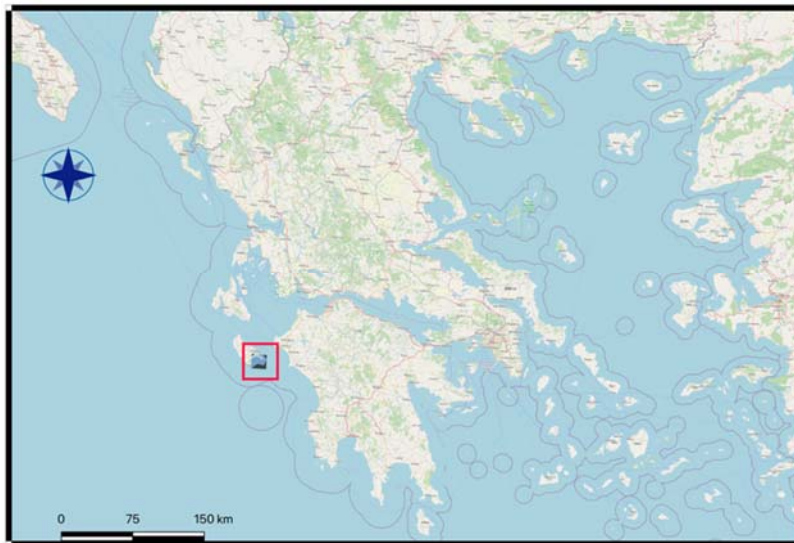


Figure 1. Map of the Study Site (Laganas bay, Zakynthos Isl./red rectangular)

2.2 Data Used

The use of high-resolution imagery investigated, acquired from Pleiades satellite constellation. Especially, the Pleiades image (DS_PHR1A_201505070930456_FR1_PX_E020N37_1220_01318) used in this research dated on 07 May 2015 (time: 09h 31min 51.6562sec) which covers an area of 157.00 km² (cloud coverage 0%). It is georeferenced in the Coordinate Reference System (CRS) EPSG 32634 (WGS84, UTM 34Z, North) and is designated as "Pleiades Standard Ortho" product. The Pleiades image utilized to extract the bathymetry of Laganas bay by using a specific model named Hybrid Bio-optical Transformation (HBT) described in detail in [21].

The ICESat-2 altimetry data downloaded free of charge from www.openaltimetry.org site. Altimetry information over sea area of Laganas bay analysed of the dates of 18.09.2019, 18.12.2019 and 16.12.2020. Ground truth data also used in the framework of the present research for validation purposes. The mentioned data collected during a bathymetric survey organized and coordinated by University of Aegean, in Gerakas bay area, which is a coastal area located at the eastern part of Laganas

bay (Figure 2). The field bathymetric dataset collected on 10 May 2015, which is a date closely to the date of Pleiades imagery used. The aforementioned in-situ data acquired by using a single-beam echosounder and an RTK/GPS receiver. Raw bathymetric data processed and cleaned from systematic errors and blunders. Finally, a total of 381 soundings used for validation scope. The ground truth data utilized for evaluating the final SDB model computed using the HBT method as well as the bathymetry measured by ATLAS03 in particular dates.

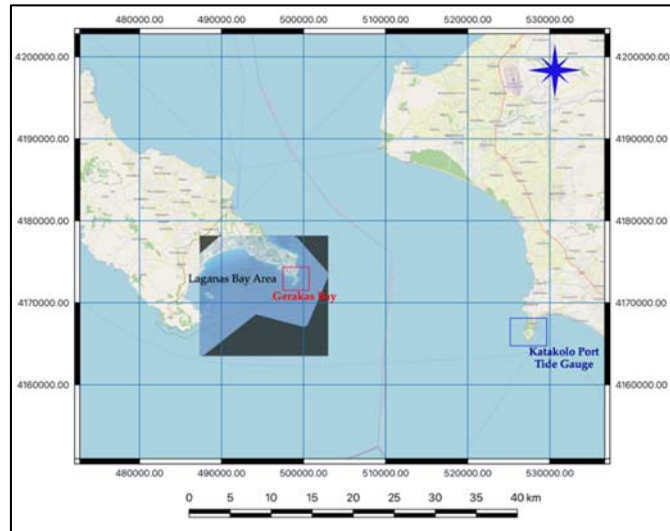


Figure 2. Bathymetry resulted using HBT Model

2.3 Methodology

Initially, the altimetry data of ATLAS08 sensor downloaded, free of charge, in *.csv format, from relevant NASA site (www.openaltimetry.org). The track number No. 1265 and its ground track 2 (gt2) selected as more appropriate, since it collects data with minimal refraction, since it beams to the direction of the sensors nadir. Photon's altimetry data are referred to ellipsoidal height (WGS84). To convert photons ellipsoidal heights to Orthometric heights (Geoid heights-EGN2008), the Geoid Height (N) should be known in order to be subtracted from photons heights (Orthometric height (H)= Ellipsoidal Photon height (ICESat-2 heights (h) – Geoid Height(N)). The Geoid Height (N) data for Zakynthos Island downloaded (free of charge) from International Center for Global Gravity Field Models site (ICGEM) (<http://icgem.gfz-potsdam.de/>). ATLAS08 photons heights transformed to Mean Sea Level (MSL) heights. The MSL photons heights compared and validated with the ground truth (field bathymetric) data which referred to MSL vertical datum as well as to the mean sea level of the Tide Gauge of Katakolo Port, which is the closer tide gauge in the area located at 35.0 km from the study area. The Katakolo tide gauge sea level data downloaded, free of charge, from the IOC monitoring site (<http://www.ioc-sealevelmonitoring.org/>).

Afterwards, the Hybrid Bio-optical Transformation (HBT) applied to Pleiades imagery according to the model described by Mavraeidopoulos et al. [21]. The Pleiades image further corrected for the sunglint error by applying the NIR band of Pleiades imagery according to the algorithm developed by Kay et al. [22]. Imagery is also corrected for water column effects based on Lyzenga's methodology [23] and the relevant water bio-optical properties ($b_b(\lambda)$, $\alpha(\lambda)$, $K_d(\lambda)$) computed using the Quasi-Analytical Algorithm (QAA) of Lee et al. [24]. The relations of the bio-optical properties validated and utilized in order to classify the image in subareas of common water optical properties. Moreover, the ratios of the abovementioned water optical properties calculated along with their natural logarithms.

Then, a regression analysis takes place between the seabed photons heights and the ratios of bio-optical properties at the classified subareas (areas of common water optical properties). The equation with the best correlation between the ICESat-2 data and bio-optical ratios is used to compute the bathymetry in each classified subarea. The final Satellite Derived Bathymetry (SDB) model of the entire area is created by merging the SDB computed for each subarea. A final regression analysis takes place to validate the

bathymetry derived exclusively from space-borne depths. The final bathymetry results also evaluated with the field area collected in past at the area of Gerakas bay (eastern Laganas sea area).

3 RESULTS

Satellite Derived Bathymetry (SDB) model using Hybrid Bio-Optical Transformation is presented in figure 3 that follows. Using data from relevant NASA's cyberinfrastructure platform for discovery, access, and visualization of ICESat-2 data (<https://openaltimetry.org/data/icesat2/>), it was found out that the data set of the 16th of Dec 2020, (track no. 1265), comes over Gerakas bay, where field bathymetric data were also available. Undertaken the abovementioned analysis, a good fit between field data collected during the bathymetric survey of Gerakas Bay dated of 10 May 2015 and the field bathymetry from ICESat-2 acquired on 16 Dec 2020, figured out. The small deviation observed could be resulted from seabed change in the time period between the two campaigns or the possible error in depth reduction of bathymetric data from the local vertical datum information (tide reduction). Hence, having in mind that the photons heights represent in essence the bathymetry along-track no. 1265 in WGS84 (ITRF2014 reference frame), a regression analysis performed between ICESat-2 heights and satellite derived bathymetry from HBT model.

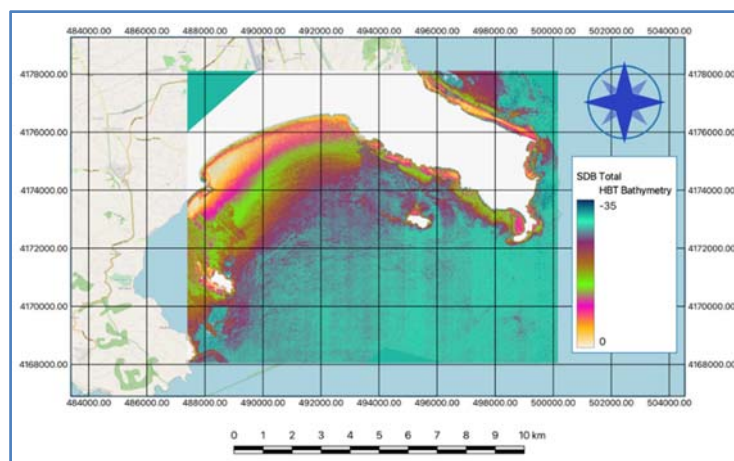


Figure 3. Bathymetry resulted using HBT Model

4 CONCLUSIONS

Ports and coastal area bathymetry is required for a wide range of scientific and engineering applications since coastal waters are areas very dynamically changed. It is still a challenge the fact that exploiting the techniques of remote sensing, depths can be modeled over large or/and remoted coastal areas, consisted of dangerous hazards, submerged objects and steep mor-phology of seabed, included a wide range of benthic diversity. The capability to derive Ba-thymetry (SDB) using Hybrid Bio-Optical Transformation combined with spaceborne ground truth data from ICESat-2 could introduce new perspectives to the coastal management issues.

Experiments shown that after relevant data processing and analysis, the ICESat-2 data can be exploited to calibrate high-resolution imagery, in order to provide coastal bathymetry. The maximum seabed depth measured by ICESat-2 was about -29.0 m. Bathymetry derived from satellite imagery using HBT model, was in good fit with the bathymetry measured by ICESat-2, when the latter was validated with the orthometric photons heights gave a determination coef-ficient of $R^2 = 0.906-0.969$ and an average $RMSE = 2.70$ m. The resulted Root Mean Squared Error is a combination of the accuracy of the geolocation of ICESat-2 data, the sea state at the time of image acquisition and the photons vertical uncertainty.

Further research is required to improve the accuracy of the method described in this article with the scope to reduce the average RMSE. However, the methodology adopted here seems to be functioning. Bathymetry data derived from exclusively spaceborne data can be used in a diverse range of objectives

related to marine management, by monitoring coastal environmental parameters and providing the interested stakeholders and planners with cheap but very significant ecosystems information.

Data Availability Statement

Pleiades Data used in this research provided free of charge by the European Space Agency in the framework of the acceptance of proposal of Dr. A. K. Mavraeidopoulos Nr. 40867 titled “Bathymetry/Hydrography Extraction from Imagery”, (ESA Cat-1/EO Data User Project ID: 40867).

Acknowledgments

The depth data from the sea area of the bay of Gerakas, Zakynthos were collected by the Associate Professor of the University of West Attica Professor Em. Oikonomou and Associate Professor of Aegean University Ep. Hasiotis in the framework of a European research program carried out in the study area, to whom I thank warmly for their free sponsorship in order to evaluate them and use them accordingly in my research.

References

- [1] European Environment Agency (2018). <https://www.eea.europa.eu>.
- [2] Hammack, J.C. (1977) LandSat goes to sea. *Photogrammetric Engineering and Remote Sensing*, 43(6), 683-691.
- [3] Lyzenga, D.R. (1978). Passive Remote Sensing Techniques for Mapping Water Depth and Bottom Features. *Applied Optics*, 17, 379-383.
- [4] Jupp, D.L.B. (1988) Background and Extensions to Depth of Penetration (DOP) Mapping in Shallow Coastal Waters. *Symposium on Remote Sensing of Coastal Zone*, Gold Coast, Queensland.
- [5] Brando, V.E.; Anstee, J.M.; Wettle, M., Dekker, A.G. (2009) A Physics-based Retrieval and Quality Assessment of Bathymetry from Suboptimal Hyperspectral Data. *Remote Sensing of Environment*, 113, 755-770. <https://doi.org/10.1016/j.rse.2008.12.003>.
- [6] Tatsuyuki, S.; Yuta, Y.; Toshio, O.; Tsutomu, Y. (2019) Satellite Derived Bathymetry Using Machine Learning and Multi-Temporal Satellite Images. *Remote Sens.*, 11(10), 1155. <https://doi.org/10.3390/rs11101155>.
- [7] Sathyendranath, S.; Platt, T.; Caverhill, C.M.; Warnock, R.E.; Lewis, M.R. (1989) Remote Sensing of Oceanic Primary Production: Computations using a Spectral Model. *Deep-Sea Res.*, 36, 431–453.
- [8] Eugenio, F.; Marcello, J.; Martin, J. (2015) High-Resolution Maps of Bathymetry and Benthic Habitats in Shallow-Water Environments using Multispectral Remote Sensing Imagery. *IEEE Trans. Geosci. Remote Sens.*, 53, 3539–3549.
- [9] Muzirafuti, A.; Crupi, A.; Barreca, G.; Randazzo, G. (2019) Shallow water bathymetry by satellite image: A case study on the coast of San Lo Capo Peninsula, Northwestern Sicily, Italy. In *Proceedings of the International Workshop on Metrology for the Sea*, Genova, Italy, 3–5 October 2019.
- [10] Apollo Mapping-The Image Hunters, High Resolution Satellite and Aerial Imagery. Available online: <https://apollomapping.com/imagery/high-resolution-imagery> (accessed on 19 March 2020).
- [11] Hussain, M.S.; Bujang, J.S.; Zakaria, M.H.; Hashim, M. (2015) The Application of Remote Sensing to Seagrass Ecosystems: An Overview and Future research Prospects. *Int. J. Remote Sens.*, 36 (1), 61-113.
- [12] Hedley, J.D.; Roelfsema, C.M.; Chollett, I.; Harborne, A.R.; Heron, S.F.; Weeks, S.; Skirving, W.J.; Strong, A.E.; Eakin, C.M.; Christensen, T.R.L.; Ticzon, V.; Bejarano, S.; Mumby, P.J. (2016) Remote Sensing of Coral Reefs for Monitoring and Management: A Review. *Remote Sens.*, 8 (2), 118.
- [13] Blandon, A.; Ermgassen, P.S.E. (2014) Quantitative Estimate of Commercial Fish Enhancement by Seagrass Habitat in Southern Australia. *Estuarine, Coastal and Shelf Science*, 141, 1-8.
- [14] Mobley, C.D.; Sundman, L.K. (2000) *Hydrolight 4.1—Users Guide*; Sequoia Scientific, Inc.: Redmond, WA, USA.
- [15] Tulloch, V.J.; Possingham, H.P.; Jupiter, S.D.; Roelfsema, C.M.; Tulloch, A.I.T.; Klein, C.J. (2013) Incorporating uncertainty associated with habitat data in marine reserve design. *Biol. Conserv.*, 162, 41-51.
- [16] Roelfsema, C.M.; Phinn, S.R. (2013) Validation in *Coral Reef Remote Sensing: A Guide for Multi-level Sensing Mapping and Assessment*; Goodman, J., Purkis, S.R., Eds.; Springer: Berlin, Germany, pp. 375-365.

- [17] Parrish, C.E.; Magruder, L.A.; Neuenschwander, A.L.; Forfinski-Sarkozi, N.; Alonzo, M.; Jasinski, M. (2019) Validation of ICESat-2 ATLAS Bathymetry and Analysis of ATLAS's Bathymetric Mapping Performance. *Remote Sens.*, *11*, 1634. <https://doi.org/10.3390/rs11141634>.
- [18] Neumann, T. A.; Brenner, A.; Hancock, D.; Robbins, J.; Saba, J.; Harbeck, K.; Gibbons, A.; Lee, J.; Luthcke, S.B.; Rebold, T. et al., 2020. ATLAS/ICESat-2 L2A Global Geolocated Photon Data, Version 3. Boulder, Colorado USA. NASA National Snow and Ice Data Center Distributed Active Archive Center. doi: <https://doi.org/10.5067/ATLAS/ATL03.003>. [assessed 20 September 2021].
- [19] Thomas, N.; Pertiwi, A. P.; Traganos, D.; Lagomasino, D.; Poursanidis, D.; Moreno, S.; and Fatoyinbo, L. (2021) Space-borne cloud-native Satellite- Derived Bathymetry (SDB) models using ICESat-2 and Sentinel-2. *Geophysical Research Letters*, *48*, e2020GL092170. <https://doi.org/10.1029/2020GL092170>.
- [20] Babbel, B. J.; Parrish, C. E.; and Magruder, L. A. (2021) ICESat-2 elevation retrievals in support of satellite-derived bathymetry for global science applications. *Geophysical Research Letters*, *48*, e2020GL090629. <https://doi.org/10.1029/2020GL090629>.
- [21] Mavraeidopoulos, A.K.; Oikonomou, E.; Pallikaris, A.; Poulos, S. (2019) A Hybrid Bio-Optical Transformation for Satellite Bathymetry Modeling Using Sentinel-2 Imagery. *Remote Sens.*, *11* (23), 2746.
- [22] Kay, S.; Hedley, J.D.; and Lavender S. (2009) Sun Glint Correction of High and Low Spatial Resolution. *Remote Sensing*, *1*, 697-730. doi:10.3390/rs1040697.
- [23] Lyzenga, D. (1981) Remote Sensing of Bottom Reflectance and Water Attenuation Parameters in Shallow Water using Aircraft and Landsat Data. *International Journal of Remote Sensing*, *2*(1), 71-82.
- [24] Lee, Z-P.; K.L. Carder; and R.A. Arnone (2002) Deriving Inherent Optical Properties from Water Color: A Multiband Quasi-Analytical Algorithm for Optically Deep Waters. *Applied Optics*, *41*(27), 5755-5772.

Seabed conditions in the embayment of Agia Efimia (Kefalonia) 2 years after the Medicane IANOS

I. Petsimeris, A. Oikonomou, A. Poulos, O. Andreadis, V. Lioupa, T. Hasiotis*

Department of Marine Sciences, University of the Aegean, University Hill, Mytilene 81100, Lesvos Isl., Greece

*Corresponding author: hasiotis@aegean.gr

Abstract

The Mediterranean tropical-like cyclone (Medicane) IANOS struck the southern Ionian Islands in September 2020, causing devastation in local infrastructures. In the eastern part of Kefalonia, Agia Efimia suffered extensive damages, whilst a mud/debris flow drained in the local port. In September 2022 a coastal survey took place to evaluate the seabed conditions in relation to the existence of sediments that may be related to the materials deposited during the Medicane, and comparatively between the port and the wider embayment. The bathy-morphological survey revealed the seafloor habitats but also the area being dredged to shallow and clean the port from IANOS materials. Also, various natural and anthropogenic targets were identified, most of them transported during the Medicane-induced mass flows. Sediment analysis showed the presence of a surficial layer influenced by human activities and remnants of IANOS materials and a subsurface layer probably corresponding to the natural bed of the embayment. The survey showed that during the intervening 2 years IANOS deposits have been mixed due to physical and human-induced processes but also highlighted the need for coastal management actions in order to reduce the anthropogenic impact and restore the environmental quality of Agia Efimia embayment.

Keywords Medicane IANOS, coastal geomorphological mapping, port sediments, geophysical survey

1 INTRODUCTION

Medicanes (Mediterranean tropical-like cyclones), though rare, are responsible for various types of catastrophic impacts on the Mediterranean coastal regions, including storm surges and erosion of low-lying areas, damages due to strong winds and high waves, landslides due to intense rainfalls (Scicchitano et al. 2021; Toomey et al. 2022). These processes account for infrastructure damages but also for loss of lives and injuries. In September 2020 IANOS Medicane, the most intense medicane ever recorded in the Mediterranean (Lagouvardos et al. 2022), stroke the western and central parts of Greece causing four casualties and severe damages in local infrastructures. In the eastern part of Kefalonia, Agia Efimia experienced damages due to widespread flooding, mud and debris flows but also due to the strong winds and waves. The surrounding Agia Efimia geological conditions and tectonic regime is responsible for an extensive zone of intensively fractured rock mass that gave the material for the extensive debris flow phenomena along the SW and central part of the Pylaros basin during IANOS (Valkaniotis et al. 2022; Diakakis et al. 2023). The same authors point that mass flows appear to be a recurring phenomenon, since alternating loose sandy-clayey material and layers of gravels, cobbles, and boulders are found along the mainstream floor draining in Agia Efimia, suggesting past flood and debris flow phenomena.

Mud/debris flows drained at the port of Agia Efimia altering the morphology and the local environment. Natural materials (i.e., branches of various sizes), but also several objects of man-made origin deposited in the port and the wider embayment. A large volume of these items was removed by volunteers and crews of the Municipality of Sami immediately after the bad weather. During summer 2022, dredging works were carried out in the port aiming to clean it from transported natural materials that had altered the relief and caused shallowing, especially in its northern part, near the pier where tourist boats are moored. In addition, the Municipality prepared plans to upgrade the existing port facilities, for improving the safety level of berthed vessels.

This study aims to evaluate the seabed conditions 2 years after IANOS (i) in relation to the existence of soft/loose sediments that may be related to the materials deposited during the bad weather conditions, and (ii) comparatively between the port and the wider embayment.

2 METHODS

The survey was carried out using a 4.8 m inflatable boat along a specific grid and a 7-m boat for coring. Navigation, positioning, bathymetry, and seabed morphology were supported by a Humminbird Helix 10 multi-parametric sonar. The sonar, although designed for general use in shallow waters, can provide high resolution information. It uses 180-240 kHz for bathymetry and 455 kHz (Chirp technology) for morphological (side scan sonar-SSS) mapping. Position accuracy was 3 m and depth accuracy 0.5% on each measurement.

In order to create accurate bathymetric and morphological maps of the study area, a dense grid of crossing survey lines was performed (Figure 1a). The total number of survey lines was 51, of which 42 had an E-W direction and a length of approximately 12 km, while 9 had a N-S direction, being ~3.5 km in length. Spacing between the W-E lines ranged from 10 to 30 m due to anchored sailing ships within the port. The bathymetric data were exported in a .csv format and then imported in QGIS. The IDW method was used in QGIS to create a 1x1 m bathymetric grid. SonarWiz was used for post-processing, analysis, and mosaicking of the collected sonographs. Processing involved bottom tracking (allowing for water column removal and an isometric record), gain setting changes, de-stripe filter and nadir filter. Finally, a georeferenced mosaic (GeoTIFF) of very high resolution (0.05 x 0.05 m) was created using a selection of overlapping records. For the inner part of the embayment records with W-E orientation were chosen, whilst on the area out of the port N-S oriented records were used giving better coverage. The total area of the SSS mosaic was ~156000m². Careful examination of both the individual SSS records and the mosaic revealed different backscatter (reflectivity) tones and geomorphological features, which were gathered to produce the geomorphological/habitat map of the study area.

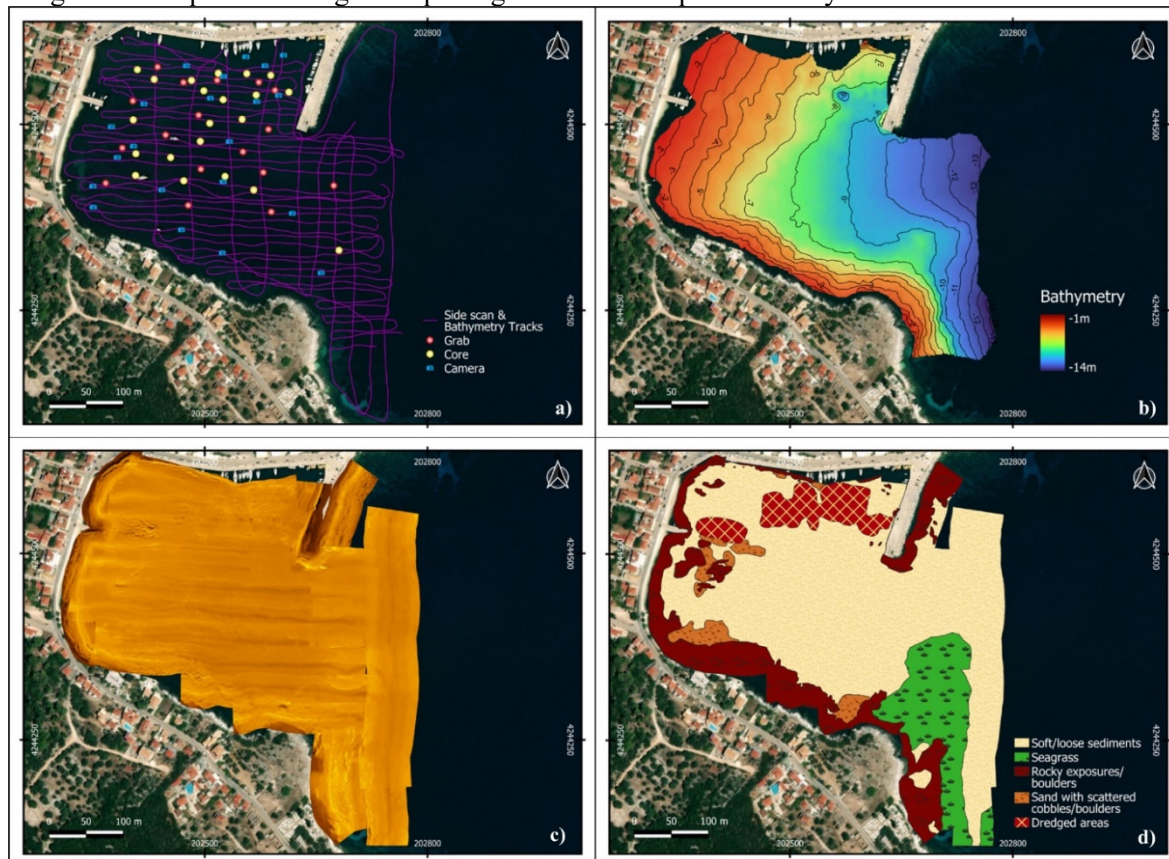


Figure 1 (a) Field data collected over Agia Efimia embayment, (b) bathymetry map deeper than ~2 m, (c) SSS mosaic and (d) geomorphological/habitat map of the study area.

For ground-truthing purposes in certain locations of interest, a drop camera was used to validate the side scan records. The total number of drop camera stations was 21 (Figure 1a). Most of the captures were located to the north (port area). A common characteristic of all the videos was the lack of visibility due to turbidity. Also, many videos evidenced debris of natural and anthropogenic origin inside the port, probably related to IANOS mud/debris flow.

A small gravity corer (1.0 m long) and a van-veen grab managed to collect 12 small sediment cores (9 attempts failed) and 17 surficial samples, respectively (Figure 1a). The sample locations were selected after thorough examination of the side scan records. In the northern part of the area the uneven seafloor and the shallow depths did not allow for core samples even after multiple attempts. In the laboratory, the plastic cores were split in half, photographed and macroscopic observations were made such as sediment color and sediment texture and layering. Grain size analysis was performed by the pipette method for the fine sediment and dry sieving for the coarser grains (Folk 1980). Statistical parameters were calculated in ϕ units ($\phi = -\log_2 d$, where d is the grain diameter in mm) using the Gradistat software (Blott and Pye 2001). All data were imported and processed in QGIS in EGSA87' (Greek grid).

3 RESULTS AND DISCUSSION

The bathymetric survey showed an even seabed with steeper slopes occurring at the southern part of the study area, in continuation to the onshore rocky outcrops (inclinations of ~11%) both in and out of the embayment (Figure 1b). The deepest area out of the embayment reached ~14 m depth. A zone of irregular microrelief was observed to the north, at the outer edge of the port, coinciding with the dredged area.

In the SSS mosaic many seabed features were visible such as areas with outcrops and boulders, a location that appeared to have been dredged as well as areas covered with soft/loose sediments. However, some features like seagrass were relatively difficult to differ from others (i.e., coarser sediments) making the study of the SSS records separately necessary. With the examination of the mosaic and the individual records habitats were mapped depending on their backscatter pattern and tone. Five backscatter (reflectivity) patterns (BP) that correspond to different types of sediments and habitats were identified (Figure 2). The first returns a low reflectivity (occasionally with and sparsely distributed small targets), it is related to the smooth relief and is indicative of fine-grained sediments. This BP covers the larger part of the embayment (Figure 1c,d), whilst the observed smaller targets and stripes were mainly attributed to human debris and anchor chains, respectively.



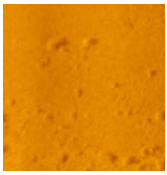

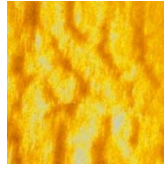

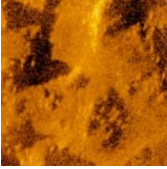

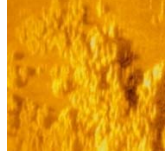

BP	SSS image	Seafloor camera snapshot	BP	SSS image	Seafloor camera snapshot
1			4		
2			5		
3					

Figure 2 Representative SSS images of the observed backscatter patterns and corresponding BP appearance on the underwater camera snapshots

The second BP is of relatively high reflectivity developing in uneven intervals and corresponds to *p. oceanica* meadows with height differences, which cover the southern part of the embayment. The third BP consists of rapid changes of high reflectivity followed by varying in extent shadows and refers to rocky exposures and/or densely distributed boulders. It is found in the shallow waters around the embayment and next to the pier. The fourth BP has a medium reflectivity with small targets of higher reflectivity followed by smaller shadows and is related to the presence of scattered coarser material (cobbles to boulders) within sandy sediments. This pattern appears in patch form, usually next to BP 3 in shallow waters. The fifth BP has mixed reflectivity tones (from low to high with acoustic shallows) in irregular intervals appearing like cavities and corresponds to the anomalous micro-relief created due to dredging operations. The latter BP is found to the north, within the port, shallower than ~7-8 m water depth. Various targets were also observed in the sonar images, and they were found to be (after inspection with the drop camera) of human (anchor scars, suspended chains, big public wheelie waste bin, tires, a small almost buried boat, etc) but also of natural origin (i.e., tree or bush branches, boulders), most of them probably carried away by the intense stream runoffs induced by IANOS.

Considering the geomorphological map (Figure 1d), and specifically the northern part (port area) it is apparent that its morphology has been clearly shaped from the dredge works. It is likely that areas closer to the dock that were dredged but do not show clear signs of this activity, were smoothed out by hydrodynamics, and are also covered by looser sediment due to the sediment transport. Seagrass meadows (mainly *p. oceanica*) start to develop in the southern part of the study area, out of the embayment, deeper than 9-10 m.

The small sediment cores (Figure 3) verified the presence of two distinct layers. The surficial layer (A) is 10-46 cm thick, fine-grained (mud to sandy mud) and consists of a surficial lamina (1-5 mm) of dark brown mud overlying dark grey or dark brown to grey or almost black muddy sediments with roots, small branches, leaves, pine needles and pieces of wood. The terrestrial origin is undisputable, however the dark to black color of the sediments is also indicative of high organic content probably related to human activities. Benthic activity appears to be absent except from a few very small biogenic fragments occasionally found in the samples. The mean size (M) ranges from 6.38 to 7.43 Ø. Mud has a high percentage (80.57-97.84%), with silt being the dominant textural class (50.08-66.27%). Sand is rare and only locally appears higher values (2.16-19.43%). Gravels were not observed in the surface layer (A). Standard deviation (σ) ranges from 2.36 to 2.97 Ø, indicating very poorly graded sediments.

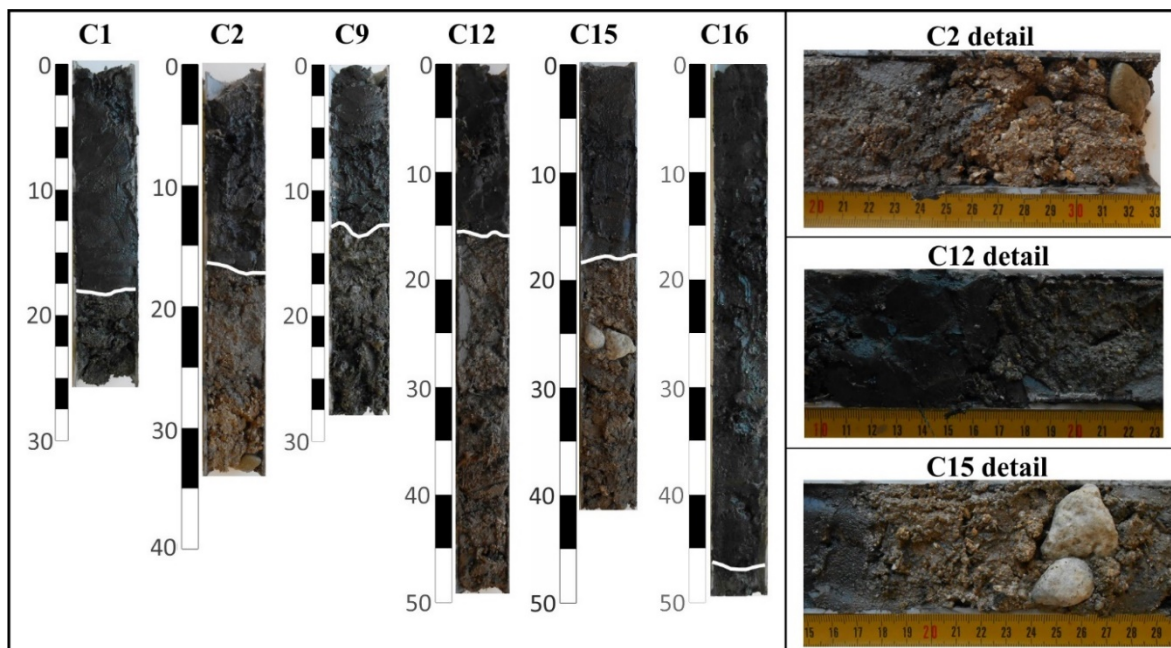


Figure 3 Small sediment cores collected over Agia Efimia embayment showing the contact (white lines along the cores) between the surficial (A) and the subsurface (B) layers. Close up photos illustrating the sharp change in color and consistency between the two layers

The subsurface layer (B) is usually separated by a distinct unconformity from layer A, it consists of sandy mud to gravely muddy sands, locally with small gravels, it is brown to grey-brown in color with biogenic fragments of various sizes and occasionally with remnants of seaweeds. The existence, locally, of small pieces of leaves/plants of terrestrial origin is possibly related to older stream runoff deposits. It seems that layer B represents the natural sedimentary bed of the embayment. The mean size M ranges from 2.22 to 6.91 ϕ indicating a wide range of the various textural classes (gravel: 0-11.71%; sand: 15.33-75.84%; silt: 12.86-55.67%; clay: 6.59-33.48%), with the coarser classes attaining high values. Standard deviation ranges from 2.56 to 3.37 ϕ , suggesting very poorly sorted sediment, similarly to the surficial layer (A).

The grab sediments also mimic the consistency of layer A, being fine-grained (mud: 64.19-98.44%), with slightly coarser material (gravel: (0.86-3.83%; sand: 1.56-34.29%) observed to the northwest but also to the central part of the port, probably related to mixing during the dredging works as well as to sediments from shallower waters.

Table 3 Average values of the sediment textural classes and of the main statistical parameters (mean (M) and standard deviation (σ)) for the surficial (A) and the subsurface (B) layers and the grab samples

	Gravel %	Sand %	Silt %	Clay %	M (ϕ)	σ (ϕ)
Surficial layer (A)	0.00	8.85	57.68	33.47	7.02	2.61
Subsurface layer (B)	3.06	44.23	35.39	17.32	4.32	2.91
Grabs	1.28	18.04	52.96	28.21	6.12	2.91

It is evident that during the intervening period between IANOS Medicane and the present sampling (about 2 years), mixing of the sediments took place (a) with materials of anthropogenic origin (mainly sewage) flowing into the bay, (b) due to hydrodynamics (waves and coastal currents) and (c) probably, to a lesser extent, due to seasonal disturbance from the mooring of vessels. It becomes obvious that, at present, the main concern must be the adoption of management plans in order to reduce human intervention and improve/restore the environmental quality of the wider area.

References

- Blott SJ, Pye K (2001) Gradistat: A Grain Size Distribution and Statistics Package for the Analysis of Unconsolidated Sediments. *Earth Surf Proc Landf* 26:1237–1248
- Diakakis M, Mavroulis S, Filis C, Lozios S, Vassilakis E, Naoum G, Soukis K, Konsolaki A, Kotsi E, Theodorakidou D, Skourtsos E, Kranis H, Gogou M, Spyrou N, Katsetsiadou K, Lekkas E (2023) Impacts of Medicanes on geomorphology and infrastructures in the eastern Mediterranean, the case of Medicane Ianos and the Ionian Islands in Western Greece. *Water* 15, 1026. <https://doi.org/10.3390/w15061026>
- Folk R (1980) *Petrology of Sedimentary Rocks*. Hemphill Publishing Company, Austin, Texas
- Lagouvardos K, Karagiannidis A, Dafis S, Kalimeris A, Kotroni V (2022) Ianos – A hurricane in the Mediterranean. *Americal Meteorological Society* 103(6):1621-1636. <https://doi.org/10.1175/BAMS-D-20-0274.1>
- Scicchitano G, Scardino G, Monaco C, Piscitelli A, Milella M, De Giosa F, Mastronuzzi G (2021) Comparing impact effects of common storms and Medicanes along the coast of south-eastern Sicily. *Mar Geol* 439, 106556.
- Toomey T, Amores A, Marcos M, Orfila A, Romero R (2022) Coastal Hazards of Tropical-Like Cyclones Over the Mediterranean Sea. *Jour Geophys Res Ocean* 127, e2021JC017964
- Valkaniotis S, Papathanassiou G, Marinos V, Saroglou C, Zekkos D, Kallimogiannis V, Karantanellis E, Farmakis I, Zalachoris G, Manousakis J, Ktenidou O (2022) Landslides triggered by medicane Ianos in Greece, September 2020: Rapid satellite mapping and field survey. *Appl Scien* 12(23), 12443. <https://doi.org/10.3390/app1223124>

The contribution of hydrography to pockmark detection, for the port construction and maintenance optimisation, with the use of modern sonar systems

D. Kiouisi¹, E. Oikonomou¹, A. Sartampakou², P. Sartampakos^{3*}

¹Department of Surveying and Geoinformatics Engineering, University of West Attica (UNIWA), 28
Ag.Spyridonos Str, 12243, Greece

²Nikolaou Plastira Str., 187 55 Keratsini Attica, Greece

³NIREAS Engineering, 1-3 Skra Str., Athens, 17673, Greece

*corresponding author: sartabakos@yahoo.gr

Abstract

Hydrographic surveys and seabed mapping, especially in coastal areas, are of great importance, since they contribute to navigation safety and environmental protection, while playing a pivotal role in marine activities, such as economic development, constructions, hydrocarbon detection, cable laying, as well as marine research and defense. In the present work at the port of Katapolo, in Kyparissiakos Gulf, Western Peloponnese in Greece, a high resolution 3D bathymetric model was made with the use of multibeam sonar and the application of specialized hydrographic software, in order to process and analyse point-cloud data, and to detect and monitor the existence of circular seabed depressions called “pockmarks”. The main purpose of this study is to indicate the importance of Hydrography in precise seabed surveys, resulting in accurate data that can be used for the proper design and positioning of marine constructions, and for reassuring the sustainability and operational functionality of already existing harbours.

Keywords: Bathymetry, Pockmarks, Multibeam echosounder, Port construction and safety.

1 INTRODUCTION

The bathymetric surveys refer to the seabed 3D morphology, as well as to the coastline topography. In several occasions, the seafloor surveying also includes its material composition, especially in cases of submarine cable and pipeline laying, port construction and coastal engineering. The position of horizontal survey points (X,Y) is defined with the use of precise GNSS (Global Navigation Satellite Systems), for the accurate orientation and specification of the acoustic beam trajectory during each sounding, whilst the third dimension (i.e. depth Z) is computed from other devices, such as echosounders used in the present research. In order to gain 3D coordinates (X,Y,Z) for the spatial display of the natural sea bottom, depth measurements are combined with horizontal positionings at each point. The hydrographic survey took place in July 2022 at the port of Katakolo, in the Western Peloponnese, Greece (Figure 1), with the study area selected due to detection of gas seepages.

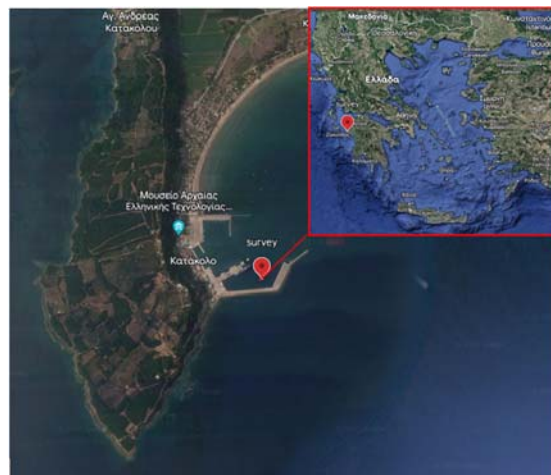


Figure 14: Chartographic illustration of Katakolo. (Source: <https://earth.google.com/>)

Along the Kyparissiakos Gulf in Kyllini, Katakolo and Kaiafas, a geological survey conducted in 2004 (Giuseppe Etiope et al., 2006) revealed gas seepages that reflect deep hydrocarbon-generation processes. Especially at Katakolo, the seepages occur both offshore and onshore of the local tourist harbour. The result of this systematic leakage is the creation of underwater craters, via the erosion of the bottom sediments called “pockmarks”, which may endanger the seafloor structural stability and damage marine constructions. According to Cathles et al. (2010), pockmarks are nearly circular depressions formed where fluids escape upward through fine-grained seafloor sediments (Figure 2). Their length-to-breadth ratio generally varies from 1 (circular) to ~1.25. The indication of pockmarks from the geological survey carried out in Kyparissiakos Gulf in 2004 are shown in Figure 3 and 4.

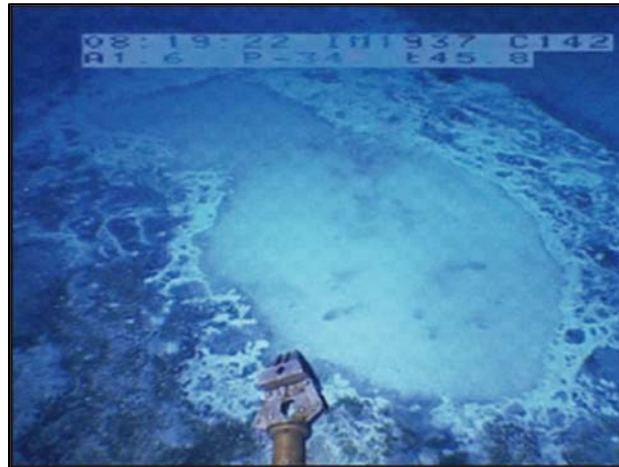


Figure 15: Submarine image of pockmark formation. (Source: Ceramicola et al, 2018)



Figure 16: Pockmark Location in Kyparissiakos Gulf.

(Source: <https://pubs.geoscienceworld.org/aapgbull/article-abstract/90/5/701/132749/Methane-and-hydrogen-sulfide-seepage-in-the>)

2 IMPACT ON PORT SAFETY

At Katakolo port there have already been previous incidents, provoked by pockmarks, that led to the destruction in some parts of the breakwater (Figure 5). Taking into account the port’s annual traffic, with a plethora of cruise boats and yachts, the dangers provoked by the pockmarks to seafloor and marine constructions may threaten both human life and ship safety. Therefore, hydrographic observations alarmingly require immediate attention and comparison with past seismic profiles recorded in the area.



Figure 4: Indication and gas seepages in the study area, from previous geological surveys. (Source: <https://pubs.geoscienceworld.org/aapgbull/article-abstract/90/5/701/132749/Methane-and-hydrogen-sulfide-seepage-in-the>)



Figure 5: Destruction at the Katakolo port breakwater in 2009

The recognition of pockmark existence is of great significance, since it contributes to the better understanding of the local seabed morphology, whilst the processing of the survey data may uncover minor anomalies in the underwater seismic profiles that otherwise might have gone undetected.

The detection of pockmark formation can efficiently be accomplished with the use of modern sonar systems, which enable obtaining seafloor images of cold seep features, as well as their acoustic character. Nevertheless, in order to achieve a better understanding of the gas seepage acoustic behaviour, a combination of surveying with backscatter data is recommended.

3 METHODOLOGY AND RESULTS

The equipment used for surveying the port bathymetry was a multibeam echosounder (with up to 120° swath coverage, 224 beams per sounding and a central frequency at 160 kHz), along with a GNSS sensor equipped with a D-GPS antenna for both horizontal positioning computations and tidal-level estimation. All depths refer to MSL (Mean Sea Level) surface, which corresponds to 0.00 m of the Hellenic Military Geographical Service control network. Moreover, hydrographic surveys should be conducted based on standards depending on the intended use. For instance, for shallow water areas, such as harbours or berthing areas as in the case of the Katakolo port, the hydrographic surveys must be conducted according to the “Exclusive order” of the 6th edition of the IHO standards manual, which requires 200% bathymetric coverage, meaning the overlapping among neighbor scannings.

For this reason, the survey in the study area implemented the boustrophedon cellular decomposition method (Choset, 2000). Additionally, in order to compute the correct depths, both water salinity and temperature were necessary to be measured near the port. For this reason a thermosalinometer device was used, and via the Mackenzie (1981) equation:

$$c(D, S, T) = 1448,96 + 4,591 * T - 5,304 * 10^{-2} * T^2 + 2,374 * 10^{-4} * T^3 + 1,34 * (S - 35) + 1,63 * 10^{-2} * D + 1,675 * 10^{-7} * D^2 - 1.025 * 10^{-2} * T * (S - 35) - 7,139 * 10^{-13} * T * D^3$$

a characteristic sound velocity $c(D, S, T)$ profile of the study area was calculated at the geographical coordinates and UTC date and time where the depth (D), temperature (T) and Salinity (S) were measured (Figure 6).

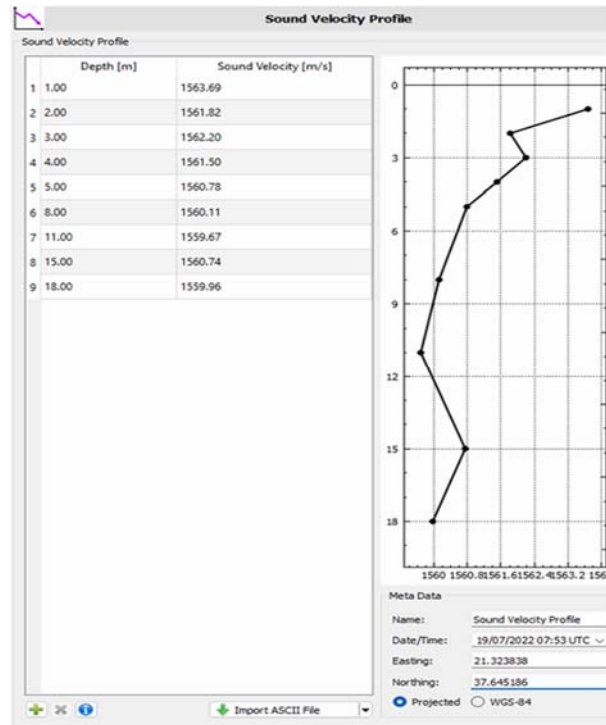


Figure 6. The sound velocity profile at the Katakolo port.

Next step was the analysis and processing of the data, which was carried out with the use of specialised modern hydrographic software. The final coordinates of the measured points were referred to the Greek Geodetic Reference System 1987 (GGRS87). The observed data had to be cleaned from noise created by factors, such as fish, anchors, sediments or fluids, using either automated filters or manually.

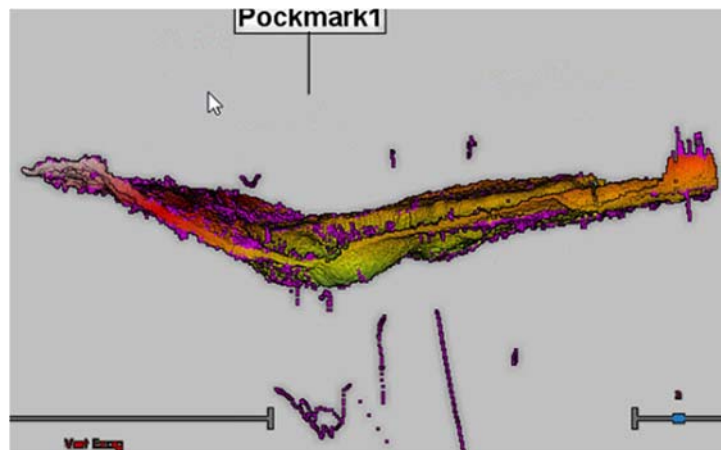


Figure 7. Pockmark detection

Therefore, it is of great significance for the hydrographer to evaluate and interpretate the data before applying any filter if, according to the survey requirements, to preserve selective noise, especially when surveying a port with the peculiarities of the study area, meaning the presence of pockmarks. Following the evaluation of the raw data, however, we came to the conclusion that any points being far below the seafloor surface were actually the result of gas leakage, which was released in the form of bubbles and distorted the orientation of the echosound beams, thus, revealing the position of pockmarks (Figure 7). Although the algorithm of automated filters may reject pockmarks as noisy data, in contrast to this work these points were preserved manually and geolocators were placed in the data to indicate the pockmark positions on the map. In addition, whilst multibeam scans combined with the dense boustrophedon

method they provided an adequate seafloor coverage, there were still seabottom areas with data gaps, which were then filled with interpolation methods, e.g. using neighbor pixels (Figure 8).

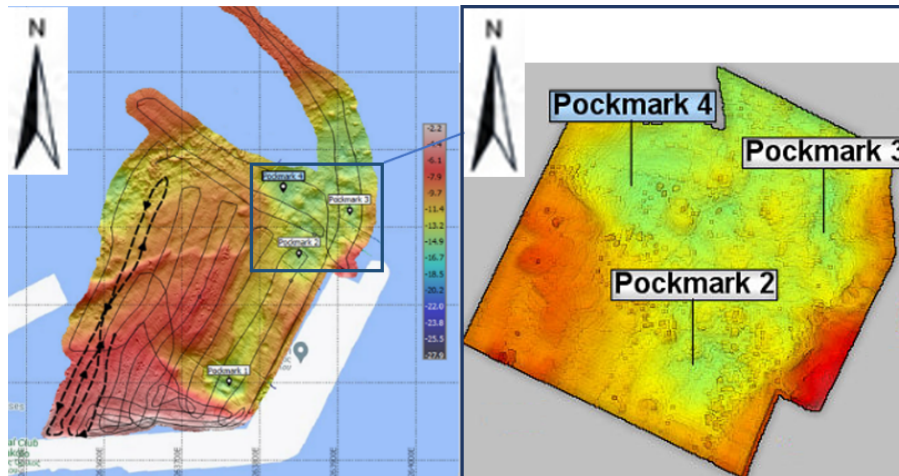


Figure 8:(a) The Katakolo port bathymetric processed data, (b) The detection of pockmarks in the study area

4 CONCLUSIONS

According to the IMO (International Maritime Organisation), which sets the technical provisions in the SOLAS (Safety Of Life At Sea) Convention, the collection and compilation of hydrographic data, as well as their publication, dissemination and keeping up-to-date in terms of safe navigation, they are all of vital importance. In order to ensure that frequent hydrographic surveys will provide adequate seabed information corresponding to the SOLAS requirements, modern Hydrography needs to provide the means for complying with these demands and standards, if to better understand seafloor mechanisms and to improve the maintenance of marine constructions and the operability of already existing ports. Furthermore, it is crucial to investigate the study area before a hydrographic survey takes place, so to detect possible peculiarities and characteristics and to accordingly adjust the field work and the data post processing. The present research points out the contribution of Hydrography and its importance for monitoring marine constructions and seabed status in the long term, with the typical example the pockmarks in the port of Katakolo, Greece. Due to lack of knowledge of their existence in the past, multiple incidents of breakwater destruction were observed in this harbour, provoked by the pockmarks. This results calls for an urgent need for hydrographic surveys at the Katakolo port on an annual basis, so that the generation rate of pockmark and possible destruction on both seabed and port facilities can be monitored, consequently allowing local authorities to potentially evaluate early enough any hazards and prevent port accidents.

References

- Choset H, (2000) Coverage of Known Spaces: The Boustrophedon Cellular Decomposition. *Autonomous Robots* 9, 247–253 doi:10.1023/A:1008958800904.
- Cathles LM, Su Z, Chen D (2010) The physics of gas chimney and pockmark formation, with implications for assessment of seafloor hazards and gas sequestration, *Marine and Petroleum Geology*, [online] vol.27, pp 82-91. <https://www.sciencedirect.com>
- Ceramicola S, Dupre S, Somoza L, Woodside J, (2018) *Cold Seep Systems. Submarine Geomorphology* (pp.367-387). Publisher: Springer.
- Etiopé G, Papatheodorou G, Christodoulou D, Ferentinos G, Sokos E, Favali P, (2006) Methane and hydrogen sulfide seepage in the northwest Peloponnese petroliferous basin (Greece): Origin and geohazard. *AAPG Bulletin*, 90 (5), 701 – 713.
- Talib KH, Othman MY, Sulaiman SAH, Wazir MAM, Azizan A, (2011) Determination of speed of sound using empirical equations and SVP. *IEEE 7th International Colloquium on Signal Processing and its Applications*, Penang, Malaysia, pp. 252-256, doi:10.1109/CSPA.2011.5759882.





2nd International Conference DESIGN AND MANAGEMENT OF PORT, COASTAL AND OFFSHORE WORKS

MAY 24-27, 2023

**Aristotle University's
Research Dissemination Center**
Thessaloniki, Greece

Sponsors:



Έργο: Υποστήριξη διοργάνωσης 2^{ου} Διεθνούς Επιστημονικού Συνεδρίου με θέμα «Σχεδιασμός και διαχείριση λιμενικών παράκτιων και υπεράκτιων έργων»

Πρόγραμμα - Μέτρο: «Εξωστρεφείς Δράσεις, Φυσικό Περιβάλλον και Καινοτόμες Δράσεις 2023»

Προϋπολογισμός έργου: 15000 €

Χρηματοδότηση: Πράσινο Ταμείο

Όνομα δικαιούχου: ΕΛΚΕ ΑΠΘ, ΠΟΛΥΤΕΧΝΙΚΗ ΣΧΟΛΗ – ΤΜΗΜΑ ΠΟΛΙΤΙΚΩΝ ΜΗΧΑΝΙΚΩΝ

Under the auspices:







DMP CO 2023



**LABORATORY OF MARITIME ENGINEERING
AND MARITIME WORKS**

**Civil Engineering Department
Aristotle University of Thessaloniki**

University Campus: Thessaloniki, 54124 Greece

ISSN: 2945-1299

ISBN: 978-960-99922-6-8 (set e-book)

ISBN: 978-960-99922-8-2 (Vol. II e-book)